ResearchOnline@JCU

JAMES COOK UNIVERSITY AUSTRALIA

This file is part of the following work:

**Sharan, Ashneel Ajinesh (2025)** ***Development of efficient mathematical, machine learning, simulation-optimisation and digital twin models for managing saltwater intrusion in Pacific Island coastal aquifers.*** **PhD Thesis, James Cook University.**

Access to this file is available from:

https://doi.org/10.25903/3dsg%2Dey19

Copyright © 2025 Ashneel Ajinesh Sharan

The author has certified to JCU that they have made a reasonable effort to gain permission and acknowledge the owners of any third party copyright material included in this document. If you believe that this is not the case, please email researchonline@jcu.edu.au

# Development of efficient mathematical, machine learning, simulation-optimisation and digital twin models for managing saltwater intrusion in Pacific Island coastal aquifers

Thesis submitted by

Ashneel Ajinesh Sharan

Bachelor of Science (Hon) (Physics) (University of Delhi, India)

Master of Science (Physics) (The University of the South Pacific, Fiji)

January 2025

In fulfilment of the requirements for the degree of

Doctor of Philosophy (PhD)

College of Science and Engineering

James Cook University

Australia



# Dedication

This thesis is dedicated to my grandparents. I am hopeful that this achievement will fulfil their dreams for me all those years ago when they decided to give me the best education possible.

# Acknowledgement

The completion of this PhD research and thesis would not have been possible without the unwavering support, encouragement, and assistance of numerous individuals, organisations, family, and friends.

First and foremost, I owe a deep debt of gratitude to my supervisor, Dr. Bithin Datta, who guided me through every step of this PhD journey from the day I arrived in Townsville. I consider myself incredibly fortunate to have been mentored by Dr. Datta, whom I regard as a true blessing in my academic life. His insightful research ideas, steadfast support, and continuous motivation have been the driving forces behind my work. Words cannot fully capture the significance of his role in this endeavour, and I will be forever grateful to him. I extend my heartfelt thanks to Dr. Datta for accepting me as his PhD student and for leading me through this challenging but rewarding journey. I would also like to express my appreciation to my secondary advisor, Dr. Alvin Lal, for his valuable guidance. Special thanks are extended to the faculty and staff of the College of Science and Engineering at James Cook University for their constant support and encouragement throughout my PhD candidature.

Financial support is a crucial aspect of completing a PhD research degree, and I am deeply grateful for the assistance I received throughout my candidature. I extend my heartfelt thanks to the Graduate Research School (GRS) at James Cook University for awarding me the James Cook University Postgraduate Research Scholarship (JCUPRS), which provided essential financial stability during my three and a half years of study. I'm also thankful to GRS for waiving my tuition fees for the full four years of my PhD course. I also appreciate the College of Science and Engineering at James Cook University for offering various levels of financial support, which was instrumental in the successful completion of my research. In addition, my special and genuine gratitude goes to the TropWATER, James Cook University's Centre for Tropical Water and Aquatic Ecosystem Research, for providing me with conference registration fees of $1000 AUD.

I am also deeply grateful to my research group members and colleagues at James Cook University for their ongoing motivation and inspiration. In particular, I want to acknowledge Dilip, Rabindra, Juan, Tejas and Teddy for their support and encouragement throughout my PhD journey.

Finally, I would like to thank my extended family members, especially my grandparents, for their constant support. My wife, Nilma, always provided substantial moral support and always encouraged me to complete the thesis. I would like to thank Nilma for all her patience, support, and belief in me, which enabled me to complete this dissertation. I would also like to thank my son, Adrith, who helped me destress by playing with me.

I recognise that no words of acknowledgment can fully compensate for the invaluable contributions of all those mentioned. Nevertheless, with sincere gratitude, I thank each of them for their generous support and outstanding contributions.

To end with, thank you, God.

*"Ananyascintayanto mam ye janah paryupasate, tesham nityabhiyuktanam yoga-kshemam vahamy aham."* Bhagavad Gita 9.22

This verse conveys a sense of divine support and guidance, reflecting the spirit of gratitude for those who have supported me.

## Statement of contribution of others

This thesis was carried out under the supervision of Dr Bithin Datta, who initially agreed with the research concept provided to him. I was responsible for creating the computational and technical framework, conducting numerical simulations, and analysing the results. Throughout the writing process, Dr Datta offered valuable suggestions and feedback. I authored the manuscripts for journals and conference papers and prepared oral and poster presentations for conferences, with input from Dr Datta. He also reviewed and provided insightful comments on all articles, papers and presentations.

James Cook University generously provided financial support through the James Cook University Postgraduate Research Scholarship, and travel assistance for conference participation was funded by the College of Science and Engineering and TropWATER.

I would also like to thank Dr Dilip Kumar Roy and Dr Alvin Lal for reviewing, editing, and providing useful comments on my journal papers, as well as providing me with artificial intelligence codes that assisted me in developing multiple machine learning models. Dr Krishna Kotra also provided me with the hydrogeological data from Vanuatu, which helped me to develop, calibrate and validate the numerical simulation model. Dr Kotra and Dr Roy also reviewed, edited and provided valuable comments on my journal papers.

The contribution of co-authors in my published papers was less than 15%. I did more than 85% of the work, including conceptualisation, investigation, methodology, writing the original draft, review and editing, and visualisation.

# Abstract

Population growth and rapid industrialisation have imposed excessive demand for groundwater in Pacific Island countries (PICs). To meet this demand, over-pumping of groundwater is practised in the majority of the PICs, which eventually causes saltwater intrusion (SWI) in coastal aquifers. In addition, the geographical location of PICs makes them more vulnerable to natural means of SWI. However, other anthropogenic activities and natural factors also cause groundwater contamination and SWI in PICs. SWI poses a significant threat to the sustainability of coastal aquifers in small PICs, driven by both anthropogenic and natural factors. This thesis focuses on developing efficient, reliable, and robust methodologies to manage SWI in these aquifers using mathematical models, machine learning, simulation-optimisation (S-O), and digital twin (DT) technologies. It further examines how climate change, human activities, and natural disasters impact groundwater resources across PICs. By addressing these challenges, the research contributes to the long-term sustainability of groundwater resources vital for these nations' development.

A comprehensive analysis was conducted to evaluate the effects of anthropogenic activities and natural factors on groundwater resources, focusing on Tonga. This study is the first to investigate various aspects of climate change and how it ultimately affects groundwater resources in Tonga. Limited studies have been done on the evaluation of groundwater use sustainability in Tonga, and so far, no specific investigation has been reported on the links between salinity trends, over-abstraction, long-term rainfall patterns, net recharge, sea level rise and $CO_2$ emissions on groundwater in Tonga. Hence, this study provides novel insights into Tonga's groundwater condition and opens pathways for further studies in the domain of groundwater research.

Historical data revealed that increased groundwater pumping in Tongatapu has caused significant salinity to increase over 42 years. Concurrently, long-term rainfall and net recharge have declined over 61 years, largely due to reduced precipitation and atmospheric heating from rising carbon dioxide ($CO_2$) emissions. Rising sea levels have exacerbated SWI, further contaminating coastal aquifers. This analysis highlights the urgent need for innovative management strategies that incorporate climate change mitigation, reduced abstraction rates, and carbon footprint reduction. These findings

underline the necessity of advanced modelling techniques, such as 3D numerical and AI-based models, for improved SWI prediction and management.

To address the SWI challenges in PICs, a SEAWAT-based 3D numerical simulation model was developed for an illustrative study area testing different SWI management scenarios. While field data limitations restricted precise calibration, hydrogeological parameters and boundary conditions were incorporated to simulate the system's response under seven scenarios. The scenarios included changing the barrier wells (BWs), injection wells (IWs), recharge, hydraulic head, hydraulic conductivity and grid size. Apart from salt, leachate and engine oil were also modelled in the current study area to see how they affect the freshwater wells over time. The scenario-based sensitivity analysis tests indicate that IWs, recharge, and hydraulic conductivities are highly sensitive, and with the proper modification, SWI can be managed or regulated. The sensitivity of grid size showed that the simulated results varied within the 10% range of different gird sizes. Moreover, it was also found that the rise in sea level or coastal heads by 0.3m-1m does not significantly cause further SWI in aquifers. However, a sea level rise above 1m would increase SWI rates. The results from this study are very crucial in this modern era when freshwater needs in coastal areas, especially PICs, are rapidly increasing, and fresh groundwater resources are declining. The novel outcome presented in this study opens pathways for further detailed modelling and numerical studies in the field of SWI management strategies development.

To enhance the realism of these models, randomised hydraulic conductivities (RHCs) were introduced to simulate aquifer heterogeneity. Using MATLAB, over 10000 randomised K values were generated for three hydraulic conductivity ranges (K-1 = 15 to 25 m/day, K-2 = 5 to 40 m/day, and K-3 = 2 to 100 m/day) and integrated into MODFLOW, MT3DMS and SEAWAT. The random integers and Halton Sequence were used to generate random hydraulic conductivities. The illustrative study area was selected for this simulation, leveraging available hydrogeological and raster data. Results indicated that RHCs reduced computational burdens and made the models more representative of field conditions. Importantly, SEAWAT demonstrated convergence under heterogeneous conditions, affirming its capability for complex simulations. This study is crucial, and the novel insight from this study is that this is the first study to randomise hydraulic conductivities in the SEAWAT code to develop a numerical model

for a coastal aquifer. The methods used to randomise the hydraulic conductivities are also the first to be used in this study.

After successfully developing and simulating the 3D numerical model using the SEAWAT code for the illustrative study area, a similar methodology was applied, and a 3D model was developed for a real study area. The methodology was applied to Tagabe coastal aquifer, which mostly supplies the groundwater to the capital city, Port Vila, in Vanuatu. The knowledge gained from this study is novel and of foremost importance for Vanuatu and all other surrounding island nations in the Pacific region, as it will provide optimal SWI management strategies by considering uncertainties, including climate change. This study also provides new knowledge to stakeholders and/or bore drilling companies who want to harvest groundwater in Vanuatu, as it gives them the benchmark of fresh groundwater's daily or yearly production rates.

The study on Tagabe coastal aquifer marks the first SEAWAT-based numerical model developed, calibrated, and validated using field data for Vanuatu. Scenario testing identified that a combination of BWs and IWs offered the most effective SWI mitigation strategy. Additionally, sea level rise projections up to 2043 indicated limited immediate impact under current estimates but underscored the need for extended modelling to account for uncertainties and higher sea level scenarios. The study also highlighted the need to balance BW and production well (PW) pumping rates to prevent unintended consequences, such as increased SWI or saline water disposal challenges. Hence, optimal SWI management strategies are needed for managing water in Tagabe coastal aquifer.

To optimise SWI management strategies further, an S-O methodology was developed, combining numerical simulation with machine learning-based surrogate ensemble models. Twelve surrogate models were trained using input-output patterns from SEAWAT simulations. The top five models ranked using Shannon’s entropy weight, were selected to form ensemble models for each monitoring location. These ensemble models, externally linked to a Controlled Elitist Multi-Objective Genetic Algorithm (CEMOGA), successfully optimised SWI management strategies by resolving conflicting constraints. The results from the S-O models are of global significance as they build on the current knowledge of utilising machine learning models in SWI predictions. This study will contribute to the knowledge of which surrogate or ensemble is robust, computer-efficient and accurate in predicting the SWI of a complex and heterogeneous

real island aquifer. A large number of surrogates and ensembles would also provide a benchmark for the accuracy of SWI predictions in an island coastal aquifer. Another important aspect of using multi-objective S-O is that it uses a limited number of input-output training patterns to train the surrogate models. This approach saved computational time and provided efficiency in developing the surrogate models. Hence, using fewer input-output datasets is another novelty of the S-O model. The results will provide justifications of which decision theories are important in selecting surrogate and ensemble models. Moreover, the results will also highlight the importance of using CEMOGA algorithm in drawing up robust multi-objective SWI management strategies in Vanuatu.

The S-O model achieved Pareto optimal solutions, maximising PW pumping, minimising BW pumping, and maintaining salt concentrations below allowable limits. Validation of these solutions showed minimal relative errors (<7%) between surrogate ensemble and numerical models, affirming their reliability. The S-O methodology also demonstrated the potential of machine learning in groundwater management. Surrogate ensemble models reduced computational burdens and effectively predicted SWI with limited datasets. However, implementing and validating optimal strategies in real-world scenarios necessitated a more dynamic approach, leading to the development of a DT model for the Tagabe coastal aquifer.

The DT framework integrated the 3D numerical model, surrogate ensemble models, and S-O techniques to create a virtual replica of the aquifer. Simulated data from illustrative field sensors triggered real-time updates between the physical and virtual systems. The DT was used to optimise pumping strategies under five scenarios of maximum allowable salt concentrations (ranging from 0.45 to 1.15 kg/m$^3$). Scenario 3 (0.75 kg/m$^3$) offered the best balance, allowing 17,317 m$^3$/day of PW pumping and 202 m$^3$/day from BWs. Higher salt concentration scenarios increased extraction rates but required greater BW pumping, highlighting trade-offs between sustainability and resource demand. The DT demonstrated a relative error of less than 10%, confirming its reliability for SWI management.

This innovative application of DT in SWI management underscores its transformative potential for sustainable water resource governance. The application of DT in SWI management in coastal aquifers has not been applied yet. By enabling real-time monitoring, simulation, and optimisation, the DT provided critical insights into

future scenarios and adaptive management strategies. Its integration of smart sensors and feedback loops promises enhanced decision-making and resource conservation, setting a global precedent for groundwater management. The results from this thesis demonstrate that numerical models, surrogate ensemble models, S-O methodologies, and DTs are effective tools for managing SWI in coastal aquifers. The findings offer actionable strategies for policymakers, water managers, and stakeholders in PICs, enabling sustainable groundwater extraction and long-term aquifer protection. The methodologies and insights developed can also be adapted to other regions globally facing similar challenges, contributing to the broader field of groundwater resource management.

# List of publications during PhD Candidature

## Peer-reviewed journal articles

1. Sharan. A., Lal, A., & Datta, B. (2021). A review of groundwater sustainability crisis in the Pacific Island countries: Challenges and solutions. Journal of Hydrology, 603, 1-15. https://doi.org/10.1016/j.jhydrol.2021.127165
2. Sharan. A., Lal, A., & Datta, B. (2023). Evaluating the impacts of climate change and water over-abstraction on groundwater resources in Pacific island country of Tonga. Groundwater for Sustainable Development, 20, 1-7. https://doi.org/10.1016/j.gsd.2022.100890
3. Sharan. A., Datta, B., & Lal, A. (2023). Integrating numerical modelling and scenario-based sensitivity analysis for saltwater intrusion management: Case study of a complex heterogeneous island aquifer system. Environmental Monitoring and Assessment, 195(553), 1-22. https://doi.org/10.1007/s10661-023-11159-z
4. Sharan, A., Datta, B., & Lal, A. (2024). Stochastic Application in the Numerical Simulation Model for Groundwater Salinity Management and Decision-Making. In: Ghute, B.B., Diwate, P. (eds) Geospatial Technologies for Integrated Water Resources Management. GIScience and Geo-environmental Modelling. Springer, Cham. https://doi.org/10.1007/978-3-031-57777-2_12
5. Sharan. A., Datta, B., Lal, A., & Kotra, K. (2024). Management of saltwater intrusion using numerical modelling techniques in the small Pacific Island country of Vanuatu. Environmental Monitoring and Assessment, 196(120), 1-20. https://doi.org/10.1007/s10661-023-12245-y

## Articles under review

1. Sharan. A., Roy, D.K., Datta, B., & Lal, A. (2024). A multi-objective simulation-optimisation model for managing saltwater intrusion in a coastal aquifer for a Pacific Island country: Case study of Vanuatu. *Journal of Hydrology*.
2. Sharan. A., Datta, B., Roy, D.K., & Lal, A. (2024). Conceptual development and implementation of a digital twin model for managing saltwater intrusion of an island coastal aquifer. *Water Resources Research.*

## Peer-reviewed conference proceeding

1. Sharan. A., Lal, A., Roy, D.K., & Datta, B. (2024). Prediction of saltwater intrusion using numerical and surrogate modelling: Case study of Tagabe coastal aquifer, Vanuatu. *Proc., International CleanUp Conference*, Cooperative Research Centre for Contamination Assessment and Remediation of the Environment (CRC-Care), 15-19 September, Adelaide, Australia, 1-2.

## Oral conference presentations

1. Sharan. A., Lal, A., & Datta, B. (2023). Management of saltwater intrusion using 3D numerical modelling: a first for Pacific Island country of Vanuatu. *The Society of Environmental Toxicology and Chemistry (SETAC*), Townsville, Australia.
2. Sharan. A., Lal, A., & Datta, B. (2023). Stochastic application in numerical simulation model for groundwater salinity management and decision-making. *Australasian Groundwater / New Zealand Hydrological Society Joint Conference,* 28 Nov – 1 Dec 2023, Auckland, New Zealand.
3. Sharan. A., Lal, A., Roy, D.K., & Datta, B. (2024). Prediction of saltwater intrusion using numerical and surrogate modelling: Case study of Tagabe coastal aquifer, Vanuatu. *International CleanUp Conference*, Cooperative Research Centre for Contamination Assessment and Remediation of the Environment (CRC-Care), 15-19 September, Adelaide, Australia, 1-2.
4. Sharan. A., Roy, D.K., Datta, B., & Lal, A. (2024). A multi-objective simulation-optimisation model for managing saltwater intrusion in a coastal aquifer for a Pacific Island country. GEOMATE Conference, the Geomate Society Thailand Chapter, 13 to 15 November 2024., Pattaya, Thailand.

# Table of contents

**Dedication** ..... **i**

**Acknowledgement** ..... **ii**

**Statement of contribution of others** ..... **iv**

**Abstract** ..... **v**

**List of publications during PhD Candidature** ..... **x**

**List of Tables** ..... **i**

**List of Figures** ..... **i**

**Chapter 1: Introduction** ..... **1**

1.1 Overview ..... 1

1.2 Outline ..... 1

1.3 Research Significance ..... 3

1.4 Aims and Objectives ..... 4

1.5 Thesis organisation and structure ..... 5

**Chapter 2: Literature review** ..... **7**

2.1 Overview ..... 7

2.2 Executive Summary ..... 7

2.3 Introduction ..... 7

2.4 PICs water resources and associated challenges – detailed background ..... 9

2.5 Background Information on Saltwater Intrusion – A Common Challenge for PICs ..... 20

2.5.1 Major solutions for saltwater intrusion in PICs ..... 22

2.6 Conclusions ..... 37

**Chapter 3: Evaluating the impacts of climate change and water over-abstraction on groundwater resources in Pacific island country of Tonga** ..... **38**

3.1 Overview ..... 38

3.2 Executive Summary ..... 38

3.3 Introduction ..... 39

3.4 Data 43

3.4.1 Study area ..... 43

3.5 Methods ..... 44

3.6 Results and Discussion ..... 44

3.7 Conclusions ..... 51

**Chapter 4: Integrating numerical modelling and scenario-based sensitivity analysis for saltwater intrusion management: case study of a complex heterogeneous island aquifer system** ..... **53**

4.1 Overview ..... 53
4.2 Executive Summary ..... 53
4.2 Introduction ..... 54
4.3 Methods ..... 59
4.3.1 Governing Equations ..... 59
4.4 Study area ..... 60
4.4.1 Model Discretisation ..... 62
4.4.2 Numerical Model and Boundary Conditions ..... 62
4.4.3 Different scenarios tested ..... 64
4.5 Results ..... 65
4.5.1 Scenario 1: Increasing the number of barrier wells ..... 65
4.5.2 Scenario 2: Increasing the hydraulic conductivity, porosity and BWs ..... 68
4.5.3 Scenario 3: Increasing the recharge rate ..... 71
4.5.4 Scenario 4: Installation of injection wells ..... 72
4.5.5 Scenario 5: Increasing the hydraulic head ..... 73
4.5.6 Scenario 6: Changing the model grid size ..... 75
4.5.7 Scenario 7: Multi-species contaminant transport ..... 77
4.6 Discussion ..... 79
4.7 Conclusions ..... 82
**Chapter 5: Stochastic application in numerical simulation model for groundwater salinity management and decision-making ..... 84**
5.1 Overview ..... 84
5.2 Executive Summary ..... 84
5.3 Introduction ..... 85
5.4 Materials and Method ..... 88
5.4.1 Study area ..... 88
5.4.2 Numerical model design ..... 91
5.4.3 Randomising hydraulic conductivities ..... 93
5.4.4 Saltwater intrusion management strategies ..... 94
5.5 Results ..... 94
5.5.1 Random integers of hydraulic conductivities ..... 94
5.5.2 Random hydraulic conductivities using Halton Sequence ..... 100
5.5.3 SWI management scenarios ..... 104
5.6 Discussion ..... 106
5.7 Conclusions ..... 107

**Chapter 6: Management of saltwater intrusion using numerical modelling techniques in the small Pacific Island country of Vanuatu ..... 109**
6.1 Overview ..... 109
6.2 Executive Summary ..... 109
6.3 Introduction ..... 110
6.4 Materials and Methods ..... 114
6.4.1 Study area ..... 114
6.4.2 Flow and solute transport model ..... 119
6.4.3 Model Calibration and Validation ..... 122
6.4.4 Simulated scenarios ..... 122
6.5 Results ..... 123
6.5.1 Calibration and Validation ..... 123
6.5.2 Base case ..... 123
6.5.3 Scenario 1: Increased population and pumping rates ..... 125
6.5.4 Scenario 2: Addition of barrier wells ..... 127
6.5.5 Scenario 3: Addition of barrier wells and injection wells ..... 130
6.5.6 Scenario 4: Sea level rise ..... 130
6.6 Discussion ..... 132
6.7 Conclusions ..... 134
**Chapter 7: A multi-objective simulation-optimisation model for managing saltwater intrusion in a coastal aquifer for a Pacific Island country ..... 136**
7.1 Overview ..... 136
7.2 Executive Summary ..... 136
7.3 Introduction ..... 137
7.4 Methodology ..... 140
7.4.1 Study area ..... 140
7.4.2 Surrogate and ensemble models ..... 146
7.4.3 Management Model ..... 155
7.4.4 Model Performance Evaluation Criterion ..... 157
7.4.5 Shannon's entropy-based decision theory ..... 158
7.5 Results and Discussion ..... 159
7.5.1 Numerical Simulation Model ..... 159
7.5.2 Surrogate and Ensemble Model ..... 161
7.5.3 Model Performance and Selection ..... 171
7.5.4 Management Model ..... 178
7.5.5 Validation of Pareto Optimal Solutions ..... 180

7.6 Conclusions ..... 183
**Chapter 8: Conceptual development and implementation of a digital twin model for managing saltwater intrusion of an island coastal aquifer ..... 185**
8.1 Overview ..... 185
8.2 Executive Summary ..... 185
8.3 Introduction ..... 186
8.4 Methodology ..... 189
8.4.1 Study area ..... 189
8.4.2 3D Numerical Simulation Model ..... 191
8.4.3 Surrogate Ensemble Model ..... 193
8.4.4 Management Model ..... 194
8.4.5 Digital Twin ..... 196
8.5 Results and Discussion ..... 201
8.5.1 3D Numerical Simulation Model ..... 201
8.5.2 Machine learning surrogate ensemble model ..... 204
8.5.3 Digital Twin ..... 214
8.5.4 Validation of Pareto optimal fronts ..... 217
8.6 Summary and Conclusions ..... 219
**Chapter 9: Conclusions and Recommendations ..... 222**
9.1 Conclusions ..... 222
9.2 Limitations and future scope of work ..... 225
**Reference ..... 227**
**Appendix A ..... 251**

# List of Tables

Table 2.1: Pacific Island countries and territories summary. Source ([1]World Population Review, 2021; [2]Falkland, 2002).....12

Table 2.2: Water monitoring devices. Adapted from Xylem (2013). .....26

Table 2.3: Common 3-D modelling codes used for SWI. .....27

Table 2.4: The summary of simulation-optimisation techniques for SWI management.31

Table 2.5: Application of SWI solutions in Kiribati (a small Pacific Island country). ...36

Table 4.1: General salinity classification (Hillel, 2000).....55

Table 4.2: Pacific Island countries profile and water resources. Source ([1]World Population Review, 2022; [2]Falkland, 2002; [3]Sharan et al., 2021). .....56

Table 4.3: Model parameters and their values used in the numerical simulations. .....64

Table 5.1: Hydrogeological parameters.....90

Table 6.1: Model parameters and the values used for the model design. .....118

Table 6.2: Location of production boreholes in Tagabe, Port Vila.....121

Table 7.1: Model parameters and the values used for the model design. Source (Sharan et al., 2024). .....145

Table 7.2: Performance criteria of twelve surrogate models at four different monitoring locations (MLs) during the model training period. .....174

Table 7.3: Performance criteria of twelve surrogate models and four ensemble models at four different monitoring locations (MLs) during the model testing period. .....174

Table 7.4: Entropy weight of performance indices. .....176

Table 7.5: Entropy weight of the individual prediction models. .....177

Table 7.6: Validation of Pareto optimal front solutions with the numerical simulation model. .....182

Table 8.1: Model parameters and the values used for the model design. Source (Sharan et al., 2024a). .....191

Table 8.2: Performance criteria of twelve surrogate models at four different monitoring locations (MLs) during the model training period. Source (Sharan et al., 2024b). .....211

Table 8.3: Performance criteria of twelve surrogate models and four ensemble models at four different monitoring locations (MLs) during the model testing period. Source (Sharan et al., 2024b). .....211

Table 8.4: Entropy weight of the individual prediction models. Source (Sharan et al., 2024b).....213

Table 8.5: Validation of Pareto optimal front solutions with the numerical simulation model for all five scenarios of the digital twin approach. .....218

# List of Figures

Figure 2.1: The Pacific Islands. .....9

Figure 2.2: Major water sources in Pacific Island countries. .....10

Figure 2.3: Fiji's total freshwater water production in year 2016. Source (WAF, 2019). .....11

Figure 2.4: Summary of all groundwater wells surveyed for seven villages in Onotoa, Kiribati. Source (Loco et al., 2020).....13

Figure 2.5: Nauru's internal water usage per day (2-4 persons) in 2015. Source (NRW, 2015).....14

Figure 2.6: Water pumping output of selected boreholes in Niue (2008). Source (Siohane and Chapman, 2009).....15

Figure 2.7: Water usage of some selected states in Palau. Source (SOPAC, 2007a). ....15

Figure 2.8: Renewable water resources per capita and number of people with access to safe drinking water in PNG. Source (Worldometer, 2021). .....16

Figure 2.9: Water temperature and salinity measurements of a borehole in Samoa. Source (Wiyot, 2015).....17

Figure 2.10: Characteristics of some selected boreholes in Solomon Islands. Source (SOPAC, 2007b). Boreholes W1 to W4 are located in White River (9.26° S 159.55° E), M1 to M3 are located in Mataniko (9.43° S 159.97° E) and K1 and K2 are located in Kombito (9.433°S 159.98°E).....17

Figure 2.11: The specific conductivity of four selected boreholes and one treatment plant in Tonga. Source (Singh, 2014). These production bores are located in Lifuka Island (19.81° S 174.34° W). The geographic locations of each bores are; Tonga Water Board (TWB) PANGAI North (19.81° S 174.35° W), TWB Hihifo North (19.813° S 174.353° W), TWB Hihifo East (19.818° S 174.356° W), TWB4 (19.817° S 174.354° W), Treatment plant is also located in Lifuka. .....18

Figure 2.12: Number of people with no access to safe drinking water in Tuvalu. Source (Worldometer, 2021).....18

Figure 2.13: Water source for seven provinces in Vanuatu. Source (SOPAC, 2007c)...19

Figure 2.14: Saltwater intrusion in a coastal aquifer system. .....21

Figure 2.15: Study area indicating pumping and barrier wells, and monitoring stations, (b) 3D model developed using FEMWATER. Reproduced from Lal and Datta (2019c).....29

Figure 3.1: The Island of Tongatapu marked with groundwater wells and salinity monitoring boreholes.....40

Figure 3.2: Groundwater pumping rates of Mataki'eua/Tongamai wellfield. .....45

Figure 3.3: Salinity concentration of various wells in Tongatapu. .....45

Figure 3.4: Rainfall (marked blue) and net recharge (marked green) for Nuku'alofa, Tonga.....46

Figure 3.5: Sea level height in Nuku'alofa. .....47

Figure 3.6: Salinity monitoring boreholes in Mataki'eua, Tonga, SMB1 (-21.15883, -175.23464), SMB2 (-21.15389, -175.24172) and SMB3 (-21.15061, -175.24494). .....49

Figure 3.7: Carbon dioxide ($CO_2$) emissions of some selected PICs. .....51

Figure 4.1: Plan view of the study area. .....61

Figure 4.2: (a-10 to a-30), (b-10 to b-30) and (c-10 to c-30) shows the plan view of the simulated results of saltwater intrusion for the controlled area, the addition of barrier wells (scenario 1) and increasing the hydraulic conductivities and porosities (scenario 2), respectively. .....66

Figure 4.3: (a-10 to a-30), (b-10 to b-30) and (c-10 to c-30) shows the plan view of the simulated results of saltwater intrusion for changing recharge (scenario 3), the addition of injection wells (scenario 4) and increasing the hydraulic heads (scenario 5), respectively. .....67

Figure 4.4: (a-10 to a-30); (b-10 to b-30); (c-10 to c-30); (d-10 to d-30); (e-10 to e-30) and (f-10 to f-30) shows the side view of the simulated results of saltwater intrusion at monitoring location 1 for the controlled area, the addition of barrier wells (scenario 1) and increasing the hydraulic conductivities and porosities (scenario 2), changing recharge (scenario 3), the addition of injection wells (scenario 4) and increasing the hydraulic heads (scenario 5), respectively. The -10, -20 and -30 represent the time steps 10, 20 and 30 years, respectively. .....69

Figure 4.5: (a to e) shows the comparison of simulated salt concentrations at various monitoring locations for the controlled area against the addition of barrier wells (scenario 1), increasing the hydraulic conductivities and porosities (scenario 2), changing recharge (scenario 3), the addition of injection wells (scenario 4) and increasing the hydraulic heads (scenario 5), respectively. .....70

Figure 4.6: (a to c) shows the box plot of simulated salt concentrations obtained by using different grid sizes, the linear correlation of 100m x 100m and 50m x 50m grid results, and the linear correlation of 50m x 50m and 25m x 25m grid results, respectively. .....76

Figure 4.7: (a-15 to a-30) shows the leachate concentrations for 15 and 30-year time steps; (a-15s to a-30s) shows the leachate concentrations for 15 and 30-year time steps after sorption and chemical reactions. (b-15 to b-30) shows the engine oil concentrations for 15 and 30-year time steps; (b-15s to b-30s) shows the engine oil concentrations for 15 and 30-year time steps after sorption and chemical reactions. .....78

Figure 5.1: Simple process of saltwater intrusion in coastal aquifers. Source (after Sharan et al., 2021). .....86

Figure 5.2: Study area.....89

Figure 5.3: a, c, e represent hydraulic conductivities randomly generated integers ranging from 15 m/d to 25 m/d, 5 m/d to 40 m/d, and 2 m/d to 100 m/d, respectively. b, d, f are hydraulic conductivities randomly generated using Halton sequence for the ranges 15 m/d to 25 m/d, 5 m/d to 40 m/d, and 2 m/d to100 m/d, respectively. ...96

Figure 5.4: Plan view of saltwater intrusion. (a-1 to a-20) for uniform hydraulic conductivities (HCs). (b-1 to b-20) for randomized hydraulic conductivities (K-1) using randomly generated integers for the range 15 m/d to 25 m/d. (c-1 to c-20)

showing randomised hydraulic conductivities (K-1.1) generated using the Halton sequence for the range 15 m/d to 25 m/d. The numbers 1, 5, 10, 15, and 20 represent the time steps of 1 year, 5 years, 10 years, 15 years, and 20 years, respectively. .97

Figure 5.5: Plan view of saltwater intrusion. (a-1 to a-20) for uniform hydraulic conductivities (HCs). (b-1 to b-20) for randomised hydraulic conductivities (K-2) using randomly generated integers for the range 5 m/d to 40 m/d. (c-1 to c-20) showing randomized hydraulic conductivities (K-2.1) generated using the Halton sequence for the range 5 m/d to 40 m/d. The numbers 1, 5, 10, 15, and 20 represent the time steps of 1 year, 5 years, 10 years, 15 years, and 20 years, respectively. .98

Figure 5.6: Plan view of saltwater intrusion. (a-1 to a-20) for uniform hydraulic conductivities (HCs). (b-1 to b-20) for randomised hydraulic conductivities (K-3) using randomly generated integers for the range 2 m/d to 100 m/d. (c-1 to c-20) showing randomized hydraulic conductivities (K-3.1) generated using the Halton sequence for the range 2 m/d to 100 m/d. The numbers 1, 5, 10, 15, and 20 represent the time steps of 1 year, 5 years, 10 years, 15 years, and 20 years, respectively. .99

Figure 5.7: a-e are salt concentrations at monitoring location 1 for time steps 1, 5, 10, 15 and 20, respectively. Uni indicates the uniform hydraulic conductivity of 20 m/d. K-1, K-2 and K-3 are hydraulic conductivities randomly generated integers for the range 15 m/d to 25 m/d, 5 m/d to 40 m/d, and 2 m/d to 100 m/d, respectively. Whereas K-1.1, K-2.3 and K-3.1 are hydraulic conductivities randomly generated using Halton sequence for the range 15 m/d to 25 m/d, 5 m/d to 40 m/d, and 2 m/d to 100 m/d, respectively. .....101

Figure 5.8: a-e are salt concentrations at monitoring location 2 for time steps 1, 5, 10, 15 and 20, respectively. Uni indicates the uniform hydraulic conductivity of 20 m/d. K-1, K-2 and K-3 are hydraulic conductivities randomly generated integers for the range 15 m/d to 25 m/d, 5 m/d to 40 m/d, and 2 m/d to 100 m/d, respectively. Whereas K-1.1, K-2.3 and K-3.1 are hydraulic conductivities randomly generated using Halton sequence for the range 15 m/d to 25 m/d, 5 m/d to 40 m/d, and 2 m/d to 100 m/d, respectively. .....102

Figure 5.9: a-e are alt concentrations at monitoring location 3 for time steps 1, 5, 10, 15 and 20, respectively. Uni indicate the uniform hydraulic conductivity of 20 m/d. K-1, K-2 and K-3 are hydraulic conductivities randomly generated integers for the range 15 m/d to 25 m/d, 5 m/d to 40 m/d, and 2 m/d to 100 m/d, respectively. Whereas K-1.1, K-2.3 and K-3.1 are hydraulic conductivities randomly generated using Halton sequence for the range 15 m/d to 25 m/d, 5 m/d to 40 m/d, and 2 m/d to 100 m/d, respectively. .....103

Figure 5.10: Plan view of saltwater intrusion encroachment management strategies. (a-1 to a-20) showing the hydraulic barriers using the barrier wells and injection wells to manage saltwater intrusion. (b-1 to b-20) showing the hydraulic barriers using only the injection wells to manage saltwater intrusion. The numbers 1, 5, 10, 15, and 20 represent the time steps of 1 year, 5 years, 10 years, 15 years, and 20 years, respectively. .....105

Figure 6.1: Earth's water resources. Source (Shiklomanov, 1993). .....111

Figure 6.2: Study area inclusive of the plan and 3D views. .....117

Figure 6.3: Observed versus simulated salt concentrations obtained during calibration (a to e) and validation stage (f to j). (a to e) represents the data from bore 1, 2, 3, 7 and

8, respectively. Similarly, (f to j) represents the data from bore 1, 2, 3, 7 and 8, respectively. ..... 124

Figure 6.4: (a-1 to a-20) shows the plan view of the simulated results of saltwater intrusion for the base case; (b-1 to b-20) increasing the pumping and number of pumping wells (scenario 1); (c-1 to c-20) addition of barrier wells (scenario 2); (d-1 to d-20) addition of injection well plus barrier wells (scenario 3); (e-1 to e-20) sea level rise (scenario 4). The numbers 1, 5, 10, 15 and 20 represent the time steps 1 year, 5 years, 10 years, 15 years and 20 years, respectively. ..... 125

Figure 6.5: (a-1 to a-20) shows the front view of the simulated results of saltwater intrusion for the base case; (b-1 to b-20) increasing the pumping and number of pumping wells (scenario 1); (c-1 to c-20) addition of barrier wells (scenario 2); (d-1 to d-20) addition of injection well plus barrier wells (scenario 3); (e-1 to e-20) sea level rise (scenario 4). The numbers 1, 5, 10, 15 and 20 represent the time steps 1 year, 5 years, 10 years, 15 years and 20 years, respectively. ..... 126

Figure 6.6: Projected population of Port Vila, Vanuatu. ..... 128

Figure 6.7: a) shows the comparison of simulated salt concentrations for different boreholes for the base case and the increased pumping and the number of pumping wells (scenario 1); b) shows the comparison of simulated salt concentrations for different boreholes for the base case the addition of barrier wells (scenario 2); c) shows the comparison of simulated salt concentrations for different boreholes for the base case the addition of injection well plus barrier wells (scenario 3); d) shows the comparison of simulated salt concentrations for different boreholes for the base case and the sea level rise (scenario 4). ..... 129

Figure 6.8: Projected sea level rise for Vanuatu, relative to 1990. Source (CRCP, 2021). ..... 131

Figure 7.1: Study area. Source (Sharan et al., 2024). ..... 141

Figure 7.2: Single-layered ANN structure. ..... 147

Figure 7.3: Simple S.V.R. model structure. ..... 149

Figure 7.4: Simple Genetic Programming model tree. ..... 149

Figure 7.5: Schematic of simple probabilistic linear regression. ..... 152

Figure 7.6: Random forest regression structure. ..... 152

Figure 7.7: Flow diagram of linked simulation-optimisation management model. ..... 157

Figure 7.8: (a-1 to a-20) shows the plan view of the simulated results of saltwater intrusion for the base case; (b-1 to b-20) increasing the pumping and number of pumping wells (scenario 1); (c-1 to c-20) addition of barrier wells (scenario 2); (d-1 to d-20) addition of injection well plus barrier wells (scenario 3); (e-1 to e-20) sea level rise (scenario 4). The numbers 1, 5, 10, 15 and 20 represent the time steps 1 year, 5 years, 10 years, 15 years and 20 years, respectively. Source (Sharan et al., 2024). ..... 160

Figure 7.9: Actual versus predicted salt concentrations of monitoring location 1 (ML1) using different machine learning algorithms during training period; **a)** – Adaptive Neuro Fuzzy Inference System (ANFIS), **b)** – Artificial Neural Network (ANN), **c)** – Multivariate Adaptive Regression Spline with Piecewise Cubic Spline (MARS_C), **d)** – Multivariate Adaptive Regression Spline with Piecewise Linear

Spline (MARS_L), **e)** – Bayesian Optimization tuned Automatic Model Selection (AMS_Bayesian), **f)** – Asynchronous Successive Halving Algorithm tuned Automatic Model Selection (AMS_ASHA), **g)** – Bi-directional Long Short term Memory Network (Bi-LSTM), **h)** – Group Method of Data Handling (GMDH), **i)** – Gaussian Process Regression (GPR), **j)** – Probabilistic Linear Regression (PLR), **k)** – Random Forest (RF) and **l)** – Support Vector Regression (SVR). .....163

Figure 7.10: Actual versus predicted salt concentrations of monitoring location 2 (ML2) using different machine learning algorithms during training period; **a)** – Adaptive Neuro Fuzzy Inference System (ANFIS), **b)** – Artificial Neural Network (ANN), **c)** – Multivariate Adaptive Regression Spline with Piecewise Cubic Spline (MARS_C), **d)** – Multivariate Adaptive Regression Spline with Piecewise Linear Spline (MARS_L), **e)** – Bayesian Optimization tuned Automatic Model Selection (AMS_Bayesian), **f)** – Asynchronous Successive Halving Algorithm tuned Automatic Model Selection (AMS_ASHA), **g)** – Bi-directional Long Short term Memory Network (Bi-LSTM), **h)** – Group Method of Data Handling (GMDH), **i)** – Gaussian Process Regression (GPR), **j)** – Probabilistic Linear Regression (PLR), **k)** – Random Forest (RF) and **l)** – Support Vector Regression (SVR). .....164

Figure 7.11: Actual Actual versus predicted salt concentrations of monitoring location 3 (ML3) using different machine learning algorithms during training period; **a)** – Adaptive Neuro Fuzzy Inference System (ANFIS), **b)** – Artificial Neural Network (ANN), **c)** – Multivariate Adaptive Regression Spline with Piecewise Cubic Spline (MARS_C), **d)** – Multivariate Adaptive Regression Spline with Piecewise Linear Spline (MARS_L), **e)** – Bayesian Optimization tuned Automatic Model Selection (AMS_Bayesian), **f)** – Asynchronous Successive Halving Algorithm tuned Automatic Model Selection (AMS_ASHA), **g)** – Bi-directional Long Short term Memory Network (Bi-LSTM), **h)** – Group Method of Data Handling (GMDH), **i)** – Gaussian Process Regression (GPR), **j)** – Probabilistic Linear Regression (PLR), **k)** – Random Forest (RF) and **l)** – Support Vector Regression (SVR). .....165

Figure 7.12: Actual versus predicted salt concentrations of monitoring location 4 (ML4) using different machine learning algorithms during training period; **a)** – Adaptive Neuro Fuzzy Inference System (ANFIS), **b)** – Artificial Neural Network (ANN), **c)** – Multivariate Adaptive Regression Spline with Piecewise Cubic Spline (MARS_C), **d)** – Multivariate Adaptive Regression Spline with Piecewise Linear Spline (MARS_L), **e)** – Bayesian Optimization tuned Automatic Model Selection (AMS_Bayesian), **f)** – Asynchronous Successive Halving Algorithm tuned Automatic Model Selection (AMS_ASHA), **g)** – Bi-directional Long Short term Memory Network (Bi-LSTM), **h)** – Group Method of Data Handling (GMDH), **i)** – Gaussian Process Regression (GPR), **j)** – Probabilistic Linear Regression (PLR), **k)** – Random Forest (RF) and **l)** – Support Vector Regression (SVR). .....166

Figure 7.13: Actual versus predicted salt concentrations of monitoring location 1 (ML1) using different machine learning algorithms during testing period; **a)** – Adaptive Neuro Fuzzy Inference System (ANFIS), **b)** – Artificial Neural Network (ANN), **c)** – Multivariate Adaptive Regression Spline with Piecewise Cubic Spline (MARS_C), **d)** – Multivariate Adaptive Regression Spline with Piecewise Linear Spline (MARS_L), **e)** – Bayesian Optimization tuned Automatic Model Selection (AMS_Bayesian), **f)** – Asynchronous Successive Halving Algorithm tuned Automatic Model Selection (AMS_ASHA), **g)** – Bi-directional Long Short term Memory Network (Bi-LSTM), **h)** – Group Method of Data Handling (GMDH), **i)**

– Gaussian Process Regression (GPR), **j)** – Probabilistic Linear Regression (PLR) , **k)** – Random Forest (RF) and **l)** – Support Vector Regression (SVR). .....167

Figure 7.14: Actual versus predicted salt concentrations of monitoring location 2 (ML2) using different machine learning algorithms during testing period; **a)** – Adaptive Neuro Fuzzy Inference System (ANFIS), **b)** – Artificial Neural Network (ANN), **c)** – Multivariate Adaptive Regression Spline with Piecewise Cubic Spline (MARS_C), **d)** – Multivariate Adaptive Regression Spline with Piecewise Linear Spline (MARS_L), **e)** – Bayesian Optimization tuned Automatic Model Selection (AMS_Bayesian), **f)** – Asynchronous Successive Halving Algorithm tuned Automatic Model Selection (AMS_ASHA), **g)** – Bi-directional Long Short term Memory Network (Bi-LSTM), **h)** – Group Method of Data Handling (GMDH), **i)** – Gaussian Process Regression (GPR), **j)** – Probabilistic Linear Regression (PLR), **k)** – Random Forest (RF) and **l)** – Support Vector Regression (SVR). .....168

Figure 7.15: Actual versus predicted salt concentrations of monitoring location 3 (ML3) using different machine learning algorithms during testing period; **a)** – Adaptive Neuro Fuzzy Inference System (ANFIS), **b)** – Artificial Neural Network (ANN), **c)** – Multivariate Adaptive Regression Spline with Piecewise Cubic Spline (MARS_C), **d)** – Multivariate Adaptive Regression Spline with Piecewise Linear Spline (MARS_L), **e)** – Bayesian Optimization tuned Automatic Model Selection (AMS_Bayesian), **f)** – Asynchronous Successive Halving Algorithm tuned Automatic Model Selection (AMS_ASHA), **g)** – Bi-directional Long Short term Memory Network (Bi-LSTM), **h)** – Group Method of Data Handling (GMDH), **i)** – Gaussian Process Regression (GPR), **j)** – Probabilistic Linear Regression (PLR), **k)** – Random Forest (RF) and **l)** – Support Vector Regression (SVR). .....169

Figure 7.16: Actual versus predicted salt concentrations of monitoring location 4 (ML4) using different machine learning algorithms during testing period; **a)** – Adaptive Neuro Fuzzy Inference System (ANFIS), **b)** – Artificial Neural Network (ANN), **c)** – Multivariate Adaptive Regression Spline with Piecewise Cubic Spline (MARS_C), **d)** – Multivariate Adaptive Regression Spline with Piecewise Linear Spline (MARS_L), **e)** – Bayesian Optimization tuned Automatic Model Selection (AMS_Bayesian), **f)** – Asynchronous Successive Halving Algorithm tuned Automatic Model Selection (AMS_ASHA), **g)** – Bi-directional Long Short term Memory Network (Bi-LSTM), **h)** – Group Method of Data Handling (GMDH), **i)** – Gaussian Process Regression (GPR), **j)** – Probabilistic Linear Regression (PLR), **k)** – Random Forest (RF) and **l)** – Support Vector Regression (SVR). .....170

Figure 7.17: Performance of all surrogate models during the training stage using Pearson correlation coefficient, Index of Agreement, Kling-Gupta Efficiency coefficient and Nash-Sutcliffe Efficiency coefficient at **a)** ML2, **b)** ML2, **c)** ML3 and **d)** ML4. .....172

Figure 7.18: Performance of all surrogate models during the training stage using Pearson correlation coefficient, Index of Agreement, Kling-Gupta Efficiency coefficient and Nash-Sutcliffe Efficiency coefficient at **a)** ML2, **b)** ML2, **c)** ML3 and **d)** ML4. .....173

Figure 7.19: Boxplots of absolute errors between actual and predicted salt concentration values at **a)** ML1, **b)** ML2, **c)** ML3, and **d)** ML4 using all twelve surrogate models. .....175

Figure 7.20: Residual of actual versus predicted salt concentrations of ensemble models. **a)** residual of an ensemble model at ML1, **b)** residual of an ensemble model at ML2, **c)** residual of an ensemble model at ML3 and **d)** residual of an ensemble model at ML4. ..... 178

Figure 7.21: Pareto optimal front of the linked simulation-optimisation management model. ..... 179

Figure 8.1: Location of the study area. ..... 190

Figure 8.2: Flow diagram of linked simulation-optimisation management model. ..... 195

Figure 8.3: Digital twin framework of a coastal aquifer. ..... 198

Figure 8.4: Numerical model simulated saltwater intrusion rates in Tagabe coastal aquifer with production bores (B1-B8): **a)** length of saltwater intrusion after 5 years of current pumping regimes in Tagabe; **b)** length of saltwater intrusion after 10 years of current pumping regimes in Tagabe; **c)** length of saltwater intrusion after 20 years of current pumping regimes in Tagabe. ..... 202

Figure 8.5: Side view cross-sections of salt concentration of layer 1 with production bores (B1-B8): **a)** length of saltwater intrusion after 5 years of current pumping rates in Tagabe; **b)** length of saltwater intrusion after 10 years of current pumping rates in Tagabe; **c)** length of saltwater intrusion after 20 years of current pumping rates in Tagabe. ..... 203

Figure 8.6: Actual versus predicted salt concentrations of monitoring location 1 (ML1) using different machine learning algorithms during training period; **a)** – Adaptive Neuro Fuzzy Inference System (ANFIS), **b)** – Artificial Neural Network (ANN), **c)** – Multivariate Adaptive Regression Spline with Piecewise Cubic Spline (MARS_C), **d)** – Multivariate Adaptive Regression Spline with Piecewise Linear Spline (MARS_L), **e)** – Bayesian Optimization tuned Automatic Model Selection (AMS_Bayesian), **f)** – Asynchronous Successive Halving Algorithm tuned Automatic Model Selection (AMS_ASHA), **g)** – Bi-directional Long Short term Memory Network (Bi-LSTM), **h)** – Group Method of Data Handling (GMDH), **i)** – Gaussian Process Regression (GPR), **j)** – Probabilistic Linear Regression (PLR), **k)** – Random Forest (RF) and **l)** – Support Vector Regression (SVR). ..... 205

Figure 8.7: Actual versus predicted salt concentrations of monitoring location 2 (ML2) using different machine learning algorithms during training period; **a)** – Adaptive Neuro Fuzzy Inference System (ANFIS), **b)** – Artificial Neural Network (ANN), **c)** – Multivariate Adaptive Regression Spline with Piecewise Cubic Spline (MARS_C), **d)** – Multivariate Adaptive Regression Spline with Piecewise Linear Spline (MARS_L), **e)** – Bayesian Optimization tuned Automatic Model Selection (AMS_Bayesian), **f)** – Asynchronous Successive Halving Algorithm tuned Automatic Model Selection (AMS_ASHA), **g)** – Bi-directional Long Short term Memory Network (Bi-LSTM), **h)** – Group Method of Data Handling (GMDH), **i)** – Gaussian Process Regression (GPR), **j)** – Probabilistic Linear Regression (PLR), **k)** – Random Forest (RF) and **l)** – Support Vector Regression (SVR). ..... 206

Figure 8.8: Actual versus predicted salt concentrations of monitoring location 3 (ML3) using different machine learning algorithms during training period; **a)** – Adaptive Neuro Fuzzy Inference System (ANFIS), **b)** – Artificial Neural Network (ANN), **c)** – Multivariate Adaptive Regression Spline with Piecewise Cubic Spline (MARS_C), **d)** – Multivariate Adaptive Regression Spline with Piecewise Linear

Spline (MARS_L), **e)** – Bayesian Optimization tuned Automatic Model Selection (AMS_Bayesian), **f)** – Asynchronous Successive Halving Algorithm tuned Automatic Model Selection (AMS_ASHA), **g)** – Bi-directional Long Short term Memory Network (Bi-LSTM), **h)** – Group Method of Data Handling (GMDH), **i)** – Gaussian Process Regression (GPR), **j)** – Probabilistic Linear Regression (PLR), **k)** – Random Forest (RF) and **l)** – Support Vector Regression (SVR). .....207

Figure 8.9: Actual versus predicted salt concentrations of monitoring location 4 (ML4) using different machine learning algorithms during training period; **a)** – Adaptive Neuro Fuzzy Inference System (ANFIS), **b)** – Artificial Neural Network (ANN), **c)** – Multivariate Adaptive Regression Spline with Piecewise Cubic Spline (MARS_C), **d)** – Multivariate Adaptive Regression Spline with Piecewise Linear Spline (MARS_L), **e)** – Bayesian Optimization tuned Automatic Model Selection (AMS_Bayesian), **f)** – Asynchronous Successive Halving Algorithm tuned Automatic Model Selection (AMS_ASHA), **g)** – Bi-directional Long Short term Memory Network (Bi-LSTM), **h)** – Group Method of Data Handling (GMDH), **i)** – Gaussian Process Regression (GPR), **j)** – Probabilistic Linear Regression (PLR), **k)** – Random Forest (RF) and **l)** – Support Vector Regression (SVR). .....208

Figure 8.10: Spider plots of three major performance measures of twelve surrogate models for different monitoring locations: **a)** Index of Agreement values for twelve surrogate models during the testing period; **b)** Kling-Gupta Efficiency Coefficient values for twelve surrogate models during the testing period; **c)** Nash Sutcliffe Efficiency Coefficient values for twelve surrogate models during the testing period; **d)** Index of Agreement values for twelve surrogate models during the training period; **e)** Kling-Gupta Efficiency Coefficient values for twelve surrogate models during the training period; **f)** Nash Sutcliffe Efficiency Coefficient values for twelve surrogate models during the training period. .....210

Figure 8.11: Boxplots of absolute errors between actual and predicted salt concentration during the training stage at **a)** ML1, **b)** ML2, **c)** ML3, and **d)** ML4 using all twelve surrogate models. Pink dots indicate outliers. .....212

Figure 8.12: Observed versus predicted salt concentrations using surrogate ensemble models at **a)** ML1, **b)** ML2, **c)** ML3 and **d)** ML4. .....214

Figure 8.13: Pareto optimal fronts of the linked simulation-optimisation management model based on different scenarios for digital twin. **a)** Scenario 1 with a maximum allowable salt concentration of 0.45 kg/m3, **b)** Scenario 2 with a maximum allowable salt concentration of 0.55 kg/m3, **c)** Scenario 3 with a maximum allowable salt concentration of 0.75 kg/m3, **d)** Scenario 4 with a maximum allowable salt concentration of 0.90 kg/m3, **e)** Scenario 5 with a maximum allowable salt concentration of 1.15 kg/m3. .....216

# Chapter 1: Introduction

## 1.1 Overview

This chapter describes the background of the problem statement – saltwater intrusion in coastal aquifers. Section 1.2 of this chapter outlines the theoretical background, causes and solutions of managing saltwater intrusion in Pacific Island countries. Section 1.3 of this chapter talks about the significance of this research. Section 1.4 outlines the aims and objectives of this thesis. Lastly, Section 1.5 describes the thesis organisation and structure.

## 1.2 Outline

Water of suitable quality for drinking is essential for life on Earth. Often referred to as "Blue Gold" due to its immense value (Vidal, 2002; Collins, 2015), drinking water is sourced from various locations, with groundwater being one of the oldest and most utilised. Groundwater is freshwater stored beneath the Earth's surface in the spaces between rocks or in saturated zones (Margat and Gun, 2013). It occurs in two subsurface zones: the zone of aeration, which holds less water bound to soil and rock by capillary forces, and the zone of saturation, where water completely fills the pores and spaces in the rocks, separated by the water table (Baldwin and McGuinness, 1963). Of the approximately 3% of the Earth's water classified as freshwater, 95% is stored as groundwater, with surface water accounting for 3.5% and soil moisture making up 1.5%. However, only 0.36% of freshwater is easily accessible for use (Leopold, 1947). Groundwater supports over 2 billion people globally (~32%) and accounts for about one-third of freshwater consumption worldwide (Morris et al., 2003; Famiglietti, 2014; Gorelick and Zheng, 2015). In coastal regions, which host more than 70% of the global population, groundwater plays a critical role in meeting water demands (Bear et al., 1999). While 50% of groundwater is used for drinking, 40% serves industrial purposes, and 20% is used for irrigation (Foster and Chilton, 2003; Hao et al., 2018).

Groundwater systems are highly dynamic and complex, shaped by various physical and environmental factors. Groundwater recharge occurs naturally through precipitation and infiltration, while discharge takes place via springs, streams, and wells. The interconnectedness of groundwater and surface water is crucial for sustaining aquatic ecosystems and fulfilling water demands across multiple sectors (Alley et al., 1999).

However, over-extraction of groundwater can result in resource depletion, land subsidence, and saltwater intrusion in coastal areas. The quality of groundwater is a critical component of its management. It is vulnerable to contamination from both natural and human-induced sources, such as agricultural runoff, industrial discharges, and septic systems. Polluted groundwater poses serious risks to public health and the environment and is often expensive and challenging to remediate (Li et al., 2021). Consequently, the regular monitoring and management of groundwater quality are essential to ensure the sustainability of these resources.

Climate change further complicates groundwater management. Variations in precipitation patterns and rising temperatures can influence groundwater recharge rates and distribution. Additionally, extreme weather events such as droughts and floods can have profound impacts on groundwater systems (UNESCO, 2021). Implementing effective management strategies such as water conservation, land use regulation, and pollution control is vital to mitigating the effects of climate change and ensuring the long-term availability and quality of groundwater.

Over-abstraction, industrialisation, growing population and extensive agricultural usage impose significant constraints on groundwater availability and use. One of the major impacts of unplanned constant use of groundwater is saltwater intrusion (SWI) in coastal aquifers. SWI occurs when saltwater infiltrates freshwater aquifers due to excessive groundwater pumping, sea-level rise, or other anthropogenic activities. This phenomenon, driven by differences in the density of saltwater and freshwater as well as hydraulic gradients within aquifers, can severely degrade groundwater resources, ecosystems, and the communities that depend on them (Werner et al., 2013). Proactive measures are necessary to address these challenges and safeguard groundwater resources in such vulnerable regions.

SWI is a growing problem around the globe, including smaller island nations. In Pacific Island Countries (PICs), groundwater sources are mainly affected by SWI in coastal aquifers due to their geographic locations and excessive use of groundwater. In PICs, groundwater is also the main source of fresh water for domestic use and irrigation. To ensure the future sustainability of valuable groundwater resources in coastal areas, the development and implementation of groundwater monitoring, management, and prevention techniques are essential.

The current study will provide various SWI management strategies and techniques using mathematical, empirical, numerical and machine learning-based models. The knowledge gained from this study is novel and important for small island nations in the Pacific region, as it will provide optimal SWI management strategies by considering uncertainties, including climate change and sea level rise. The strategies provided will help protect groundwater resources for future use and help reduce saline water contaminations. In addition, this study will also provide new knowledge, and policymakers and water engineers will use the results from this study in modelling, planning, and decision-making to conserve and utilise the water resources of coastal aquifers.

## 1.3 Research Significance

Various natural, climate and anthropogenic impacts threaten the freshwater aquifers around the globe and in PICs. The land area of PICs is small and fully surrounded by ocean water, which leads to SWI more often by natural means. Also, the groundwater in PICs is also contaminated by anthropogenic means. Freshwater reserves in coastal aquifers are continuously degrading, necessitating sustainable management strategies and policies. It is surprising to note that while threats to groundwater reserves are acknowledged, research, conception and implementation of water management frameworks have been very poor.

The problem of coastal aquifer management remains a practical concern in many parts of the world. This proposed research fills this gap by providing improved techniques for regulating groundwater withdrawals without compromising groundwater reserves in coastal aquifers. In addition, the application of management strategies in a real-life case study aquifer is a key feature of this study. This application will also help in developing efficient and improved regional-scale coastal aquifer management strategies for similar coastal aquifers subjected to SWI.

Moreover, the present study will be useful to groundwater users, consultants, engineers, firms, stakeholders, and policymakers in developing robust and optimum monitoring, management, and prevention techniques to minimise the impact of SWI on coastal aquifers. The simulated-synthetic (S-S) data will be used with reference to PICs for the sustainable management of groundwater resources. SEAWAT-based modelling, new surrogate ensemble models, coupled simulation-optimisation models would be used

to provide optimum solutions for SWI management in coastal aquifers. The development of various methodology components will be tested utilising simulated synthetic and field data. A digital twin model will be developed for the real site aquifer or a specific part of the aquifer better to evaluate the SWI and groundwater management system performance. Digital twin technology is fairly new in water sectors and it has not been used in groundwater or coastal aquifer systems. The developed SWI management methodologies will be validated with real-life aquifer data from a selected PIC, e.g., Vanuatu, to test the performance of the developed methodology for the actual management of coastal SWI.

Furthermore, this proposed research focuses on coastal aquifer management efforts, building research capabilities and providing results of substantial benefit in an area critical to a nation's sustainability. This research fills a major gap in current coastal aquifer management capabilities and application, especially to tropical PIC, by delivering improved, reliable, robust and practical management solutions. Lastly, the developed coastal aquifer management methodology will help solve current SWI problems and possibly avoid or explore future unforeseen problems. The outcome of this work will impart new knowledge and permit better long-term regional-scale management, planning, and governance of precious yet fragile groundwater resources in coastal aquifers.

Climate change and other natural disasters impacting the groundwater quality will also be incorporated. This study, when completed, will provide new tools and techniques, especially for application in PICs with the primary freshwater sources coming from groundwater resources. The results from this proposed study will be useful in addressing the salinity intrusion process and the consequences related to climate change.

## 1.4 Aims and Objectives

The aim of this research is to develop more efficient, reliable and robust mathematical, machine learning, simulation-optimisation and digital twin models for managing saltwater intrusion of Pacific Island coastal aquifers for the long-term sustainability of groundwater resources. This study also aims to analyse the anthropogenic factors and natural disasters affecting groundwater resources in Pacific Island countries (PICs).

The specific objectives of this study are as follows:

Objective 1: Explore the plausible impact of climate change in terms of sea level rise and $CO_2$ emission levels on groundwater withdrawal and groundwater quality for a natural aquifer system in a Pacific Island country.

Objective 2: Develop and evaluate simulated-synthetic aquifer data-based models integrating numerical modelling and scenario-based sensitivity analysis for saltwater intrusion management using a complex heterogeneous island aquifer.

Objective 3: Develop and evaluate a numerical simulation model using randomised hydraulic conductivities and stochastic application of simulated-synthetic data for groundwater salinity management and decision-making.

Objective 4: Develop and evaluate a SEAWAT-based 3-dimensional numerical model to simulate and predict groundwater salinity concentrations in a real case study aquifer system in a Pacific Island country.

Objective 5: Develop and evaluate a multi-objective simulation-optimisation-based model for sustainable management of Pacific Island coastal aquifer systems, incorporating surrogate ensemble models as approximate predictors of salinity concentrations.

Objective 6: Develop and implement a digital twin model of a Pacific Island country aquifer system using real-time data to further evaluate management strategies under various management and input uncertainties scenarios.

## 1.5 Thesis organisation and structure

This thesis consists of nine chapters. The main contents of chapters 2, 3, 4, 5, and 6 have been published in peer-reviewed journals, while chapters 7 and 8 are under review. References to published and under-reviewed articles are given at the beginning of each chapter. A summary of the major contents of each chapter is given below.

Chapter 1 provides the broad framework of the coastal aquifer management problem, the thesis aims and objectives, and the thesis structure.

Chapter 2 provides a detailed background, literature review and knowledge gap on managing saltwater intrusion in coastal aquifers for Pacific Island countries.

Chapter 3 evaluated the impacts of climate change and water over-abstraction on groundwater resources in the Pacific island country of Tonga.

Chapter 4 uses a complex heterogeneous island aquifer system to integrate numerical modelling and scenario-based sensitivity analysis for saltwater intrusion management.

Chapter 5 uses randomised hydraulic conductivities and stochastic application for groundwater salinity management and decision-making in numerical simulation models.

Chapter 6 provides saltwater intrusion management strategies using numerical modelling techniques in the Pacific Island country of Vanuatu.

Chapter 7 deals with the surrogate ensembles and multi-objective simulation-optimisation model for managing saltwater intrusion in a coastal aquifer for a Pacific Island country.

Chapter 8 describes the conceptual development and implementation of a digital twin model for managing saltwater intrusion of an island coastal aquifer.

Chapter 9 discusses the summary, conclusions and recommendations for future work.

# Chapter 2: Literature review

The main contents of this chapter have been published and copyrighted as outlined below:

**Sharan, A**., Lal, A., & Datta, B. (2021). A review of groundwater sustainability crisis in the Pacific Island countries: Challenges and solutions. *Journal of Hydrology*, 603, 1-15. https://doi.org/10.1016/j.jhydrol.2021.127165

## 2.1 Overview

This chapter comprehensively reviews the groundwater sustainability crisis in different Pacific Island countries. It also identifies different water sources in Pacific Island countries, the significant challenges groundwater faces, and solutions or strategies for monitoring, managing, and preventing the identified challenges.

## 2.2 Executive Summary

Population growth and rapid industrialisation have imposed excessive demand for groundwater in Pacific Island countries (PICs). To meet this demand, over-pumping of groundwater is practised in majority of the PICs, which eventually causes saltwater intrusion (SWI) in coastal aquifers. The geographical location of PICs makes them more vulnerable to natural means of SWI. However, anthropogenic activities also cause groundwater contamination in PICs. The main objectives of this review are to identify the water sources in PICs, the major challenges groundwater faces, and solutions or strategies for monitoring, management, and prevention of the identified challenges. This study has revealed that SWI is highly common in PICs and that there is a knowledge gap with limited research on groundwater. This review also highlights that the use of the latest technologies, 3D modelling, simulation-optimisation techniques, artificial intelligence, relevant policies and regulations on groundwater and mass awareness will help in monitoring, managing and preventing SWI and other ways of contamination in coastal aquifers for PICs.

## 2.3 Introduction

Water of acceptable quality and fit for drinking purposes is essential for survival on Earth. Water is so precious that it is also termed as Blue Gold! (Vidal, 2002; Collins, 2015). Drinking water can be available from various sources, with groundwater being the oldest and widely used water source. Groundwater is merely freshwater present

underneath the Earth's surface between rock spaces or in saturated zones (Margat and Gun, 2013). Groundwater is found in two zones beneath the Earth surface, namely, zone of aeration and zone of saturation, separated by the water table. The zone of aeration has less water held to the soil and rocks by capillarity force, whereas the zone of saturation is filled with water in all the rock spaces and its pores (Baldwin and McGuinness, 1963). Approximately 3% of the world's water is freshwater, of which 95% is groundwater, 3.5% is surface water and 1.5% is soil moisture. However, only 0.36% of freshwater is readily available for usage (Leopold, 1947). More than 2 billion people (~32%) are dependent on groundwater (Morris et al., 2003), or approximately one-third of freshwater is consumed globally (Famiglietti, 2014; Gorelick and Zheng, 2015). More than 70% of the world's population living in coastal areas is directly and indirectly linked with groundwater (Bear et al., 1999). Groundwater is not only used for drinking but for other purposes as well. Only 50% of groundwater is used as drinking water, 40% and 20% are used for industrial and irrigation, respectively (Foster and Chilton, 2003; Hao et al., 2018).

The use of groundwater has increased due to population growth, agriculture, environmental demands, tourism, increased living standards and industrialisation (Hanjra and Qureshi, 2010; Howard, 2015; Neumann et al., 2015; Hamed et al., 2018). Groundwater is highly demanding in this era, including Pacific Island countries (PICs). The PICs are surrounded by the largest and deepest ocean in the world – the Pacific Ocean (NOAA, 2021), yet people do not have access to safe drinking water. Pacific Island consists of 22 countries with ~550,000 $km^2$ of land area (Weber, 2007), of which some selected country profiles are given in Table 2.1 and the map of PICs is shown in Figure 2.1.

The rise in sea level, climate change and water usage has mandated us to do a thorough review, largely focusing on the groundwater crisis, challenges and solutions in PICs. This review will provide an in-depth analysis of twelve major PICs water resources, water challenges, saltwater intrusion (SWI) and salinity levels in some selected boreholes. This review is different from other research work as it will discuss the knowledge gap and the amount of research conducted on sustaining groundwater resources, which will help other researchers focus on areas where significant work is needed in PICs. Moreover, this study will provide robust solutions for monitoring, managing and preventing SWI and other groundwater contaminants.

## 2.4 PICs water resources and associated challenges – detailed background

The PICs are spread out geographically, with Papua New Guinea (PNG) being the largest and Nauru being the smallest. All the PICs listed in Table 2.1 share groundwater as a common natural resource.

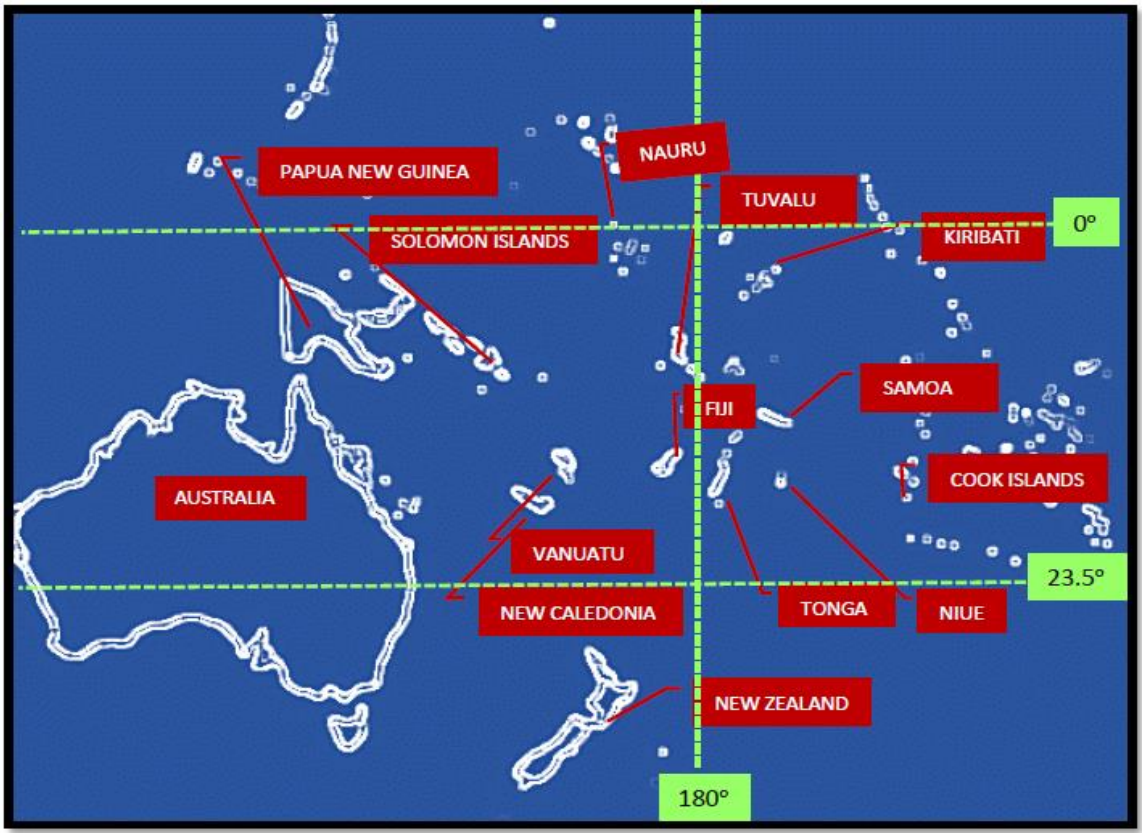



Figure 2.1: The Pacific Islands.

The major water sources in these twelve PICs are shown in Figure 2.2. These twelve PICs use groundwater from aquifer systems, wells and boreholes. Apart from groundwater, around 67% of them use rainwater, 33% use surface water and 12% of countries use desalination plants to purify water for daily needs, as deduced from Figure 2.2. The twelve PICs' background, water resources and challenges will be discussed as follows: **(1) Cook Islands (21.24° S, 159.78° W)** comprises 15 widely spread islands clustered in Southern and Northern groups with tropical climates (Carruthers, 2009). The country's major income is tourism. However, it also gained from agriculture, offshore banking, and black pearls (CIA, 2021). There is great potential for groundwater in this country. However, it needs further studies and better monitoring and management plans. The major concerns for Cook Islands groundwater are saltwater intrusion (SWI) in coastal aquifers, high demand or reticulated usage of water for

agriculture, contamination of groundwater due to the leakage of lavatory septic tanks, waste from animal farms located near rivers and streams, lack of vivid water usage and supply policies (Antoniou et al., 2018).

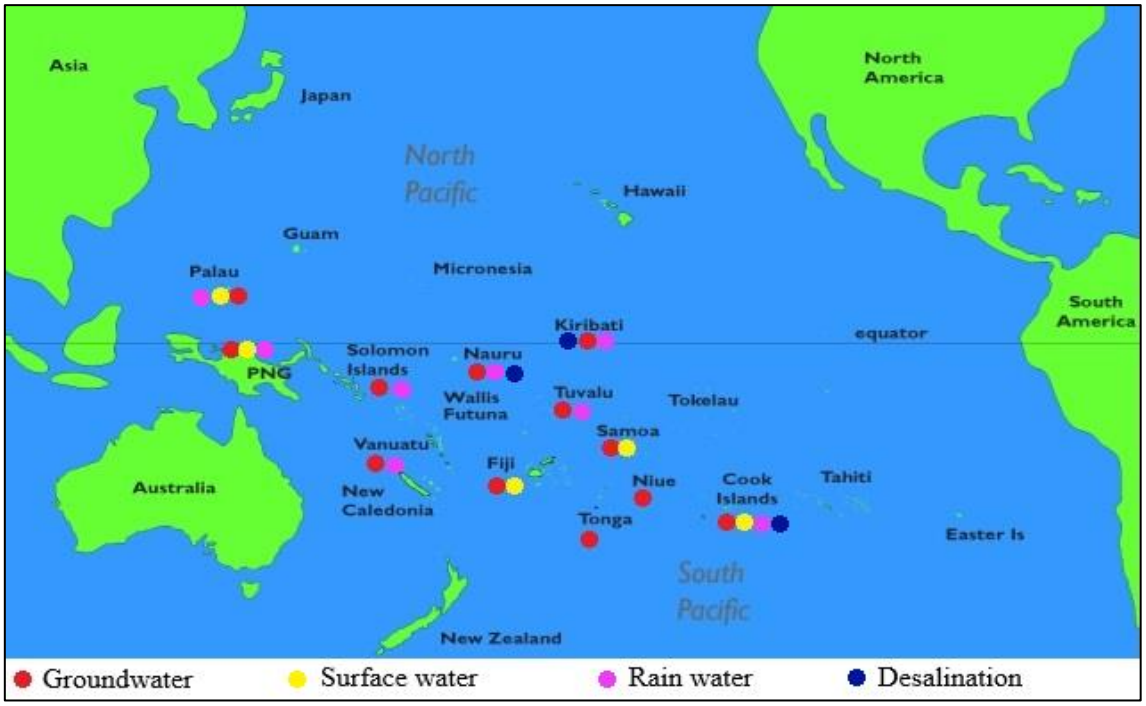



Figure 2.2: Major water sources in Pacific Island countries.

**(2) Fiji (17.71° S, 178.06° E)** is a much more developed country when compared with other PICs with tropical climates. The primary income for Fiji is from tourism, agriculture, sugar exports, and minerals (Gounder, 2020). Rural and low-lying island communities extensively use groundwater for daily needs in all aspects. Groundwater usage started in the 1970s by digging boreholes, and currently, more than 800 boreholes are registered in Fiji's Mineral Resource Department (IGRAC, 2016). Fiji produces more than 120000 mega litres of water annually from 55 water treatment plants (WAF, 2019). The monthly freshwater production in Fiji for the year 2016 is shown in Figure 2.3.

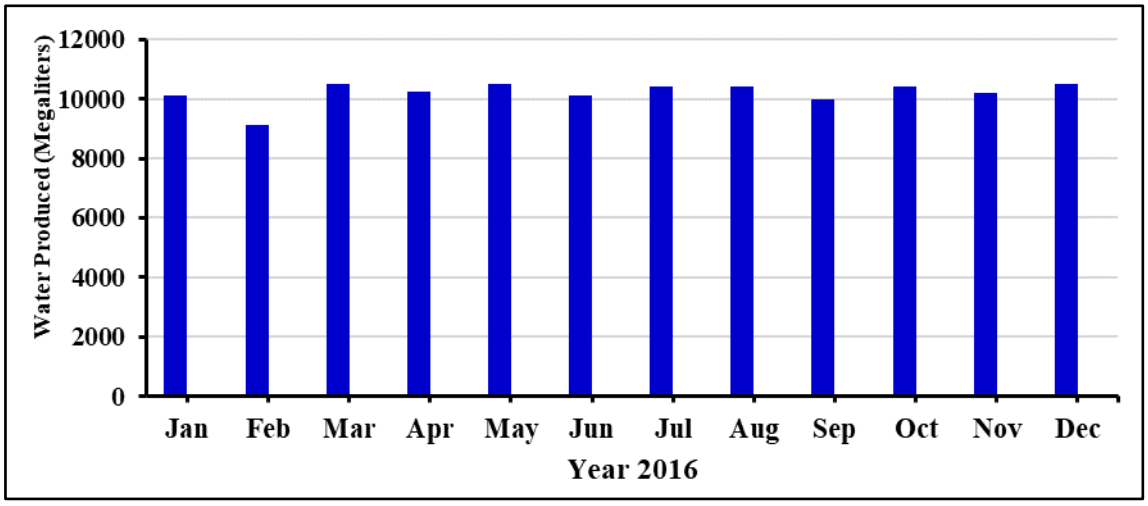



Figure 2.3: Fiji's total freshwater water production in year 2016. Source (WAF, 2019).

Fiji lacks thorough monitoring of groundwater reserves, issuing rights in groundwater exploration to public and private sectors and SWI monitoring (Mimura, 1999).

Table 2.1: Pacific Island countries and territories summary. Source ([1]World Population Review, 2021; [2]Falkland, 2002).

| **Country[1]** | **Sub-Region[1]** | **Approximate Population (in 2020)[1]** | **Land Area (per km sq.)[1]** | **Island Geology[2]** |
|---|---|---|---|---|
| Cook Islands | Polynesia | 17564 | 236 | Atoll, volcanic, volcanic & limestone |
| Fiji | Melanesia | 896445 | 18272 | Volcanic, limestone, atoll |
| Kiribati | Micronesia | 119449 | 811 | Majority atoll, 1 limestone |
| Nauru | Micronesia | 10824 | 21 | Limestone |
| Niue | Polynesia | 1626 | 260 | Limestone |
| Palau | Micronesia | 18094 | 459 | Limestone, volcanic |
| Papua New Guinea (PNG) | Melanesia | 8947024 | 462840 | Atolls, coral Is., volcanic, limestone |
| Samoa | Polynesia | 198414 | 2842 | Volcanic |
| Solomon Islands | Melanesia | 686884 | 28896 | Atolls, volcanic, limestone |
| Tonga | Polynesia | 105695 | 747 | Volcanic, limestone, limestone & sand, mixed |
| Tuvalu | Polynesia | 11792 | 26 | Atoll |
| Vanuatu | Melanesia | 307145 | 12189 | Majority volcanic, sand & limestone |

Limited and outdated policies and legislations on SWI management, over-pumping, pollution and contamination control exist. Moreover, detailed information and data on groundwater parameters, technical skills and public awareness are lacking in Fiji (Carpenter et al., 2007). **(3) Kiribati (3.37° S, 168.73° W)** has 33 atolls and has a hot and humid tropical climate. The economic income for this country is mainly from foreign aid, seafood export, copra farming and limited tourism (Webb, 2020; CIA, 2021). Groundwater is the major water source for the people on the island (Lal and Datta, 2019b). They have reliable and extensive data on more than 80 groundwater boreholes starting from the 1980s. Water salinity plants are also operational in the outer islands of Kiribati. However, more investment should be made by the government in sanitation and improving the quality of water (Webb, 2020). Onotoa Island in Kiribati has 184 wells, which supply groundwater. The details of these wells and the water salinity levels are shown in Figure 2.4. The issues and challenges that come with excessive usage of groundwater in Kiribati include SWI, animal waste contamination (Loco et al., 2015), lack of constant and extensive monitoring with world-class technologies, lack of exploring and using other water sources for drought periods, land ownership issues, lack of proper policies on use and monitoring the groundwater (Carpenter et al., 2007). Sea level rise is also a major concern for Kiribati, which causes SWI (Aung et al., 2009).

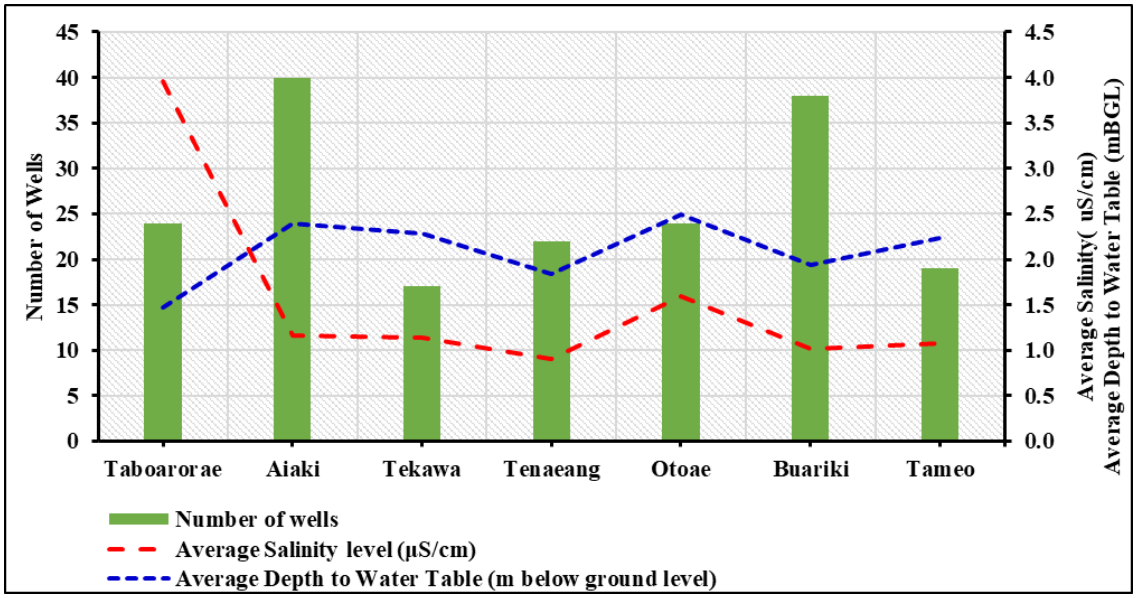



Figure 2.4: Summary of all groundwater wells surveyed for seven villages in Onotoa, Kiribati. Source (Loco et al., 2020).

**(4) Nauru (0.52° S, 166.93° E)** is a single limestone island with a very hot and humid climate due to its geographical location. The island is mainly dependent on foreign

aid, fishing, tourism and agroforestry (Clifford et al., 2018). Harvesting of rainwater and shallow groundwater is widely available on the island. The average water usage for 2-4 persons in Nauru is shown in Figure 2.5. The subsurface water issues are SWI (Alberti et al., 2017), contamination from sewage systems and long droughts. Nauru also lacks policies on the usage and monitoring of groundwater and awareness to the public. Moreover, the land and groundwater sources are mainly owned by the public. Hence, government involvement is limited. Mining also disturbed and destroyed ~64% of the whole of Nauru and its natural environment, including groundwater (Carpenter et al., 2007).

**(5) Niue (19.05° S, 169.87° W)** is also a single island with a tropical climate. Agriculture is the major source of income for Niueans, along with the export of honey, coconut cream, sale of postal stamps and vanilla (Butler, 2004; CIA, 2021). This country is only dependent on groundwater, which is being overexploited due to an increase in demand (Carpenter et al., 2007). Some selected boreholes and their submersible pumping (SP) capacity per day are shown in Figure 2.6. There are many challenges in Niue related to water resource, which includes a lack of proper planning, development and management of groundwater, lack of skills, competencies and technology to minimise water contamination and wastewater management (IGRAC, 2016).

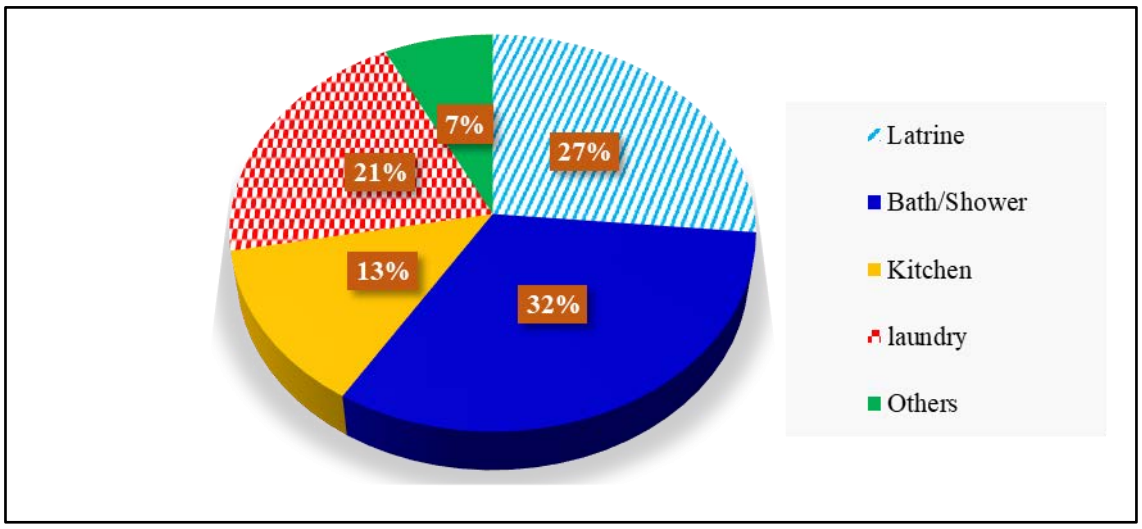



Figure 2.5: Nauru's internal water usage per day (2-4 persons) in 2015. Source (NRW, 2015).

**(6) Palau (7.52° N, 134.58° E)** Palau has around 350 islands with a tropical climate, where tourism and foreign aid are major economic contributors (IMF, 2019). Agriculture and fishing exports also contribute to the island's economic growth (Miles, 2020). The majority of the population has access to treated water or surface water. However, Palauans

also use groundwater. The detailed information on the water usage for nine states in Palau is shown in Figure 2.7.

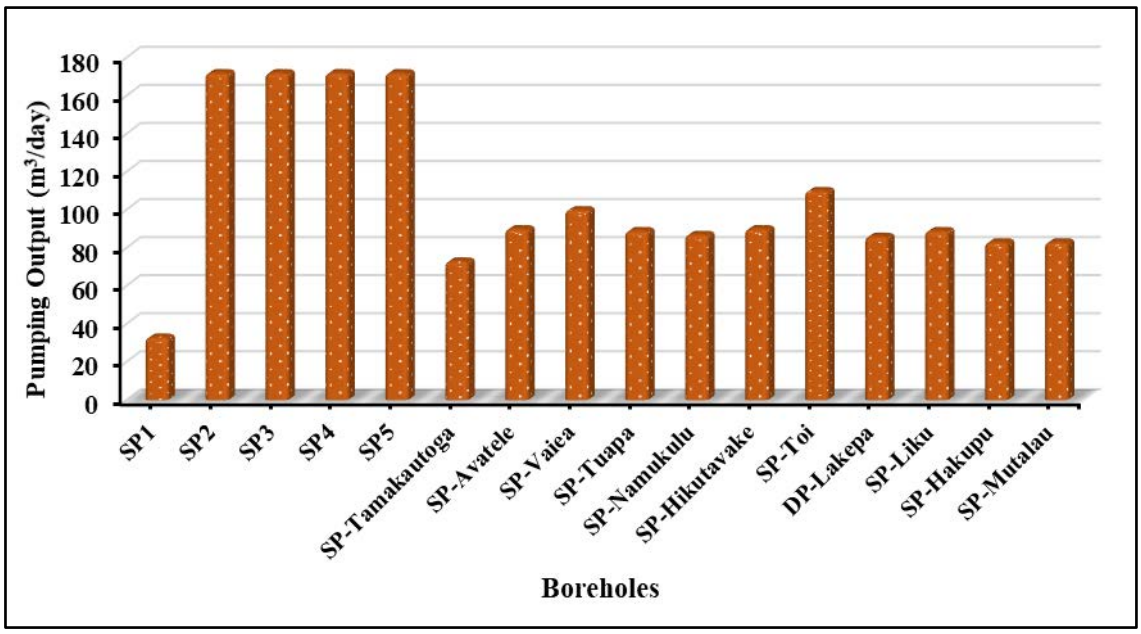



Figure 2.6: Water pumping output of selected boreholes in Niue (2008). Source (Siohane and Chapman, 2009).

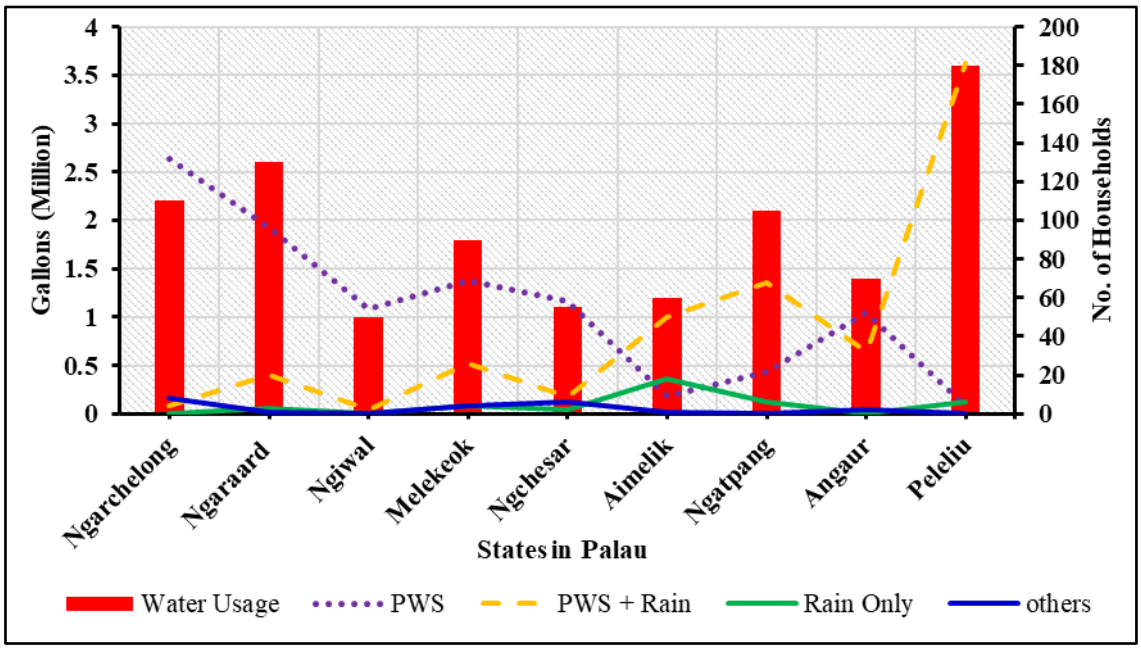



Figure 2.7: Water usage of some selected states in Palau. Source (SOPAC, 2007a).

Unlike other PICs, Palau also has challenges associated with water resources, including sea level rise and SWI (Mcleod et al., 2019; Miles, 2020), massive deforestation, sediment erosion, pesticide, lack of wastewater management, technologies for water resource assessment and monitoring (Carpenter et al., 2007; IGRAC, 2016). **(7) Papua New Guinea (PNG) (6.32° S, 143.96° E)** is divided into two regions, half of

which falls in Oceania and half towards Indonesia or north of Australia, with an overall tropical climate (IGRAC, 2016). The primary income for PNG is from agriculture, mining, forestry, crude oil production and refinery (Howes et al., 2019; Schmidt et al., 2020). PNGs renewable water resources are declining at a considerable rate. The details are shown in Figure 2.8. The number of people who do not have access to safe drinking water has grown since 1992. Groundwater is safer and more reliable in PNG. However, the country also uses surface water and effluent water for daily needs. Groundwater is at risk due to population growth, industrialisation, fewer strategies to minimise contamination measures and SWI (Wolanski et al., 1997). PNG also lacks proper policies and control on the usage of agricultural chemicals and fertilisers, which additionally increases the groundwater threat (Carpenter et al., 2007).

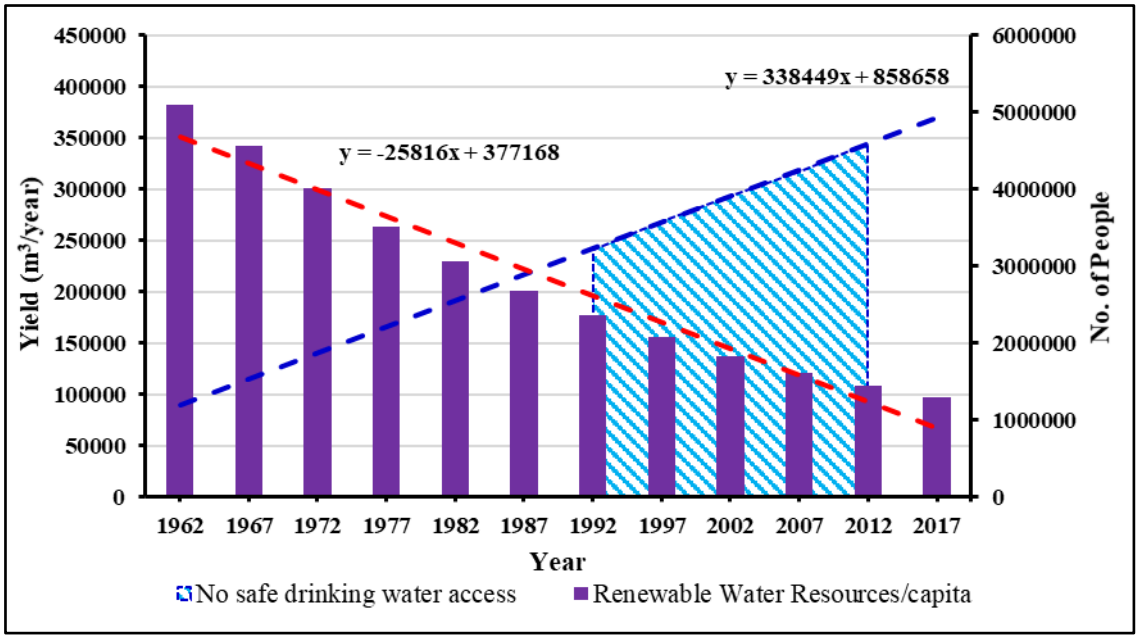



Figure 2.8: Renewable water resources per capita and number of people with access to safe drinking water in PNG. Source (Worldometer, 2021).

**(8) Samoa (13.76° S, 172.10° W)** has nine volcanic islands with hot and humid weather year-round. Agriculture, fish exports, tourism and copra are major economic boosters for the country (Sialaoa, 2003; Amosa, 2012). Surface and groundwater are both used for daily needs, with approximately ten boreholes under operation (Berthe et al., 2014). The water temperature and salinity levels in a selected borehole are shown in Figure 2.9. Population growth, industrialisation and drought induce challenges to water sources, especially groundwater (Berthe et al., 2014). SWI, lack of wastewater management, soil and sediment erosion, and other anthropogenic factors affect groundwater in the country (IGRAC, 2016). **(9) Solomon Islands (9.65° S, 160.16° E)**

consists of 347 islands with very humid climate throughout the year. Logging or log exports are major income generators for the country, with a high amount of minerals untouched, which can further increase the country's income (Gay, 2016). Rainwater and groundwater are two major sources of water supply on the island.

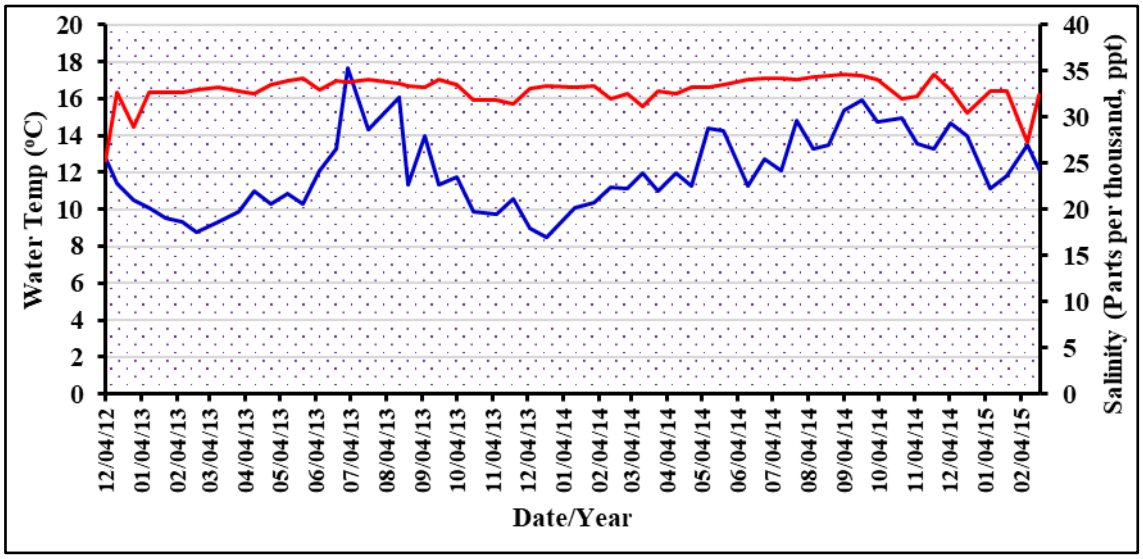



Figure 2.9: Water temperature and salinity measurements of a borehole in Samoa. Source (Wiyot, 2015).

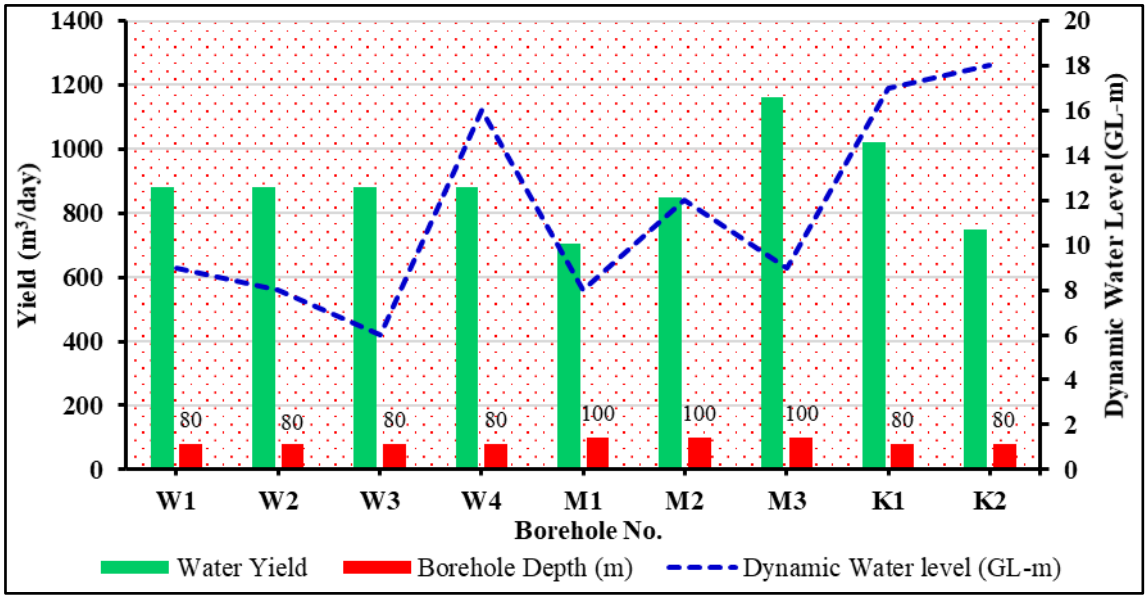



Figure 2.10: Characteristics of some selected boreholes in Solomon Islands. Source (SOPAC, 2007b). Boreholes W1 to W4 are located in White River (9.26° S 159.55° E), M1 to M3 are located in Mataniko (9.43° S 159.97° E) and K1 and K2 are located in Kombito (9.433°S 159.98°E).

The characteristics of some selected boreholes are shown in Figure 2.10. Increases in population, sea level rise, climate change, excessive logging and SWI are some of the major causes of groundwater contamination (Quigley et al., 2016; World-Bank, 2018).

Moreover, wastewater management, human resources, groundwater competencies, robust information and data, chloride and total dissolved solids, public awareness and lack of policies are also added challenges to the current water sources (Carpenter et al., 2007; IGRAC, 2016).

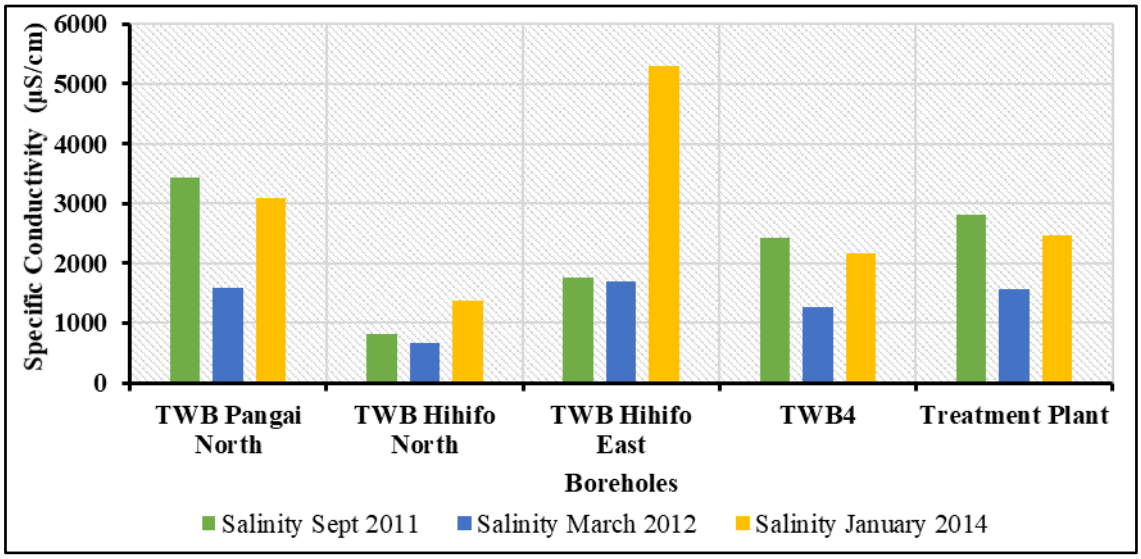



Figure 2.11: The specific conductivity of four selected boreholes and one treatment plant in Tonga. Source (Singh, 2014). These production bores are located in Lifuka Island (19.81° S 174.34° W). The geographic locations of each bores are; Tonga Water Board (TWB) PANGAI North (19.81° S 174.35° W), TWB Hihifo North (19.813° S 174.353° W), TWB Hihifo East (19.818° S 174.356° W), TWB4 (19.817° S 174.354° W), Treatment plant is also located in Lifuka.

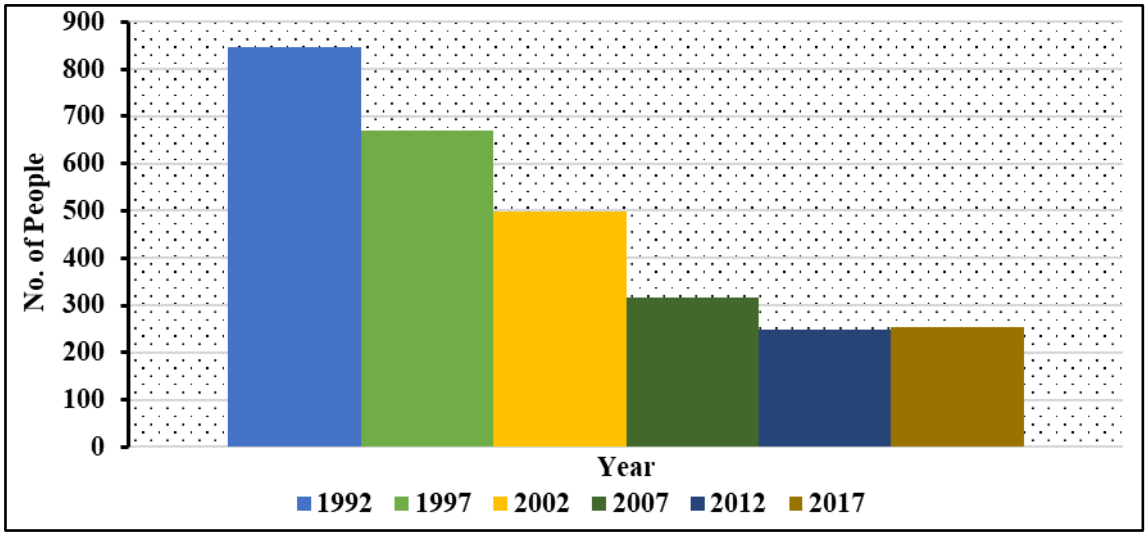



Figure 2.12: Number of people with no access to safe drinking water in Tuvalu. Source (Worldometer, 2021).

**(10) Tonga (21.18° S, 175.19° W)** has 171 small islands and semi-tropical weather, with agriculture and tourism being the primary foreign exchange earners for the country (Harkness, 2001; CIA, 2021). This country is primarily dependent on groundwater and

has around 124 water supply wells and 16 boreholes. The salinity levels on some selected boreholes are shown in Figure 2.11. Some challenges on groundwater sources are SWI due to over-pumping, improper disposal of pesticides, insecticides, factory and human waste, droughts, soil and sediment erosion, sea level rise and climate change (Harkness, 2001; IGRAC, 2016; Babu et al., 2018). Comprehensive laws on land ownership, management and protection of water resources, and better sanitation policies or practices do not exist in Tonga (Carpenter et al., 2007). **(11) Tuvalu (7.12° S, 177.65° E)** has nine atoll islands with tropical climates comprising of monsoon and dry seasons. Granting fishing licences in Tuvaluan water generates significant income for the country (Mellor, 2003; Milan et al., 2016). The number of people who do not have access to safe drinking water declined over the years, as shown in Figure 2.12. The groundwater is not used for drinking but for other purposes like agriculture, lavatories and washing because it is highly contaminated due to improper disposal of factory, human and animal waste, chemicals, oil, fuel, coastal erosion and SWI (Fujita et al., 2013; Milan et al., 2016). Tuvalu is in the dark when it comes to groundwater monitoring, usage and management due to a knowledge gap, a lack of policies and awareness.

Lastly, **(12) Vanuatu (15.38° S, 166.96° E)** has 80 islands with tropical climate. The country's primary income sources are agriculture, fishing and tourism (Verdone and Seidl, 2012; Duncan, 2016). The country uses groundwater and rainwater as primary water sources and has four groundwater monitoring stations (Foster and Willetts, 2018). The water source for seven provinces is shown in Figure 2.13.

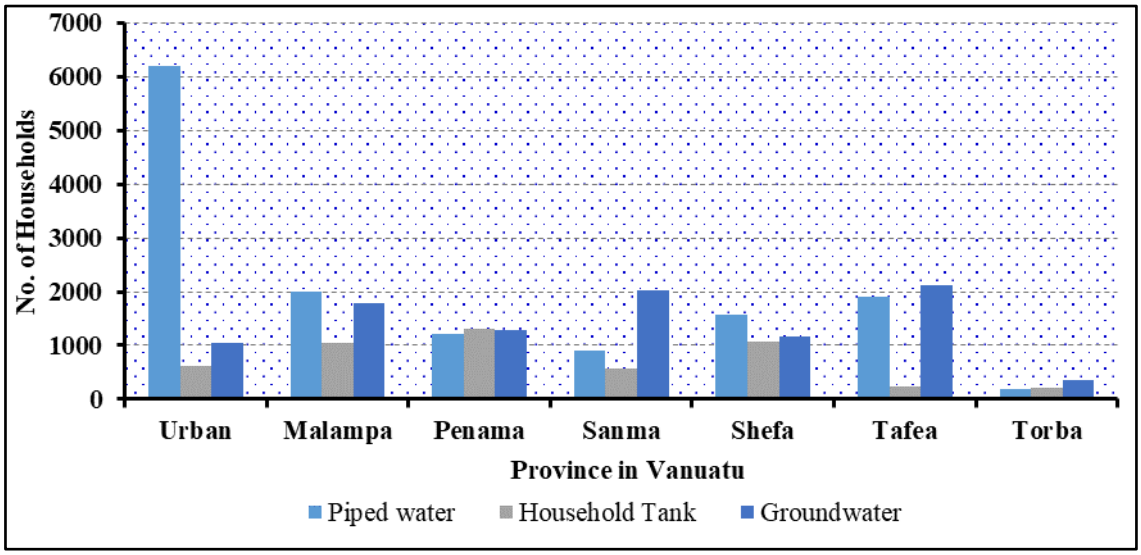



Figure 2.13: Water source for seven provinces in Vanuatu. Source (SOPAC, 2007c).

Some of the challenges for the groundwater in this country are SWI, sea level rise, poor solid and liquid waste disposal, and lack of proper policies and procedures for water resource assessment, usage, monitoring and management (Foster et al., 2019; Devlin et al., 2020). Moreover, the lack of proper data, technology and competencies are some of the additional challenges Vanuatu faces regarding groundwater (Carpenter et al., 2007; IGRAC, 2016). These twelve PICs use groundwater, are vulnerable to frequent water contaminations and are linked with a common environmental challenge.

## 2.5 Background Information on Saltwater Intrusion – A Common Challenge for PICs

A thorough PICs profile and literature have identified saltwater intrusion (SWI) as a major concern for PICs due to population growth, increase in abstraction on water demand, industrialisation and sea level rise. All these issues also have a huge impact on coastal aquifers (e.g. Reilly and Goodman, 1987; Alley et al., 1999; Sherif and Singh, 2002; Zektser et al., 2005; Michael et al., 2017). Coastal aquifers are predominantly a link between hydrogeology systems and the ocean, which are hydraulically connected with the sea. Freshwater aquifers provide drinking water in urban and rural sectors, as well as agricultural, irrigation, and industrial use. The interaction between groundwater and seawater is a process of surface and subsurface water, which is also referred to as the intrusion of saltwater or seawater into coastal aquifers. Intrusion generally occurs when the density of the groundwater is less than that of seawater when they hydraulically interact with each other (Mohsen et al., 1990; Khublaryan et al., 2008). The process of SWI in coastal aquifer systems is shown in Figure 2.14. Huge groundwater abstraction causes extra SWI sip-in and the formation of depression and ascension zones, further indicating the SWI severity. Withdrawing excessive amounts of groundwater from confined aquifers results in the formation of huge depression cones with a radius greater than 100 km, causing extensive amounts of SWI (Freeze and Cherry, 1979; Iodkazis and Mokrik, 1981; Gregorauskas., 1986; Gregorauskas., 1987; Frolov and Yushmanov., 1998; Bear et al., 1999).

SWI in coastal aquifers is a major concern, and researchers around the globe are showing immense interest in this environmental phenomenon (e.g. Post and Abarca, 2009; Werner et al., 2013; Meyer et al., 2019; Wang et al., 2019). Senthilkumar et al. (2019) studied the integrated SWI of the coastal region of Thriuvallur district (13.25° N, 80.01° E), Tamil Nadu in South India using integrated geophysical and geochemical

methodologies to assess the SWI. The authors found NaCl in majority of the water samples, indicating SWI in the area of study due to over pumping. Costal et al. (2020) studied the groundwater through-flow and SWI in high-quality coastal aquifers using more than 30 years of well-based data from SWI monitoring sites in the south-west of Western Australia. The authors reported that the SWI is a major groundwater problem in coastal regions and the SWI monitoring tools should be specifically designed for coastal areas.

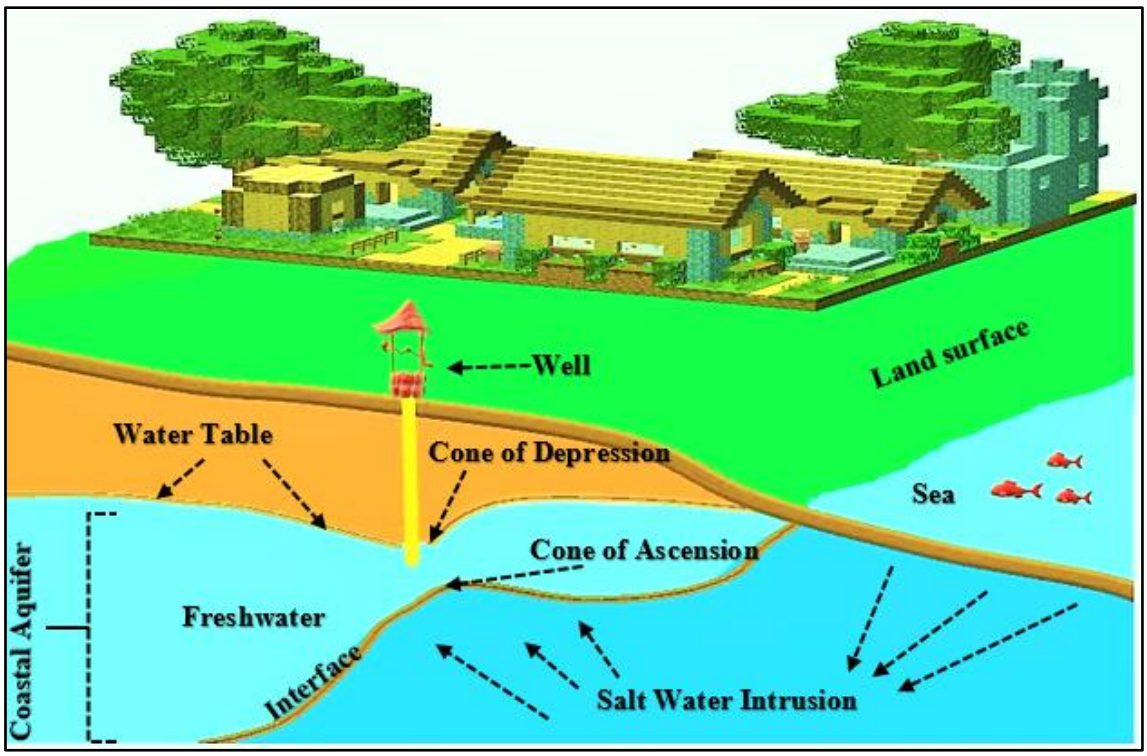



Figure 2.14: Saltwater intrusion in a coastal aquifer system.

In PICs, there is very little research being conducted on SWI and groundwater, even though PICs are vulnerable to this environmental problem (Burns, 2002; Carpenter et al., 2007; Velde et al., 2007; White and Falkland, 2010; IGRAC, 2016). The land area of PICs is small and fully surrounded by ocean water, which leads to SWI more often by natural means. Some studies on groundwater contamination due to SWI in PICs are given in (e.g. Hay and Kaluwln, 1993; Ghassemi et al., 1996; Mourits, 1996; Dawe, 2001; Singh et al., 2001; Presley, 2005; Carruthers, 2009; Fletcher and Richmond, 2010; Fussel, 2012; Bendixson et al., 2014; Lal and Datta, 2019a; 2019b). All these studies have reported that due to the immense use and abstraction of groundwater, SWI contaminates the groundwater and makes it unusable for a longer timeframe. Closing the groundwater sites for a period of time and switching to other water sources or new boreholes is the only

option for preventing SWI for some PICs. Robust research should be conducted on PICs groundwater, as it is highly vulnerable. Researchers around the world can also do case studies on PICs and do experimental setups for robust and accurate SWI data collection. These data can be used to draw the solutions for monitoring, managing and preventing SWI.

### 2.5.1 Major solutions for saltwater intrusion in PICs

Numerous techniques have been developed and adapted by an immense number of researchers around the world to monitor, manage, and prevent SWI in coastal aquifers. This section will clearly discuss the solutions that researchers around the world have adopted and the solutions recommended in this review allow PICs and others to adopt to minimise and eliminate SWI and groundwater problems in general. Some of the commonly used techniques to identify, locate, interface, salinity levels and severity of SWI in aquifers use (1) geochemical techniques (e.g. Edet and Okereke, 2001; Allen et al., 2001; Sherif et al., 2005), (2) geophysical methods (e.g. Fitterman and Deszcz-Pan, 2001; Ekwurzel et al., 2001; Sherif et al., 2010), (3) experimental studies (e.g. Koch and Starke, 2001; Van et al., 2004; Chang and Clement, 2012) and (4) mathematical modellings (e.g. Henry, 1959; Cooper, 1959; Sbai et al., 1998; Bower et al., 1999; Aharmouch and Larabi, 2001). Households that depend solely on groundwater can face many issues without getting clean and freshwater. Hence, prevention of SWI is very important due to the impact it poses on freshwater.

#### *2.5.1.1 Physical ways of preventing SWI*

The common physically used SWI prevention techniques are **(a) relocation of abstraction wells**, where the freshwater wells can be relocated by digging new ones on higher grounds or away from the sea would prevent SWI (Todd, 1974; Maimone et al., 2004; Dogan and Fare, 2008). **(b) Reduction in pumping rates** reduces the chance of SWI. However, it can reduce the volume of water supply if there is no other water source to meet the escalated demand (Sherif and Al-Rashed, 2001; Maimone et al., 2004; Abarca et al., 2006). **(c) Increasing the aquifer's natural recharge** assists the aquifers with extra surface water, whereby the retained water from rain infiltrates into the subsurface, increasing the amount of groundwater ratio and preventing SWI. However, this technique requires highly permeable land or soil structure, or else, natural recharge can last for a longer period due to the infiltration process (Ru et al., 2001; Calvache and Pulido-Bosch,

1997). **(d) Artificial aquifer recharge** assists the groundwater by manually adding water to the ground. The excess surface water, desalinated water and treated wastewater are directed into the ground near pumping wells or boreholes so they can be infiltrated into the aquifer, increasing the volume of groundwater (Bouwer, 2002; Papadopoulou et al., 2005; Shammas, 2008). **(e) Pumping of saline groundwater** will increase the water volume and reduce the chance of SWI in the groundwater. This technique reduces the volume of saline water underground and protects abstraction wells from upconing (Soldal et al., 1994; Sherif and Hamza, 2001; Barrett et al., 2002; Rastogi et al., 2004). **(f) Forming a groundwater circulation well** allows a vertical circulation flow by pumping groundwater from the aquifers through a screen in a single well and injecting it back into the aquifer through different screens. This vertical circulation forms a circular pattern between pumping and recharge screens, acting as a hydraulic barrier for controlling SWI in coastal aquifers (Herrling et al., 1991; Gonen and Gvirtzman 1997; Stamm 1998; Vats et al. 2020). This technique is mostly suited for coastal areas (Prusty and Farooq, 2020), hence, PICs should employ this technique to prevent SWI.

The use of the six physical ways of preventing SWI mentioned above are effective. However, very few studies have been conducted and reported on PICs regarding the use of these physical techniques. Hence, PICs need to keep a proper record of all groundwater-related data to find a better physical way of preventing SWI in coastal aquifers. Moreover, more research and funds are needed to physically visit groundwater sites in PICs for a better understanding of the groundwater problems and to propose the best solutions for protecting the groundwater and preventing SWIs.

#### *2.5.1.2 Robust Monitoring*

Comprehensive monitoring strategies must be employed by the countries facing SWI issues in coastal aquifers using the latest technologies and devices. The contaminated groundwater monitoring is challenging, as it can be triggered naturally or by anthropogenic means. Hence, robust monitoring should generally include but not be limited to field surveys, state-of-the-art technologies and devices, temporal and spatial data collection and analysis, evaluating the on-hand information and implementing proper management processes (Melloul and Goldenberg, 1997).

Electrical resistivity tomography (ERT) and electromagnetic (EM) devices using multi-electrode, multi-channel systems, 2-dimensional, 3-dimensional and 4-dimensional

surveys are used to monitor groundwater (Auken et al., 2006; Loke et al., 2013). Acworth and Dasey (2003) used the ERT technique to examine the hyporheic zone and found a widespread mixing region of seawater and permeated rainwater underground. The authors reported that to understand the electrical images clearly, borehole data should be combined with geophysical or geological surface-based data. Andersen et al. (2007) studied the discharge of nitrate-containing groundwater into a coastal marine environment using a multi-electrode profiling system to plot the subsurface distribution of freshwater in a coastal aquifer. Their results indicated a freshwater discharge at the small scale governed by limited heterogeneities. Kirkegaard et al. (2011) used an electromagnetic measuring device to study the salinity distribution in heterogeneous coastal aquifers to depths of 200 m below the surface and reported that there is a huge relationship between geographical heterogeneity and groundwater salinity.

Moreover, the Saltwater Monitoring System (SAMOS) is a monitoring system developed by Grinat et al. (2010), which is comprised of a vertical electrode chain mounted in a backfilled borehole that monitors the zone of transition thoroughly. SAMOS is useful mainly because the electrode array covers the zone of transition and is powered by the solar system. Hence, it can operate in any location. SAMOS also generate automatic measurements daily with telemetric data transfer (Grinat et al., 2010). Ronczka et al. (2020) used SAMOS to observe freshwater-saltwater interfaces and their dynamics, whereby the authors were able to get clear data on transition zones showing saline and freshwater interaction. However, the authors indicated that a longer period of groundwater monitoring data is needed for optimum results. Subsurface monitoring devices (SMDs) are automatic, remote-controlled and multisensory tools used for SWI. SMDs can be used for sampling, testing, logging and profiling SWI. Tal et al. (2019) used SMD for SWI monitoring and found that SMDs are reliable because of high-resolution temporal and spatial data output, which can be transmitted through the World Wide Web and can be analysed and interpreted in real time.

Anumalla et al. (2005) used smart sensors to monitor groundwater and designed a monitoring system based on a wireless network linked to pressure sensors. Moreover, some sensors are linked to the Global Positioning System (GPS) and satellite communications system, which records the groundwater data (SachinAmreiss et al., 2020). PICs have few monitoring devices. However, they need to be updated, and state-of-the-art technologies are needed for robust monitoring. Some of the sample sensors and

latest devices for monitoring water and measuring different parameters are given in Table 2.2. These water monitoring devices are very useful in groundwater and SWI detections. PICs can use some of these devices, which are cheap, handy and reliable for robust monitoring of groundwater quantity and quality.

Table 2.2: Water monitoring devices. Adapted from Xylem (2013).

| Monitoring Type | Applications | Measuring parameters | Sample(s) |
|---|---|---|---|
| Sampling and testing (e.g. Professional Plus, ProODO, Pro20, Pro30) | Groundwater<br>Wastewater<br>Aquaculture<br>Surface water<br>Industrial | Temperature, Dissolved oxygen, pH, ORP, Conductivity Level, Specific conductance, Salinity, Total dissolved solids, Barometric pressure, Ammonia, Calcium, Chlorine |  |
| Sampling, Logging & Profiling (e.g. 600LS sonde, 600XL/M sondes, 600XL/M V2 sondes) | Short-term studies, lake and stream sampling, groundwater wells, tide gauge measurements, water level, sound velocity profiles, saltwater intrusion, hydrographic surveying, coastal research and fisheries | Conductivity, Temperature, Depth, Vented level, pH, ORP, Dissolved oxygen, Turbidity, Nitrate, Ammonium, Chloride, Salinity and Sound speed |  |
| Long-term Monitoring (e.g. 6600 V2 Sonde, 600OMS V2 sonde, EXO1 sonde, EX02 sonde) | Continuous monitoring, source water, lake profiling, dredging underway sampling, PAR studies, algal bloom monitoring, coastal studies and saltwater intrusion | Conductivity, Temperature, Dissolved oxygen, Chlorophyll, Blue-green algae, Turbidity, Rhodamine, Depth, Vented level, PAR, pH, ORP and fDOM |  |
| Hydrological Monitoring (e.g. Storm 3 Browser-based Data logger) | Water level monitoring, reservoirs and tanks, remote data delivery, real-time alerts | Well and aquifer water levels. |  |
| Continuous Monitoring and Control (e.g. 5200A Monitor) | Wastewater process monitoring Aquaculture monitoring and control | Conductivity, Temperature, Dissolved oxygen, Salinity Turbidity, TSS, Ammonium, Nitrate. |  |

Table 2.3: Common 3-D modelling codes used for SWI.

| 3D Modelling Codes | Common characteristics | Reference |
|---|---|---|
| FEMWATER | Finite-element model, Graphical user interface, Saturated and unsaturated flow, Maximise total pumping from production wells and minimise total pumping from production wells. | (Dhar and Datta 2009; Roy and Datta 2017; Lal and Datta 2019c) |
| FEFLOW | Finite-element model, Graphical user interface, Saturated and unsaturated flow, HYDROCOIN salt-dome, Elder and Henry problems are tested. | (Watson et al., 2010; Zheng et al., 2018) |
| SEAWAT | Finite-difference model, Graphical user interface, Saturated flow only, Uses MODFLOW and MT3D models, HYDROCOIN salt-dome, Elder, Henry and rotating fluids problems are tested. | (Cherubini and Pastore 2011; Webb and Howard 2010; Kourakos and Mantoglou 2013) |
| SUTRA | Finite-element model, Graphical user interface, Saturated and unsaturated flow, HYDROCOIN salt-dome, Elder and Henry problems are tested, Minimise total net recharge, SWI and total cost. | (Nishikawa et al. 2009; Javadi et al. 2015) |
| MOCDENS3D | Finite-difference model, Graphical user interface, Saturated flow only, Elder, Henry and rotating fluids problems are tested. | (Bakker et al., 2004; Giambastiani et al. 2007; Vandenbohede and Lebbe 2011). |
| MARUN | Finite-element model, Graphical user interface, Saturated and unsaturated flow, Only tested for Henry's problem. | (Boufadel et al., 2011; Li and Boufadel 2011). |
| SWAT-MODFLOW | This is new integrated Soil and Water Assessment Tool (SWAT) and MODFLOW, Finite-difference model, Graphical user interface. | (Sabzzadeh and Shourian, 2020; Wang and Chen, 2021) |
| QSWATMOD | Quantum Geographic Information System based graphical user, Finite-difference model, Model written in Python. | (Park et al., 2019) |

### *2.5.1.3 Use of 3D models*

Numerous modelling methodologies and codes are used to understand, monitor, and prevent SWI in coastal aquifers. A tremendous amount of research has been done focusing on developing and using analytical and numerical models for forecasting the level of SWI in coastal aquifers. There are two basic approaches used in numerical modelling. **(1) Sharp interface** operates on the assumption that saltwater and freshwater are immiscible liquids parted by sudden and unexpected interfaces (Bear and Verruijt, 2012). This approach is simple and requires less computational load. However, it can be less accurate and will not give the desired results (Person et al., 1998; Zhou et al., 2005; Kacimov and Sherif, 2006; Choquet et al., 2016). **(2) Diffusive interface** operates on the assumption that saltwater and freshwater are miscible liquids separated by a zone of transition. This interface uses density-dependent flow and transport models (Voss and Souza, 1987). This approach provides more realistic results for homogeneous and heterogeneous coastal aquifer systems (Nguyen, 2016). A diffusive interface is also known as a density-dependent numerical model.

The common modelling codes used in groundwater studies are summarised in

Table 2.3. From all the models given, SEAWAT can test all four problems (namely, Elder, Henry/Hilleke, HYDROCOIN salt dome and rotating fluids problem), as it uses combined MODFLOW and MT3D models. Few PICs used FEMWATER for modelling and groundwater monitoring (Lal and Datta, 2019a; 2019c). However, there is a vast opportunity to explore and use other 3D models in PICs for managing SWI in coastal aquifers. A sample 3D model developed from FEMWATER is shown in Figure 2.15. The 3D model helps to indicate SWI, explain non-linear flow and transport processes and maximise or minimise total groundwater pumping rates. The PICs that are highly dependent on groundwater must use 3D models to monitor, manage and prevent SWI.

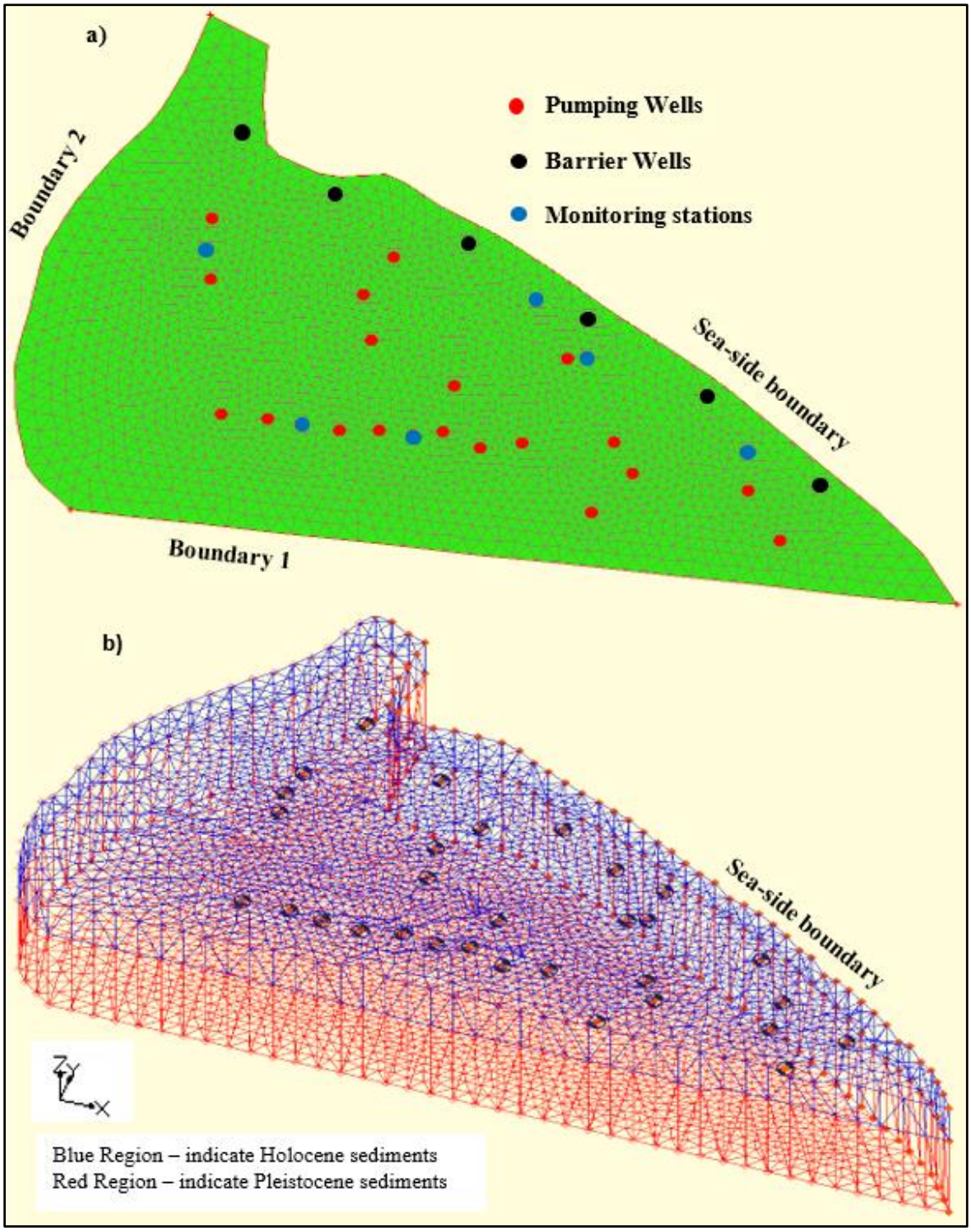



Figure 2.15: Study area indicating pumping and barrier wells, and monitoring stations, (b) 3D model developed using FEMWATER. Reproduced from Lal and Datta (2019c).

#### *2.5.1.4 Artificial intelligence*

SWI monitoring, management and prevention methodology requires accurate and precise results, whereby a simulation-optimisation (S-O) approach using artificial intelligence (AI) or machine learning can help to achieve the optimum strategies replacing complex numerical simulation models (Dhar and Datta, 2009; Sreekanth and Datta, 2010;

Christelis and Mantoglou, 2016; Roy and Datta, 2020). The S-O process ranges from simple to complex based on the number of inputs and types of models. A simple S-O uses the output of the simulation process by an optimisation model to provide the appropriate feedback to achieve the optimum result, which then re-guides the input parameters in the simulation model (Carson and Maria, 1997; Syberfeldt et al., 2013).

The S-O method is one of the most commonly used and effective approaches for coastal aquifer management purposes. Numerical simulation modelling can estimate various management strategies on aquifer systems, but it cannot find the best solutions instantly because of its descriptive nature. Hence, an optimisation algorithm can be combined with a numerical simulation model in an S-O structure to find optimum management strategies for coastal aquifers (Mantoglou et al., 2004; Abarca et al., 2006; Roy et al., 2016). Moreover, S-O helps to identify the optimal strategy in SWI management, gives simultaneous results, removes the complexity of analysis and allows the governing body to draw policies for using groundwater (Ataie-Ashtiani et al., 2013). Some of the studies and S-O techniques are summarised in Table 2.4. This research work provides different types of numerical and optimisation techniques used by several researchers under density-dependent and sharp interface models. The majority of the authors reported that using the S-O technique gives optimum results for coastal aquifer problems.

Coupling the numerical simulation model with optimisation models requires a large amount of computational time. Hence, it is computationally demanding (Lal and Datta, 2019a). Therefore, to minimise this time-related issue, S-O is coupled with data-driven mathematical models, known as surrogate models. Forrester et al. (2008) gave a comprehensive review of the theory, architecture and use of the surrogate modelling approach in Engineering. Surrogate modelling approaches have been used by various researchers, including (Sreekanth and Datta, 2010; Roy and Datta, 2018; Lal and Datta, 2017; 2018; 2019a; 2019b). These studies combined S-O modelling with surrogate modelling to find the optimum management strategies for SWI in coastal aquifers.

Table 2.4: The summary of simulation-optimisation techniques for SWI management.

| Modelling Type | Simulation Model | Data-Driven Models (approximate simulators) | Optimisation Model | Reference |
|---|---|---|---|---|
| DD | 3D advective dispersion flow and transport process equation proposed by Huyakorn et al. (1987) | ANN | GA | Bhattacharjya and Datta (2005) |
| DD | SEAWAT | - | EASS | Kourakos and Mantoglou (2009) |
| DD | FEMWATER | ANN | GA | Dhar and Datta (2009) |
| DD | FEMWATER | ANN & GP | NSGA II | Sreekanth and Datta (2010) |
| DD | SUTRA | ANN | GA | Ataie-Ashtiani et al. (2013) |
| DD | SUTRA | - | NSGA II | Javadi et al. (2015) |
| DD | FEMWATER | MARS - Ensemble | CEMOGA | Roy and Datta (2019) |
| DD | FEMWATER | SVR-Ensemble | GA | Lal and Datta (2019b) |
| DD | FEMWATER | GP - Ensemble | NSGA II | Sreekanth and Datta (2011) |
| SI | Ghyben-Herzberg relationship (Analytical) | - | ECACO | Ataie-Ashtiani and Ketabchi (2011) |
| SI | Ghyben-Herzberg relationship (Analytical) | RBFN | DE | Papadopoulou et al. (2010) |
| SI | Analytical | - | GA | Cheng et al. (2000) |
| SI | Analytical | - | LP & NLP | Mantoglou (2003) |
| SI | Analytical(MODFLOW) | - | EA & NLP | Mantoglou et al. (2004) |
| SI | Analytical | - | LP & DE | Karterakis et al. (2007) |
| SI | SHARP | ANN | SA | Rao et al. (2004) |

DD – Density Dependent model, SI – Sharp Interface model, LP – Linear Programming, NLP – Non-Linear Programming, ANFIS – Adaptive Neuro-Fuzzy Inference System, ANN – Artificial Neural Network, EA – Evolutionary Algorithm, GA – Genetic Algorithm, EASS – Evolutionary Annealing Simplex Scheme Optimisation Algorithm, RBFN – Radial Basis Function Network, DE – Differential Evolution, SA – Simulated Annealing, ECACO – Elitist Continuous Ant-Colony Optimisation, NSGA II – Non-Dominated Sorting Genetic Algorithm, CEMOGA – Controlled Elitist Multi-Objective Genetic Algorithm, MARS – Multivariate Adaptive Regression Spline.

Single surrogate models have some uncertainties in predicting the optimum management strategies. However, to overcome this issue, multiple surrogates are combined for robust and accurate results, known as ensemble models (Wu et al., 2008; Zhou, 2012; Zhou et al., 2013). Substituting numerical models with ensemble models produces reliable results when coupled with the S-O framework. However, its application in SWI and coastal aquifer problems is limited. Sreekanth and Datta (2011), Roy and Datta (2017a; 2017b) and Lal and Datta (2019a; 2019c) used ensemble models for multi-objective, multi-layered and multi-realisation groundwater management strategies in coastal aquifers. All these authors reported that the various uncertainties in management strategies are addressed with clarity while using an ensemble modelling approach.

The PICs have yet to use common numerical models, optimisation techniques, coupled S-O approaches, surrogate and ensemble models, and digital twin models. Lal and Datta (2019a; 2019b; 2019c) only studied using the S-O, surrogate and ensemble modelling approaches to find the optimum SWI management strategies for the Bonriki aquifer system in Kiribati. The majority of the PICs use groundwater for everyday needs (refer to Figure 2.2). Therefore, all PICs should use S-O and AI to thoroughly monitor and draw up optimum management strategies for controlling SWI in coastal aquifers.

#### *2.5.1.5 Digital Twin*

The use of smart sensors for remote monitoring and feedback is essential in managing SWI and water resources. One of the emerging technologies used in engineering disciplines (apart from water) is digital twins (DT). A DT, a virtual representation of a physical system updated in real-time, is an emerging technology with transformative potential across industries (Liu et al., 2021; Tao et al., 2022). It enables predictive analysis, performance monitoring, and decision-making, enhancing efficiency and reducing risks. Initially developed for aerospace, DT applications have expanded to manufacturing, healthcare, and urban planning (Attaran and Celik, 2023). Globally and in PICs, DT models have not been applied to SWI management. Hence, using DT will provide a comprehensive, real-time depiction of an aquifer system, incorporating critical information throughout its lifecycle.

#### *2.5.1.6 Robust groundwater policies and regulations*

The use of groundwater and SWI monitoring state-of-the-art devices, 3D models and codes, and S-O, ensemble models, and AIs in coastal aquifers provide optimum

monitoring, management, and prevention strategies. Using these strategies, the governing body of a country, including PICs, can draw up policies and regulations to eliminate groundwater-related problems, including SWI. These policies and regulations should address groundwater pumping rates, pumping time, supply and demand, pricing and trading, permissions for well or borehole drilling, depths of wells or boreholes, and installing water meters for recording and detecting uncontrolled leaks (Giordana and Montginoul, 2006; GWPR, 2016). Based on these policies, the governing body of a PIC can regulate heavy fines and penalties for lawbreakers. These regulations should be imposed on all the people using groundwater and the future investors, water companies, farmers, and anyone directly or indirectly associated with groundwater.

A limited number of countries around the world have policies regulating groundwater management and preventing SWI (Scheidleder et al., 1999). Also, many countries have yet to regulate proper policies in relation to SWI management in coastal aquifers (Livingston and Garrido, 2004). Kelly (2006) used the 1989 Island County (48.19° N, 122.58° W) SWI policy and pointed out the limitations associated with it and the need for revising the existing policy. The old policies on groundwater should be revised, and new rules and regulations have to be adapted due to the increased demand for groundwater in recent years. Alberti et al. (2017) studied SWI in Nauru and reported that due to overexploitation and increased pollution through anthropogenic activities, groundwater must be protected using strict rules and regulations

There is a study gap for PICs in terms of better policies, rules and regulations in the identification, monitoring, management and prevention strategies of SWI. No research has been conducted for PICs about scrutinising the old groundwater protection policies and finding the drawbacks and limitations associated with the SWI management strategies. Very few PICs have proper policies and regulations for protecting the groundwater. The old policies and regulations must be revised by adding more ways to protect the groundwater from natural and anthropogenic activities. Wastewater management, water usage for agriculture, household needs, industrialisation, animal waste and water resource planning should also be addressed in the new policies to protect the groundwater for current and future generations.

#### *2.5.1.7 Awareness program*

Creating community awareness is also one of the major ways of protecting groundwater, preventing SWI and other contaminations in coastal aquifers. Those countries that have all the rules and regulations in relation to groundwater protection should also create public awareness on monitoring, management and prevention strategies of groundwater contamination, including SWI. Awareness is one of the significant aspects of preventing anthropogenic means of groundwater contamination, yet limited research on ways of awareness is reported. Public awareness and support is very important for water management. Due to continuous population growth and impaired water supply, future generations will have many challenges, including the accessibility of clean and freshwater (Weinrich et al., 2012).

Mokhtar et al. (2018) studied the groundwater flow and SWI in Fum Al Wad coastal aquifer located in Laayoune (27.15° N, 13.19° W) and reported that the farmers using groundwater for irrigation and other purposes must be thoroughly informed of the serious issues associated with overexploitation and over pumping of groundwater. Maity et al. (2018) reported that lack of awareness amongst farmers, unwilling involvement of the governing bodies and unavailability of other water sources in the Purba Midnapur district (21.94° N, 87.78° E) poses major hurdles in implementing aquifer improvement plans. Carpenter et al. (2007) reported that the majority of the PICs lack public awareness, community involvement and knowledge of monitoring, management and prevention of SWI and other contaminations of groundwater.

PICs are affected by climate change and sea level rise (Sharan and Kumar, 2021), thus posing a natural effect on groundwater and SWI. Anthropogenic effects are also very common in PICs in relation to SWI (Carpenter et al., 2007), therefore, (1) thorough awareness through community involvement must be done. This can be achieved by establishing committees or groups that look after groundwater sites in their area and ensure that all policies, procedures and regulations are followed. (2) Curriculum design for primary and secondary education sectors. The younger generation should be taught about the pros and cons of using groundwater, or they will face huge water problems in the future. (3) University courses must be developed focusing on educating all aspects of groundwater and its protection. The existing courses can be revised by adding the latest

technologies, techniques and devices. (4) PICs need more research and funding to conduct groundwater-related research and projects and create mass awareness.

Apart from groundwater-related problems, PICs are also prone to severe cyclones, droughts, and other natural disasters. Hence, research must be very active in PICs to protect the freshwater, its people and the country as a whole. (5) Conducting seminars and awareness sessions to the general public and the targeted companies or industries using groundwater. (6) Targeting NGOs, political, traditional and religious leaders for conveying and conducting the awareness programs. (7) Teaching the public, farmers and industries of harvesting rainwater and using other water sources to avoid overexploitation and contamination of groundwater. These programs and ways of creating awareness will be very effective in protecting groundwater and other freshwater sources in PICs and around the globe. The SWI prevention and management techniques mentioned above would be very useful, and their applicability to PICs is of great importance. Kiribati was selected and illustrated in Table 2.5 to show the applicability of these techniques. Only Kiribati was selected due to the availability of groundwater data, whereas most of the island countries' data was unavailable.

Table 2.5: Application of SWI solutions in Kiribati (a small Pacific Island country).

| **Application of Saltwater Intrusion Solutions** | | | | | | |
|---|---|---|---|---|---|---|
| **Country** | **Physical Ways of Preventing SWI** | **Robust Monitoring** | **Use of 3D Models** | **Artificial Intelligence** | **Robust Policies and Regulations** | **Awareness Program** |
| Kiribati | Increasing the natural recharge in Tarawa Atoll (White et al., 2001) | Use of various devices in Bonriki aquafer for monitoring salinity, water levels and water quality (Damlamian et al., 2015) | Use of SEWAT for Bonriki groundwater modeling (Mack, 2015) | Lal and Datta (2019b) used ensemble models of Support Vector Machine Regression (SVMR) for optimal design of groundwater pumping strategies from the unconfined Bonriki aquifer | National Water Resources Policy for Kiribati is adapted for protecting all types of water sources (White and Falkland, 2010) | Robust awareness programmes practised in Kiribati are detailed in the Pacific Programme for Water Governance (White, 2007) |

## 2.6 Conclusions

The review of groundwater in Pacific Island countries (PICs) highlights several key findings related to the challenges of groundwater contamination and the strategies for effective monitoring, management, and prevention. One of the major concerns is groundwater contamination, primarily driven by SWI and improper disposal of solid and liquid waste. Despite these pressing issues, using advanced numerical models and optimisation techniques, such as simulation-optimisation approaches and surrogate and ensemble models for SWI management, remains limited in most PICs.

However, there is great potential for improvement. By integrating state-of-the-art technologies, including 3D numerical modelling, artificial intelligence, simulation-optimisation methods, and digital twin models coupled with relevant policy frameworks and increased public awareness, PICs can significantly enhance their ability to monitor and manage groundwater resources. The SWI management strategies obtained from various modelling techniques would help address anthropogenic and natural contamination in coastal aquifers.

The review also reveals a significant knowledge gap in research and the lack of attention to scrutinising outdated groundwater policies and SWI management strategies in PICs. No research has been conducted to examine the limitations of current SWI and groundwater resources management strategies, pointing to the need for more extensive studies. Moving forward, increased funding, governmental support, and international collaboration are crucial to protecting groundwater resources in PICs.

The next chapter will describe how the over-abstraction of freshwater and climate change affect the water quality and quantity of groundwater resources in one of the PICs. The next chapter's results will validate the literature review's findings on how natural and anthropogenic activities affect groundwater resources in PICs.

# Chapter 3: Evaluating the impacts of climate change and water over-abstraction on groundwater resources in Pacific island country of Tonga

The main contents of this chapter have been published and copyrighted as outlined below:

**Sharan, A**., Lal, A., & Datta, B. (2023). Evaluating the impacts of climate change and water over-abstraction on groundwater resources in Pacific island country of Tonga. *Groundwater for Sustainable Development*, 20, 1-7. https://doi.org/10.1016/j.gsd.2022.100890

## 3.1 Overview

This chapter used a large number of groundwater and climate data to show how natural and anthropogenic activities affect groundwater resources in Tonga. Over-abstraction of groundwater, increased salinity in production bores, recharge rates, increased sea level rise and carbon dioxide emissions are the major factors considered in this chapter.

## 3.2 Executive Summary

Small, low-lying Pacific Island countries are prone to climate change and water resources-related issues. The demand for water in Pacific Island countries has increased significantly due to population growth, industrialisation, tourism, and agricultural needs. Groundwater is utilised by most Pacific Island countries, and due to increasing demand, the majority of the Pacific Island countries practise over-abstraction. Climate change caused by natural means and over-abstraction of groundwater has led to saltwater intrusion into the coastal aquifers and other groundwater-related problems in several low-lying Pacific Island countries. In this study, groundwater salinity data collected over a 42-year duration from several abstraction wells in Tonga is linearly analysed to ascertain the impact of over-abstraction on groundwater resources. Climate change also affects rainfall and net recharge patterns. Hence, Tonga's long-term rainfall and net recharge patterns were linearly analysed. Also, to ascertain the climate change effect in Tonga, the sea level height and carbon dioxide emissions were linearly analysed using the data from 1993-2020 and 1960-2018, respectively. Quantitative data, linear regression and graphical linear fit techniques were used in this study for data analysis. The results from this study

indicated that over-abstraction has caused saltwater intrusion more frequently and affected groundwater quality. An increasing salinity trend of 58% was observed from 1965 till 2007. It is also evident that the higher the abstraction rates, the higher the saltwater flux sipping into the coastal aquifers. Moreover, decreasing trends were also observed in rainfall (19%) and net recharge (37%) in Tonga between 1950 to 2006. This study also revealed that the sea level and carbon dioxide emissions have increased by 5.2% and 800%, respectively. This study provides insights into why controlling abstraction rates and acting against climate change is essential concerning groundwater. These insights will be helpful for groundwater resource managers, stakeholders, and policymakers in Tonga and the broad scientific community in managing saltwater intrusions and preserving the water resource.

## 3.3 Introduction

Groundwater is one of the world's widely used and oldest water resources. Groundwater usage has increased in the last few decades due to increasing population, industrialisation, tourism, and agricultural needs. Increasing groundwater demand also increases over-abstraction, which could lead to saltwater intrusion (SWI) (Frolov and Yushmanov, 1998; Bear et al., 1999; Roy and Datta, 2018; Lal and Datta, 2019c; Roy and Datta, 2020; Francesco et al., 2021; Chakraborty and Pal, 2021). Over-abstraction of water and other anthropogenic factors can also lead to further environmental issues and contribute to a global energy crisis as the resources deplete (Chakraborty et al., 2012; Kumar et al., 2020; Chakraborty et al., 2021; Kwame and Bawa, 2022). SWI in coastal aquifers is a major environmental problem, which has increased the interest of many global researchers in solving this issue (Werner et al., 2013; Wang et al., 2019). Over-abstraction of groundwater and SWI in Pacific Island countries (PICs) are also a significant concern. The deep Pacific Ocean predominantly surrounds PICs, and saline water sip-in has become a common challenge for these countries (Sharan et al., 2021). The PICs map and the study area are shown in Figure 3.1.

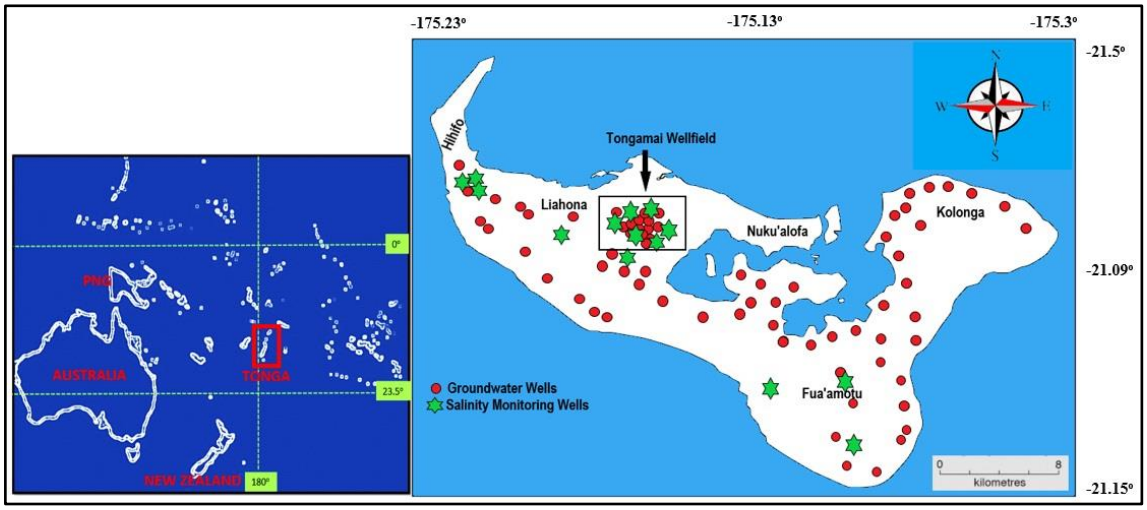



Figure 3.1: The Island of Tongatapu marked with groundwater wells and salinity monitoring boreholes.

Anthropogenic and climate change inputs jointly affect groundwater resources. Over-abstraction significantly reduces the volume of water in aquifers. It also makes the well dry and contaminates freshwater with salty water. Goode et al. (2013) reported that over-abstraction deteriorates the groundwater quality, declines the water levels and increases salinity concentrations. The majority of the PICs practise over-abstraction, including Tonga. White et al. (2020) reported that groundwater quality in Tonga has significantly deteriorated due to the over-pumping of groundwater since 1971. Hunt (1979) studied the analysis of groundwater resources in Tongatapu using the data from 39 wells and constructed a piezometric contour map. The author reported that the freshwater lens varies from 0-20m near central portions of the island, only 25-30% of rainfall reaches the groundwater table, and chloride ion ($Cl^-$) concentrations are found in the aquifers due to over-pumping. The author suggested that artificial recharge might help control the increasing Cl – ion concentrations in the aquifers.

White and Falkland (2010) studied the management of freshwater lenses on small Pacific islands and reported that over-abstraction is a major human threat to the freshwater lenses of groundwater. Moreover, the authors also stated that small island populations are about to reach the limit of sustainable groundwater abstractions. Hence, this could lead to severe SWI and other environmental risks. Groundwater problem has been identified, and there is a need for sustainable management strategies to overcome this issue. The governing bodies must adequately address the over-abstraction of groundwater in PICs. This anthropogenic input can be controlled. For instance, Dasgupta et al. (2015) and Garsallah et al. (2022) described how to treat wastewater through ultrafiltration and

nanofiltration. However, everyone needs to have a closer look at climate change factors affecting the groundwater in PICs.

Climate change also plays a significant role in determining the quality of groundwater in PICs. The sea level rise, frequency and severity of tropical cyclone occurrence, amount of rainfall and net recharge patterns, atmospheric heat, carbon dioxide ($CO_2$) emissions and Tsunami can be linked with climate change in PICs (Sharan and Kumar, 2021; Sharan et al., 2021). All these environmental issues can be inked with the SWI in PICs. The recent volcanic eruption in Tonga's vicinity has raised the risk of widespread and severe salinity increase in the groundwater system because of the Tsunami inundating large coastal areas. However, further information gathering and data analysis will be required to ascertain the extent of potential adverse impacts due to the Tsunami. A considerable amount of study was conducted on climate change effect on groundwater (e.g., Palmer et al., 1992; Bates et al., 2009; Green et al., 2011; Menberg et al., 2014; Green, 2016; Goldscheider et al., 2020). Epting et al. (2021) reported that climate change has qualitative and quantitative effects on groundwater. Barbieri et al. (2021) confirmed that groundwater is more resilient to climate change than surface water, and climate change can also affect groundwater quality by lowering the recharge.

Hay et al. (2005) studied the implications of climate change and sea level rise for small island nations of the South Pacific using vulnerability assessment methods. The responses to present-day variability indicated how the system would manage imminent climate changes. Vulnerability assessment has highlighted that small PICs are vulnerable to sea level rise caused by natural and anthropogenic means. The authors reported that climate change and rising sea levels affect groundwater quality and quantity. White et al. (2007) studied climatic and human influences on groundwater in low atolls using the data from Tarawa (1.45° N, 172.97° E), Kiribati. The authors reported that groundwater is affected by anthropogenic and natural means of climate change. The authors also reported that the atoll groundwater is mainly vulnerable to frequent El Niño Southern Oscillation-related droughts, and SWI sip-ins are frequent due to storm surges, sea level rise and human activities. Holdings et al. (2016) studied the groundwater vulnerability on small islands using qualitative data through a questionnaire survey involving local experts. The authors reported that PIC aquifers are oppressed by overpumping, climate variability and climate change. Lese et al. (2021) studied the historical and future drought impacts in Pacific islands and atolls and reported that the groundwater and other water sources would

be affected in the future due to prolonged droughts caused by climate change and climate change variability.

The majority of the PICs use groundwater. Limited research has been conducted in the PICs on groundwater and how it is affected by natural and anthropogenic means. Some relevant studies conducted on some PICs are (e.g., White et al., 2001; White et al., 2011; Alberti et al., 2017; Lal and Datta, 2019a; 2019b; 2019c). A thorough review of the groundwater sustainability crisis in the PICs was done by Sharan et al. (2021), where the authors found that PICs groundwater is overexploited and is prone to SWI by natural and anthropogenic means. The authors also reported that to minimise SWI and improve groundwater quality, PICs must use the latest SWI monitoring devices, 3D numerical modelling, machine learning algorithms and thorough community awareness. All these techniques will help to monitor, manage and prevent SWI in coastal aquifers.

Climate change caused by natural means and over-abstraction of groundwater has led to SWI in the coastal aquifers and other groundwater-related problems in several low-lying PICs. This case study is based on a small PIC, Tonga. This study uses quantitative data, linear regression, and graphical linear trends fit data analysis techniques to find the relationship between two variables. Linear trend lines were also used for a better description of the results. Groundwater salinity data from several abstraction wells in Tonga were analysed to ascertain the impact of over-abstraction on groundwater resources. Moreover, Tonga's long-term rainfall and net recharge patterns were analysed to see if groundwater is affected by climate change. Furthermore, data on sea level and carbon dioxide emissions were used to ascertain and validate the impact of climate change on Tonga.

This study is the first to investigate various aspects of climate change and how it ultimately affects groundwater resources in Tonga. Limited studies have been done on the evaluation of groundwater use sustainability in Tonga, and so far, to the best of the current knowledge, no specific investigation has been reported on the links between salinity trends, over-abstraction, long-term rainfall patterns, net recharge, sea level rise and carbon dioxide emissions on groundwater in Tonga. Hence, this study provides novel insights into Tonga's groundwater condition and opens pathways for further studies in the domain of groundwater research. Moreover, this study should be helpful for groundwater resource managers, stakeholders, and policymakers in Tonga and the broad scientific

community, the PICs, and the general Tonga community in combating saltwater intrusions and preserving the water resource.

## 3.4 Data

### 3.4.1 Study area

Tonga (21.18° S, 175.19° W) is a Polynesian country and is also known as the Kingdom of Tonga. Tonga has 171 volcanic, limestone, sand, and mixed islands, many uninhabited, with agriculture and tourism as primary economic earners. Tonga is divided into three major islands: Tongatapu, Ha'apai and Vava'u. The current population of Tonga is 105,695, whereas Nuku'alofa is the capital. Tongatapu has approximately 259 $km^2$ of total area, 31.5 km along its Northwest-Southeast way and 18.5 km along the Northeast-Southwest way (Babu et al., 2018). Tonga has ten active volcanoes, six on land and four underwater (World-data, 2022). Tonga is in the Pacific Ring of Fire, which attracts natural disasters and volcanic eruptions are one of them. On 15 Jan 2022, the Hunga Tonga-Huna Ha'apai volcano erupted in Tonga, where some nearby islands were covered in volcanic ashes. Tonga is also vulnerable to cyclones, tsunamis, earthquakes and droughts.

The study area for this research is Tongatapu (21.14° S, 175.25° W), as shown in Figure 3.1. Tongatapu is ~65 m above sea level, and the aquifers mainly consist of karst-type limestone, which is very porous (White et al., 2009). Tongatapu's geology and hydrological characteristics include a low-lying island of coral reefs and soil layers with cracks or karst macro pores. Karstification of layers indicates that aquifers are heterogeneous and anisotropic, with higher hydraulic conductivity in karstified layers. Moreover, lower conductivity can be seen in sandy layers. Hence, spatial variation is higher (Waterloo and Ijzermans, 2017). The soil type consists of clay and volcanic ash, known as Typic Argiudoll and Hapludoll (Manu, 2000). The natural forest is minimal in Tongatapu due to agriculture, which amounts to the island's vegetation.

Groundwater is the primary water source in Tonga. However, Tongans also use rain and desalinated water. Tongatapu has plenty of salinity monitoring boreholes and more than 6000 groundwater supply wells. However, not all the boreholes and wells are marked in Figure 3.1. The actual locations of the wells that were studied are shown in Figure A1:. The data was used from 56 locations in Tongatapu, and all the locations are marked in Figure A1:. The exact names of locations, the number of wells, longitude and latitude of the study area are given in Table A2. Moreover, from the locations Niutoua till Haateiho,

the groundwater data were collected on 14 Aug 2007 and from the locations Pae till Sia'atoutai, the groundwater data were collected on 15 Aug 2007, as shown in Table A2. The data was taken from the report compiled by White et al. (2009).

## 3.5 Methods

This study investigates the salinity concentrations of groundwater samples from some monitoring wells in Tongatapu. The yearly mean electrical conductivity (EC) of more than 20 wells was analysed using linear regression and graphical linear trends fit to see the effect of salinity concentrations due to the over-abstraction of groundwater from 1965 until 2007. The trend line was also shown to see the type of effect, either positive or negative. Moreover, the salinity profiles for the three monitoring wells in Mataki'eua/Tongamai (21.15° S, 175.23° W) wellfield (marked in Figure 3.1) were linearly plotted at different depths below the water table. The long-term rainfall patterns and net recharge rates from 1945 until 2006 were also linearly analysed for Nuku'alofa (21.14° S, 175.20° W) in Tongatapu. Linear regression was used to compare Tonga's average monthly rain and net recharge. The salinity data, rainfall patterns and net recharge data were taken from the report compiled by White et al. (2009) with the collaboration of the South Pacific Applied Geosciences Commission (SOPAC) (White et al., 2009).

Moreover, to see the climate change effect in Tonga, the sea level or tide height data from 1993 to 2020 were linearly plotted against the year. The tide height data of Nuku'alofa was used, and it was taken from the National Tidal Centre, Bureau of Meteorology, South Australia (NOC, 2022). Moreover, the carbon dioxide (CO2) emissions in Tonga from 1960 to 2018 were linearly plotted to strengthen and validate climate change in Tonga. The data was taken from The World Bank (WBG, 2022).

## 3.6 Results and Discussion

Tonga has minimal water management strategies, and the over-exploitation of water resources is a significant concern (Hess, 2017). To show the over-abstraction and overuse of groundwater in Tongatapu, the groundwater pumping rates of the Mataki'eua/Tongamai wellfield were linearly analysed using the data from 1966 to 2007. The results are shown in Figure 3.2. The results indicate that the pumping rate has increased with a positive slope of 1.23 and an $r^2$ value of 0.94, indicating a better representation of data. The pumping rate and the number of pumps in 2007 were ≈ 6 times higher than in 1966. Moreover, the pumping rate (litres/second) increased by 19% from

1998 till 2007. Over-abstraction of groundwater poses a possible risk of saltwater intrusions into the freshwater aquifers. Hence, the groundwater salinity trends in Tongatapu were analysed using linear trend analysis.

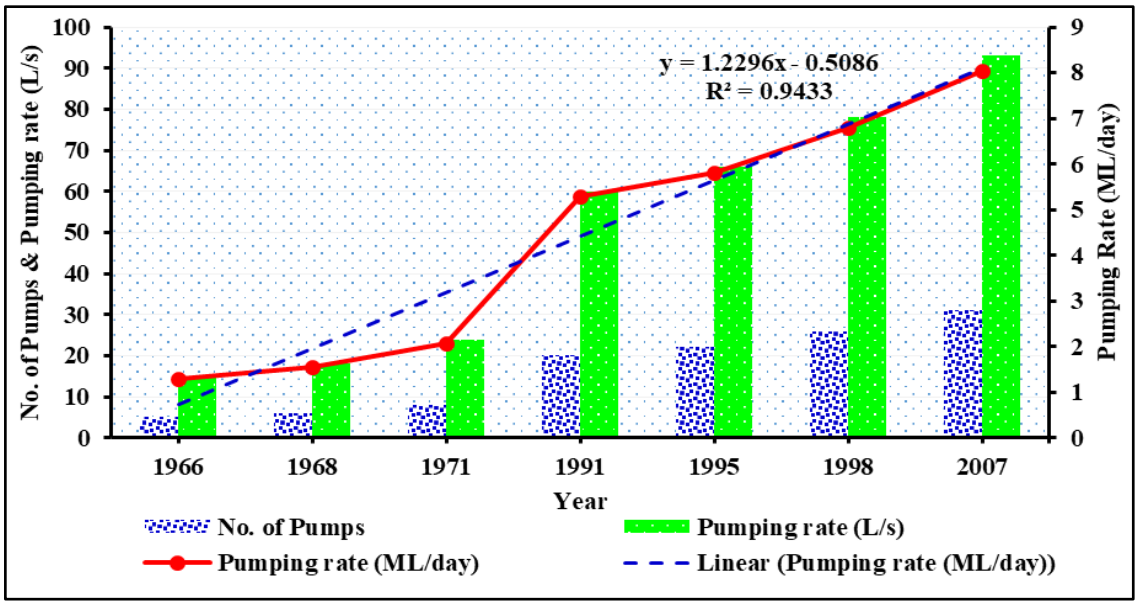



Figure 3.2: Groundwater pumping rates of Mataki'eua/Tongamai wellfield.

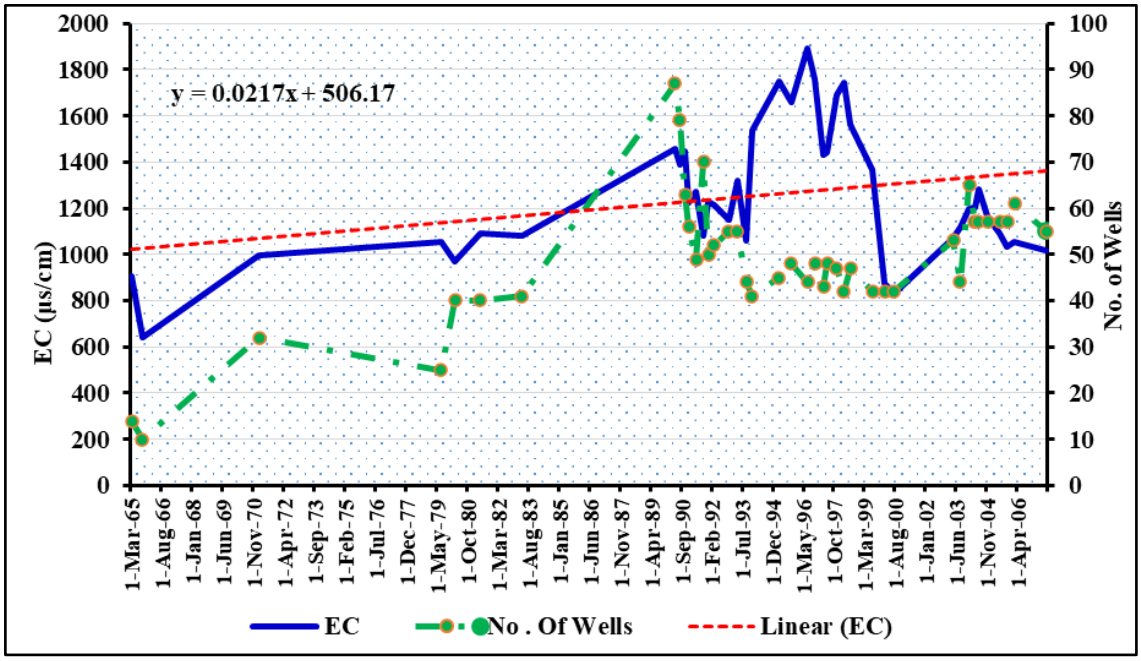



Figure 3.3: Salinity concentration of various wells in Tongatapu.

Groundwater salinity trends were determined using the electrical conductivity (EC) of several wells in Tongatapu, and the results are shown in Figure 3.3. The results indicate that EC has increased by 58% from the year 1965 with a gradient of +0.022. The average salinity concentrations of all wells indicated the lowest salinity of 353.1 mg/L in

September 1965. In contrast, the highest average salinity concentration of 1040.6 mg/L was noted in July 1996. Due to the wider time gap, the variations are higher. Moreover, the EC values were highest in 1996, and they gradually decreased till 2001 because, during that time, Tonga experienced heavy rainfall, which caused severe flooding and increased waterlogged areas. Due to this, there was a sudden decrease in the EC values, as shown in Figure 3.3. The annual rainfall patterns in Tonga are shown in Figure 3.4, from which it can be seen that from 1995 to 1996, the rainfall was minimal. Hence, the EC had a peak value. During low rainfall, the temperature was also high, which also triggered higher EC in Tongatapu. Also, from Figure 3.4, it can be seen that the rainfall from 1996 to 2001 was relatively high, gradually reducing the EC values by the dilution effect.

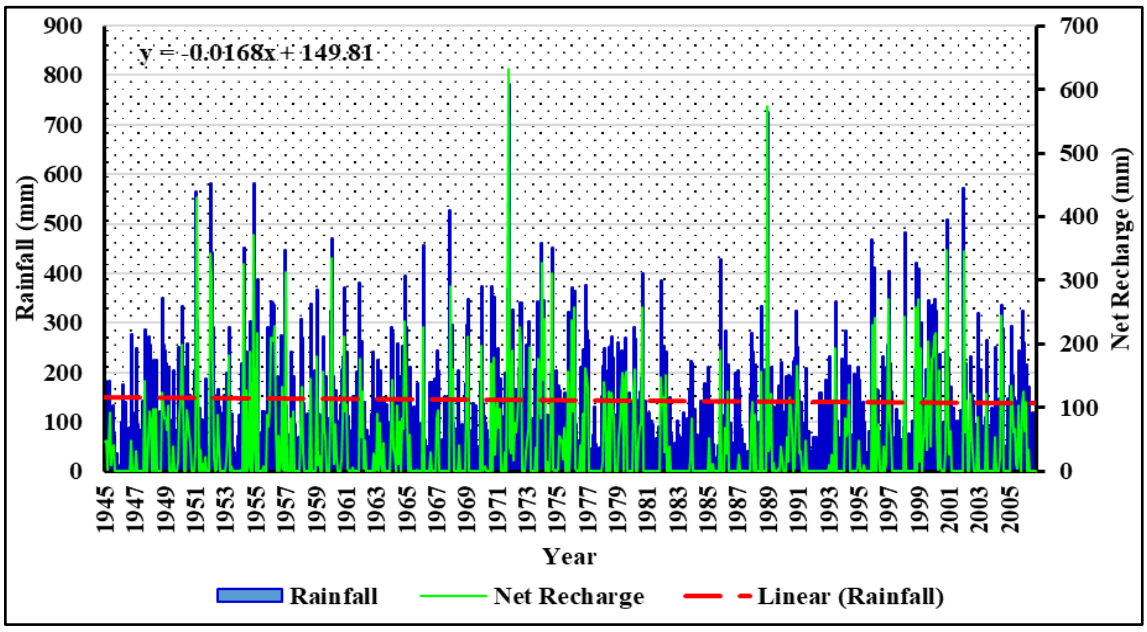



Figure 3.4: Rainfall (marked blue) and net recharge (marked green) for Nuku'alofa, Tonga.

The sea level was high in 1996 and decreased slightly till 2000, as shown in Figure 3.5. The sea level height also affected the EC. The increase in EC over the 40-year period depicts the presence of sodium chloride in the groundwater in several wells. Hence, the groundwater can be considered saline. In other words, there is a possibility of saltwater intrusions into the freshwater aquifers in Tonga, which makes the water saline. Since the pumping rates have increased, indicating over-abstraction by ≈ 6 times higher since 1966, there is a good chance of saltwater intrusion in Tongan aquifers.

Ayolabi et al. (2013) did a case study in Nigeria mapping saltwater intrusion (SWI) into coastal aquifers with geophysical and geochemical techniques and reported that SWI

has encroached into the aquifers, contaminating the water. The authors also reported that increased EC indicated a positive SWI in coastal aquifers. Moreover, Dausman and Langevin (2005), Furguson and Gleeson (2012) and Costall et al. (2020) also reported that overuse, over stress and exploitation of groundwater lead to SWI and other environmental complications. Prusty and Farooq (2020) reviewed SWI in coastal aquifers in India and reported that due to the increase in population and water demand, over-abstraction of groundwater frequently leads to SWI sip-in. Lal and Datta (2019b) studied the multi-objective groundwater management strategy under uncertainties for sustainable control of saltwater intrusion of the Bonriki coastal aquifer (1.37° N, 173.15° E) in Kiribati. The authors reported that to minimise the SWI, pumping rates must be controlled, and management models must be developed for optimum groundwater pumping.

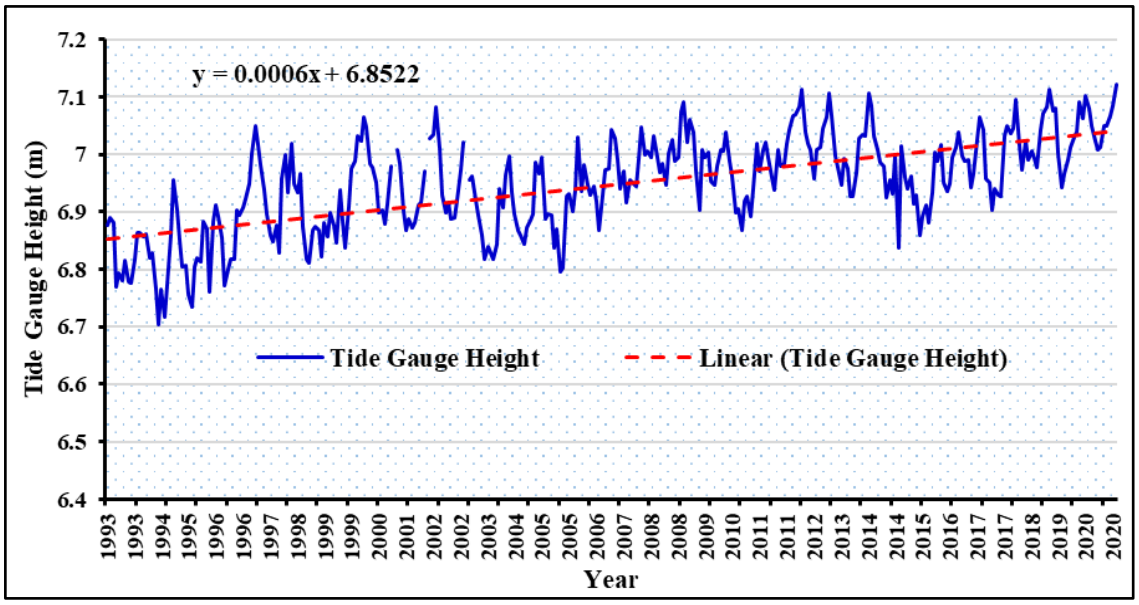



Figure 3.5: Sea level height in Nuku'alofa.

The increase in SWI in Tongatapu is mainly due to over-abstraction triggered by the increasing demand for groundwater due to daily household needs and agricultural use. The pumping rate in recent years has increased in the Mataki'eua/Tongamai wellfield, which supplies the groundwater to most of the people in Tongatapu. The increase in pumping rates in Tonga has increased the electrical conductivity of the groundwater. Hence, the freshwater wells and aquifers have more saline water, and the freshwater-saltwater interface has moved towards the landward side, possibly causing saltwater intrusion.

Moreover, the data from three salinity-monitoring boreholes in Tongatapu, namely, SMB1, SMB2 and SMB3, were also analysed, and the results are shown in Figure 3.6. As the depth below the water table increases, the salinity level also increases for all three monitoring boreholes. Moreover, 14m below the water table, EC drastically increases, indicating higher salinity concentrations. A thorough review of how the water table, EC and salinity concentrations are linked is given by Rusydi (2018). Bloomfield et al. (2020) studied variations in the salinity of deep groundwater systems and reported that groundwater becomes more saline with increasing depth below the water table. The authors also reported that total dissolved solids (TDS) vary about five orders of magnitude, increasing mineralisation with depth. Hence, the results from this study indicate that all the monitoring boreholes had higher salinity concentrations below the water table. It can be seen that over-abstraction and SWI are related. However, if the aquifers receive a good amount of recharge through rainfall, the freshwater-saltwater interface will move towards the seaward side. Therefore, the long-term rainfall and recharge patterns in Tongatapu were linearly analysed.

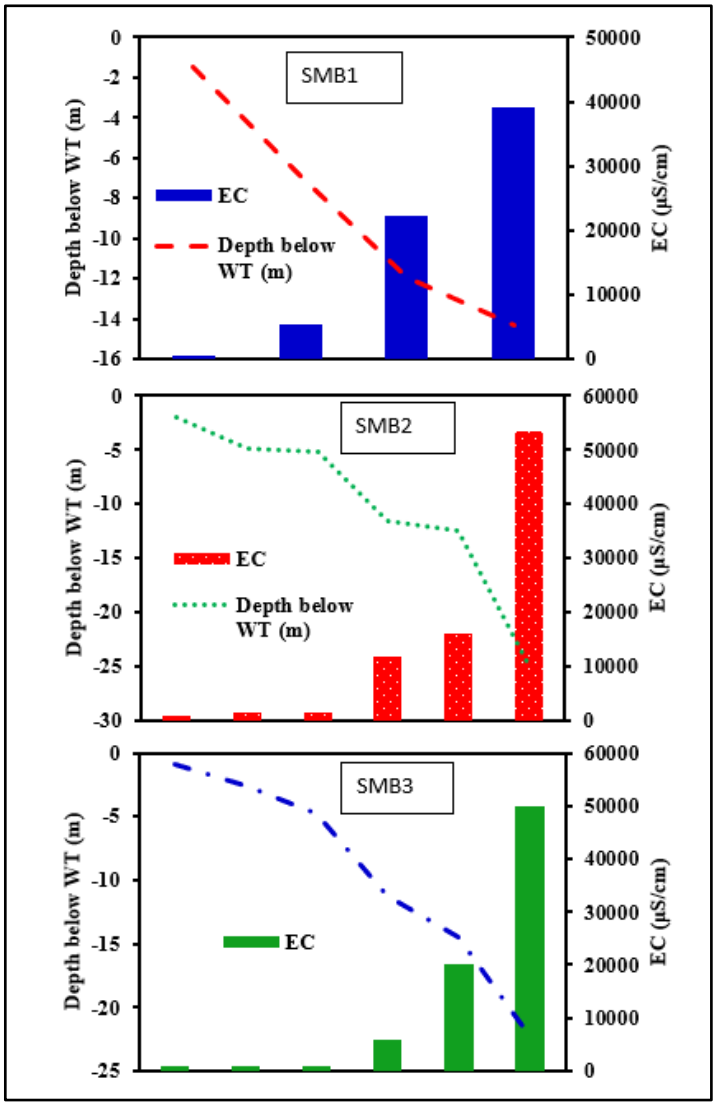



Figure 3.6: Salinity monitoring boreholes in Mataki'eua, Tonga, SMB1 (-21.15883, -175.23464), SMB2 (-21.15389, -175.24172) and SMB3 (-21.15061, -175.24494).

The long-term rainfall patterns for Nuku'alofa in Tongatapu were linearly analysed. The results are shown in Figure 3.4. The results indicate that the monthly mean rainfall has decreased by 19% from 1950 to 2006. The decrease in rainfall could be due to many factors. However, global warming caused by climate change could be one of the prominent factors for Nuku'alofa's decreased rainfall. C2ES (2022) reported that some climate models show a decrease in rainfall with increased dry periods in Tonga. Due to this decreased rainfall, the net recharge has also decreased by 37% from 1950 to 2006, as shown in Figure 3.4. The decrease in rainfall will impact the groundwater's net recharge (Owuor et al., 2016). Tongatapu island, in general, has decreased net recharge due to decreased long-term rainfall and the possibility of increased evaporation and transpiration linked with climate change and increased atmospheric heat (Dore, 2005).

Climate change can also be validated if the sea level rises, the strength and frequency of tropical cyclone occurrence, and increased carbon dioxide emission ($CO_2$). Tonga is experiencing a sea level rise of 6mm/year (Mulhern, 2020) and the severity and frequency of tropical cyclone occurrence in the past few years (MEIDECC, 2021). The rise in sea level can pose a vertical inundation of SWI into the coastal aquifers. The sea level or tide gauge height data for Nuku'alofa was linearly analysed from 1993 to 2020, and the results are shown in Figure 3.5. Sea level data was analysed to validate the plausible climate change occurrence in Tonga. The results indicate that the sea level has increased from 1993 to 2020 by 5.2%. Sea level rise is one of the major effects of climate change (Mimura, 2013). Treanor and Watson (2015) reported that Tonga is facing rising sea levels due to climate change. The rise in sea level also affects the water quality and increases water contaminations like SWI. Werner and Simmons (2009) studied the impact of sea level rise on SWI in coastal aquifers and reported that sea level rise affects the groundwater quality. Jasechko et al. (2020) studied the groundwater level observations in 250,000 coastal U.S. wells and reported that rising sea levels, land subsidence, and increased water demands would cause frequent SWI into the aquifers. Hence, the increased sea level in Nuku'alofa must have caused vertical inundation of saltwater into the aquifers, contaminating the freshwater.

$CO_2$ also plays a vital role in climate change (Pastor and Post, 1988; Lindsey, 2020). The increased $CO_2$ emissions in Tonga have led to climate variability and climate change, which has increased sea levels and eventually contaminated the coastal aquifers in Tongatapu and nearby areas. The $CO_2$ emissions in Tonga, Fiji, Papua New Guinea (PNG), and Samoa have increased from 1960 to 2018, as shown in Figure 3.7. $CO_2$ emission in Tonga alone has increased by ≈ 800% since 1960. Moreover, there was a slight increase in $CO_2$ by 5.9% from 2017 to 2018. Excessive $CO_2$ in the atmosphere can also be absorbed into groundwater, affecting the water quality (Carroll et al., 2009; Oviedo-Vargas et al., 2015). However, other studies also suggest that depleting groundwater releases $CO_2$ into the atmosphere (e.g., Macpherson, 2009; Wood and Hyndman, 2017; Mishra et al., 2018). These studies have revealed that the over-abstraction of groundwater changes the water's pH level and significantly reduces the bicarbonate level, releasing the stored $CO_2$ into the atmosphere. The link between groundwater over-abstraction and $CO_2$ released into the atmosphere must be further developed and studied for Tonga and other PICs.

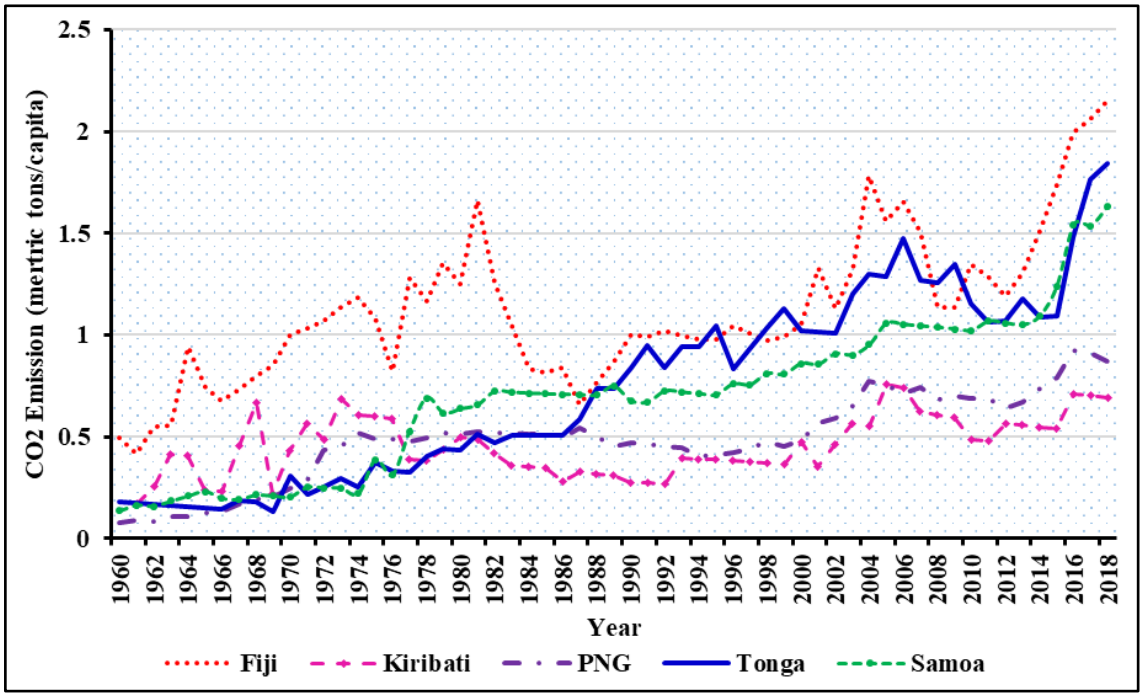



Figure 3.7: Carbon dioxide ($CO_2$) emissions of some selected PICs.

The water quality in Tonga has been affected by natural and anthropogenic factors. Over-abstraction, decreased long-term rainfall rates, decreased net recharge, rising sea level and increased $CO_2$ emissions contaminated the groundwater and caused possible saltwater encroachment in Tongatapu. The limitations of this case study were the availability of quality groundwater data. The majority of the PICs do not have quality and accessible groundwater data. Hourly or daily groundwater pumping and salinity data are needed to better understand the groundwater contaminations. Also, there is a need to separate other TDS from the groundwater to see the actual presence of salinity. However, to better understand the SWI in the coastal aquifers of Tongatapu, there is a need for 3-D modelling, AI-based modelling and decision models to manage and prevent saltwater intrusions. Using these modelling techniques will clearly indicate the presence of SWIs and provide better groundwater management strategies for controlling SWIs.

## 3.7 Conclusions

The effect of climate change and freshwater over-abstraction on groundwater resources in Tonga has been analysed using quantitative data, linear regression and linear trend analysis. Water salinity concentrations, pumping rates, long-term rainfall and net recharge, sea level and carbon dioxide ($CO_2$) emission data were used to see the effect of climate change and how over-abstraction of freshwater affects groundwater resources. Due to increasing demands, the over-abstraction and pumping rates of groundwater in

Tongatapu have significantly increased. Moreover, the salinity concentrations of several wells in Tongatapu have increased for a 42-year period. The long-term rainfall and net recharge of coastal aquifers in Tongatapu have decreased for a 61-year period. Net recharge of the coastal aquifer has decreased predominantly due to a long-term decrease in rainfall and increased heat in the atmosphere caused by excess $CO_2$ emissions, leading to evaporation and transpiration.

Moreover, an increase in sea level has caused vertical inundation of saltwater into the aquifers, contaminating the freshwater in Tongatapu. $CO_2$ emissions have significantly increased in Tonga, threatening the groundwater quality. Moreover, to find how the over-abstraction or depleting of groundwater releases $CO_2$ emissions into the atmosphere are related, a further study must be conducted in Tonga and other Pacific Island countries, as these issues have not been addressed adequately or rigorously till now. In addition, 3D and AI-based modelling studies are needed to better understand the saltwater intrusion in Tongan aquifers. This study provides insight into how natural and anthropogenic factors affect the groundwater in Tonga. Also, this study will benefit the people of Tonga and the broader scientific community by planning and focusing more on reducing abstraction rates, reducing carbon footprints, and combating climate change issues.

In the next chapter, an illustrative study (in the context of a PIC aquifer) is used to develop a 3D numerical simulation model to better understand saltwater intrusion in coastal aquifers. The chapter also provides various types of saltwater intrusion management strategies.

# Chapter 4: Integrating numerical modelling and scenario-based sensitivity analysis for saltwater intrusion management: case study of a complex heterogeneous island aquifer system

The main contents of this chapter have been published and copyrighted as outlined below:

**Sharan, A**., Datta, B., & Lal, A. (2023). Integrating numerical modelling and scenario-based sensitivity analysis for saltwater intrusion management: Case study of a complex heterogeneous island aquifer system. *Environmental Monitoring and Assessment*, 195(553), 1-22. https://doi.org/10.1007/s10661-023-11159-z

## 4.1 Overview

This chapter develops a 3D numerical model for a complex heterogeneous island aquifer to predict saltwater intrusion based on different pumping patterns. It also provides scenarios and tests uncertainties that trigger and prevent saltwater intrusion rates for a coastal aquifer.

## 4.2 Executive Summary

Population growth, industrialisation, and increasing agricultural demands have significantly stressed groundwater resources in Pacific Island countries (PICs). Climate change and sea-level rise also affect the groundwater resources in PICs. These anthropogenic and natural factors give rise to saltwater intrusion (SWI), a major growing environmental problem in the PICs. SWI is a highly non-linear process, which makes it more complex to manage. However, with the help of numerical modelling, SWI can be monitored, managed and controlled. An illustrative study area was used in the present study. The hydrogeological parameters and other boundary conditions used are similar to the PICs aquifer systems in Vanuatu. The scenarios include changing the barrier wells, injection wells, recharge, hydraulic head, hydraulic conductivity and grid size. The numerical simulation model of the study area was developed, and different scenarios were tested using SEAWAT modules. Apart from salt, leachate and engine oil were also modelled in the current study area to see how they affect the freshwater wells over time. The scenario-based sensitivity analysis tests indicate that injection wells, recharge, and hydraulic conductivities are highly sensitive, and with the proper modification, SWI can be managed or regulated. The sensitivity of grid size showed that the simulated results

varied within the 10% range of different gird sizes. Moreover, it was also found that the rise in sea level or coastal heads by 0.3m-1m does not significantly cause further SWI in aquifers. The results from this study are very crucial in this modern era when freshwater needs in coastal areas, especially PICs, are rapidly increasing, and fresh groundwater resources are declining. The novel outcome presented in this study opens pathways for further detailed modelling and numerical studies in the field of SWI management strategies development and is, therefore, beneficial for policymakers, groundwater modellers, and general scientific communities.

## 4.2 Introduction

Groundwater is the oldest and most widely used water resource on Earth, whereby 35% of water is used by humans supplied through sub-surface aquifers worldwide (Frankel, 2015). Groundwater usage has increased in the last few decades merely due to agricultural demands, population growth and industrialisation (Howard, 2015; Hamed et al., 2018). The increase in demand for groundwater resources has imposed a lot of stress and environmental problems in coastal aquifers across the globe. Saltwater intrusion (SWI) is one of the major environmental problems faced by coastal aquifers due to the over-abstraction of groundwater (Alley et al., 1999; Michael et al., 2017; Sharan et al., 2021). SWI occurs when the density of the groundwater is less than that of seawater when they hydraulically interact, forming depression and ascension zones. SWI is also described as the degradation or contamination of groundwater when the salinity of freshwater aquifers increases. Freshwater is identified by determining the total dissolved solids (TDS) present in the water. Freshwater has TDS < 1000 mg/L, whereas salty water has TDS > 35000 mg/L. Table 4.1 shows the general salinity classifications of different water types.

Pacific Island countries (PICs) use groundwater daily for drinking, cooking, washing, farming, irrigation, etc. Climate change, natural disasters, over-abstraction and other anthropogenic factors constantly affect the groundwater resources in PICs (Sharan et al., 2021). The groundwater resources in PICs are also prone to SWI problems. Hence, groundwater modelling tools are needed to tackle the SWI in the coastal aquifers in PICs. Table 4.2 summarises the twelve PICs profile, their water resources and the significant contaminants affecting their water resources. The summary vividly indicates that SWI is a major issue in small island nations affecting their coastal aquifers. The studies

conducted in managing the SWI problems are very limited in all the PICs except for Kiribati, where the research is active with some published reports and papers.

Table 4.1: General salinity classification (Hillel, 2000).

| Water Type | Total Dissolved Solids (mg/L) | Electrical Conductivity (μS/cm) | General Usage |
|---|---|---|---|
| Rainfall | ≤ 20 | ≤ 30 | Drinking and all irrigation also suitable for all livestock |
| Wastewater Effluents | 250-800 | 373-1194 | Drinking and all irrigation also suitable for all livestock |
| Freshwater | < 1000 | < 1500 | Drinking and all irrigation also suitable for all livestock |
| Brackish Water | 1000-10000 | 1501-15000 | Not suitable for drinking, but used for aquaculture, cooling water for power generation. Saline water (TDS = 2000-10000 mg/L) |
| Seawater | > 35000 | > 52000 | Not suitable for drinking or irrigation, also known as brine water, can be used for limited mining or industrial purposes. |

Coastal aquifers need to be monitored frequently, and it is essential to know the exact landward extent of saline water and freshwater discharge to maintain the saltwater-freshwater interface at equilibrium. There are numerous techniques and tools for preventing, managing and minimising SWIs. The detailed techniques and tools are thoroughly described by Sharan et al. (2021). Three-dimensional (3-D) numerical modelling techniques are one of the reliable, efficient and cost-effective tools for preventing, managing and minimising the SWIs in coastal aquifers (Lal and Datta, 2017; Roy and Datta, 2020; Sharan et al., 2021; Sharan et al., 2023). PICs have used a limited number of numerical models to manage the SWI. Some of the 3-D numerical models used in PICs groundwater management include SEAWAT (Bosserelle et al., 2015), SUTRA (Kumar, 2016) and FEMWATER (Lal and Datta, 2018; Lal and Datta, 2019). A SEAWAT-based numerical model has only been developed for the Bonriki aquifer (1.385$^{o}$ N, 173.144$^{o}$ E) in Kiribati to manage SWIs. However, more work still needs to be done, and the complexity of the conceptual model needs to be considered for the Bonriki aquifer. The SWI is a non-linear process. Hence, developing a complex model and using all possible boundary conditions will give optimum SWI management strategies.

Table 4.2: Pacific Island countries profile and water resources. Source ([1]World Population Review, 2022; [2]Falkland, 2002; [3]Sharan et al., 2021).

| Country[1] | Approximate Population (in 2020)[1] | Land Area (km sq.)[1] | Island Geology[2] | Major Source of Income[3] | Major Water Sources[3] | Major Water Contaminants or Problems[3] | Saltwater intrusion studies[3] |
|---|---|---|---|---|---|---|---|
| Cook Islands | 17595 | 236 | Atoll, volcanic, volcanic & limestone | Tourism, agriculture, pearls. | Desalination, Groundwater, Rain & Surface Water | Septic tank leakage, animal and human waste. SWI | Very limited |
| Fiji | 909466 | 18272 | Volcanic, limestone, atoll | Tourism, sugarcane, agriculture | Groundwater & Surface Water | Over-abstraction of groundwater, Waste disposals, SWI. | Very Limited |
| Kiribati | 123419 | 811 | Majority atoll, 1 limestone | Foreign aid, seafood exports, copra | Desalination, Groundwater, Rainwater | SWI, animal waste, droughts, over-abstraction., SWI | Active |
| Nauru | 10903 | 21 | Limestone | Foreign aid, seafood export, tourism, agriculture | Desalination, Groundwater, Rainwater | Sewage, long droughts, over-abstraction, SWI | Very Limited |
| Niue | 1648 | 260 | Limestone | Agriculture | Groundwater | Animal and Human waste, over-abstraction | Very Limited |
| Palau | 18233 | 459 | Limestone, volcanic | Agriculture and Seafood | Groundwater, Rain & Surface Water | Deforestation, sediment erosion, pesticides, human and animal waste | Very Limited |
| Papua New Guinea (PNG) | 9292169 | 462840 | Atolls, coral Is., volcanic, limestone | Agriculture, mining, crude oil | Groundwater, Rain & Surface Water | Farm chemicals, fertilizers, over-abstraction, SWI. | Very Limited |
| Samoa | 202239 | 2842 | Volcanic | Agriculture, seafood export, tourism, copra. | Groundwater & Surface Water | sediment erosion, human and animal waste, SWI | Very Limited |
| Solomon Islands | 721159 | 28896 | Atolls, volcanic, limestone | Log exports | Groundwater, Rainwater | Animal & human waste, over-abstraction, SWI, logging | Very Limited |

| Country[1] | Approximate Population (in 2020)[1] | Land Area (km sq.)[1] | Island Geology[2] | Major Source of Income[3] | Major Water Sources[3] | Major Water Contaminants or Problems[3] | Saltwater intrusion studies[3] |
|---|---|---|---|---|---|---|---|
| Tonga | 107749 | 747 | Volcanic, limestone, limestone & sand, mixed | Agriculture, tourism | Groundwater | Farm chemicals, animal waste, fertilizers, over-abstraction, SWI. | Very Limited |
| Tuvalu | 12066 | 26 | Atoll | Fishing licence to foreign vessels | Groundwater & Rainwater | Highly contaminated groundwater, animal, factory, human waste, chemicals, erosion, SWI | Very Limited |
| Vanuatu | 321832 | 12189 | Majority volcanic, sand & limestone | Agriculture, seafood export, tourism | Groundwater & Rainwater | SWI, animal, factory, human waste, chemicals | Very Limited |

SEAWAT-based numerical simulation models are developed using finite difference techniques. SEAWAT code is used for complex geometrics and geological settings, including SWI, submarine groundwater discharge, brine transport and groundwater flow near salt domes (Cobaner et al., 2012). Guo et al. (2019) studied the effects of sea-level fluctuations, groundwater pumping, and inland recharge on SWI in complex coastal aquifers. The authors developed the numerical model using SEAWAT and calibrated the hydrogeological parameters using real-time data. The authors found that their simulated groundwater level and salt concentrations were comparable with the results from the observation wells. Moreover, they also reported that high and low tides portray a major role in SWI in coastal aquifers.

Hagagg (2019) used the SEAWAT code to examine the level of SWI in the Karstic aquifer of El Negila (30.75º N, 30.698º E). The author tested the scenarios, including increased sea-level heights and pumping activities for 2022. The author reported that the SWI would increase if the pumping rates and sea level heights increased. Hamidi et al. (2021) used the SEAWAT code to model the SWI for the Rmel-Oulad Ogbane coastal aquifer in Larache, Morocco. The authors focused on two scenarios which include climate change and sea-level rise (SLR). The authors reported that the over-pumping of groundwater and SRL caused by climate change are the primary drivers of SWI in coastal aquifers. Moreover, the authors also reported that climate change also reduces the natural recharge, which eventually reduces the fresh groundwater resources.

The SLR, climate change, and over-abstraction of groundwater affect the quantity and quality of groundwater resources in PICs. These factors also cause SWI in coastal aquifers. Hence, managing the anthropogenic and natural factors affecting groundwater resources is very important. A numerical modelling approach is considered for this study to establish proper links between climate change, SLR and over-abstraction. This study will test different scenarios, and sensitivity analysis will be conducted by changing various parameters in the model domain. Moreover, multi-species contaminants will be introduced and modelled within the model domain. To the best of the current knowledge, some combinations of different scenarios tested in this study have never been investigated in previous studies. Moreover, the combined SWI and other species flow and transport will be the first for PICs. This study will be beneficial to hydrogeologists and groundwater professionals in considering various scenarios while developing their models using SEAWAT. Moreover, this study will provide better scenarios capable of managing SWIs.

Also, this study will show how multi-species contaminants are transported in coastal aquifers using SEAWAT, which will benefit lawmakers in drawing up policies for controlling these contaminant species before they contaminate the freshwater wells.

## 4.3 Methods

Saltwater intrusion is a complex non-linear process that requires mathematical models like numerical models to build the case simulation and provide management strategies for controlling saltwater intrusion. The numerical simulation model was developed using SEAWAT modules in Groundwater Modelling System (GMS). SEAWAT numerical code was developed to simulate 3D, variable density, transient groundwater flow in porous medium combining MODFLOW and MT3DMS programs. MODFLOW solves the non-linear variable density flow equations, and MT3DMS solves the non-linear temporal and spatial salt or solute transport equations (Guo and Langevin, 2002).

### 4.3.1 Governing Equations

The variable-density flow process solves the following form of the variable-density groundwater flow equation (tensors and vectors are shone in bold) (Langevin et al., 2008).

$$\nabla \cdot \left[\rho \frac{\mu_0}{\mu} \mathbf{K_0} \left( \nabla h_0 + \frac{\rho - \rho_0}{\rho_0} \nabla z \right)\right] = \rho S_{s,0} \frac{\partial h_0}{\partial t} + \theta \frac{\partial \rho}{\partial C} \frac{\partial C}{\partial t} - \rho_s q'_s , \qquad (4.1)$$

where $\rho_0$ is the fluid density [kg/m$^3$] at the reference concentration and reference temperature, $\mu$ is dynamic viscosity [kg/md], $\mathbf{K_0}$ is the hydraulic conductivity tensor of material saturated with the reference fluid [m/d], $h_0$ is the hydraulic head [m] measured in terms of the reference fluid of a specified concentration and temperature (as the reference fluid is commonly freshwater), $S_{s,0}$ is the specific storage [1/m], defined as the volume of water released from storage per unit volume per unit decline of $h_0$, $t$ is time [d], $\theta$ is porosity [dimensionless], $C$ is salt concentration [kg/m$^3$], $q'_s$ is a source or sink [1/d] of fluid with density $\rho_s$.

The integrated MT3DMS Transport process solves the following form of the solute transport equation.

$$\left(1 + \frac{\rho_b K_d^k}{\theta}\right)\frac{\partial(\theta C^k)}{\partial t} = \nabla \cdot (\theta \mathbf{D} \cdot \nabla C^k) - \nabla \cdot (\mathbf{q} C^k) - q_s' C_s^k + \sum_{k=1}^{N} R_k \qquad (4.2)$$

where $\rho_b$ is the bulk density (mass of the solids divided by the total volume) [mg/m$^3$], $K_d^k$ is the distribution coefficient of species $k$ [m$^3$/kg], $C^k$ is the concentration of species $k$ [kg/m], **D** is the hydrodynamic dispersion coefficient tensor [m$^2$/d], **q** is specific discharge [m/d], and $C_s^k$ is the source or sink concentration [kg/m$^3$] of species $k$. $R_k$ ($k=1, \ldots N$) is the chemical reaction term (kg/m$^3$d) of species $k$.

In previous versions of SEAWAT, $\frac{\mu_0}{\mu}$ was approximated as one, and thus viscosity effects were neglected, and fluid density was treated as a simple linear function of only one solute species. In SEAWAT version 4, fluid density and viscosity can be calculated using concentrations from one or more solute species. These equations of state relate the density and viscosity terms in equation 4.1 to one or more of the MT3DMS species concentrations ($C^k$) in equation 4.2. By allowing one or more of the MT3DMS species to affect fluid density and viscosity, variable-density groundwater flow can be coupled with simultaneous solute and heat transport (Langevin et al., 2008). Moreover, the previous version of SEAWAT and variable density groundwater flow and transport equations are given in by Guo and Langevin (2002) and Zheng and Wang (1999).

## 4.4 Study area

An illustrative study area representing an island aquifer system was used to simulate the 3D saltwater intrusion process and test different SWI management scenarios. The one-layer unconfined aquifer used in this study was 125.58 km$^2$. The aquifer system considered was complex, heterogeneous and isotropic in nature, with different values of hydraulic conductivities and porosities in the horizontal direction. The hydraulic conductivities for area portions 1, 2 and 3 are 10 m/d, 15 m/d, and 20 m/d, respectively. Also, the porosities for area portions 1, 2 and 3 are 0.2, 0.28 and 0.32, respectively. The study area consisted of an ocean boundary, three rivers, pumping wells, barrier wells, monitoring wells, industrial waste and oil dumping sites, as shown in Figure 4.1. The dumping site is assumed to be leaking at a prolonged rate, whereby the leachate and oil are seeping into the groundwater system. The annual rainfall for the area was 115 inches/year (3937 mm/year).

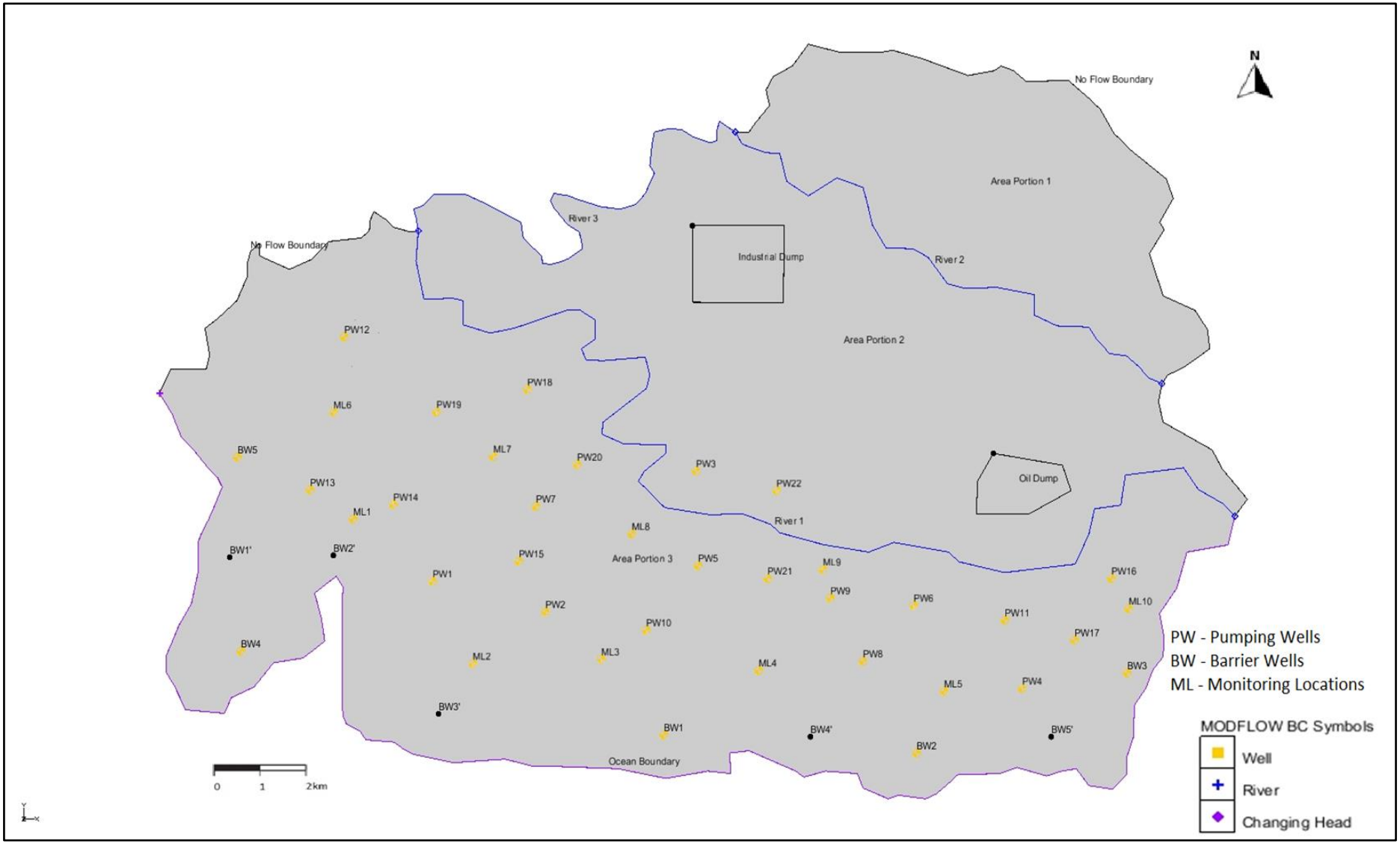



Figure 4.1: Plan view of the study area.

The illustrative study area is an actual groundwater pumping site in Vanuatu (15.3767° S, 166.9592° E) in Pacific Island countries (PICs). PICs do not have enough groundwater data to calibrate and validate groundwater models. Due to the unavailability of the hydraulic heads, groundwater pumping and water concentration data, the area was treated as an illustrative study area utilising the field data to the extent available to resemble the PICs aquifer system. The dumping site and the number of wells and rivers created in the model domain are added to introduce more complexity to the model. However, some boundary conditions and hydrogeological parameters are realistic and taken from the actual study area in Vanuatu.

### 4.4.1 Model Discretisation

The MODFLOW-2000 module was used to develop the conceptual model domain of the current study area. The length of the study area in the X-direction was 13822.15m, the length in Y-direction was 9083.80m, and the length in Z-direction was 100m. The cell size used to create the finite-difference grids was 50m x 50m. The number of nodes was 1010748, and the number of cells was 50414. The grid top elevation was 200m, and the grid bottom elevation was 100m.

### 4.4.2 Numerical Model and Boundary Conditions

The study area was divided into three small area portions representing an island aquifer system. Area portion 1 had fine to medium-grained sand, area portion 2 had coarse-grained sand and area portion 3 had sand/gravelly sand. The top boundary was a free surface, and the bottom boundary was treated as a no-flow boundary. There were three no-flow boundaries within the model domain. One was between rivers 1 and 2, the other was towards the northeastern side, and the third no-flow boundary was on the western side of the model domain. The boundary on the south side of the model domain was the coastal side boundary, and it was considered the specified head (constant head boundary), with the heads being at 181m each for two different nodes. River 1 head value of the eastern boundary was 182m, and 190m of the northwestern boundary. River 2 head value of the eastern boundary was 188m, and 195m of the northwestern boundary. River 3 head value on the western side was 190m, whereas 195m was on the northeastern boundary. The thickness of the aquifer was 95m. 22 pumping wells and 10 monitoring location wells were uniformly placed along the model domain.

The barrier wells and injection wells were also introduced in the model domain after testing different SWI management strategies. Pumping wells act as the sink to the system, whereas injection wells can be considered as sources to the system. The uniform pumping of 10000 $m^3$/d from 22 pumping wells was considered. The pumping rates and locations of production wells were not changed in order to compare the most effective scenarios for managing saltwater intrusions. Also, changing the pumping rates could have increased the simulations time and the numerical modelling would have become computationally expensive. However, the rates of pumping have been altered by adding barrier wells and injection wells. Recharge was also used as a source to the model domain uniformly. The recharge rates and other hydrogeological parameters used in the development of the model are given in Table 4.3.

The conceptual model was developed and simulated in a steady state using MODFLOW. The simulated heads were then used as initial heads for the transient simulation in MT3DMS and SEAWAT. The maximum stress period used was 10950 days. The hydraulic head values were simulated in a steady state until the difference in heads was not large. Then, these heads were used as initial heads in transient simulations. The initial salt concentrations were assumed to be zero as there was no salinity data from Vanuatu. If some data was available, then it could have been used to simulate the initial concentrations. The advection, dispersion, source and sink mixing packages and chemical reaction packages were used for solute transport. The simulated species are defined as salt in the MODFLOW and MT3DMS modules. Once the flow and solute modules were ready, SEAWAT-version 4 modules was initiated using the variable-density flow (VDF) package. To calculate the internodal density within the model domain, an upstream-weighted algorithm within the SEAWAT module was used. The freshwater density was used as the reference fluid density in the SEAWAT module. The density and concentration slope constant factor F was also used to prevent the model to over-estimate the freshwater lens. If F = 0, then as the concentration changes, there will be no change in the density. Hence, the results will be similar to the results simulated by MT3DMS. Hence, SEAWAT was used to generate the results because it uses VDF (freshwater and seawater) to make the freshwater lens difficult to circulate freely, forming a zone of transition.

Table 4.3: Model parameters and their values used in the numerical simulations.

| Definition | Values | S.I. Units |
|---|---|---|
| Area Portion 1 (Fine to Medium-Grained Sand) | Hydraulic Conductivity, K = 10<br>Porosity = 0.2 | K = m/d<br>Porosity = dimensionless |
| Area Portion 2 (Coarse-Grained Sand) | Hydraulic Conductivity, K = 15<br>Porosity = 0.28 | |
| Area Portion 3 (Sand/Gravelly Sand) | Hydraulic Conductivity, K = 20<br>Porosity = 0.32 | |
| Horizontal Anisotropy | 1 | dimensionless |
| Freshwater Density | 1000 | $kg/m^3$ |
| Seawater Density | 1025 | $kg/m^3$ |
| Saltwater Concentration | 35 | $kg/m^3$ |
| Specific Storage | 0.0035 | 1/m |
| River conductance | 1 | m/d |
| Longitudinal dispersivity | 20 | m |
| Recharge | 0.0004 | m/d |
| Stress Period | 30 | years |
| Density/Con. Constant, F | 0.7143 | dimensionless |
| Leachate Recharge Concentration | 30000 | $kg/m^3$ |
| Bulk Density | 60000 | $kg/m^3$ |
| Oil Recharge Concentration | 20000 | $kg/m^3$ |
| Leachate Dissolved Rate | 0.00005 | 1/d |
| Leachate sorbed Rate | 0.00005 | 1/d |
| Leachate sorption const. | 0.000006 | $m^3/kg$ |
| Oil sorption const. | 0.000003 | $m^3/kg$ |
| Oil Dissolved Rate | 0.00008 | 1/d |
| Oil sorbed Rate | 0.00008 | 1/d |

### 4.4.3 Different scenarios tested

The numerical simulation model was developed using the SEAWAT module, and the different scenarios were tested to find the best SWI management strategies in coastal aquifers. Seven different scenarios were tested, and the sensitivity analysis was done to see how the model would behave if different parameters were changed. The different scenarios include the changes in barrier wells, injection wells, hydraulic conductivities and porosities, recharge rates, hydraulic heads, multi-species and grid size. The finite-difference method was to discretise the grids. The finite-difference grid method allows us to change different parameters without changing the grid size and node locations. However, using the finite-element method, it is challenging to test different scenarios using different parameters because every time, the mesh will change, eventually changing

the mesh size and node locations. Hence, conducting the sensitivity analysis becomes more challenging.

## 4.5 Results

### 4.5.1 Scenario 1: Increasing the number of barrier wells

The current study area had 5 barrier wells (BWs) placed uniformly near the ocean boundary. In this scenario, the number of BWs was increased by 50%. The 5 additional BWs were also placed uniformly in the model domain along the ocean boundary and marked as BW′, as shown in Figure 4.1. The study area was initially modelled without using any BWs. It was also modelled using 5 BWs and then increasing the number of BWs by 50%. The results did not show significant variations in the salt concentrations in either of the situations. Hence, the model was simulated using 5 BWs, and the salt concentration at various MLs was tested to see how the BWs would change if the BWs were increased at uniform locations. The model domain was mapped with 10 BWs, and all the other boundary conditions and hydrogeological parameters remained the same. The BWs acted as the sink to the system, and the pumping rate of the 5 BWs was considered as 12000 $m^3$/d.

SEAWAT simulation was carried out, and the result was recorded at various time steps. The plan view of the 3-time steps (10, 20, 30 years) with the 50% increased BWs are shown in Figure 4.2(b-10 to b-30). Figure 4.2(a-10 to a-30) shows the base case results or the controlled simulated results. The movement of saline water towards the PWs is clearly shown in the different time steps. The side view at ML1 was also recorded, and the results are shown in Figure 4.4(a-10 to a-30). The graph clearly shows how the SWI occurs at ML1 in 30 years. The variations in the salt concentration in the model domain are shown in the plan view and the side view, Figure 4.2(b-10 to b-30) and Figure 4.4(b-10 to b-30), respectively. The figures with the numbers after the letter indicates the year to which the simulated result corresponds. The side view of this scenario was taken at ML 1. Hence, Figure 4.5a and Figure 4.4(b-10 to b-30) shows how the concentration was decreased at ML 1. However, seaward of ML 1, the concentration was ≈ 39.5 kg/$m^3$, shown in red.

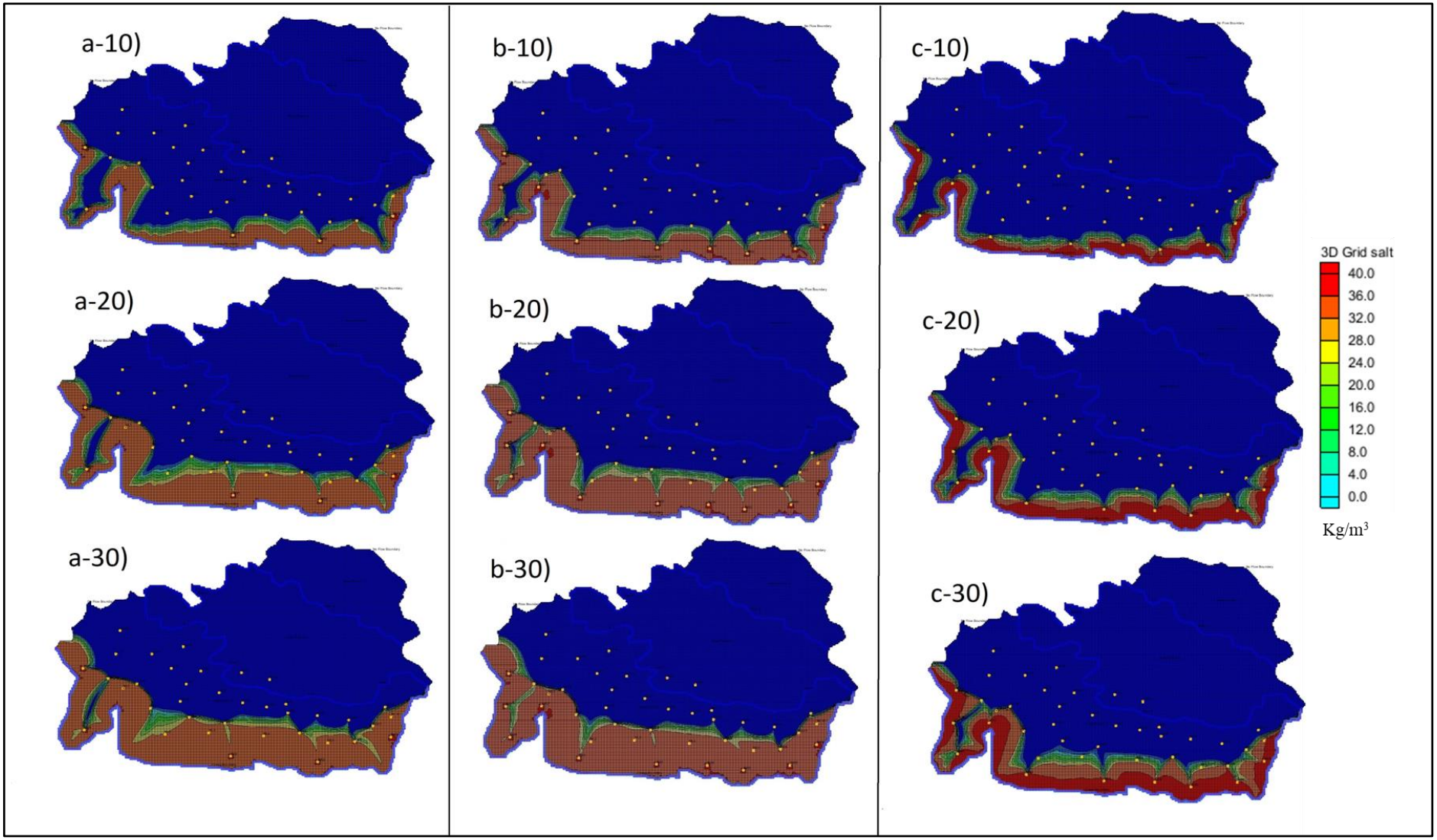



Figure 4.2: (a-10 to a-30), (b-10 to b-30) and (c-10 to c-30) shows the plan view of the simulated results of saltwater intrusion for the controlled area, the addition of barrier wells (scenario 1) and increasing the hydraulic conductivities and porosities (scenario 2), respectively.

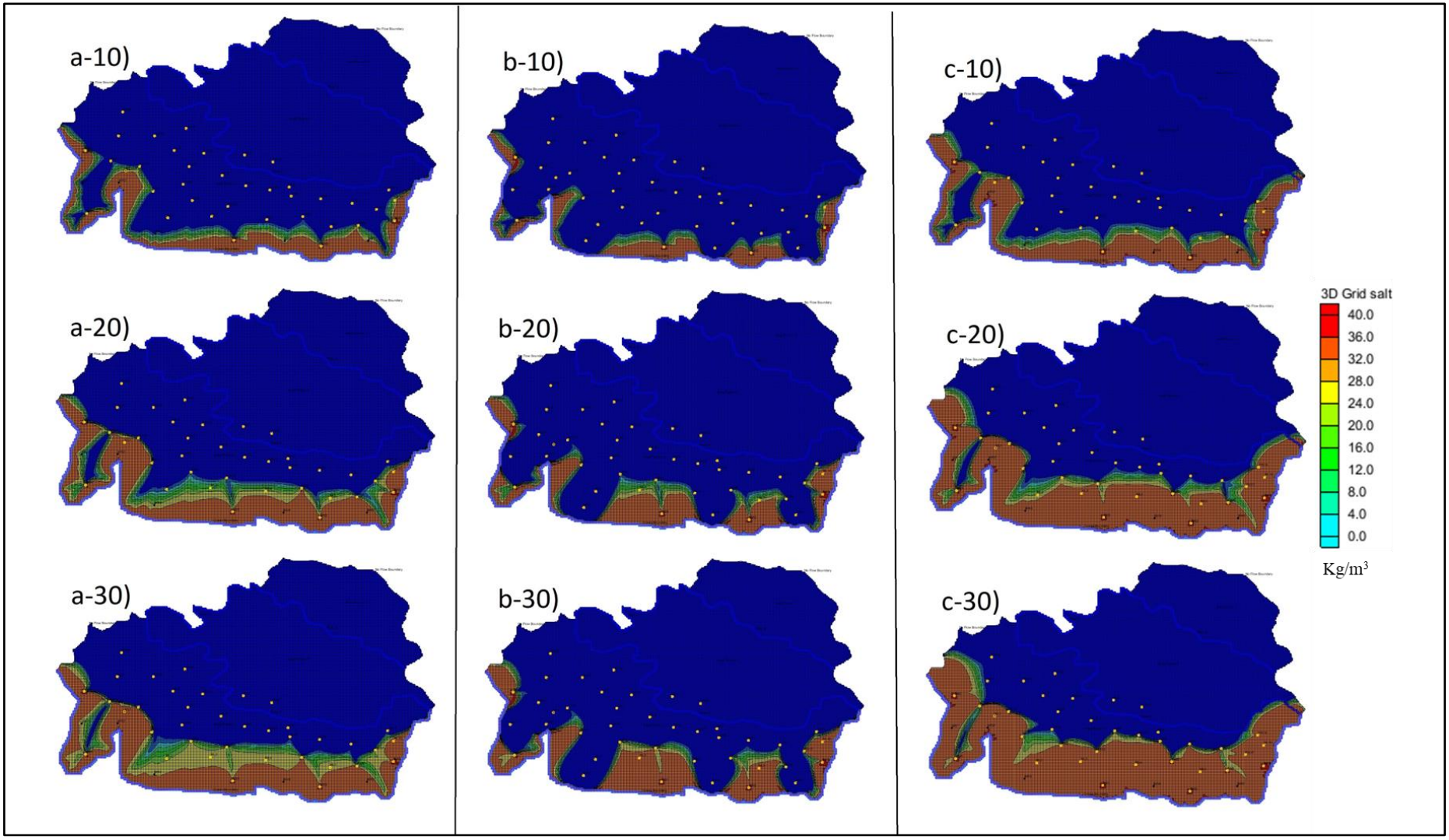



Figure 4.3: (a-10 to a-30), (b-10 to b-30) and (c-10 to c-30) shows the plan view of the simulated results of saltwater intrusion for changing recharge (scenario 3), the addition of injection wells (scenario 4) and increasing the hydraulic heads (scenario 5), respectively.

Moreover, 10 monitoring location wells (ML) were uniformly placed in the model domain to record the salt concentration values. The salt concentration after 10 years, 20 years and 30 years were plotted against the salt concentrations of these MLs without BW′ and any changes in the boundary conditions or hydrogeological parameters. To compare the changes in the salt concentrations at various MLs, a bar graph was plotted using the concentrations at 10 MLs with the new simulated values and the initial simulated values referred to as controlled values for this research. The comparison of different salt concentrations at different MLs is shown in Figure 4.5a. MLs 1-5 and 10 showed the changes in the concentrations, whereas MLs 6-9 did not show significant changes bearing the concentrations values close to 0 kg/m$^3$.

The salt concentrations for ML 1 at 10- 20- 30-year time step were decreased by 31.57%, 2.85% and 1.76%, respectively. For ML 2, the salt concentration at the 10-year time step was 0.054 kg/m$^3$, whereas the salt concentration for the initial set-up was 0.00053 kg/m$^3$. The 20-year time step and 30-year time step show 78.05% and 4.03% increase in salinity, respectively. For ML 3, no significant changes were noted for the 10-year time step, whereas 20-year and 30-year time steps show a 7.11% and 0.77% increase in salinity. For ML 4, 72.58%, 1.53% and 0.90% increments of salt concentration were noted for 10- 20- 30-year time steps, respectively. Similarly, for ML 5 and 10, the 10-year time step showed a significant increment of salt concentration, whereas the increase was relatively small for 20 and 30-year time steps.

### 4.5.2 Scenario 2: Increasing the hydraulic conductivity, porosity and BWs

The hydraulic conductivities and porosities in different area portions were increased by 50% from the initial values. The new hydraulic conductivities for area portions 1 to 3 were 20 m/d, 30 m/d and 40 m/d, respectively. The new porosity values for area portions 1 to 3 were 0.4, 0.54 and 0.64, respectively. Also, the extra BWs which was introduced in scenario 1 were also maintained in scenario 2. The plan view of the salt concentrations at different time steps for scenario 2 is shown in Figure 4.2(c-10 to c-30). From the graph, it can be seen that the saltwater flow into the aquifer from 10 to 30 years is reduced. However, the salt concentrations near the coastline have increased to a value of 39 kg/m$^3$. In addition, the saltwater did not reach PWs 1, 2, 8 and 10. Whereas, in the scenarios without changing the hydraulic conductivity and porosity, it shows the saltwater encroachments of the PWs close to the coastline.

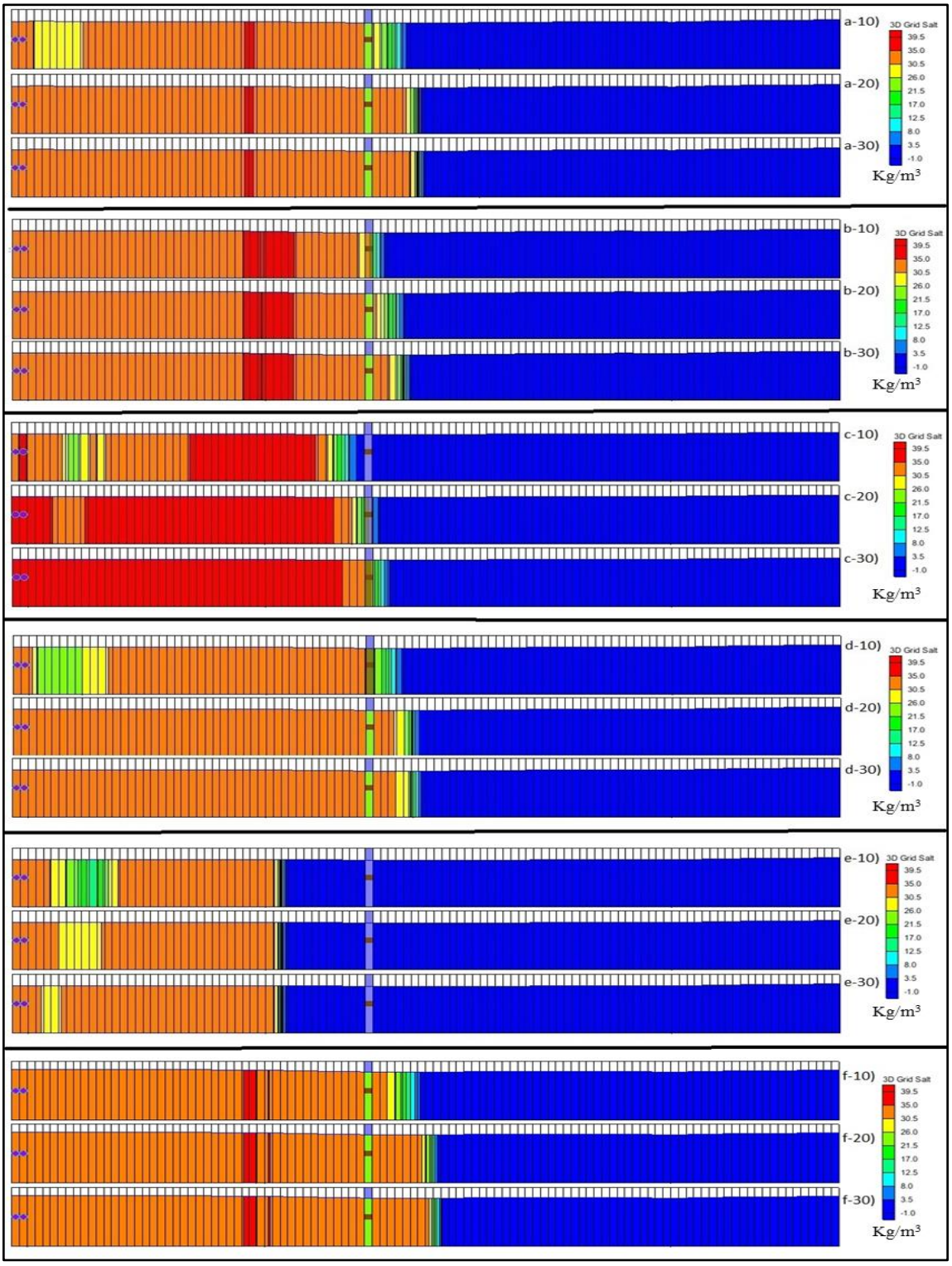



Figure 4.4: (a-10 to a-30); (b-10 to b-30); (c-10 to c-30); (d-10 to d-30); (e-10 to e-30) and (f-10 to f-30) shows the side view of the simulated results of saltwater intrusion at monitoring location 1 for the controlled area, the addition of barrier wells (scenario 1) and increasing the hydraulic conductivities and porosities (scenario 2), changing recharge (scenario 3), the addition of injection wells (scenario 4) and increasing the hydraulic heads (scenario 5), respectively. The -10, -20 and -30 represent the time steps 10, 20 and 30 years, respectively.

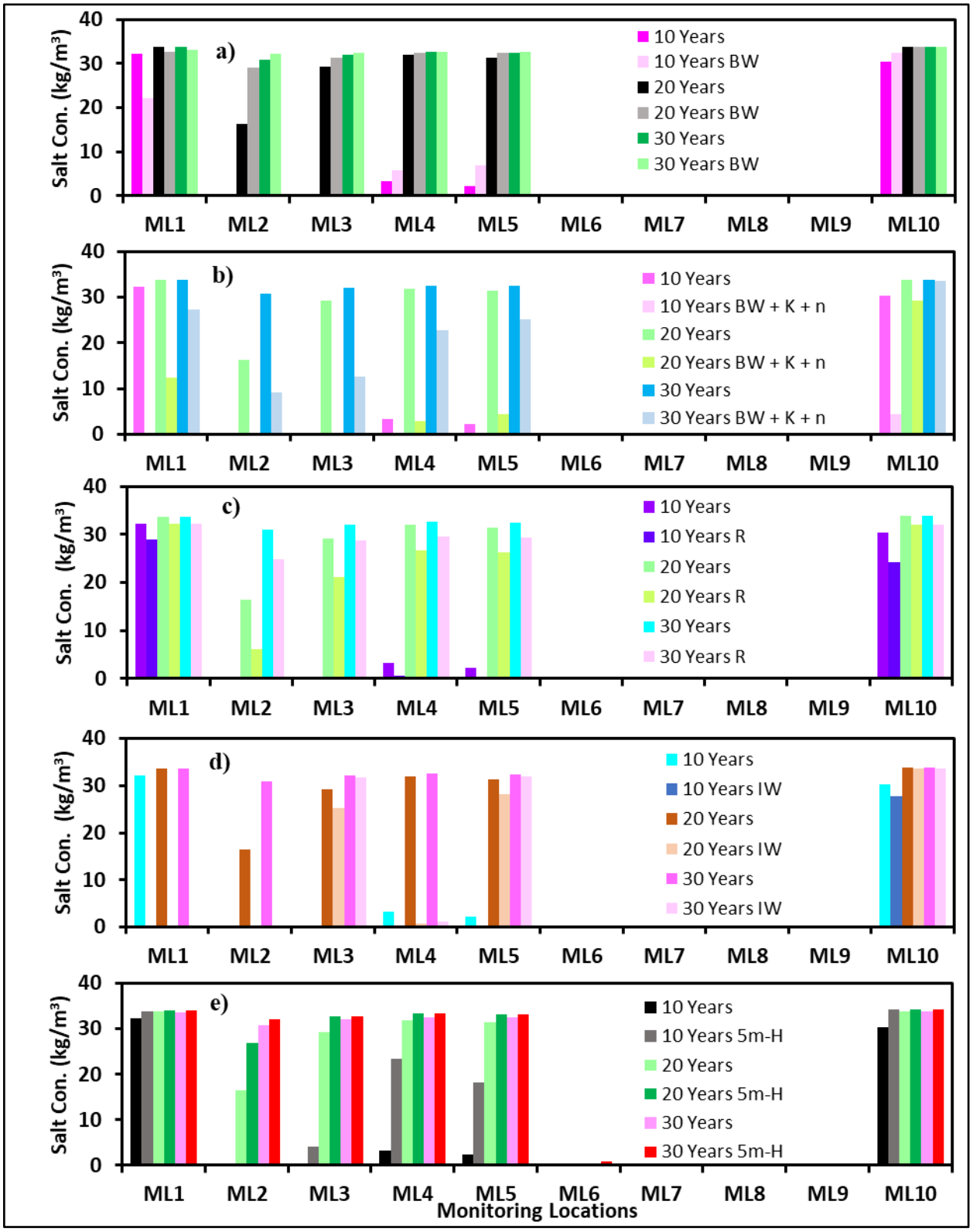



Figure 4.5: (a to e) shows the comparison of simulated salt concentrations at various monitoring locations for the controlled area against the addition of barrier wells (scenario 1), increasing the hydraulic conductivities and porosities (scenario 2), changing recharge (scenario 3), the addition of injection wells (scenario 4) and increasing the hydraulic heads (scenario 5), respectively.

The side view of scenario 2 was viewed from ML 1, and the results are shown in Figure 4.4(c-10 to c-30). From the graph, it can be seen that as the hydraulic conductivity and porosity increase, the saltwater concentration decreases. Also, the salt concentration towards the southwest of ML 1 has increased, as shown in dark red colours. These salt concentrations and SWI can be compared with the side view of scenario 1.

Moreover, the salt concentrations at 10 MLs were recorded after the SEAWAT simulation with increased hydraulic conductivities, porosities and BWs′. Only three-time step data was recorded to minimise the computational burden. A bar graph was plotted to compare the changes in the salt concentrations at various MLs with the controlled simulated results. The comparison of different salt concentrations at different MLs is shown in Figure 4.5b. MLs 1-5 and ML 10 showed the changes in the concentrations, whereas MLs 6-9 did not show any significant changes bearing the concentrations values close to 0 kg/m$^3$. The salt concentration decreased vastly at all MLs when the hydraulic conductivity and porosity increased.

The salt concentration at ML1 for the controlled simulated result was 32.248 kg/m$^3$, whereas the simulated concentration at ML 1 for this scenario was 0.0388 kg/m$^3$ for a 10-year time step. The difference in these two concentrations resulted in a 99.88% decrease in the salt concentration. Moreover, there was a 63.34% decrease at the 20-year time step and an 18.83% decrease at the 30-year time step for ML 1. Similarly, for ML 2, a 99.99%, 99.46% and 70.43% decrease in salt concentrations for 10- 20- and 30-year time steps were observed, respectively. For ML 3 and 4 at the 10- and 20-year time step, the concentrations decreased by more than 90%. However, the salt concentration for ML 3 at 30-year time steps decreased by 60.9%, and for ML 5, it decreased by 30.04%. A similar range of % decrease was noted for ML 5. For ML 10, at 10- 20- 30-year time steps, the salt concentration was decreased by 85.19%, 13.52% and 0.30%, respectively. Moreover, with increasing time, the difference in the salt concentrations at various MLs will be very less. To achieve this, the model was run for a longer time. However, in real life, there are a lot of uncertainties, and prediction becomes challenging.

### 4.5.3 Scenario 3: Increasing the recharge rate

The initial recharge value for the entire model domain was 0.0004 m/d. However, in this scenario, the recharge rate was increased into the model domain by 50%. The new recharge value for this scenario was 0.0008 m/d. All the other parameters and boundary

conditions remained the same. The BWs were also reduced to 5 as this was the initial set-up for the controlled or illustrative study area. The plan view of the salt concentrations at 3 different time steps for this scenario is shown in Figure 4.3(a-10 to a-30). The controlled results indicate that the salt concentrations for the coastal MLs (MLs 1-5, 10) are ≈ 35 kg/m$^3$, as shown in Figure 4.2(a-10 to a-30). The significant changes in the SWI show after 20 years as the saltwater concentrations are lower than 30 kg/m$^3$ for the coastal side MLs.

The side view of the saltwater movement into the coastal aquifer for this scenario was viewed from ML 1, and the results are shown in Figure 4.4(d-10 to d-30). The side view can be easily compared with other scenarios. However, the controlled side view was used to interpret the results. From Figure 4.4(d-10 to d-30), it can be seen that the salt concentrations at various grids around the ML 1 have decreased. The brackish water zone was also increased, as shown on the left side of Figure 4.4(d-10). The salt concentrations at 10 MLs were recorded for 3-time steps and compared with the initial simulated concentrations. A bar graph was also plotted for this scenario, and the results are shown in Figure 4.5c.

The bar graph was only significant for MLs 1-5 and 10, whereas MLs 6-9 had salt concentration values very close to 0 kg/m$^3$. From the bar graph, it can be seen that for all time steps, the concentration decreases if the recharge increases by 50%. The 10-year time step showed a considerable decrease in salt concentrations, with MLs 4 and 5 showing 81.98% and 78.79%, respectively. The 20-year and 30-year time steps for MLs 4-5 portrayed a 16.4% and 9.3% decrease, respectively. Similarly, other MLs showed a considerable percentage decrease in salt concentration for a 10-year time step, whereas, for 20-year and 30-year, the percentage decrease was not higher than 20%.

### 4.5.4 Scenario 4: Installation of injection wells

The number of BWs was 5 in the initial model set-up, and the same number of injection wells (IWs) was placed uniformly along the coastal boundary. IWs act as the groundwater system's source, adding water to the aquifers and increasing the total water volume. IWs were placed in the exact location where the extra BWs were placed and marked as BW′, as shown in Figure 4.1. The volume of water injected into the aquifer was 12000 m$^3$/d and was constant for the 30-year stress period. The plan view of the simulated results of this scenario is shown in Figure 4.3(b-10 to b-30). The results were

compared with the controlled simulated results. Adding IWs shows significant changes in saltwater flow into the aquifer system. The continuous pumping using PWs and injecting using IWs did not allow the saltwater to reach PWs 13, 14 and 15, even after 30 years.

The side view of ML 1 was also captured to see the saltwater movement after adding IWs, and the results are shown in Figure 4.4(e-10 to e-30). The results indicate that the salt water did not reach ML 1 for 10- 20- 30-year steps. Moreover, the brackish water zones were also formed, as shown on the far left side of all bars in the side view for this scenario. The IWs significantly reduced the salt concentrations around the surrounding area. It forms a barrier, and approximately within 1km of range, the saltwater does not come close to the PWs.

The salt concentrations were also recorded at various MLs after simulating the model using SEAWAT modules. The simulated results from this scenario were compared with the initial results. The salt concentrations for 10 MLs from this scenario and the controlled salt concentrations are shown in Figure 4.5d. MLs 1-5 and 10 showed the changes, whereas MLs 6-9 had salt concentrations of ≈ 0 kg/m$^3$. The salt concentration for all 3-time steps at ML 1 was 0.00067 kg/m$^3$. A significant 99.99% decrease in the salt concentration was noted compared with the initial simulated salt concentrations. Similar results were noted at ML 2 and ML 4. ML 3 had an 86.31% decrease for a 10-year time step, whereas the 20-year time step showed a 13.59% decrease, and the 30-year time step showed a 0.98% decrease. ML 10 showed an 8.6% decrease in salt concentrations at 10-year time steps, whereas it did not show significant variations in the salt concentrations for 20 and 30-year time steps.

### 4.5.5 Scenario 5: Increasing the hydraulic head

The hydraulic head was raised on the coastal boundary by 5m. The final coastal head values for the eastern and western nodes were 186m, respectively. The other head values of other boundaries remained the same. Also, other hydrogeological parameters remained the same. Initially, the head was raised by 1m. However, no significant change was noted in the simulated results. Hence, it was raised by a significant amount in this scenario. The plan view of the simulated results is shown in Figure 4.3(c-10 to c-30). The current result from this scenario was compared with the initial simulated results. The results indicate that raising the head on the coastal boundary allows the saltwater to flow

more easily into the model domain or the aquifer. All 3-time steps,10- 20- 30-year, showed that saltwater had moved further into the model domain when compared with the model where the heads were not raised.

The side view of the saltwater movement was also viewed at ML 1, and the results are shown in Figure 4.4(f-10 to f-30). The bars from Figure 4.4(a-10 to a-30) differentiates the salt concentrations at all 3-time steps. More saltwater has moved into the model domain, as shown from the side view as well. On the seaward of ML 1 grids, the salt concentrations at all 3-time steps show a considerable salt concentration of 39.5 kg/m$^3$, marked in red. Increasing the hydraulic head shows significant changes in the salt concentration compared with other scenarios, as shown in Figure 4.4.

Similar to other scenarios, after changing the head values at the coastal boundary, the simulation was performed using the SEAWAT module. The new simulated salt concentrations were compared with the initial simulated salt concentrations at various locations in the study area. Salt concentrations at 10 MLs were compared using bar graphs, as shown in Figure 4.5e. The salt concentrations at MLs 1-5 and 10 were significant, whereas the salt concentrations at ML 6 were slightly significant only for the 30-year time step. MLs 7-9 had salt concentration values of ≈ 0 kg/m$^3$. The salt concentration at ML 1 at 10- 20- 30-year steps increased by 4.93%, 0.79% and 0.81%, respectively. At ML 2, the salt concentration for a 10-year tie step was ≈ 0 kg/m$^3$, whereas, with time, the salt concentration at a 20-year time step increased by 63.9% compared with the initially simulated salt concentrations at these locations. However, a slight increase in the concentration was noted for the 30-year time step for ML 2.

The concentration at ML 3 for a 10-year time step was 4.01 kg/m$^3$, whereas the controlled simulated concentration was 0.00053 kg/m$^3$. For 20-year and 30-year time steps, the concentration increased by 11.78% and 2.19%, respectively. For ML 4 at 10- 20- 30-year time steps, the salt concentration increased by 607%, 4.66% and 2.18%, respectively. For ML 5 at 10- 20- 30-year time steps, the salt concentration increased by 701%, 5.94% and 2.47%, respectively. For ML 6, the concentration at the 30-year time step was 0.89 kg/m$^3$, whereas, at other time steps, it was ≈ 0 kg/m$^3$. The ML 10 showed fewer variations in the concentrations for this scenario. However, the concentrations were increased by 12.86%, 1.62% and 1.70% for the 10- 20- 30-year time steps, respectively.

### 4.5.6 Scenario 6: Changing the model grid size

The initial grid size for developing the numerical simulation model was 50m x 50m. In this scenario, two different grid sizes were used to discretise the model domain. Firstly, the grid size was reduced to 25m x 25m, and the salt concentrations at 10 MLs were recorded. Secondly, the grid size was increased to 100m x 100m, and the salt concentrations were again recorded for all MLs. The different salt concentrations at two different grid sizes were compared with the 50m x 50m grid salt concentrations. The box-and-whisker plot was produced to compare all three grid-size sensitivities, and the results are shown in Figure 4.6a.

The box-and-whisker plot for all three grid sizes at 10- 20- 30-year time steps for 10 MLs are plotted side by side. For the 10-year time step, the mean values for 25m x 25m, 50m x 50m and 100m x 100m are 16.03 kg/m$^3$, 11.38 kg/m$^3$ and 12.07 kg/m$^3$, respectively. For the 20-year time step, the mean values for 25m x 25m, 50m x 50m and 100m x 100m are 33.68 kg/m$^3$, 29.40 kg/m$^3$ and 29.45 kg/m$^3$, respectively. For the 30-year time step, the mean values for 25m x 25m, 50m x 50m and 100m x 100m are 34.99 kg/m$^3$, 32.58 kg/m$^3$ and 32.59 kg/m$^3$, respectively. Moreover, one outlier was noted for the 25m x 25m grid at a 20-year time step. This outlier was from ML 2, with a value of 27.79 kg/m$^3$. All other values were within the 34 to 35 kg/m$^3$ range.

The regression correlation between the 25m x 25m, 50m x 50m and 100m x 100m grid size and the changes in the concentrations at each MLs were also analysed, and the results are shown in Figure 4.6(b-c). The correlation between the 50m x 50m and 100m x 100m grid shows that for 10- 20- 30-year time steps, the coefficient of determination ($R^2$) value was 0.986, 0.999 and 0.987, respectively. Moreover, the correlation between the 50m x 50m and 25m x 25m grid shows that for 10- 20- 30-year time steps, $R^2$ value was 0.913, 0.961 and 0.434, respectively. The low value of $R^2$ was observed for the correlation between the 30-year salt concentrations of 50m x 50m and 25m x 25m. However, the average percentage change between the two sets of concentrations at ML 1-5 and 10 was 7.49%. Moreover, the time taken by the model to converge for 25m x 25m, 50m x 50m and 100m x 100m were 57 minutes, 5 minutes and 1 minute, respectively.

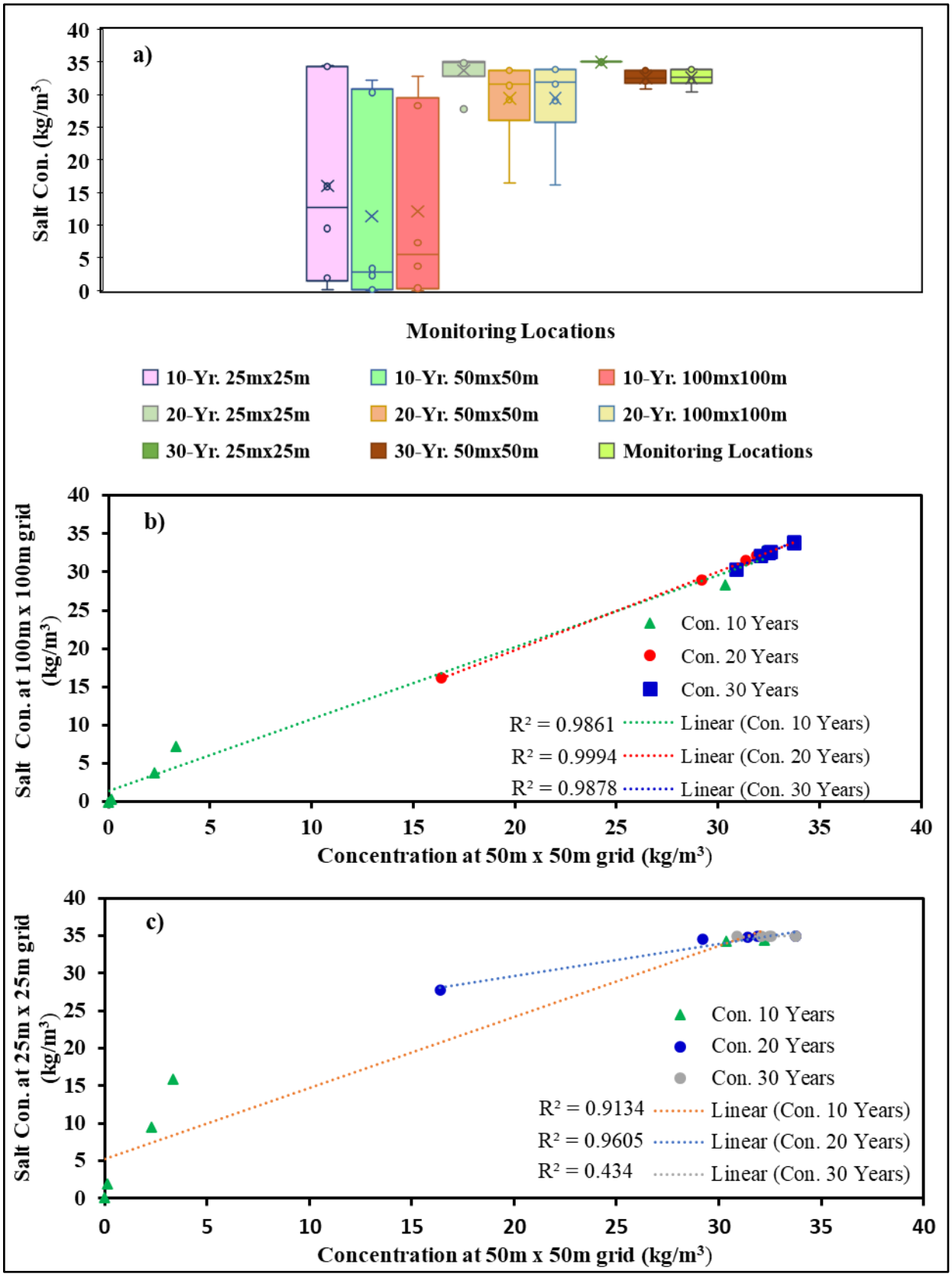



Figure 4.6: (a to c) shows the box plot of simulated salt concentrations obtained by using different grid sizes, the linear correlation of 100m x 100m and 50m x 50m grid results, and the linear correlation of 50m x 50m and 25m x 25m grid results, respectively.

### 4.5.7 Scenario 7: Multi-species contaminant transport

The numerical simulation model was made more complex by adding two contaminants towards the northern and eastern sides of the model domain, as shown in Figure 4.1. An industrial dumping site was at the northern side of the model domain, and some fluids were leaking into the ground due to the cracks in the industrial concrete dump. Similarly, there was a big automotive workshop towards the eastern side of the study area, near river 1. The automotive workshop does car servicing, and due to improper disposal of automotive engine oil, some leak into the ground. For this scenario, SEAWAT was used to simulate the leachate from the industrial dump site and oil leakage from the automotive workshop into the illustrative study area. The parameters used to solve the coupled flow and transport equations for two different species are given in Table 4.3.

The stress period for leachate and oil contaminants was 30 years. Simultaneously solving the flow and transport equations at every node, the SEAWAT simulated the multi-species contaminants, and the results are shown in Figure 4.7. Figure 4.7(a-15 and a-30) are the simulated results for leachate at 15-year and 30-year time steps, respectively. As the stress period increases, the leachate spreads and moves with the groundwater flow in the unconfined aquifer. The leachate reached PW3 after 30 years and contaminated the well with a leachate concentration of ≈ 600 kg/m$^3$. Similarly, Figure 4.7(b-15 and b-30) are the simulated results for engine oils at 15-year and 30-year time steps, respectively. Parts of river 1 and PW11 were slightly contaminated at a 15-year time step with engine oils. However, at a 30-year time step, the parts of river 1, PW11 and PW6 were highly contaminated with engine oils. The concentration of oil at PW6 and PW11 was 450 kg/m$^3$ and 283 kg/m$^3$, respectively.

Leachate and engine oil were initially simulated with advection, dispersion, sources, and sink packages from MT3DMS modules. However, in reality, some solutes get sorbed and dissolved into the groundwater system. Hence, chemical reaction packages were also included in MT3DMS, and the results are shown in Figure 4.7(a-15-s to b-30-s), where -15-30 indicates the time steps and -s indicates the inclusion of sorption in the simulated results. Sorption is when the liquid contaminants get attached to the charged soil particles. The bond between the ions can be weak or covalent bonds. The sorption process makes the contaminants travel and disperses at much slower rates. Figure 4.7(a-15-s and a-30-s) demonstrate sorption. Including the sorption process, the water from

PW3 is safe even after 30-year time steps. Similarly, Figure 4.7(b-15-s and b-30-s) demonstrates the sorbed oil in the aquifer. After 30 years, the PW6 was not affected. However, the engine oil has reached near PW11, and after a few more years, it will contaminate the well.

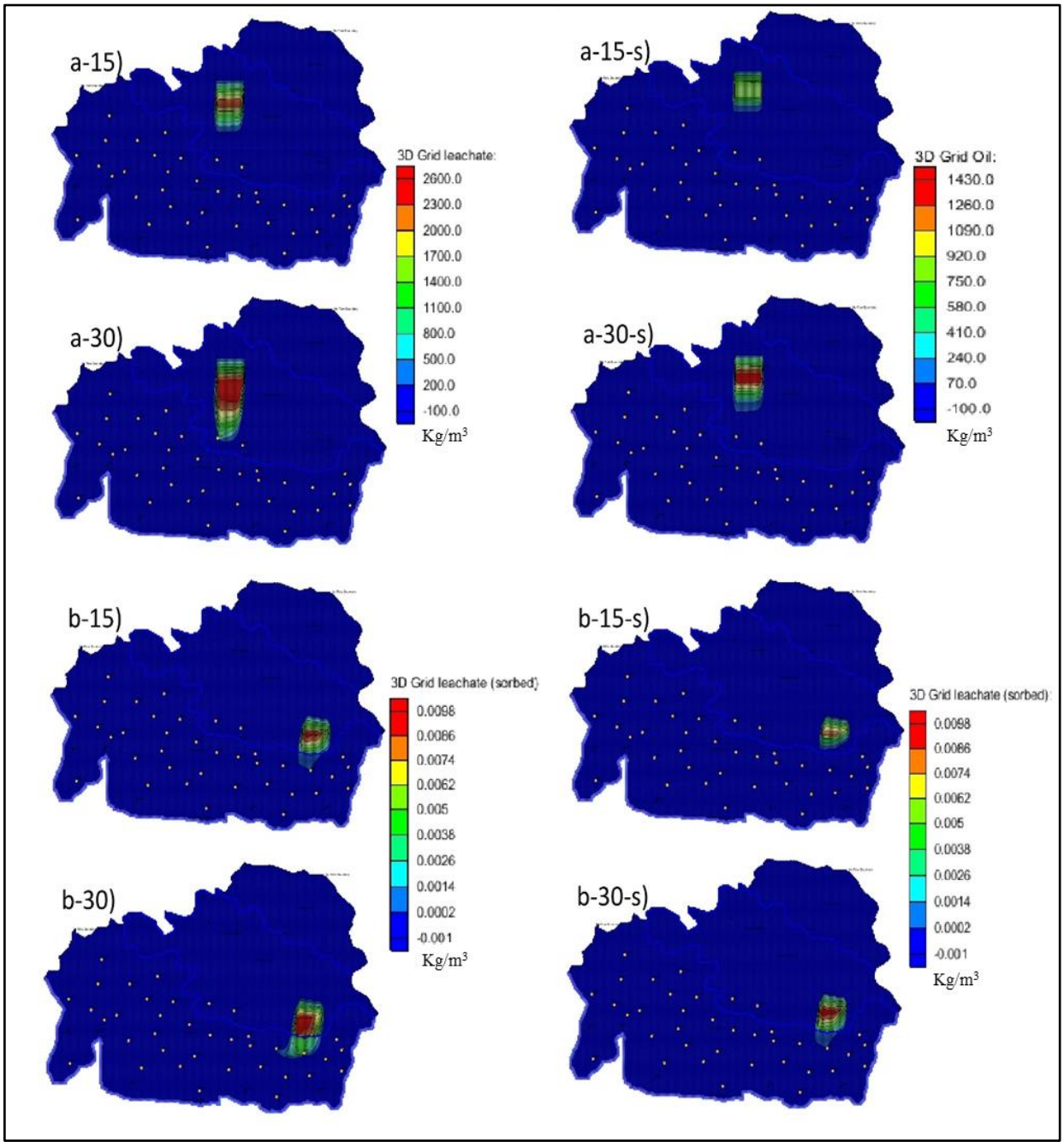



Figure 4.7: (a-15 to a-30) shows the leachate concentrations for 15 and 30-year time steps; (a-15s to a-30s) shows the leachate concentrations for 15 and 30-year time steps after sorption and chemical reactions. (b-15 to b-30) shows the engine oil concentrations for 15 and 30-year time steps; (b-15s to b-30s) shows the engine oil concentrations for 15 and 30-year time steps after sorption and chemical reactions.

## 4.6 Discussion

The SWI in the coastal aquifer is a significant concern for PICs. An illustrative study area in the context of PICs was considered for this study to manage and control the SWI. Different scenarios that affect the SWI in coastal aquifers were tested. The scenarios presented in this study were the first for PICs. Moreover, the multi-species contaminants were modelled to see how they affect the freshwater wells. Based on these scenarios, the governing bodies can draft and implement the SWI and other contaminant management policies.

The scenarios that effectively showed the decline in SWI in coastal aquifers were increasing the injection wells (IWs) and the aquifer's recharge. The salt concentration and SWI are highly sensitive to hydraulic conductivity as well. The increase in barrier wells (BWs) was also helpful in controlling the SWI. Armanuos et al. (2020) studied how the BWs control SWI in sloping unconfined aquifers and found that BWs are very effective in facilitating the retreat of SWI in coastal aquifers. Similarly, the results also indicate that SWIs are controlled by adding BWs. However, the placement of barrier wells has to be carefully considered. In the current study, the BWs were uniformally placed in the model domain, which reduced the SWI in some areas, whereas some areas had increased SWIs.

The BWs simulated results in plan view showed that the hydraulic gradient is towards the sea. Hence, the saltwater moves away from the BWs and flows in a different direction, eventually causing the concentrations at MLs to increase. However, in other locations, the salt concentrations have decreased. Therefore, introducing BWs and placing them in the model domain is essential. Hence, the best possible locations can be simulated for placing and digging BWs to prevent the SWI and contaminating the freshwater wells using trial-and-error methods. Optimisation methods can also be used to find the optimal locations of BWs that can manage the SWIs. However, this component was not included in the current study. Therefore, placing the BWs is essential if they were to be used to control SWI in coastal aquifers. However, BWs sometimes remove more freshwater than salty water, decreasing freshwater resources (Pool and Carrera, 2010). Also, the disposal of abstracted saline water can also become an issue (Kumar, 2006).

Adding the injection wells (IWs) can effectively control the SWI if placed in the correct locations. IWs can reduce the SWI and change the saline water flow directions.

However, the injection wells could be placed near the toe of the saltwater wedge in models if the toe location is known. Luyun and Momii (2011) reported that IWs would be more effective if placed at the saltwater wedge's toe. The authors also reported that deeper barrier penetration and closer to the coast would effectively control SWI. Similarly, in the current study, the modelled results showed that the BWs and IWs placed closer to the coast and near the toe of the saltwater wedge effectively reduced salt concentrations in various monitoring location wells (MLs). However, the addition of BWs and IWs can be costly and time-consuming.

The recharge is also a vital boundary condition that needs to be considered when modelling and pumping groundwater. Sometimes the recharge can be the only source to the system that can keep the freshwater volume within limits and prevent the wells from drying up. In one of the scenarios, the recharge of the entire model domain was increased by 50%, and the results were quite fascinating. The salt concentration at various MLs was reduced. Hence, increasing the recharge reduces the SWI. Similar results were also reported by Motallebian et al. (2019) and Hussain et al. (2019).

The model sensitivity of hydraulic conductivity and porosities was also tested, where it was found that the higher the hydraulic conductivity, the lesser the saltwater moves into the model domain. The hydraulic conductivities were also reduced and the results were simulated. It showed that the SWI into the model domain was increased. The increase was shown because the hydraulic gradient was from the northern side of the model to the southern side (coastal boundary). The head was lower in the coastal boundary. Hence, the saltwater would travel less if hydraulic conductivities were increased. Also, the higher amounts of pumping enabled a lot of drawdowns, which must have reduced the SWI rates. However, the results were the opposite after changing the head of the coastal side to be higher than the northern boundary.

In the current study, it was found that if the hydraulic gradient is from land-ocean and has significant pumping wells, increasing the hydraulic conductivity will decrease the SWI. If the hydraulic gradient is from ocean-land and has significant pumping wells, increasing the hydraulic conductivity will increase the SWI. The increased hydraulic conductivities resulted in higher SWI, and decreased hydraulic conductivities reduced SWI. The reduction in SWI by reducing the hydraulic conductivities was also reported by Dror et al. (2004) and Strack et al. (2016). Both these studies used laboratory

experiment setups. Hence, in the current study, the developed numerical models demonstrated similar results.

Moreover, the hydraulic gradient plays a vital role in SWI, as shown in the results. During the initial model design, modellers must carefully incorporate the hydraulic head values based on the field observations. This will help to provide better arguments on whether to increase or decrease the hydraulic conductivities to control the SWI. Hydraulic conductivities can be artificially increased or decreased by injecting the compressed air into the soil consisting of the coastal aquifers (Dror et al., 2004). Christiansen (1944) earlier reported that the trapped air can significantly reduce the hydraulic conductivities, whereas the loss of trapped air can significantly increase the hydraulic conductivities of soil. Changing the hydraulic conductivities will have significant effects on SWI in coastal aquifers.

Climate change and sea-level rise (SLR) were also considered in this study, where the hydraulic heads of the coastal side were increased due to increasing sea levels. The global projected SLR is ≈ 0.3m by the year 2050 (Rebecca, 2022). Initially, the heads were increased by adding 0.3m to the coastal heads, then increasing it by 1m. The results did not show significant variations in the salt concentrations at various MLs if the heads were increased to 1m. Loaiciga et al. (2011) also tested the SLR scenarios within 0.5-1m and reported that SLR would have minor contributions to SWIs. However, to see the actual SWIs due to SLR, the heads were increased by 5m, and then the SWI was significant. Increasing the heads on the coastal boundaries allows more SWI into the model domain. Therefore, an increase in sea level by a significant amount only contributes to SWI. However, at the current global SLR projections, the SWIs are not significant. Hence, climate change and SLR may increase the SWIs for coastal aquifers in future.

The sensitivity of grid size to the final model simulated results was also tested. Changes in grid size (discretisation) does influence the numerical simulation results. Therefore, it is essential to ensure that discretisation does not vary the simulation results by more than an acceptable (e.g., 5-10%) range. The current results revealed that the increase or decrease in the grid size of the simulated results did not vary more than 10%. However, the computational burden was increased when the grid size was decreased. It took approximately 57 minutes for the model to converge. The grids have to be selected

based on the accuracy of model convergence, computational time and outputs should not vary much. Moreover, according to Barnett et al. (2012), if the grids are refined locally, the increase in node spacing or grid size between adjacent elements must be maintained in limits to avoid computational burdens with significant contrasts in cell size. The authors also stated that as a rule of thumb, a factor of 1.5 should be kept as the maximum ratio of the volumes of neighbouring cells. Hence, for the current study, 50m x 50m cells were ideal in computations.

Studies on multi-species contaminants using SEAWAT in PICs have not been done so far. Also, to the best of the current knowledge, very few studies have been conducted showing SWI and other contaminants. However, this is the first study where SWI and the other two species are modelled using SEAWAT. In the current study, salt, leachate and engine oil were used as contaminants. They were modelled using dispersion, advection and chemical reaction packages inbuilt the latest version of SEAWAT. The current model tested how the three species affect the freshwater lens with time. The saltwater intrusion, leachate and engine oil plumes were clearly shown in the results section. However, as shown in the results, sorption and adsorption rates were also added to the leachate and engine oils, which reduced the plume size. Al-Hashimi et al. (2021) reported that sorption, adsorption, and other chemical reactions reduce the contaminations and can help in remediations.

## 4.7 Conclusions

The groundwater modelling for an illustrative study area in the context of Pacific Island countries (PICs) is presented in this work. An actual aquifer and pumping locations were treated as the illustrative study area because the hydraulic head and enough pumping data were unavailable to calibrate and validate the model. However, some of the hydrogeologic parameters and boundary conditions were realistic. The multi-species solute and heat transport module SEAWAT was used to model the study area. Seven different scenarios were tested using SEAWAT. The scenarios presented here and the different sensitivity analysis conducted in this study have never been conducted for PICs. The model and the simulated results were sensitive to various parameters presented in this study. The main aim of the scenario testing was to manage or control the saltwater intrusion into the current coastal aquifer.

The scenarios that provided the best saltwater intrusion management strategies were using injection wells to pump freshwater near the toe of the saltwater wedge, increasing the recharge of the system, using barrier wells and decreasing or increasing the hydraulic conductivities. The hydraulic gradient will determine whether to increase or decrease the hydraulic conductivities to manager SWI. The location of placing the barrier wells is essential, and it can be achieved by placing the wells within the model domain using the trial-and-error method and simulating the lowest salt concentrations at various monitoring locations and pumping wells. Furthermore, the rise in sea level by 0.3 to 1m did not substantially impact SWI rates. Moreover, it is essential to ensure that changes in the grid size do not vary the simulation results by more than an acceptable (5-10%) range.

Multi-species contaminants can be modelled using SEAWAT, and different packages can be used to see the flow, direction and size of the contaminant plumes. The current study established that the application of advection, sorption, adsorption and other chemical reactions slows the flow velocity and direction of the contaminant plumes. The limitation of this study was that there were not enough field hydraulic head, pumping, and water concentrations at various locations. The model could have been calibrated and validated if there were field data. However, PICs do not have all the required data to develop a numerical model using SEAWAT. Moreover, PICs do not have data for other contaminants like engine oil and leachate. PICs need funding and expertise for ground-level work in setting up the groundwater monitoring equipment. Hence, with the field data, better SWI management strategies and models could be developed for PICs.

The current chapter developed a 3D model to simulate saltwater intrusion. However, the next chapter further develops a 3D model using complex boundary conditions. The 3D model is developed using randomised hydraulic conductivities. Most aquifers are heterogeneous and anisotropic. Hence, to simulate the actual geology type of an aquifer, the hydraulic conductivities were randomised, and different scenarios were modelled in the next chapter.

# Chapter 5: Stochastic application in numerical simulation model for groundwater salinity management and decision-making

The main contents of this chapter have been published and copyrighted as outlined below:

**Sharan, A**., Datta, B., & Lal, A. (2024). Stochastic Application in the Numerical Simulation Model for Groundwater Salinity Management and Decision-Making. In: Ghute, B.B., Diwate, P. (eds) Geospatial Technologies for Integrated Water Resources Management. GIScience and Geo-environmental Modelling. Springer, Cham. https://doi.org/10.1007/978-3-031-57777-2_12

## 5.1 Overview

This chapter develops a 3D model using randomly generated hydraulic conductivities. It also tests the sensitivity analysis using randomised hydraulic conductivities and provides different saltwater intrusion management strategies for a coastal aquifer.

## 5.2 Executive Summary

Groundwater modelling is the process of creating mathematical representations of groundwater systems to simulate the flow and transport of water and solutes in subsurface environments. It is a crucial tool for understanding and managing groundwater resources, particularly in areas where water scarcity is a concern. Groundwater numerical simulation models can predict future water availability, assess the impacts of land use changes on groundwater resources, and evaluate the effectiveness of water management strategies. In the present study, a 3D numerical simulation model was developed using SEAWAT numerical code. An illustrative study area was used to test different scenarios that can help manage saltwater intrusion in a coastal aquifer. Randomised hydraulic conductivities were also used in 3D model simulations. The scenarios tested in this study used different hydraulic barriers in mitigating saltwater intrusion. The results from this study indicated that using injection wells and barrier wells reduces saltwater intrusion rates. Moreover, it was also demonstrated that using randomised hydraulic conductivities at different nodes is possible using the SEAWAT code. The results from this study are essential in changing the modern world where water is scarce. The noble outcome presented in this study provides insights for groundwater modellers in managing saltwater intrusion in coastal

aquifers. However, the complexity of groundwater systems and the limitations of available data mean that modelling is still an ongoing challenge, and uncertainty is always a factor to consider. Nevertheless, with continued improvements in modelling techniques and increased data availability, groundwater modelling is poised to remain a vital tool for groundwater salinity management and overall decision-making.

## 5.3 Introduction

Groundwater is an essential natural resource that plays a significant role in supporting human activities and sustaining ecosystems. It is defined as the water that is stored beneath the Earth's surface in permeable rock layers called aquifers. Groundwater is an essential source of drinking water, accounting for approximately 20% of the global freshwater supply (UNESCO, 2021). Additionally, it is widely used for irrigation, industrial processes, and other domestic purposes. Groundwater resources are unevenly distributed across the globe, and some regions, such as arid and semi-arid areas, rely heavily on this resource for their livelihoods (Scanlon et al., 2012; Sharan et al., 2021).

Groundwater systems are complex and dynamic, influenced by various physical and environmental factors. The recharge of groundwater occurs through natural processes such as precipitation and infiltration, while discharge occurs through springs, streams, and wells. The interaction between groundwater and surface water is vital for maintaining the health of aquatic ecosystems and meeting water demands for different sectors (Alley et al., 1999). However, excessive groundwater pumping can lead to depletion and subsidence of the land surface and saltwater intrusion in coastal areas (Sharan et al., 2023a; b).

Groundwater quality is also an essential aspect of groundwater management. Groundwater can become contaminated by natural and human-made sources, such as agricultural chemicals, industrial waste, and septic systems. Contaminated groundwater can pose significant risks to public health and the environment and be difficult and costly to remediate (Li et al., 2021). Therefore, monitoring and managing groundwater quality are crucial for ensuring the sustainability of groundwater resources. Climate change is also a growing concern for groundwater management.

Changes in precipitation patterns and temperatures can affect groundwater recharge rates and alter the distribution of groundwater resources. Additionally, extreme weather events such as floods and droughts can significantly impact groundwater systems

(UNESCO, 2021). Effective management strategies such as water conservation, land use planning, and pollution control are necessary to mitigate the effects of climate change on groundwater resources and ensure their long-term availability and quality.

Groundwater use in coastal regions and small island nations like Pacific Island countries (PICs) is widespread. Excessive usage of groundwater leads to saltwater intrusions (SWI). SWI is a growing concern in coastal regions where freshwater aquifers are close to the coastline. It occurs when saltwater infiltrates and replaces freshwater in coastal aquifers due to excessive pumping of groundwater, sea-level rise, and other human activities (Sharan et al., 2021). The process of saltwater intrusion is driven by the differences in density between saltwater and freshwater, as well as the hydraulic gradients in the aquifer system (Werner et al., 2013). Once SWI occurs, it can significantly impact the quality and quantity of groundwater resources and the ecosystems and human communities that depend on them. The simple process of SWI is shown in Figure 5.1.

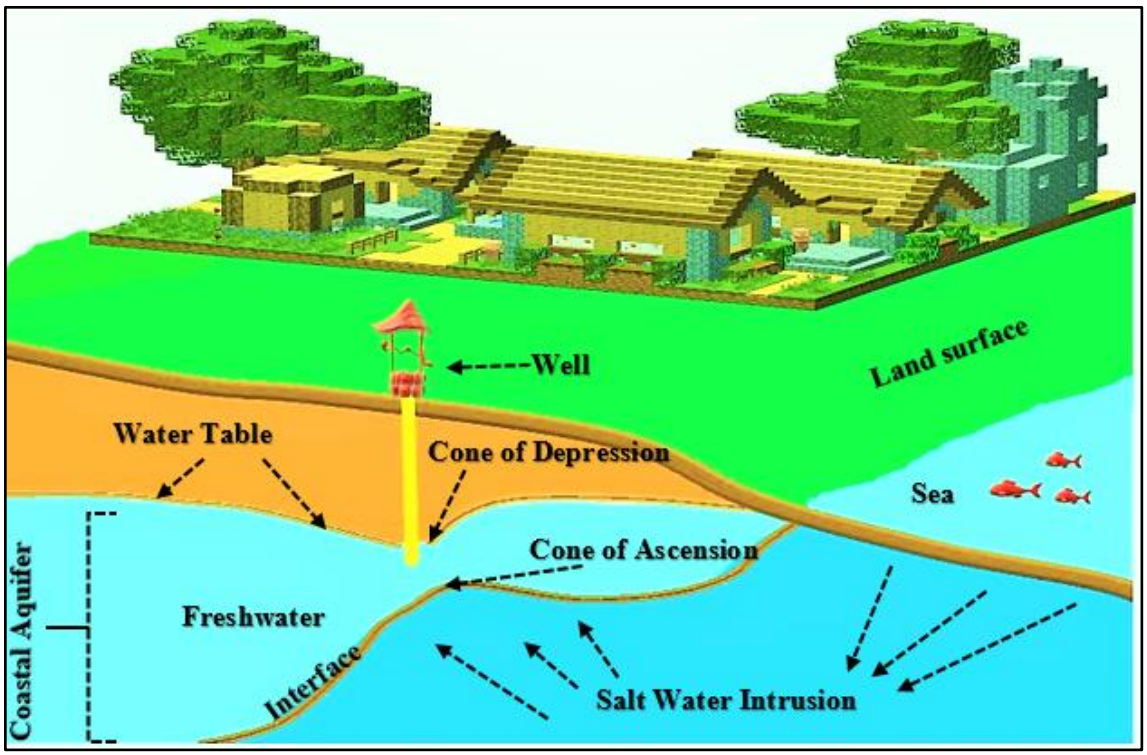



Figure 5.1: Simple process of saltwater intrusion in coastal aquifers. Source (after Sharan et al., 2021).

The impacts of SWI on coastal aquifers can be severe. The intrusion of saltwater can reduce the availability of freshwater resources, making it difficult for communities and industries to access water for drinking, agriculture, and other purposes. Additionally, the increased salinity of the groundwater can adversely affect the environment and

wildlife, particularly in wetlands and estuaries where freshwater and saltwater ecosystems intersect. SWI can also lead to increased corrosion of infrastructure, such as pipes and wells, which can have economic implications for communities and industries.

Effective management strategies are necessary to mitigate the impacts of SWI on coastal aquifers. These strategies can include reducing groundwater pumping rates, promoting water conservation measures, and implementing artificial recharge methods, such as injecting treated wastewater or surface water into the aquifer system (Sharan et al., 2023a; b). Additionally, monitoring the quality and quantity of groundwater resources is essential for identifying early warning signs of saltwater intrusion and acting before it becomes a significant problem. Collaborative approaches involving government agencies, water users, and other stakeholders are crucial for ensuring the long-term sustainability of coastal aquifers.

Numerical modelling is one of the primary techniques used to draw up robust SWI management strategies around the globe (Lal and Datta, 2019). However, using the correct code to develop the numerical models is also challenging due to the availability of quality groundwater data. Sharan et al. (2023a;b) used a complex heterogenous illustrative study area to test different scenarios that can manage SWI in the context of small island nations. The authors used simulated-synthetic data and SEAWAT code to develop their models. However, they used realistic hydrogeological data and boundary conditions from a particular Pacific Island country. The authors found that injection wells and increased recharge reduce SWI.

Hagagg (2019) utilised the SEAWAT programme to investigate the extent of saltwater intrusion (SWI) in the El Negila karstic aquifer at coordinates 30.75° N and 30.698° E. The researcher evaluated various scenarios, such as increased sea levels and pumping rates, for 2022. The study found that if the pumping rates and sea level heights increase, the SWI would also increase. Similarly, Hamidi et al. (2021) employed the SEAWAT model to simulate the SWI in the Rmel-Oulad Ogbane coastal aquifer in Larache, Morocco. The focus of the study was on two scenarios, which were climate change and sea-level rise (SLR). The research found that the over-pumping of groundwater and SLR due to climate change were the main factors responsible for SWI

in coastal aquifers. Additionally, climate change was found to reduce natural recharge, decreasing fresh groundwater resources.

Moreover, several studies have used the SEAWAT code to model the SWI and provide some strategies to mitigate the SWI. However, very few or, to the best of the current findings, no one has used randomised hydraulic conductivity (RHC) in SEAWAT modelling. Hydraulic conductivity is a crucial hydrogeological parameter that is important when developing a numerical model. RHC is a technique used in groundwater modelling to simulate spatial heterogeneity in aquifer properties. This approach involves assigning different hydraulic conductivity values to different cells in the model domain based on a probability distribution function.

This study will use the RHC values in the SEAWAT code to develop a numerical model for an illustrative study area. The results will be compared with the normal or uniform hydraulic conductivities with the RHC. The study will also show how vital the RHC are in heterogeneous aquifers and its application in improving the model predictions. Some hydraulic barriers, like injection wells and barrier wells, were also tested to mitigate the SWI in this study. This study is critical, and the novel insight from this study is that, to the best of the current knowledge, no studies have used randomised hydraulic conductivities in the SEAWAT code to develop a numerical model for a coastal aquifer. The methods used to randomise the hydraulic conductivities are also the first to be used in this study. This study will explain why RHC is better than using uniform hydraulic conductivities. The results from this study will assist hydrogeologists and groundwater modellers in easily randomising hydraulic conductivities. Also, the water managers and governing bodies may use the strategies discussed in this study to draw robust water policies for any coastal region.

## 5.4 Materials and Method

### 5.4.1 Study area

The study area for this research was Suva (18.14$^{o}$ S, 178.42$^{o}$ E), the capital of Fiji. Fiji is a beautiful tropical paradise in the South Pacific Ocean, known for its breathtaking beauty and warm hospitality. This archipelago of more than 300 islands offers stunning white sandy beaches, crystal-clear turquoise waters, and lush greenery, making it a dream destination for beach lovers and nature enthusiasts. The country's rich cultural heritage is deeply rooted in the traditions of its indigenous Fijian people, as well as the influences of

Indian, Chinese, and European settlers. Visitors to Fiji can immerse themselves in the vibrant local culture, enjoy a range of water activities such as snorkelling and diving, and explore the stunning landscapes that include pristine rainforests, waterfalls, and volcanic peaks.

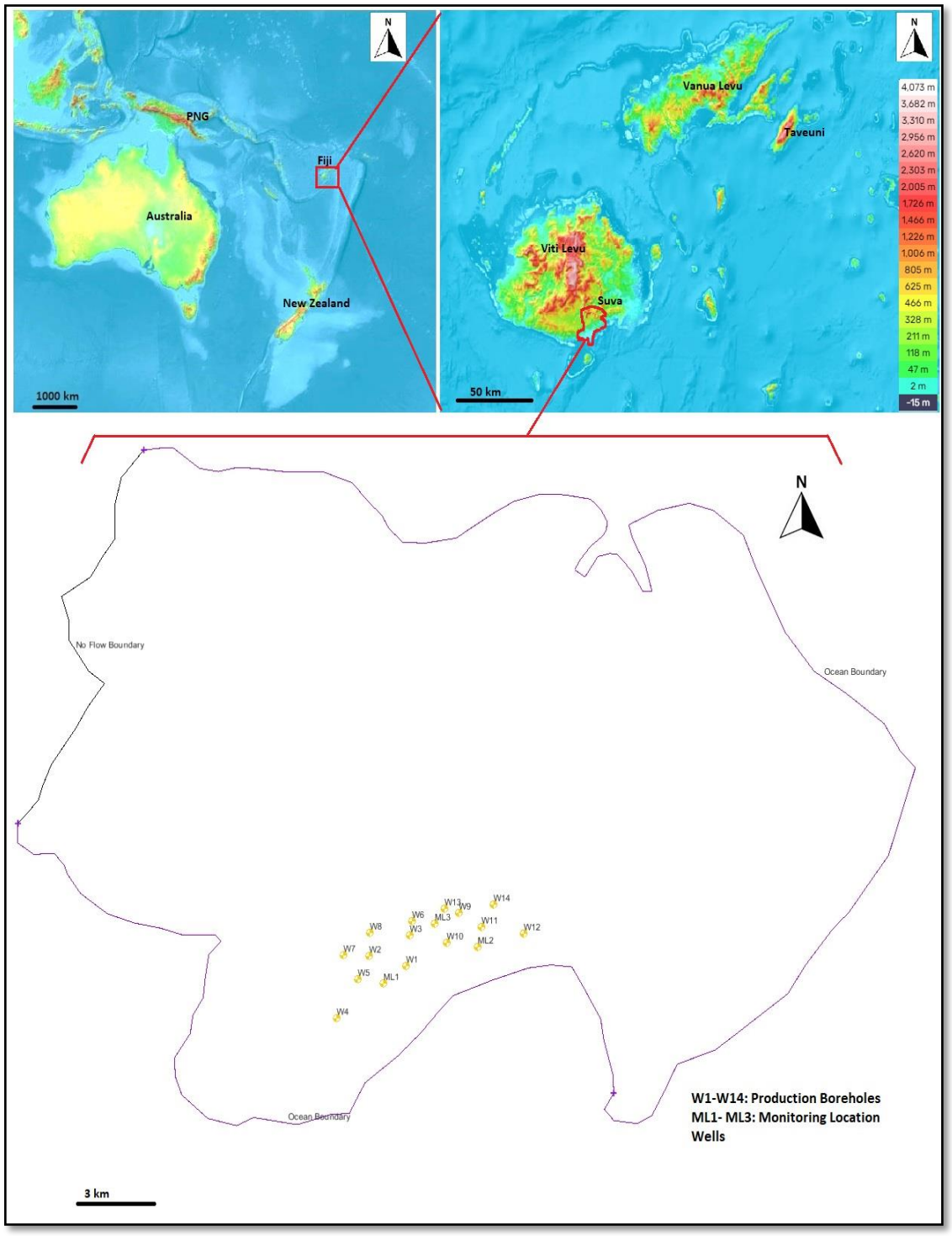



Figure 5.2: Study area.

The hydrogeology of Suva, Fiji, plays a crucial role in the city's water supply and management. Suva, the capital and largest city of Fiji, is located on the southeastern coast of the main island, Viti Levu. The region's hydrogeology is characterised by a combination of volcanic and sedimentary formations, which influence the availability and quality of groundwater resources (Shorten, 1990). The freshwater source in Suva is both surface water and groundwater, where the latter is obtained from aquifers present in the volcanic and sedimentary rocks underlying the area (Sharan et al., 2021). Volcanic rocks, such as basalt, offer favourable conditions for groundwater storage and flow due to their porosity and permeability. These aquifers are often tapped through wells or boreholes to extract water for various purposes, including domestic, agricultural, and industrial use.

However, the hydrogeological system in Suva is not without challenges. As the city experiences significant population growth and urbanisation, there is an increasing demand for water, putting pressure on the limited groundwater resources. Additionally, the proximity of Suva to the coast poses the risk of saltwater intrusion, where saltwater from the ocean can infiltrate and contaminate freshwater aquifers, particularly during periods of low rainfall or excessive pumping. Suva and other South Pacific countries are also influenced by other natural disasters, including sea level rise and frequent cyclones (Sharan, 2022; Sharan, 2023).

The location of the study area in Suva is shown in Figure 5.2. The elevations, some hydrogeological parameters and boundary conditions are used from the study area. However, due to the unavailability of the data from Suva, the site was treated as an illustrative study area. Treating the study area as illustrative gave us opportunities to test various scenarios that can be implemented in future. The wellfield and the number of boreholes for this study area were all assumed. Also, the pumping rates were synthetically simulated. The boundary conditions and hydrogeological parameters used for this study are shown in Table 5.1.

Table 5.1: Hydrogeological parameters.

| **Definition** | **Assigned field values** | **S.I. Units** |
|---|---|---|
| Layer 1 (Sand and gravel) | Uniform Hydraulic Conductivity, K = 20 | K = m/d |
| Recharge | 0.00027 | m/d |
| Porosity | 0.3 | dimensionless |
| Horizontal Anisotropy | 1 | dimensionless |
| Freshwater Density | 1000 | $kg/m^3$ |
| Seawater Density | 1025 | $kg/m^3$ |

| Definition | Assigned field values | S.I. Units |
|---|---|---|
| Saltwater Concentration | 35 | kg/m$^3$ |
| Specific Storage | 0.00035 | 1/m |
| Specific yield | 0.001 | - |
| River conductance | 10 | m$^2$/dm |
| Longitudinal dispersivity | 20 | m |
| Density/Con. constant, F | 0.7143 | dimensionless |

### 5.4.2 Numerical model design

SEAWAT code was used to develop the numerical simulation model in this study. The numerical code SEAWAT is employed to simulate the movement of groundwater in porous mediums, incorporating three-dimensional (3D) representation, variable density, and transient flow. This is achieved by integrating the MODFLOW and MT3DMS programs. Within this framework, MODFLOW is responsible for solving the nonlinear equations related to variable-density flow, while MT3DMS focuses on addressing the nonlinear equations governing the temporal and spatial transport of salt or solutes (Guo and Langevin, 2002).

#### *5.4.2.1 Governing equations*

The variable-density flow process solves the following form of the variable-density groundwater flow equation (tensors and vectors are shown in bold) (Langevin et al., 2008).

$$\nabla \cdot \left[\rho \frac{\mu_0}{\mu} \mathbf{K_0} \left( \nabla h_0 + \frac{\rho - \rho_0}{\rho_0} \nabla z \right)\right] = \rho S_{s,0} \frac{\partial h_0}{\partial t} + \theta \frac{\partial \rho}{\partial C} \frac{\partial C}{\partial t} - \rho_s q'_s \qquad (5.1)$$

where $\rho_0$ is the fluid density [kg/m$^3$], $\mu$ is dynamic viscosity [kg/md], $\mathbf{K_0}$ is the hydraulic conductivity tensor [m/d], $h_0$ is the hydraulic head [m] measured in terms of the reference fluid of a specified concentration and temperature (as the reference fluid is commonly freshwater), $S_{s,0}$ is the specific storage [1/m], defined as the volume of water released from storage per unit volume per unit decline of $h_0$, $t$ is time [d], $\theta$ is porosity [dimensionless], $C$ is salt concentration [kg/m$^3$], $q'_s$ is a source or sink [1/d] of fluid with density $\rho_s$.

The integrated MT3DMS Transport process solves the following form of the solute transport equation.

$$\left(1 + \frac{\rho_b K_d^k}{\theta}\right) \frac{\partial(\theta C^k)}{\partial t} = \nabla \cdot (\theta \mathbf{D} \cdot \nabla C^k) - \nabla \cdot (\mathbf{q} C^k) - q'_s C_s^k + \sum_{k=1}^{N} R_k \qquad (5.2)$$

where $\rho_b$ is the bulk density (mass of the solids divided by the total volume) [mg/m$^3$], $K_d^k$ is the distribution coefficient of species $k$ [m$^3$/kg], $C^k$ is the concentration of species $k$ [kg/m], **D** is the hydrodynamic dispersion coefficient tensor [m$^2$/d], **q** is specific discharge [m/d], and $C_s^k$ is the source or sink concentration [kg/m$^3$] of species $k$. $R_k$ ($k=1, \ldots N$) is the chemical reaction term (kg/m$^3$d) of species $k$.

#### *5.4.2.2 Flow and transport model*

The conceptual model was developed using MODFLOW-2000 code for the study area. The total area of the regional study location was approximately 450 km$^2$. The X, Y, and Z lengths were 25.6 km, 17.6 km and 0.1 km, respectively. A 200 m x 200 m cell size finite-difference grid was created for a single layer. The random hydraulic conductivities were used for different ranges to make the model complex and heterogeneous. Since most Pacific Island countries have hydraulic head values close to the surface, the head values were assumed within the range of 9-10 m. 14 production wells were randomly created, and the transient pumping rates were assigned. The pumping rates ranging from 10 m$^3$/d to 30000 m$^3$/d were randomly generated in MATLAB. Three monitoring location (ML) wells were also created to monitor the water quantity and quality for the study area.

Once the boundary conditions and hydrogeological parameters were assigned, the flow model was simulated for 20 years. The simulation of 20 years was done to find the initial conditions that can be used for the transport model. After 5 years, the head values did not vary much. Hence, the head values corresponding to the 5$^{th}$ year were used for the transport model. The species salt was introduced in MT3DMS, and the 20-year stress period was set. Packages like advection, dispersion, sources, and sink were also used in transport model simulations. The initial concentrations of the aquifer and wells were assumed to be 0.3 kg/m$^3$. The values were assumed because Suva did not have data on groundwater. SEAWAT was then introduced to simulate the saltwater intrusion and solve flow and transport equations simultaneously. The SEAWAT was initiated, and results were noted. In the initial simulations, the uniform hydraulic conductivity of 20 m/d was used for the whole layer. The other simulations were carried out using random hydraulic conductivities (RHC).

### 5.4.3 Randomising hydraulic conductivities

#### *5.4.3.1 Random integers*

Using random hydraulic conductivities (RHC) in a numerical simulation model is challenging. Also, the best random number generation methods play an important role. Initially, random positive integers were generated for three different ranges in this study. The first range of hydraulic conductivities (HC) was from 15 m/d to 25 m/d, the second range of integers was from 5 m/d to 40 m/d, and the third range of integers was from 2 m/d to 100 m/d. Approximately 11000 random integers were generated in MATLAB for all three ranges mentioned earlier. The code used to generate the integers is given below;

```
random_numbers = randi([X, Y], 1, Z);

disp(random_numbers);
```

where X is the lower limit of the range, Y is the upper limit of the range, and Z is the total number of random numbers required to generate.

These integers were then carefully matched with the active region of the HCs in MODFLOW. All three ranges were imported into the model domain, and scenarios were simulated.

#### *5.4.3.2 Random Halton sequence*

Halton sequence was used to generate random HC for all three ranges, similar to the ranges used to generate random integers above. Roy and Datta (2020) used the Halton sequence to generate the transient groundwater pumping rates and found that the values are evenly distributed all over the field. Loyola et al. (2016) also reported that the Halton sequence produces better results than other sampling methods. To test the simulation model, the Halton sequence of HC was generated using MATLAB. The MATLAB code used to generate HC using the Halton sequence is given below.

```
lower_bound = X;
upper_bound = Y;
num_dimensions = 1;
num_points =Z;
halton_sequence = haltonset(num_dimensions);
halton_points = net(halton_sequence, num_points);
```

```
random_numbers = lower_bound + (upper_bound - lower_bound) *
                 halton_points;
disp(random_numbers);
```

where X is the lower limit of the range, Y is the upper limit of the range, and Z is the total number of random numbers required to generate.

The random Halton sequence HCs were imported in MODFLOW and simulated for all three ranges for 20-year stress periods. Moreover, the salt concentrations at various monitoring locations were compared randomly for all the sets of HCs generated.

### 5.4.4 Saltwater intrusion management strategies

To manage the saltwater intrusion (SWI) in the current coastal aquifer, 2 different scenarios were also tested. The first scenario was using barrier well pumping and injection well pumping near the coast. Ten injection wells (IWs) and ten barrier wells (BWs) were placed uniformly as a barrier to manage SWI in the freshwater wells. The uniform pumping rates of 30000 $m^3$/d were assigned to IWs and BWs in MODFLOW. Moreover, the scenario using only the injection wells with a uniform injection rate of 30000 $m^3$/d was also tested. The use of only BW pumping was also tested. However, the BWs did not show promising results in managing SWI in the model domain. Therefore, the results merely using BWs as a SWI mitigating technique were not presented for the current study.

## 5.5 Results

### 5.5.1 Random integers of hydraulic conductivities

The random integers of K-1, K-2 and K-3 (hydraulic conductivity) were randomly generated. The values ranging K-1 =15 m/d to 25 m/d, K-2 = 5 m/d to 40 m/d and K-3 = 2 m/d to 100 m/d. The random distribution of K-1, K-2 and K-3 are shown in Figure 5.3a, c and e, respectively. Different distribution ranges were used in numerical model simulations. The plan view of the K-1 simulation is shown in Figure 5.4(b-1 to b-20). The numbers 1-, 5-, 10-, 15-, and 20- represent the time steps of 1 year, 5 years, 10 years, 15 years, and 20 years, respectively. The 5 different time-steps plan views were shown and compared with the plan view using the uniform HC of 20 m/d. The plan view of the K-1 simulation is shown in Figure 5.4(b-1 to b-20). The 5 different time-steps plan views were compared with the plan view of uniform HC shown in Figure 5.4(a-1 to a-20). Moreover,

the plan view of the K-2 simulation is shown in Figure 5.5(b-1 to b-20), and the plan view of the K-3 simulations is shown in Figure 5.6(b-1 to b-20).

The plan view does not significantly show the variations in SWI magnitudes. However, to clearly see the different HC values on the salt concentrations, the three monitoring locations (MLs) were assigned, and the results were noted. The difference in salt concentration using different HC ranges for ML1 for the 5 time-steps of 1-, 5-, 10-, 15-, and 20 years are shown in Figure 5.7a-e. The salt concentration was compared with the random HC for all corresponding time-steps. Similarly, the difference in salt concentration using different HC ranges for ML2 and ML3 for the 5 time-steps are shown in Figure 5.8a-e and Figure 5.9a-e, respectively. The difference in salt concentration for 1 year stress period for all MLs is not significant. However, for other time-steps, the variations are significant.

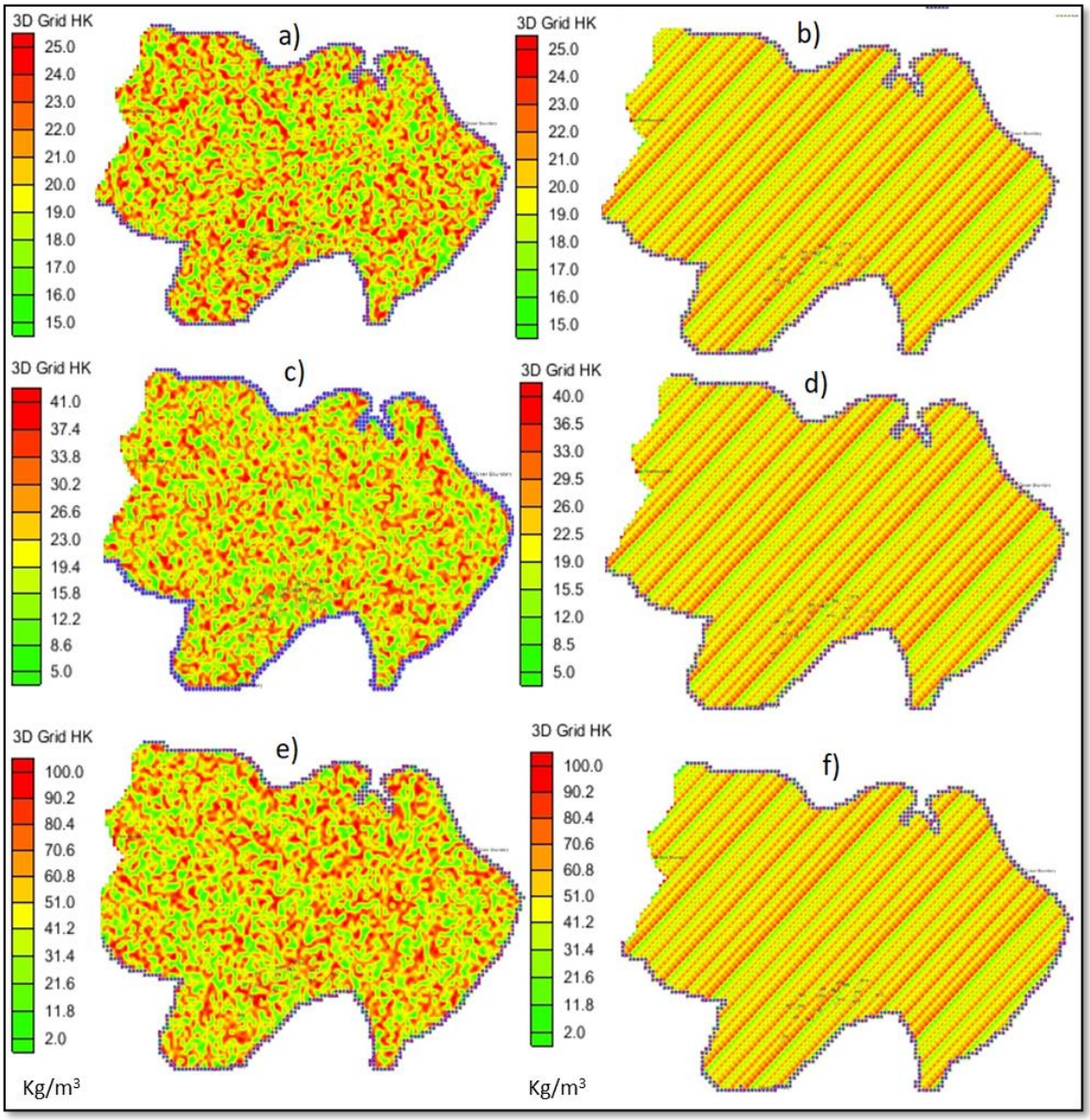



Figure 5.3: **a, c, e** represent hydraulic conductivities randomly generated integers ranging from 15 m/d to 25 m/d, 5 m/d to 40 m/d, and 2 m/d to 100 m/d, respectively. **b, d**, f are hydraulic conductivities randomly generated using Halton sequence for the ranges 15 m/d to 25 m/d, 5 m/d to 40 m/d, and 2 m/d to100 m/d, respectively.

The use of uniform HC of 20 m/d compared with the K-1 for ML1 for 5-, 10-, 15-, and 20-year time-steps vary by -0.04%, 1.52%, 2.58% and -0.04%, respectively. The minus sign indicates the percentage decrease in the salt concentration for the variable K-1 compared with uniform HCs. All these variations for ML1 are less significant. Moreover, the variations in salt concentrations of uniform HC of 20m/d compared with K-1 for ML2 for 5-, 10-, 15- and 20-year time-steps vary by -0.23%, 1.64%, 0.11% and 0.01%, respectively. Again, the variations are not significant. Furthermore, the variations of uniform HC compared with K-1 at ML3 for 5-, 10-, 15- and 20-year time-steps vary

by 0.16%, 43.77%, 5.71% and 0.90%, respectively. A significant variation was noted for the 10-year time-step.

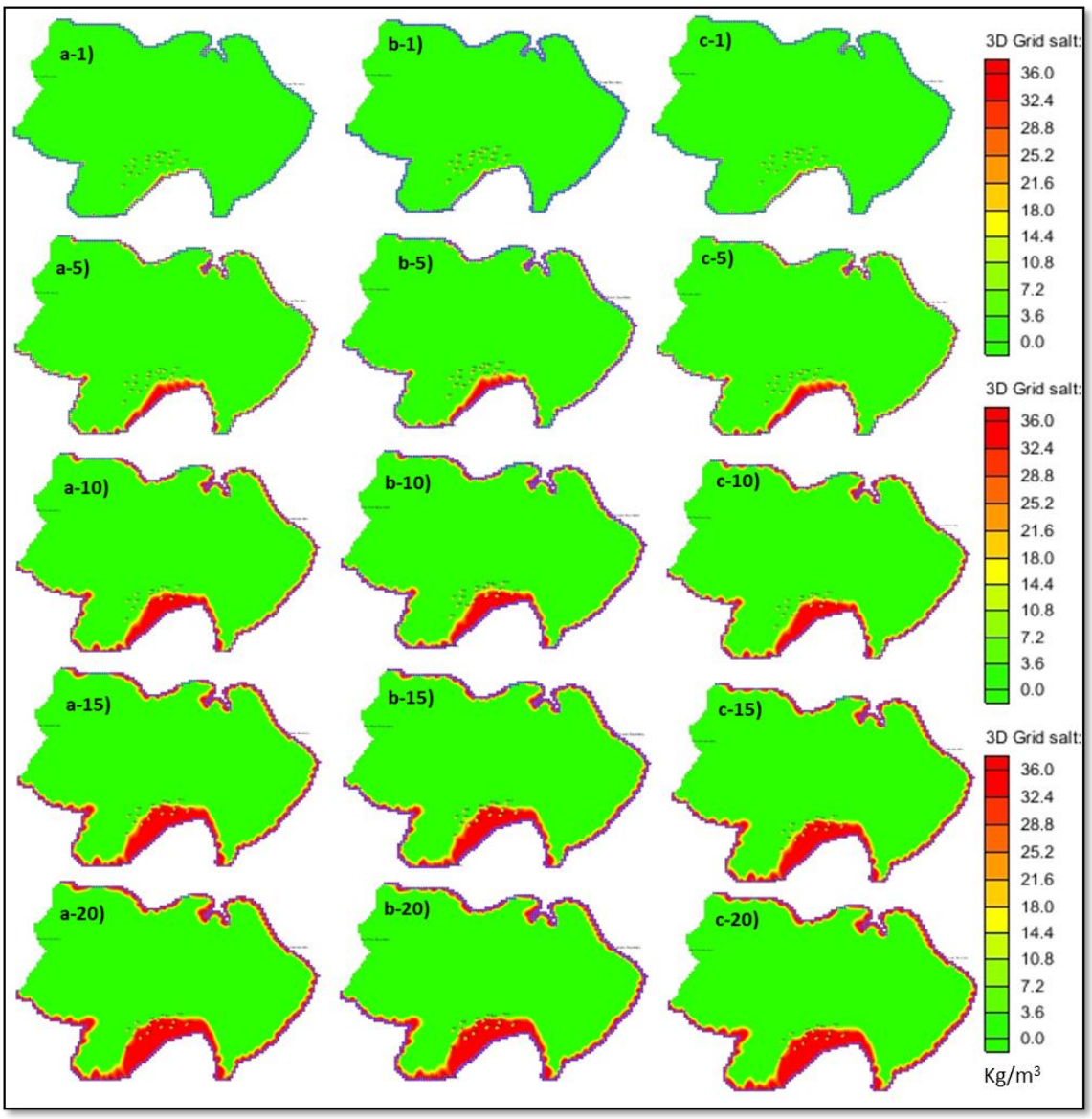



Figure 5.4: Plan view of saltwater intrusion. (a-1 to a-20) for uniform hydraulic conductivities (HCs). (b-1 to b-20) for randomized hydraulic conductivities (K-1) using randomly generated integers for the range 15 m/d to 25 m/d. (c-1 to c-20) showing randomised hydraulic conductivities (K-1.1) generated using the Halton sequence for the range 15 m/d to 25 m/d. The numbers 1, 5, 10, 15, and 20 represent the time steps of 1 year, 5 years, 10 years, 15 years, and 20 years, respectively.

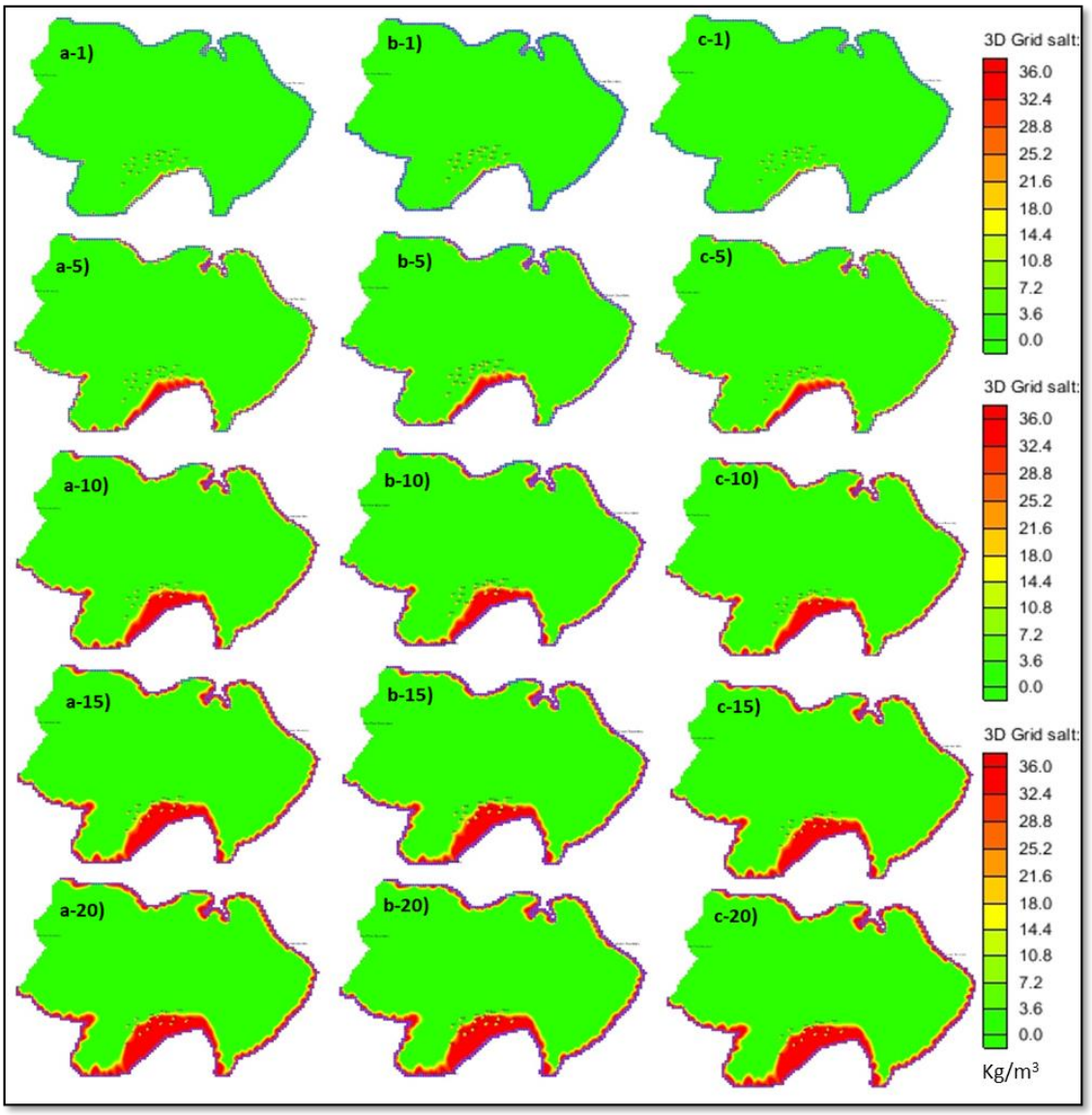



Figure 5.5: Plan view of saltwater intrusion. (a-1 to a-20) for uniform hydraulic conductivities (HCs). (b-1 to b-20) for randomised hydraulic conductivities (K-2) using randomly generated integers for the range 5 m/d to 40 m/d. (c-1 to c-20) showing randomized hydraulic conductivities (K-2.1) generated using the Halton sequence for the range 5 m/d to 40 m/d. The numbers 1, 5, 10, 15, and 20 represent the time steps of 1 year, 5 years, 10 years, 15 years, and 20 years, respectively.

Similarly, the variations of salt concentration using uniform HC of 20 m/d with K-2 for ML1 for 5-, 10-, 15- and 20-year time-steps vary by 1.31%, 169.8%, -0.52% and -3.38%, respectively. The minus sign indicates the percentage decrease in the salt concentration for the variable K-2 compared with uniform HCs. The variations are not significant, except for time-step of 10-year. Moreover, the comparison of uniform HC and K-2 for ML2 at similar time-steps as above vary by 69.08%, -0.57% and -0.64% and -0.05%, respectively. The variations are not significant, except for the 5-year time-step.

Furthermore, comparing uniform HC and K-2 for ML3 at similar time-steps as above vary by 0.34%, 2.48%, -30.36%, and -13.41%, respectively. The variations are not significant, except for the 5-year time-step. For the K-2 range, the salt concentration significantly decreased at ML3 for 15- and 20-year time-steps.

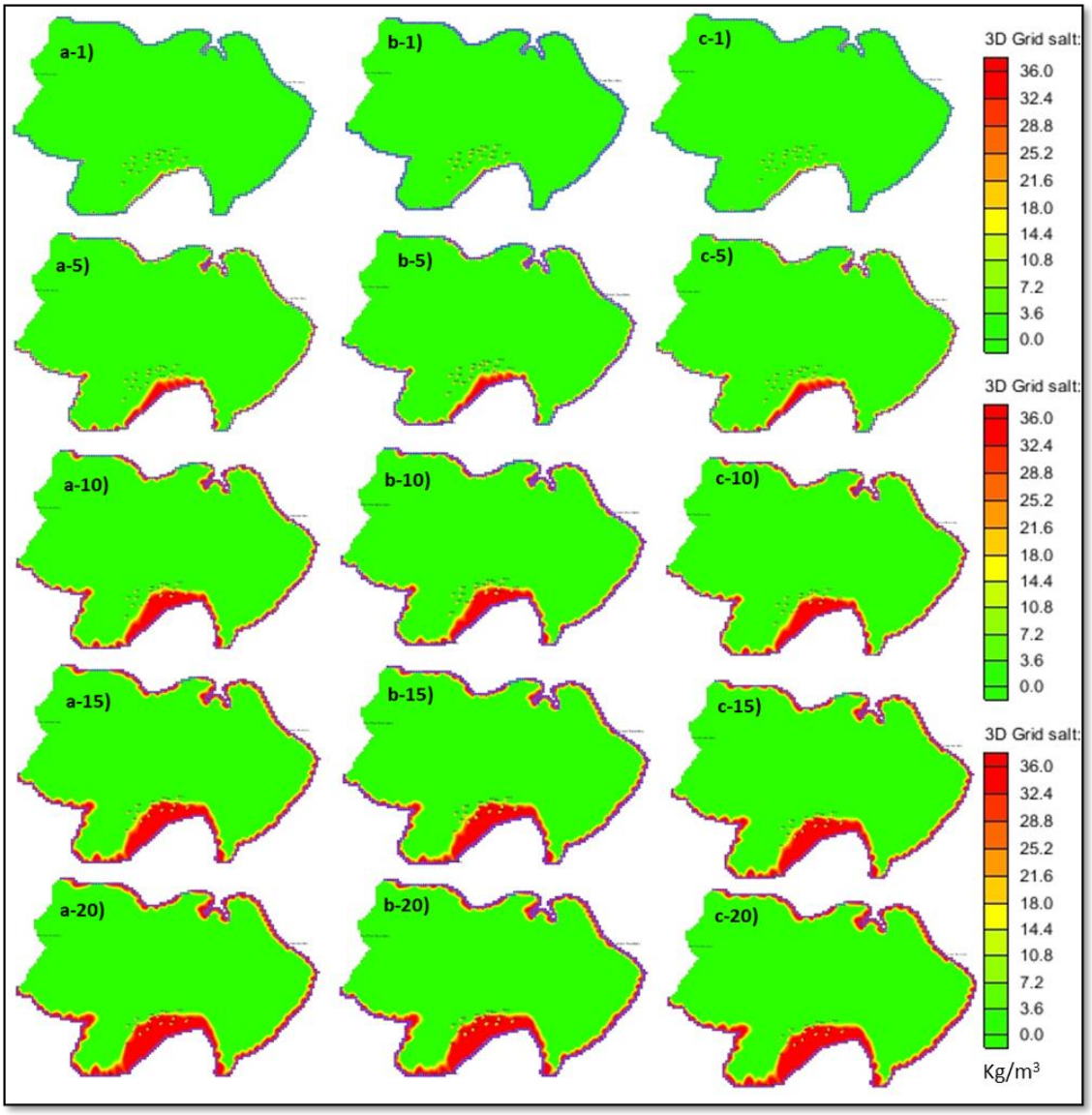



Figure 5.6: Plan view of saltwater intrusion. (a-1 to a-20) for uniform hydraulic conductivities (HCs). (b-1 to b-20) for randomised hydraulic conductivities (K-3) using randomly generated integers for the range 2 m/d to 100 m/d. (c-1 to c-20) showing randomized hydraulic conductivities (K-3.1) generated using the Halton sequence for the range 2 m/d to 100 m/d. The numbers 1, 5, 10, 15, and 20 represent the time steps of 1 year, 5 years, 10 years, 15 years, and 20 years, respectively.

The K-1 and K-2 simulated salt concentrations were also compared for 1-, 5-, 10-, 15- and 20-year time-steps at ML1, indicating the variations by -0.03%, 1.35%, 165.8%,

-3.02% and -3.34%, respectively. The minus sign indicates the percentage decrease in the salt concentration for variable K-2 compared with variable K-1. A significant increase in salt concentration was noted at a 10-year time-step. Similarly, for ML2, the variations of 1.81%, 69.47%, -2.17%, -0.75%, and -0.06%, respectively, were noted. The variations are insignificant, except for an increase in salt concertation by 69.47% at a 5-year time-step. Moreover, at ML3, the variations of -0.003%, 0.18%, -28.27%, -34.13%, and -4.18% for 1-, 5-, 10-, 15- and 20-year time-steps were noted, respectively.

### 5.5.2 Random hydraulic conductivities using Halton Sequence

The random values of HCs were also generated using the Halton sequence code. The three ranges K-1.1, K-2.1 and K-3.1 were generated. Where the range of K-1.1 =15 m/d to 25 m/d, K-2.1 = 5 m/d to 40 m/d and K-3.1 = 2 m/d to 100 m/d. The random distribution of K-1.1, K-2.2 and K-3.1 are shown in Figure 5.3b, d and f, respectively. Halton sequence generated very close values, nearly making the hydraulic conductivities uniform in the y-direction. At the same time, the x-direction was more random and heterogeneous. All three HC ranges were imported in MODFLOW, the values were mapped, and the numerical model was simulated. The plan view of SWI using K-1.1 is shown in Figure 5.4(c-1 to c-20). Also, the plan view using K-2.1 and K-3.1 are shown in Figure 5.5(c-1 to c-20) and Figure 5.6(c-1 to c-20), respectively. The plan view from Figure 5.4, Figure 5.5 and Figure 5.6 shows SWI using different HCs, as discussed above.

The more significant variations in salt concentrations using different HCs are shown in Figure 5.7 to Figure 5.9. The results using uniform HC of 20 m/d for all 5 time-steps were compared with the results simulated using K-1.1, K-2.1 and K-3.1. The variations in salt concentration for ML1 using uniform HC and K-1.1 are -0.04%, -3.79%, -0.96% and 0.07% for 5-, 10-, 15-, and 20-year time-steps, respectively. For the 1-year time-step, the variations are not significant. The minus sign indicates the percentage decrease in salt concentration using K-1.1 compared with uniform HC. Similarly, the variations in salt concentration for ML2 for the 4 time-steps are -1.13%, -0.15%, -0.03% and 0.007%, respectively. The variations at ML2 are not significant using K-1.1. Moreover, the variations for ML3 for 4 time-steps are -0.05%, -8.98%, -1.56% and -0.2%, respectively. The results also indicate minor variations at ML3 for K-1.1.

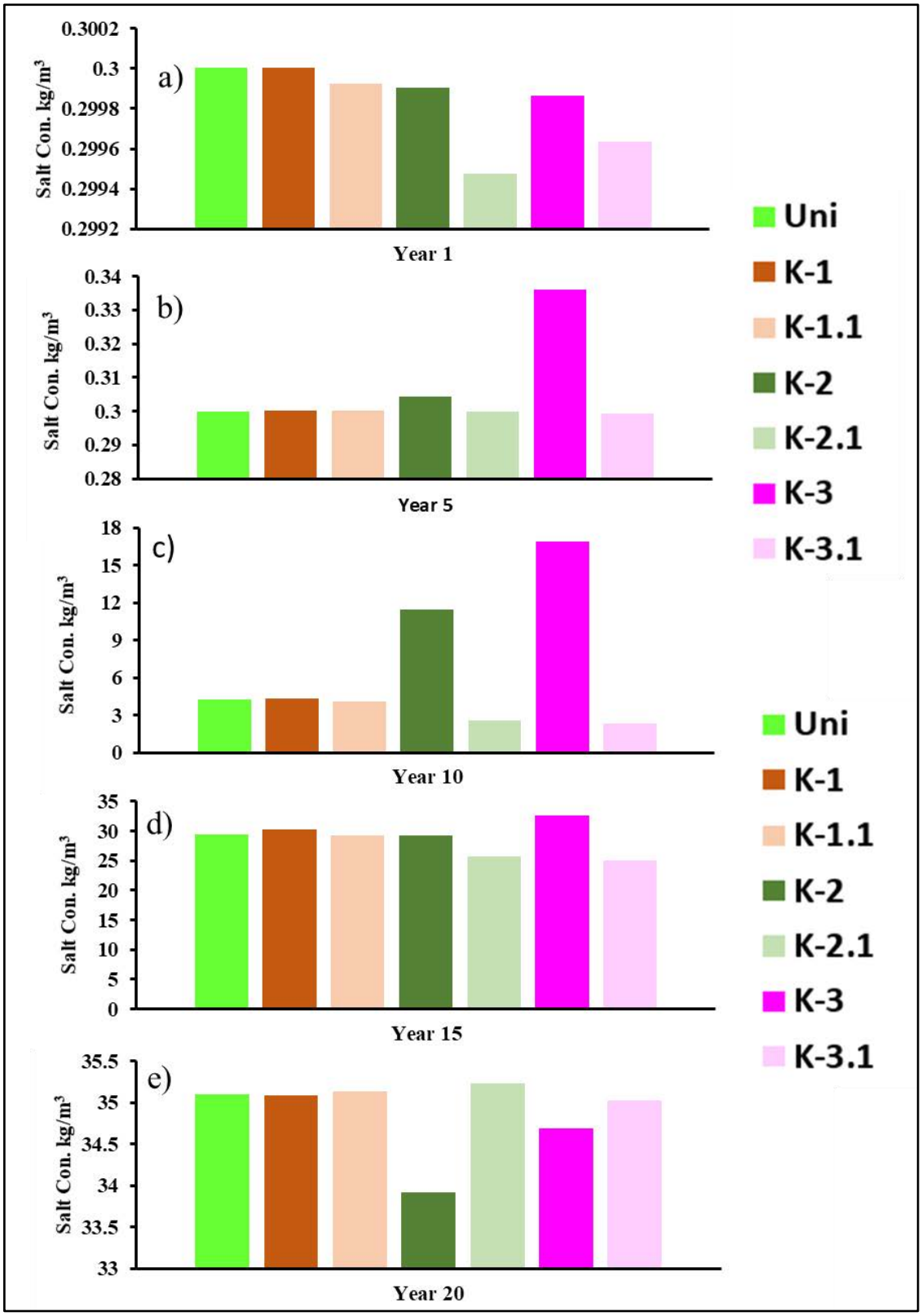



Figure 5.7: **a-e** are salt concentrations at monitoring location 1 for time steps 1, 5, 10, 15 and 20, respectively. Uni indicates the uniform hydraulic conductivity of 20 m/d. K-1, K-2 and K-3 are hydraulic conductivities randomly generated integers for the range 15 m/d to 25 m/d, 5 m/d to 40 m/d, and 2 m/d to 100 m/d, respectively. Whereas K-1.1, K-2.3 and K-3.1 are hydraulic conductivities randomly generated using Halton sequence for the range 15 m/d to 25 m/d, 5 m/d to 40 m/d, and 2 m/d to 100 m/d, respectively.

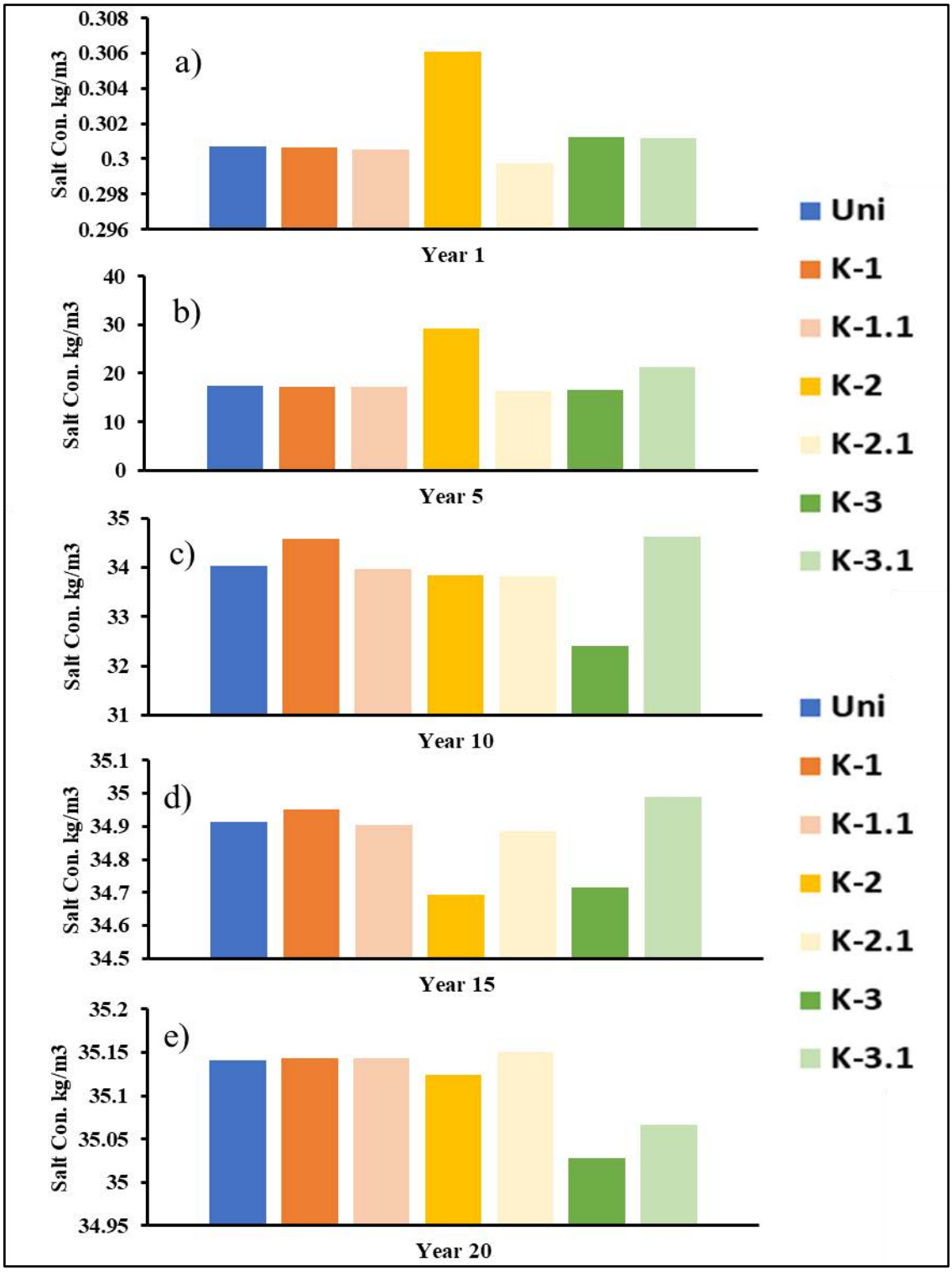



Figure 5.8: **a-e** are salt concentrations at monitoring location 2 for time steps 1, 5, 10, 15 and 20, respectively. Uni indicates the uniform hydraulic conductivity of 20 m/d. K-1, K-2 and K-3 are hydraulic conductivities randomly generated integers for the range 15 m/d to 25 m/d, 5 m/d to 40 m/d, and 2 m/d to 100 m/d, respectively. Whereas K-1.1, K-2.3 and K-3.1 are hydraulic conductivities randomly generated using Halton sequence for the range 15 m/d to 25 m/d, 5 m/d to 40 m/d, and 2 m/d to 100 m/d, respectively.

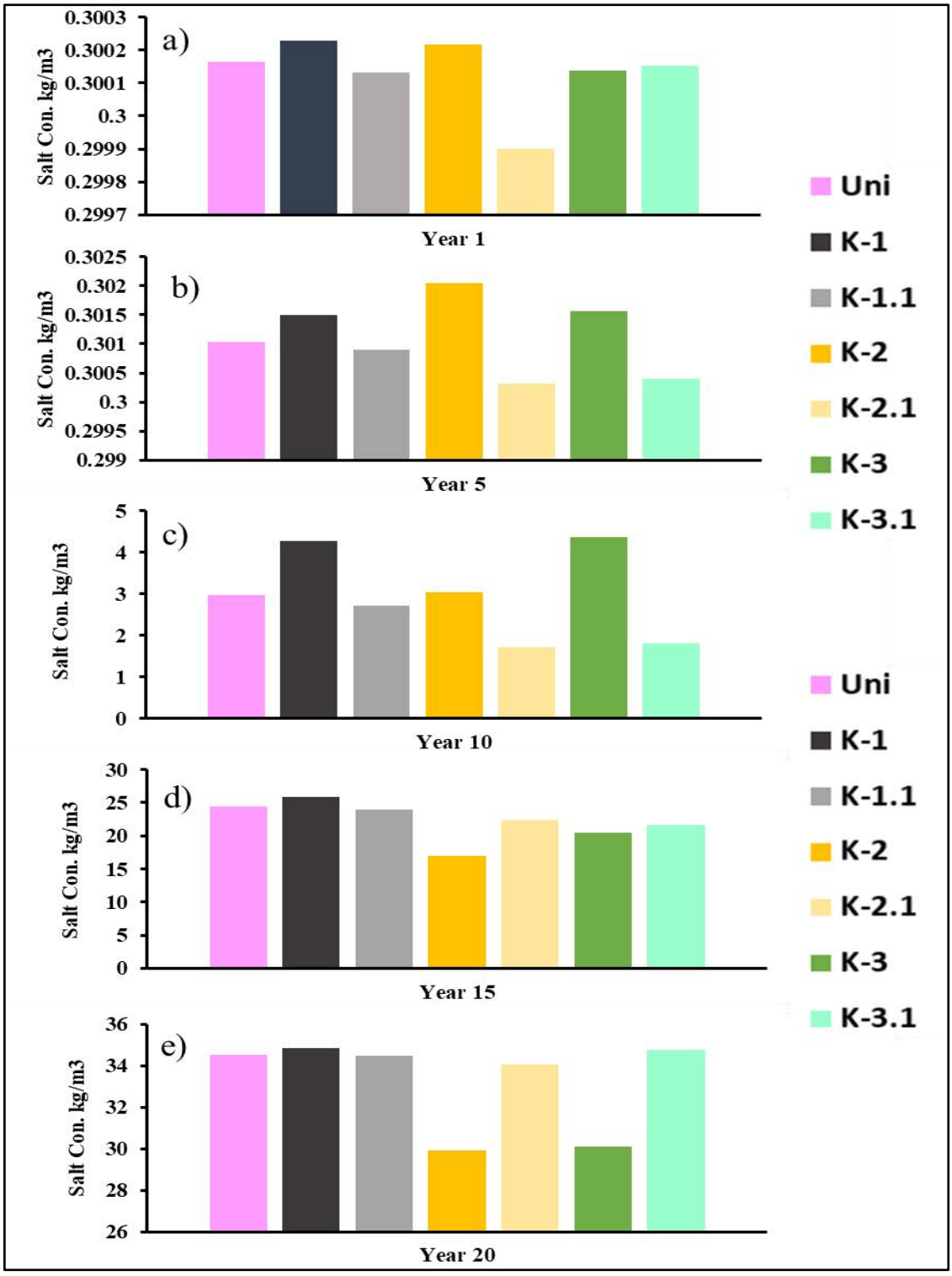



Figure 5.9: **a-e** are alt concentrations at monitoring location 3 for time steps 1, 5, 10, 15 and 20, respectively. Uni indicate the uniform hydraulic conductivity of 20 m/d. K-1, K-2 and K-3 are hydraulic conductivities randomly generated integers for the range 15 m/d to 25 m/d, 5 m/d to 40 m/d, and 2 m/d to 100 m/d, respectively. Whereas K-1.1, K-2.3 and K-3.1 are hydraulic conductivities randomly generated using Halton sequence for the range 15 m/d to 25 m/d, 5 m/d to 40 m/d, and 2 m/d to 100 m/d, respectively.

Moreover, the results obtained using the K-2.1 range of HC values were compared with uniform HC values for ML1, ML2 and ML3 in Figure 5.7, Figure 5.8 and Figure

5.9, respectively. For ML1, the variations in K-2.1 and uniform HC are -0.15%, -39.86%, -12.52% and 0.35% for 5-, 10-, 15-, and 20-year time-steps, respectively. For similar time-steps, the variations at ML2 were -5.87%, -0.63%, -0.09% and 0.03%, respectively. The variations at ML2 are not significant. Moreover, the variations at ML3 were -0.24%, -42.53%, -8.52% and -1.36%, respectively. The decrease in salt concentration was noted for all 4 time-steps at ML3. The minus sign indicates the percentage decrease in salt concentration using K-2.1 compared with uniform HC.

Furthermore, the salt concentrations using the K-3.1 HC range compared with uniform HC for ML1, Ml2 and ML3 are also shown in Figure 5.7, Figure 5.8 and Figure 5.9, respectively. The variations in salt concentration at ML1 compared with K-3.1 and uniform HC are -0.37%, -42.04%, -15.02% and -0.24%, corresponding to 5-, 10-, 15-, and 20-year time-steps, respectively. The minus sign indicates the percentage decrease in salt concentration using K-3.1 compared with uniform HC. The variations at ML2 are 23.35%, 1.74%, 0.22% and -0.21% for similar time-steps as ML1 above. The salt concentrations have increased at ML2 using K-3.1. Moreover, the variations in salt concentration at ML3 are -0.22%, -39.38%, -11.07% and 0.55%, respectively. The salt concentrations have mainly decreased using K-3.1 at ML3.

### 5.5.3 SWI management scenarios

Two scenarios were mainly tested in this study for managing the SWI. The first strategy was using hydraulic barriers inclusive of injection wells (IWs) and barrier wells (BWs). Uniform pumping and injection rates were assigned to the BWs and IWs along the coastline to prevent SWI from entering freshwater wells. The plan view of the SWI rates using BWs and IWs is shown in Figure 5.10(a-1 to a-20). Where 1-, 5-, 10-, 15-, and 20 years represent different time-steps, respectively. The results indicate the SWI has decreased and did not reach the production wells. However, during the 10-, 15-, and 20-year time steps, some SWI is shown near Well 11 and Well 12. A second strategy was introduced to overcome the contamination of freshwater wells.

The second strategy for managing SWI in freshwater wells was using only the IWs, which has demonstrated how SWI can be easily managed. Similarly, uniform water injection rates were assigned to the IWs along the coastline in front of production wells, as shown in Figure 5.10(b-1 to b-20). From the plan view, it can be seen that the SWI has

significantly decreased. However, some drawbacks are associated with IWs and BWs, which are discussed in the next section.

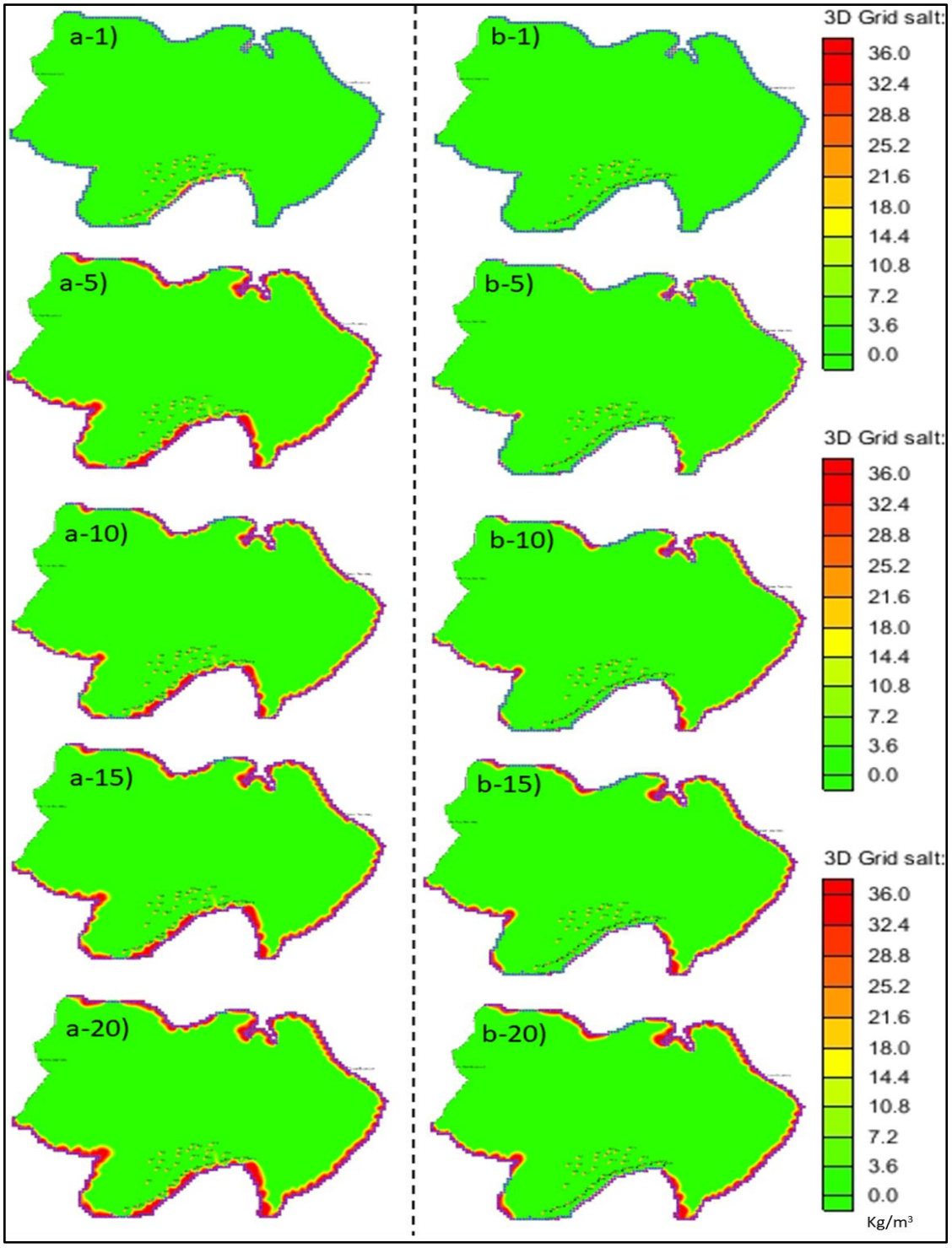



Figure 5.10: Plan view of saltwater intrusion encroachment management strategies. (a-1 to a-20) showing the hydraulic barriers using the barrier wells and injection wells to manage saltwater intrusion. (b-1 to b-20) showing the hydraulic barriers using only the injection wells to manage saltwater intrusion. The numbers 1, 5, 10, 15, and 20 represent the time steps of 1 year, 5 years, 10 years, 15 years, and 20 years, respectively.

## 5.6 Discussion

The use of random hydraulic conductivities (RHCs) in SEAWAT numerical simulation was one of the primary aims of this study. The hydraulic conductivities (HCs) were randomly generated in MATLAB. Two methods were used to generate the RHC. Random integers and Halton sequence codes were used to generate RHCs. To the best of the current knowledge, the method used to generate RHC is the first to be used in the SEAWAT code to simulate SWI for coastal aquifers. Moreover, RHCs are also the first to be used in MODFLOW for such an extensive range of HCs, as discussed in the result section. Zhang and Pinder (2000) generated RHC fields using Latin hypercube sampling (LHS) for groundwater modelling and found that it required fewer realisations to achieve a given level of accuracy. The authors also reported that LHS reduces the computational cost of solving groundwater flow and transport problems.

Malekpour et al. (2018) used the log-normal distribution method to generate the random HC values for a sample size <= 1000. The authors found that the uncertainty increases with time using log-normal distributions. Zhang (2002) reported that the Monte Carlo simulation method is better at generating the realisations RHCs by averaging the realisations. Different studies have used some techniques of randomising the HCs. However, the method proposed in this study is used for the first time. Also, the computational time or the model convergence time was reduced using the random integers and Halton sequence of the K values compared with the uniform K convergence time.

Moreover, using the random integers and random Halton sequence, K values had some convergence time for all the K ranges. However, deciding which one was the better random generator was complex, which became the limitation of this study. To better realise RHCs, real hydrogeological and HC data are needed from the field. The real data will calibrate, validate the model, and compare the outputs using random HC generators. The availability of groundwater data is not available in the Pacific Islands countries (Sharan et al., 2021), which makes it challenging to determine which random generator is better. However, it can be clearly stated that using RHC over uniform HCs reduces computational time. Also, using RHCs makes the study area heterogeneous and more realistic.

In addition, the use of hydraulic barriers was also introduced in managing the SWI for the Suva coastal aquifer. The scenario that proved to manage the SWI effectively was using the IWs. Similar results were also obtained by Sharan et al. (2023). The authors used an illustrative study area and simulated various scenarios that can manage SWI in coastal aquifers. The authors reported that IWs significantly reduce the SWI in the model domain. In this study, BW and IW were used for groundwater pumping. The results were not appealing as some wells were contaminated with saltwater. Therefore, only using IWs significantly managed the saltwater-contaminated wells.

However, using the IWs and BWs is also costly and associated with other risks (Sharan et al., 2023). If only the IWs are used, a source of freshwater that will be injected using the IWs would be needed. This can reduce the amount of freshwater from nearby rivers. Also, if the BWs are used, the disposal of withdrawn salty water becomes problematic. Therefore, other techniques like physical barriers can solve these issues (Abdoulhalik et al., 2022; Kaleris and Ziogas, 2023). SWI management is a complex process that needs to be carefully studied and modelled.

## 5.7 Conclusions

The use of RHCs in the SEAWAT-based numerical simulation model was developed for three different hydraulic conductivity (K) ranges. Random integers and Halton sequence techniques were used to generate more than 10000 random values of K for the range K-1=15 m/d to 25 m/d, K-2 = 5 m/d to 40 m/d and K-3 = 2 m/d to 100 m/d. All three ranges of K were generated using both techniques in MATLAB. The K values were imported in MODFLOW, and the SEAWAT was simulated. Moreover, the SWI management strategies were also simulated for the study area. The study area was from Suva, Fiji. However, the study area was treated as an illustrative study area due to the unavailability of the groundwater data. However, some hydrogeological parameters, boundary conditions, elevations and raster data were taken from Suva.

The results indicated that using the RHCs reduces the computational burden on numerical simulation models. Also, the realisation of the hydraulic conductivities was included in the model simulations, which made the study area heterogeneous and realistic. The results did not vary much while using random integers and Halton sequences. However, the Halton sequence generated very close values, nearly making the hydraulic

conductivities uniform in the y-direction. In contrast, the x-direction was more random and heterogeneous.

Moreover, the SWI management strategy simulated for the current study indicates that using hydraulic barriers like barrier wells (BWs) and injection wells (IWs) mitigates the SWI in coastal aquifers. IWs significantly reduced SWI compared to using BWs alone or IWs plus BWs simultaneously. This study also reported that hydraulic barriers can be costly, and disposal of salty water can be an issue.

The limitations of this study were the availability of the groundwater data, field hydraulic conductivities of the study area, pumping data, and salinity data, which could have been used to calibrate and validate the model. Also, if the actual hydraulic conductivity, hydraulic head or salinity data had been available, it would have been easier to decide the best random number generator used in this study. Moreover, to measure the best RHC generator and the best range to use, a real site with quality groundwater and bore log data must be used. In the future, researchers can use the methodology proposed in this study and apply it to the real study area that has sufficient data. Since this is the first time the random integers and Halton sequence of K values were simulated in SEAWAT-based numerical modelling, the methodology developed here could have many other applications in groundwater studies.

In Chapters 4 and 5, different methodologies were developed and tested for managing saltwater intrusion. Using a similar methodology, a real study area in a Pacific Island country was used to develop, calibrate, validate, and provide saltwater intrusion management strategies in the next chapter.

# Chapter 6: Management of saltwater intrusion using numerical modelling techniques in the small Pacific Island country of Vanuatu

The main contents of this chapter have been published and copyrighted as outlined below:

**Sharan. A**., Datta, B., Lal, A., & Kotra, K. (2024). Management of saltwater intrusion using numerical modelling techniques in the small Pacific Island country of Vanuatu. *Environmental Monitoring and Assessment*, 196(120), 1-20. https://doi.org/10.1007/s10661-023-12245-y

## 6.1 Overview

This chapter develops a 3D groundwater model for a real coastal aquifer in a Pacific Island country. It provides saltwater intrusion management strategies using numerical modelling techniques.

## 6.2 Executive Summary

Small island countries like Vanuatu are facing the brunt of climate change, sea level rise (SLR), tropical cyclones and limited or declining access to freshwater. The Tagabe coastal aquifer in Port Vila (the capital of Vanuatu) shows the presence of salinity, indicating saltwater intrusion (SWI). This study aims to develop and evaluate effective SWI management strategies for Tagabe coastal aquifer. To manage SWI, the numerical simulation model for the study area was developed using the SEAWAT code. The flow model was developed using MODFLOW and the transport model was developed using MT3DMS. Whereby SEAWAT solved flow and transport equations simultaneously. The model was calibrated, and different scenarios were evaluated for the management of SWI. The SLR was also considered in the model simulations. The results indicated that increased population, pumping rates and SLR affect the SWI rates. To manage the SWI, hydraulic barriers like barrier wells and injection wells, which effectively managed SWI in Tagabe coastal aquifer were introduced. The results from this study are significantly important whereby, the water managers, site owners, and governing bodies can use the management strategies presented in this study to create policies and regulations for managing SWI rates in Port Vila. Additionally, the water industry, private businesses, and investors who wish to extract groundwater from the Tagabe can use this study as a reference for daily or yearly freshwater production rates without the risk of SWI.

## 6.3 Introduction

Water resources are fundamental for the sustainability and survival of all living beings on Earth and beyond. This precious commodity is declining; only 3% of all water is freshwater, and out of this 3%, 31.4% is usable, whereas 68.6% are ice caps and glaciers. Moreover, groundwater reserves are approximately 30.1%, whereas surface water sources are 1.3% (Shiklomanov, 1993). The percentage of water resources remaining on our planet is shown in Figure 6.1. From the graph, it can be shown that the majority of the freshwater available is groundwater. However, these groundwater resources are also constantly threatened by natural and anthropogenic means (Khatri and Tyagi, 2015; Vengadesan and Lakshmanan, 2019; Li et al., 2021; Sharan et al., 2023).

Groundwater is the primary water source for the Pacific Island countries (PICs) (Sharan et al., 2021). Almost all PICs use groundwater for their daily needs, which puts groundwater under threat. The major environmental threat of coastal aquifers in PICs is saltwater intrusion (SWI) (Kotra et al., 2022). SWI occurs when the seawater moves towards the landward side, changing the freshwater-saltwater pressure gradients. The SWI is an environmental threat in PICs and all around the globe in coastal regions (ACASA, 2011). The management of SWI is crucial, especially in small island countries that are predominantly surrounded by oceans. The SWI management in PICs is minimal due to the unavailability of expertise, proper groundwater data management, and unavailability of specialised monitoring devices (Sharan et al., 2021). Very few PICs thoroughly monitor and collect accurate groundwater data, for instance, Kiribati (1.84$^{o}$ N, 157.38$^{o}$ W) (Lal and Datta, 2019c). The coastal aquifers in Kiribati have been extensively studied with some numerical and AI-based modelling techniques that provide optimal SWI management strategies (e.g., Lal and Datta, 2019a; 2019b). Other limited studies conducted in PICs include Nauru (0.52$^{o}$ S, 166.93$^{o}$ E) (Alberti et al., 2017) and Tonga (21.18$^{o}$ S, 175.19$^{o}$ W) (White et al., 2011; Sharan et al., 2023).

The use of numerical-based modelling techniques is complex and computationally expensive. However, they are mainly the first source of SWI management tools in groundwater. Later comes the AI-based modelling techniques, utilising the results from numerical models. Moreover, without the input-output patterns from a numerical model, one cannot develop accurate AI-based models. Therefore, numerical models are crucial for developing curative solutions to reduce SWI (Hamidi et al., 2021). Numerical

modelling has been extensively applied to manage SWI around the globe (e.g., Andersen et al., 1988; Bobba, 2002; Giambastiani et al., 2007; Dhar and Datta, 2009; Lee et al., 2023; Stein et al., 2023). All these studies used numerical modelling techniques to provide optimal SWI management strategies for coastal aquifers. Numerical models are mainly developed using the finite element method (FEM) or finite difference method (FDM). However, the models developed using the latter methods use grids, which makes it easier to test the optimum SWI management scenario (Werner et al., 2013; Sharan et al., 2023). Different codes can be used in FDM to model groundwater flow and transport, such as MODFLOW, MT3DMS, PHT3D, and SEAWAT.

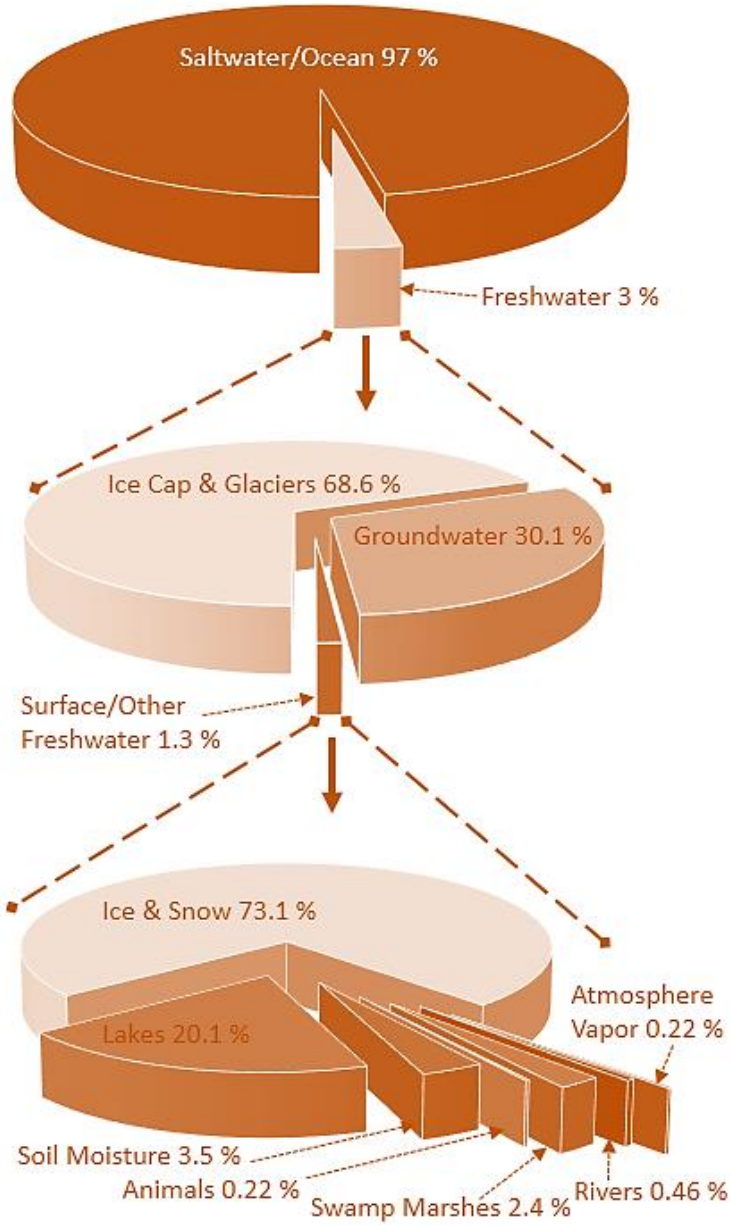



Figure 6.1: Earth's water resources. Source (Shiklomanov, 1993).

SEAWAT numerical codes have been relatively applied in managing the SWI in coastal aquifers around the globe. Lin et al. (2008) used the SEAWAT code to develop a numerical simulation model to investigate the amount of SWI in the Gulf Coast aquifers of Alabama (32.31° N, 86.90° W), USA. The authors calibrated and validated their model using the hydraulic head values. The calibrated model was used to predict the future SWI in Alabama. The authors reported that the extent of SWI has increased during a 40-year simulation period. The authors also stated that due to population growth and more water demands, the SWI would be more severe in future. Romanazzi et al. (2015) developed a numerical simulation model for managing a Mediterranean karstic coastal aquifer affected by SWI and climate change. The authors used the SEAWAT code to develop their model and used the hydraulic head and the salinity data to calibrate and validate the model. The calibrated model was simulated to predict three future scenarios: climate change, different types of discharge and SLR. The authors reported that all the scenarios tested showed non-negligible effects on coastal groundwater. The authors also suggested that to manage SWI, the current water technologies must be modified, water to be recycled, and aquifers must be artificially recharged.

Casillas-Trasvina et al. (2019) applied the SEAWAT code to develop a numerical simulation model to assess multi-source SWI under natural and pumping conditions in the Great Maputo aquifer (25. 97° S, 32.57° E), Mozambique. The authors used hydraulic heads, discharges and salt concentrations to calibrate and validate the model. The calibrated model was used to test different scenarios, including the impacts of SLR and projected abstraction rates. The results indicated that SWI is higher for the scenarios tested. The authors also reported that management strategies must be drawn, and using a more significant number of scattered production wells that can be operated with lower pumping rates will prevent the saltwater upconing. Abd-Elhamid et al. (2020) provided the SWI management strategies for Biscayne aquifer in Florida, USA using numerical modelling. The authors suggested that extending the coastline towards the sea using coastal earth-fill would increase the land surface area and reduce SWI rates. However, this technique of managing SWI could damage the existing coastal ecosystems and marine organisms. Also, this land reclamation technique could be very costly and could have low hydraulic conductivity for reclaimed soil.

Dibaj et al. (2020) developed a numerical model using SEAWAT to simulate the SWI in the Pingtung coastal aquifer (22.70° N, 120.44° E) in Taiwan under the influence

of SLR and changing abstraction regimes. The model was calibrated and validated using the observed head values. The authors used the calibrated model to predict the future SWI in the aquifer. Three management scenarios were examined, including the SLR, pumping rates and relocation of production wells. The authors reported that all three scenarios affect the extent of SWI in their study area. Moreover, all the layers of the aquifer were affected by SWI. However, the middle layer was least affected by SWI when compared with the top and bottom layers.

Said and Yurtal (2022) used the SEAWAT code to develop a numerical simulation model to predict the SWI in the coastal aquifer of Bosaso Plain (11. 28° N, 49.19° E), Somalia. The authors calibrated and validated the model using the hydraulic head and total dissolved solid concentrations. The calibrated model was used to predict SWI by changing pumping patterns. The authors reported that SWI mainly affects the coastline, and increasing the pumping will cause SWIs to reach 6.2 km inland by 2040. Moreover, the authors also reported that reducing the pumping rates by 50% will reduce SWI significantly. Abd-Elaty and Polemio (2023) used the SEAWAT numerical code to provide SWI management strategies for the Gaza Strip (32.35° N, 34.31° E) aquifer in Palestine. The authors used the SLR and the reduction in fresh groundwater storage to show SWI impacts. The authors found that SWI was more severe if the SLRs and pumping increased. They suggested that using cutoff wells and check dams effectively managed SWI.

The majority of the studies mentioned earlier have used different scenarios in testing and mitigating the SWI. However, a different approach would be approached here. The use of a numerical simulation model to manage SWI in PICs is minimal, which forms the central focus area of this research. The present study tends to develop first-ever SWI management techniques using 3D numerical simulation models for Vanuatu (15.38° S, 166.96° E) in the South Pacific region. To the best of the current knowledge, no study has been conducted in Vanuatu that safeguards groundwater or provides SWI management strategies. In this study, the increase in population and pumping rates will be raised in transient mode gradually. The standing water levels or the hydraulic head values are also raised gradually to factor in the SLR with time. The combination of barrier well and injection well will also be modelled in this study.

The knowledge gained from this study is novel and of foremost importance for Vanuatu and all other surrounding island nations in the Pacific region, as it will provide optimal SWI management strategies by considering uncertainties, including climate change. Moreover, as mentioned above, the scenarios evaluated are the first for an island nation in the Pacific region, making this study necessary for the smaller island nations. The results are beneficial for drawing up robust SWI management strategies in Vanuatu. These strategies will help protect groundwater resources for future use and reduce saline water contaminations. In addition, this study also validates strategies that could be used to increase the abstraction rates and simultaneously restrict SWI into the coastal aquifers of Vanuatu. Finally, this study provides new knowledge to stakeholders and/or bore drilling companies who want to harvest groundwater in Vanuatu, as it gives them the benchmark of fresh groundwater's daily or yearly production rates.

## 6.4 Materials and Methods

### 6.4.1 Study area

#### *6.4.1.1 Country profile and geology*

Vanuatu is located on the eastern side of Australia and comprises eighty-three islands, some volcanic and mountainous, while others are coral atolls. The country has little over 300,000 people, and its capital is Port Vila. Vanuatu is known for its stunning natural beauty, with lush rainforests, pristine beaches, and clear waters. The country is a popular destination for tourists who enjoy snorkelling, scuba diving, and hiking in the mountains. According to a report by the World Travel and Tourism Council (WTTC), tourism significantly contributes to Vanuatu's economy, amounting to 35.5% of its GDP in 2019 (WTTC, 2021). In addition to tourism, Vanuatu's economy is also supported by agriculture, fishing, and forestry. The country is known for producing tropical fruits, such as coconuts, bananas, and pineapples, as well as coffee and cocoa beans.

Vanuatu is a culturally diverse nation, with over one hundred indigenous languages spoken across its islands. The country has a rich cultural heritage, with traditional practices such as custom dancing and sand drawing still practised today. Vanuatu's culture and traditions have been recognised by UNESCO, which has designated several sites in the country as World Heritage Sites, including the Chief Roi Mata's Domain and the Cultural Centre in Port Vila (UNESCO, 2021). However, like many small island nations, Vanuatu is vulnerable to natural disasters and the impacts of climate change. The country

has experienced severe tropical cyclones, volcanic eruptions, and earthquakes in recent years, which have caused considerable damage to infrastructure and livelihoods (VMGD, 2023; Sharan, 2022; Sharan, 2023). The government of Vanuatu has recognised the importance of building resilience to these threats and has taken steps to incorporate climate change adaptation and disaster risk reduction measures into its development planning (SPC, 2015; CRCP, 2021).

The country is divided into six provinces: Malampa, Penama, Sanma, Shefa, Tafea and Torba. The province Shefa is in the country's centre, consisting of two major islands, Epi and Efate. Port Vila is the capital of Vanuatu, located on Efate Island, with an area of approximately 980 $km^2$. The primary focus of this research is based on Efate Island. Efate has diverse geology, including volcanic rocks, limestones, and alluvial deposits, which several geological processes have shaped. In addition to volcanic rocks, the island has several limestone and alluvial deposits. The limestone deposits are in the central and eastern parts of the island and were formed from the accumulation of marine organisms such as corals and shells.

Furthermore, the alluvial deposits are in the coastal plains and were formed by the erosion and deposition of sediment from nearby rivers and streams (Bath et al., 1986). Several geological processes, including volcanic activity, tectonic movements, and erosion, have also shaped the island. The volcanic activity on the island has created several volcanic features, including the Yasur volcano, one of the most active and accessible volcanoes in the world (Pfeiffer, 2023). Tectonic movements have also shaped the island's topography, with several faults and folds. Erosion has also played a significant role in shaping the island's landscape, with the coastal areas being highly susceptible to erosion due to their low elevation and proximity to the sea (Stewart et al., 2010).

#### *6.4.1.2 Groundwater site hydrogeology*

The water supply in Port Vila comes from the Tagabe catchment (17.70° S, 168.32° E). The study area for this research is Tagabe coastal aquifer, shown in Figure 6.2. The hydrogeology of this area is complex and influenced by the island's geology, rainfall patterns, and land use. According to a report by the Vanuatu Geohazards Observatory (VGO), the Tagabe catchment area has a fractured volcanic rock aquifer system composed of basalts and andesites (VGO, 2015). A study by the United Nations Development Programme (UNDP) identified several factors affecting groundwater

recharge in the Tagabe Catchment area, including rainfall patterns, land use, and soil characteristics (UNDP, 2016). Tagabe catchment supplies water to the residents, businesses, agriculture, and manufacturing industries in Port Vila. However, with the rapid urbanisation and population growth of Port Vila and the push to increase tourism and infrastructure, there will be a higher demand for freshwater per person, putting more pressure on the Tagabe freshwater aquifer. Climate change will also make Port Vila and Vanuatu more vulnerable, further jeopardising the ability to support current and future users of the Tagabe water (TRCMP, 2018).

Tagabe catchment has eight active production boreholes which supply water in Port Vila. The log of borehole EF378 data from 1994 suggested that the Tagabe aquifer can be considered two layers. The first layer has sand and gravel, whereas the second is mainly limestone. The depth of layer one goes to 80 m, and then limestone is below that. Therefore, to cater for any uncertainties, only 20 m of limestone as layer 2 was considered. Moreover, the Tagabe coastal aquifer is heterogeneous, shallow, and unconfined. Tagabe coastal aquifer has two active rivers, Sono and Tagabe river, which also acts as a source to the Tagabe aquifer. The area modelled is approximately 57 $km^2$, with eight boreholes operating in close proximity.

The Department of Water Resources, Government of Vanuatu, supplied the groundwater data. However, the data was limited. The dataset included bore pumping data from 2017 to 2022 and the electrical conductivity of some bores from 2019-2021. The hydraulic head values were not available, nor were the initial concentrations. Limited data was used to develop our numerical model, calibrate and validate, and test different scenarios that can manage SWI in Tagabe coastal aquifer. The hydrogeological parameters and other boundary conditions were taken from the bore log data and the report by Depledge (1994). The report can be shared with the mutual consent from the Government of Vanuatu. The report mentioned that hydraulic conductivity was between 20 m/d to 45m/d based on the soil types. Moreover, the specific storage value of approximately 0.000035 1/m was assumed based on the limited data from the report. Vanuatu receives a lot of rain and 90% can be runoff. Therefore, 7.5% of the rainfall as recharge and 3% as evapotranspiration were used for this study. Other hydrogeological parameters and boundary conditions used from the field are given in Table 6.1.

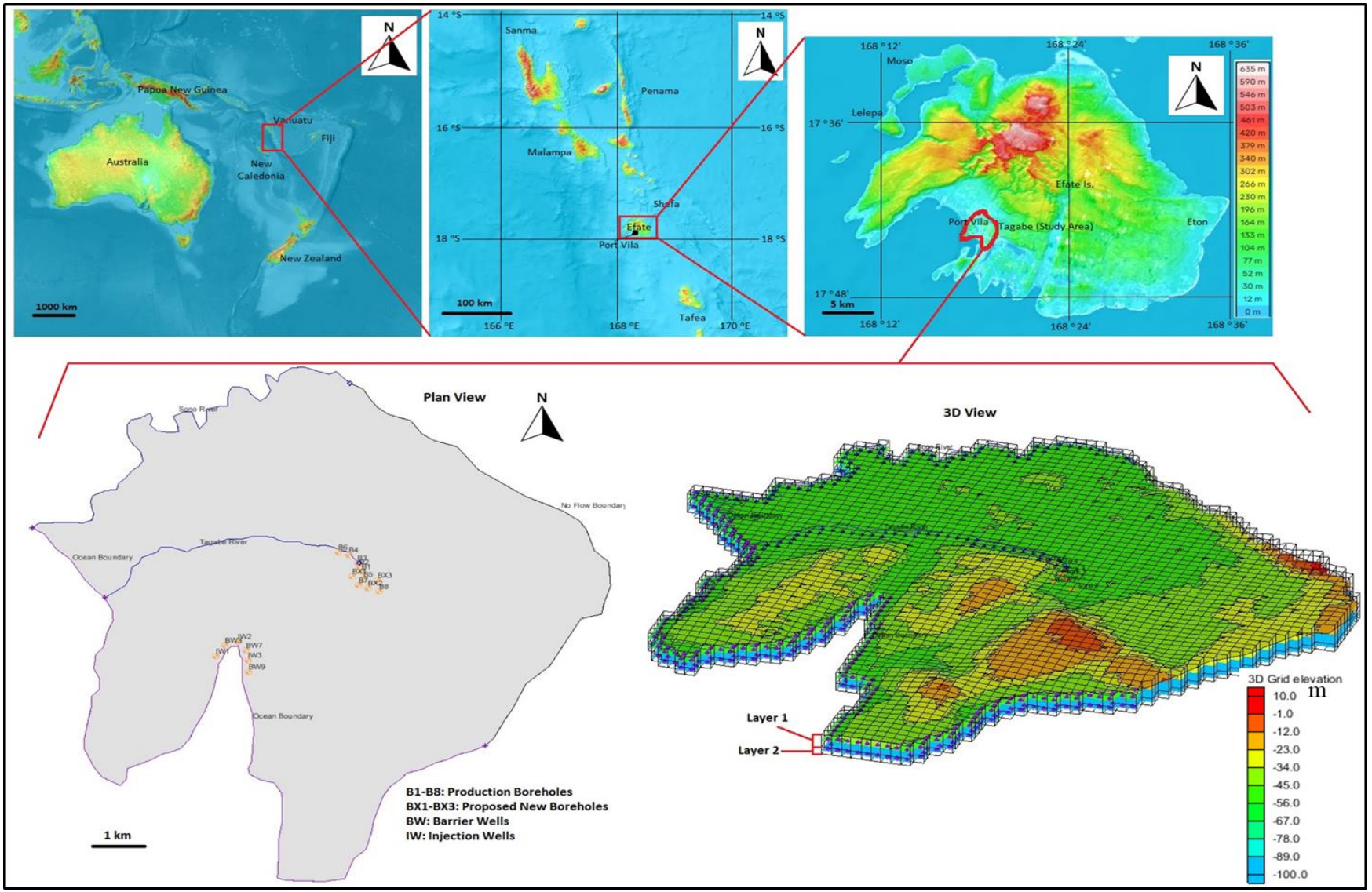



Figure 6.2: Study area inclusive of the plan and 3D views.

Table 6.1: Model parameters and the values used for the model design.

| **Definition** | **Assigned field values** | **Calibrated values** | **S.I. Units** |
|---|---|---|---|
| Layer 1 (Sand and gravel) | Hydraulic Conductivity, K = 20<br>Porosity = 0.35 | Hydraulic Conductivity, K = 25.5<br>Porosity = 0.45 | K = m/d<br>Porosity = dimensionless |
| Layer 2 (Limestone) | Hydraulic Conductivity, K = 35<br>Porosity = 0.45 | Hydraulic Conductivity, K = 40<br>Porosity = 0.55 | |
| Recharge | 0.0004 | 0.000271 | m/d |
| Horizontal Anisotropy | 1 | | dimensionless |
| Freshwater Density | 1000 | | $kg/m^3$ |
| Seawater Density | 1025 | | $kg/m^3$ |
| Saltwater Concentration | 35 | | $kg/m^3$ |
| Specific Storage | 0.000035 | | 1/m |
| River conductance | 1 | | $m^2/dm$ |
| Longitudinal dispersivity | 30 | | m |
| Density/Con. constant, F | 0.7143 | | dimensionless |

### 6.4.2 Flow and solute transport model

Developing management strategies for SWI is a complicated and nonlinear process that can be addressed using mathematical models such as numerical simulation models. In order to simulate and manage SWI, a numerical simulation model was developed using SEAWAT code within the Groundwater Modeling System (GMS). SEAWAT uses a numerical code to replicate 3D, variable density, and transient groundwater flow in porous mediums by combining the MODFLOW and MT3DMS programs. MODFLOW solves the nonlinear variable density flow equations, while MT3DMS addresses the nonlinear temporal and spatial salt or solute transport equations, as described by Guo and Langevin (2002).

#### *6.4.2.1 Governing Equations*

The variable-density flow process solves the following form of the variable-density groundwater flow equation (tensors and vectors are shone in bold) (Langevin et al., 2008).

$$\nabla \cdot \left[\rho \frac{\mu_0}{\mu} \mathbf{K_0} \left( \nabla h_0 + \frac{\rho - \rho_0}{\rho_0} \nabla z \right)\right] = \rho S_{s,0} \frac{\partial h_0}{\partial t} + \theta \frac{\partial \rho}{\partial C} \frac{\partial C}{\partial t} - \rho_s q'_s \,, \qquad (6.1)$$

where $\rho_0$ is the fluid density [kg/m$^3$] at the reference concentration and reference temperature, $\mu$ is dynamic viscosity [kg/md], $\mathbf{K_0}$ is the hydraulic conductivity tensor of material saturated with the reference fluid [m/d], $h_0$ is the hydraulic head [m] measured in terms of the reference fluid of a specified concentration and temperature (as the reference fluid is commonly freshwater), $S_{s,0}$ is the specific storage [1/m], defined as the volume of water released from storage per unit volume per unit decline of $h_0$, $t$ is time [d], $\theta$ is porosity [dimensionless], $C$ is salt concentration [kg/m$^3$], $q'_s$ is a source or sink [1/d] of fluid with density $\rho_s$.

The integrated MT3DMS Transport process solves the following form of the solute transport equation.

$$\left(1 + \frac{\rho_b K_d^k}{\theta}\right) \frac{\partial(\theta C^k)}{\partial t} = \nabla \cdot (\theta \mathbf{D} \cdot \nabla C^k) - \nabla \cdot (\mathbf{q} C^k) - q'_s C_s^k + \sum_{k=1}^{N} R_k, \qquad (6.2)$$

where $\rho_b$ is the bulk density (mass of the solids divided by the total volume) [mg/m$^3$], $K_d^k$ is the distribution coefficient of species $k$ [m$^3$/kg], $C^k$ is the concentration of species $k$ [kg/m], $\mathbf{D}$ is the hydrodynamic dispersion coefficient tensor [m$^2$/d], $\mathbf{q}$ is

specific discharge [m/d], and $C_s^k$ is the source or sink concentration [kg/m$^3$] of species *k*. $R_k$ (*k=1, ...N*) is the chemical reaction term (kg/m$^3$d) of species *k.*

SEAWAT's earlier versions assumed that $\frac{\mu_0}{\mu}$ was equal to one, resulting in viscosity effects being ignored and fluid density being considered as a simple linear function of only one solute species. In SEAWAT version 4, fluid density and viscosity can be computed using concentrations from one or more solute species. These equations of state link the density and viscosity terms in equation 6.1 to one or more of the MT3DMS species concentrations ($C^k$) in equation 6.2. By permitting one or more MT3DMS species to affect fluid density and viscosity, variable-density groundwater flow can be paired with simultaneous solute and heat transport (Langevin et al., 2008). The previous edition of SEAWAT and the variable density groundwater flow and transport equations can be found in the studies by Guo and Langevin (2002) and Zheng and Wang (1999).

#### *6.4.2.2 Conceptual and flow model design*

The MODFLOW-2000 code was used to develop the conceptual model of the Tagabe coastal aquifer. The length in the model domain's X, Y and Z directions were 7.50 km, 7.61 km, and 0.1 km, respectively. A 100 x 100 m cell size was used to create 3D finite-difference grids for the entire model domain. Two layers were created with different values of hydraulic conductivities in both layers. The uniform hydraulic conductivities of layer 1 and 2 was assigned as 20 m/d and 35 m/d, respectively. The porosities of layer 1 and layer 2 were also assigned as 0.35 and 0.45, respectively. Layer 1 was from 0 to -80 m, while layer 2 was from -80 to -100 m. The southern part of the model domain was the specified head boundary (CHB), while the eastern side was no flow boundary. The northwestern side was the Sono River, connected to the ocean boundary and no-flow boundary. The no-flow boundary was assigned merely because the groundwater flows parallel to the no-flow boundary. Tagabe River is connected to the ocean boundary from the southwestern side and goes up to the middle of the model domain. Tagabe River is near the production bore and the Vanuatu International Airport.

The observed hydraulic head values from the boreholes in Tagabe were not available. However, only one value of each borehole was provided, which was recorded in 2019. Approximate head values were assigned to the boundaries using the given head values. The CHB values for the western and southeastern nodes were assigned as 9 m and 8.8 m, respectively. The head values were assigned in such a way that the hydraulic

gradient was slightly towards the landward side. This was done because the initial conditions and head values were unknown, but the salinity was present in the Tagabe coastal aquifer, indicating a landward-side hydraulic gradient.

Moreover, the head values of the Sono River for the western and northern nodes were assigned as 9.2 m and 9 m, respectively. At the same time, the head values for Tagabe River at the western and in the centre of the model domain nodes were assigned as 9.2 m and 7 m, respectively. All eight boreholes (B1-B8) were added to the model domain using their specific geographic locations from Table 6.2. The actual transient pumping values from 2017 to 2021 were also assigned to each bore. Furthermore, all the hydrogeological parameters and boundary conditions, wells, pumping values and head values were mapped to MODFLOW and the steady-state simulation was carried out for 20 years to establish the initial conditions.

Table 6.2: Location of production boreholes in Tagabe, Port Vila.

| Borehole Number | Location | |
|---|---|---|
| | Latitude (S) | Longitude (E) |
| B1 | 17.710828 | 168.323633 |
| B2 | 17.710253 | 168.323403 |
| B3 | 17.709753 | 168.323186 |
| B4 | 17.708767 | 168.322242 |
| B5 | 17.711758 | 168.323814 |
| B6 | 17.708433 | 168.321072 |
| B7 | 17.712467 | 168.323269 |
| B8 | 17.713261 | 168.325547 |

#### *6.4.2.3 Solute transport model design*

Upon successful convergence of the flow model, the solute transport solver, MT3DMS, was introduced, and the simulation was changed from a steady state to a transient state by adding the 5-year simulation periods. The head values from the steady-state simulations were used as initial heads in the transient flow simulations. The solute salt was added to MT3DMS, and a uniform initial salt concentration of 0.1 kg/m$^3$ was assigned in the model domain. The advection, dispersion, source and sink mixing packages were used for solute transport in MT3DMS. SEAWAT-version 4 code was then introduced to solve the solute transport equations with the help of MT3DMS. A variable-density flow package was utilised to solve solute transport for freshwater and saltwater fluids.

Moreover, in the SEAWAT module, freshwater density was selected as the standard fluid density. A constant factor, F, was also applied to the density and concentration slope to prevent the model from overestimating the freshwater lens. If F were set to zero, then the density would not change with a change in concentration, providing similar results to those obtained from MT3DMS simulations. However, SEAWAT was preferred for generating results as it incorporates a variable-density flow (VDF) that restricts the free movement of freshwater and seawater, forming a transitional zone for the freshwater lens.

### 6.4.3 Model Calibration and Validation

SEAWAT was initiated for the 5-year period considering the pumping data from 2017-2021. However, only the electrical conductivity (EC) data of boreholes B1, B2, B3, B7 and B8 were available to calibrate the model. The EC data was only available from 2019-2021. However, some data was missing from the year 2021. Hence, the EC data from 2019 and 2020 was used to calibrate the model. EC was converted to parts per million (ppm) or milligrams/litre (mg/L) by multiplying the EC, measured in microseimens/centimetre (μS/cm), values by 0.55 (Landscape-SA., 2015; Rusydi, 2018). Then, mg/L was divided by 1000 to convert the salt concentration to kg/m$^3$. The limitation of this calibration process was that the flow model was not calibrated because the observed head values were unavailable. Hence, only the secondary data was used in the calibration process. Calibrating the model with secondary data was difficult and time-consuming, especially when the initial concentrations were unknown. However, the initial salt concentrations, recharge value, hydraulic conductivities and porosities were adjusted using the trial-and-error method and multiple simulations to get the desired results.

After calibrating the model, it was simulated for the next 20 years, from 2022 to 2043. The results from the calibrated model became the base case for this study. Using the calibrated model and stress period, various scenarios were tested and simulated that can manage the SWI for Tagabe coastal aquifer.

### 6.4.4 Simulated scenarios

Once the numerical simulation model was developed, calibrated and validated, the base case simulation was run for 20 years to see the extent of SWI in the Tagabe coastal aquifer. The simulated results indicated extensive SWI. Therefore, scenarios that could

manage SWI were evaluated considering uncertainties like climate change. The scenarios included (1) an increase in population and pumping rates, (2) the use of barrier wells, (3) the use of barrier wells plus injection wells and (4) a sea level rise. These scenarios were compared with the base case, and the optimal SWI management strategies were suggested for Tagabe coastal aquifer.

## 6.5 Results

### 6.5.1 Calibration and Validation

The model was calibrated using the techniques mentioned in Section 6.4.3. The observed salt concentrations of March, May, July, September, November 2019 and February 2020 were used in the calibration process. The months of April, June, August, October and December 2020 were used to validate the model. These months were chosen based on the quality and availability of the data points. The calibration and validation results of different boreholes are shown in Figure 6.3. The initial salt concentration that gave the desired results was 0.3 kg/m$^3$. The model was simulated for 5 years (2017-2021). However, the calibration started from 3$^{rd}$ year (2019), which gave us a good correlation ($R^2 > 0.9$) between observed and simulated values because the initial concentration was automatically readjusted based on transient pumping rates. If complete data were available, calibration would have started using the data from 2017. Therefore, the initial concentrations had to be assigned as < 0.3 kg/m$^3$. The calibrated model was then used to test different scenarios.

### 6.5.2 Base case

Tagabe coastal aquifer has eight operational boreholes that supply the water to the capital city of Vanuatu. Based on the current field pumping data, MODFLOW interpolated the transient pumping data for a 20-year period which was used to predict the SWI in Tagabe coastal aquifer. The calibrated model was simulated for 20 years, and the SWI was recorded. The plan view of the model domain for the base case is shown in Figure 6.4(a-1 to a-20). Five different time-steps results were recorded after the simulation. The front view of the base case simulation results was also recorded, as shown in Figure 6.5(a-1 to a-20). The numbers 1-, 5-, 10-, 15-, and 20- indicate 1-year, 5-year, 10-year, 15-year and 20-year time steps. The contours indicate the SWI into Tagabe coastal aquifers. Red indicates > 30 kg/m$^3$ salt concentration, whereas light blue indicates ~ 0 kg/m$^3$ salt concentration.

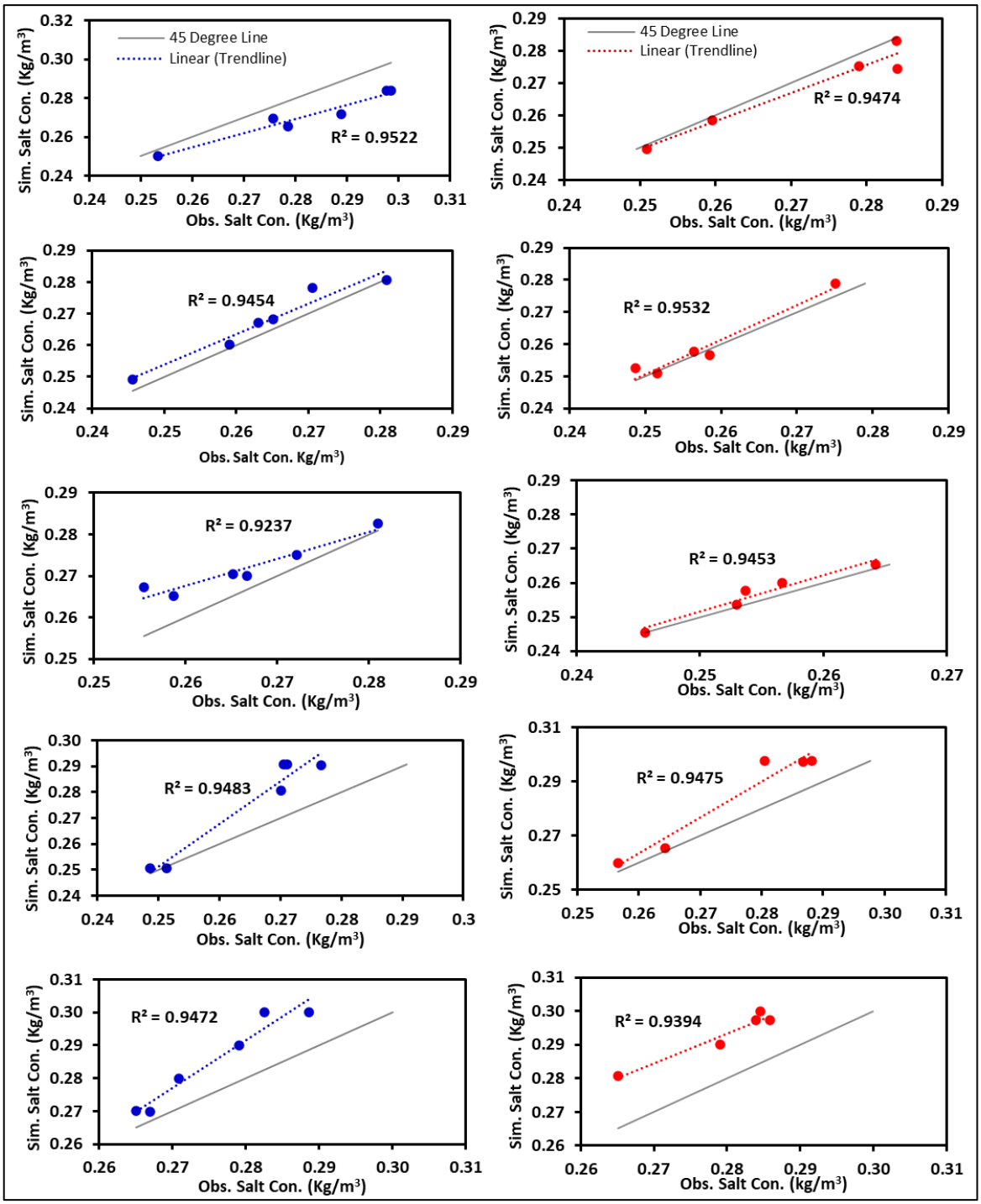



Figure 6.3: Observed versus simulated salt concentrations obtained during calibration (a to e) and validation stage (f to j). (a to e) represents the data from bore 1, 2, 3, 7 and 8, respectively. Similarly, (f to j) represents the data from bore 1, 2, 3, 7 and 8, respectively.

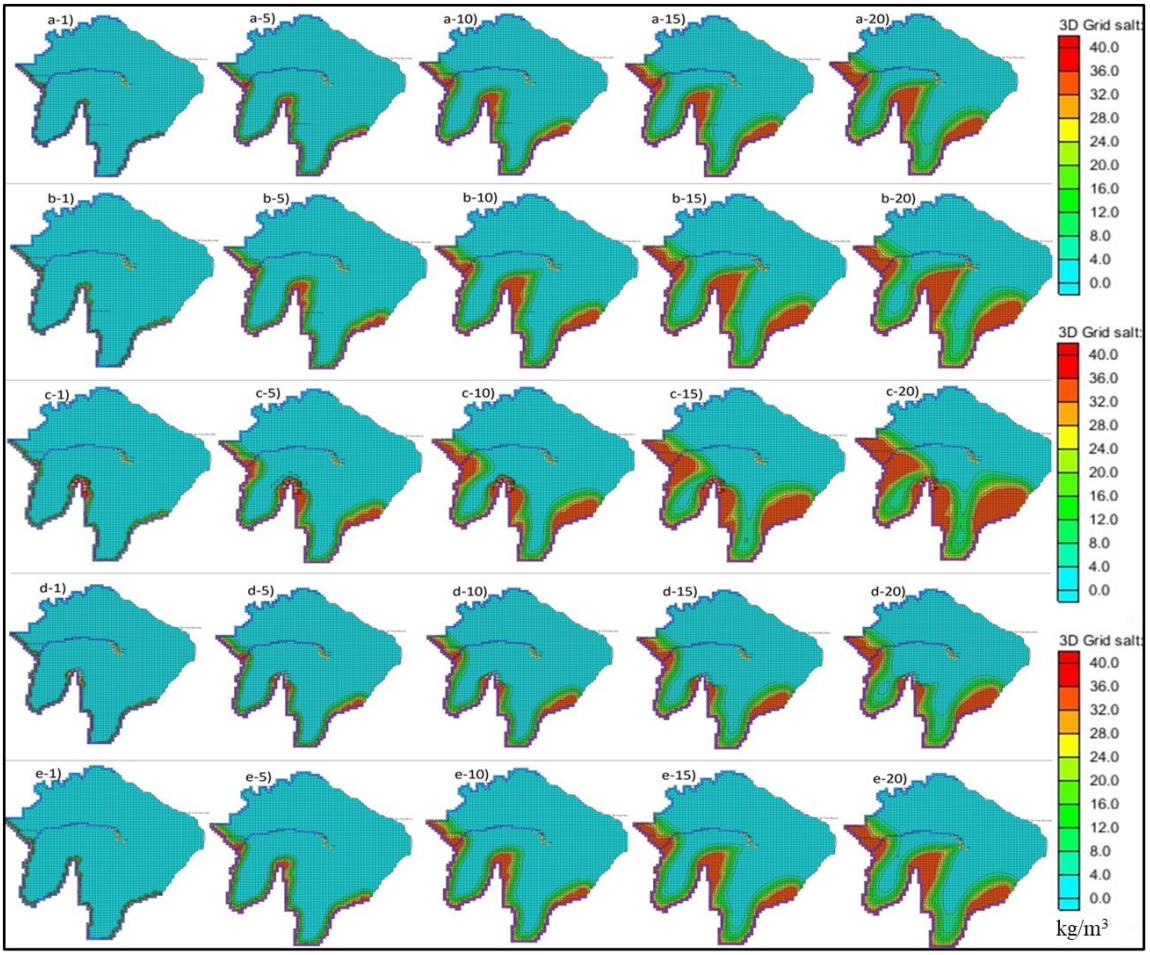



Figure 6.4: (a-1 to a-20) shows the plan view of the simulated results of saltwater intrusion for the base case; (b-1 to b-20) increasing the pumping and number of pumping wells (scenario 1); (c-1 to c-20) addition of barrier wells (scenario 2); (d-1 to d-20) addition of injection well plus barrier wells (scenario 3); (e-1 to e-20) sea level rise (scenario 4). The numbers 1, 5, 10, 15 and 20 represent the time steps 1 year, 5 years, 10 years, 15 years and 20 years, respectively.

### 6.5.3 Scenario 1: Increased population and pumping rates

Population growth is inevitable in future. A higher population will lead to higher water demand in all sectors. Since Tagabe coastal aquifer is the only water supplier in Port Vila, the uncertainties must be carefully considered while predicting the SWI rates. The projected population growth rates of Port Vila for 20 years are given in Figure 6.6. The projections were made based on the live population forecasts given by the World Population Review (WPR) (WPR, 2023). As per WPR, the population of Vanuatu will grow by 2.39%, 2.31%, 2.2%, 2.11% and 1.98% for the years 2022, 2027, 2032, 2037 and 2043, respectively. Based on these projections and using the actual population of Port Vila from City Population (CP) for the year 2020 (CP, 2023), it was found that by 2043,

the population of Port Vila will be approximately 54668. The projected population till 2043 is an increase of ~10% compared to 2020.

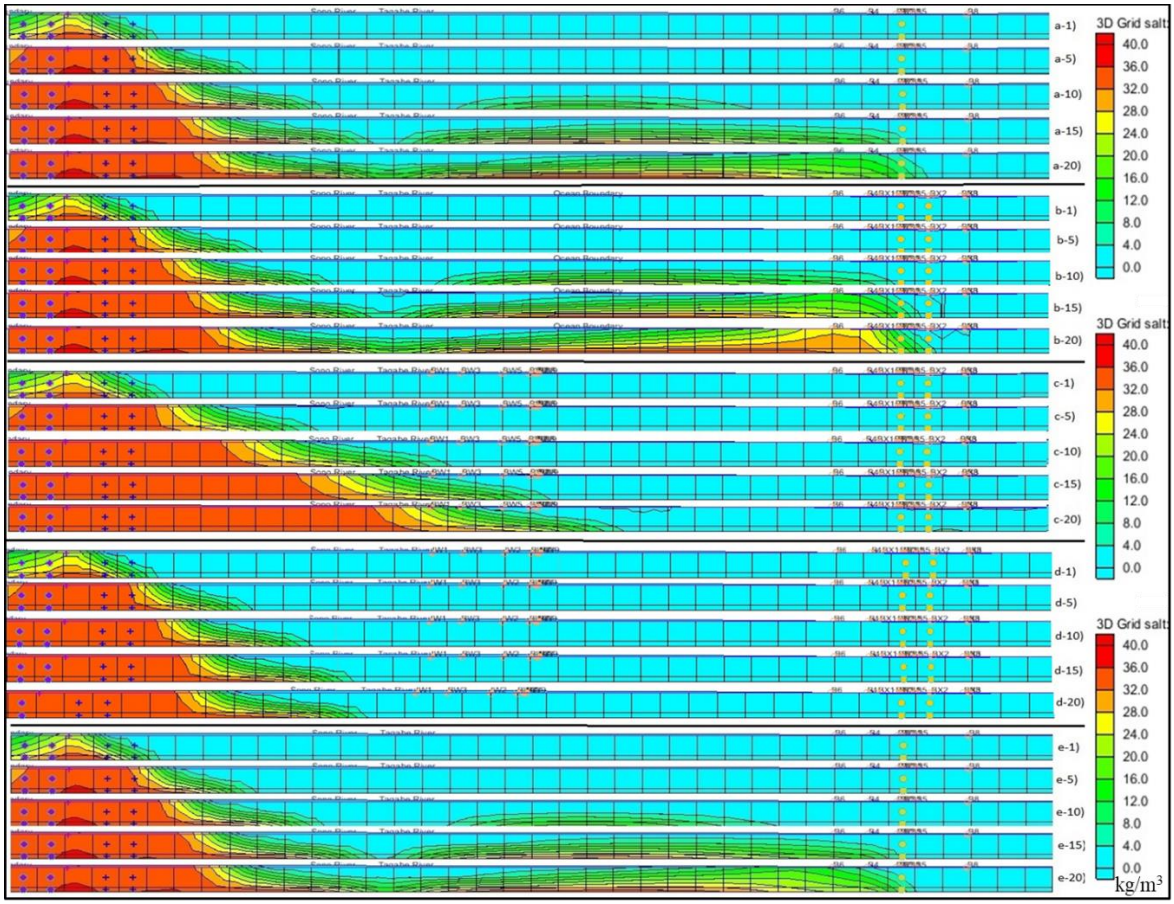



Figure 6.5: (a-1 to a-20) shows the front view of the simulated results of saltwater intrusion for the base case; (b-1 to b-20) increasing the pumping and number of pumping wells (scenario 1); (c-1 to c-20) addition of barrier wells (scenario 2); (d-1 to d-20) addition of injection well plus barrier wells (scenario 3); (e-1 to e-20) sea level rise (scenario 4). The numbers 1, 5, 10, 15 and 20 represent the time steps 1 year, 5 years, 10 years, 15 years and 20 years, respectively.

Moreover, the transient pumping rates were increased for all boreholes by 10% based on population growth. Also, three more boreholes were added to cater for the higher demand and marked as BX1, BX2 and BX3, as shown in Figure 6.2. The transient pumping rates similar to bores 7 and 8 were assigned to the three new boreholes. The changes made in the conceptual model were mapped to MODFLOW and MT3DMS then SEAWAT was initiated. The plan view and front view of the simulated SWIs of this scenario for 5 time-steps are shown in Figure 6.4(b-1 to b-20) and Figure 6.5(b-1 to b-20), respectively. The results indicated that the extent of SWI has further contaminated the Tagabe freshwater aquifer compared with the base case. The contours in these figures

also indicated that increasing the pumping rates and the number of boreholes further increases the SWI.

Moreover, the salt concentration of the bores 1, 3, 7 and 8 for 1-year, 5-year, 10-year, 15-year and 20-year time-steps were recorded to further look at the exact amount of changes in the salt concentration. Figure 6.7a compares the salt concentration of different time-steps and bores for the base case and scenario 1. Not many changes were shown for the first two time-steps. However, the last three time-steps did show some significant changes. The percentage increase in salt concentration from base case to scenario 1 for bore 1 during the time-steps of 10, 15 and 20 years are 86.34%, 759.32% and 273.75%, respectively. Moreover, the percentage increase for bore 7 at 3 time-steps as bore 1 was 209.79%, 277.78% and 117.05%, respectively. Bores 3 and 8 did not show significant changes compared to the base case, which could have been the effect of transient and automatic pumping data interpolation in MODFLOW.

### 6.5.4 Scenario 2: Addition of barrier wells

Using the same parameters and boundary conditions from scenario 1, six barrier wells (BWs) were added to prevent the SWI from encroaching into the model domain. Based on the initial simulations, the BWs were systematically placed near the coast to prevent the upconing of the saline water. The BWs acted as a barrier in preventing the saltwater from moving towards the landward side and contaminating the freshwater, hence the name. The plan view of the simulated results for this scenario is shown in Figure 6.4(c-1 to c-20). From the results, the extent of encroachment has significantly decreased when compared with the base case and scenario 1. However, the SWI from the southeast side of the model shows an increment for all 5 time-steps. The increment is shown because the BWs were not added near the southeast coast. However, adding BWs has prevented the saline water from reaching the freshwater wells, as shown in the plan view.

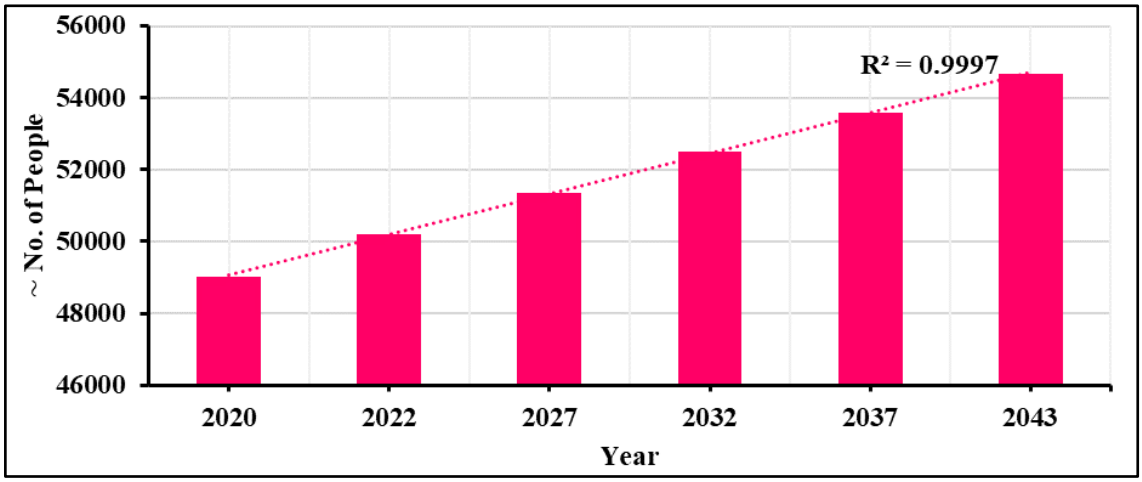



Figure 6.6: Projected population of Port Vila, Vanuatu.

The front view of the study area is also used to show our results for SWI better after adding BWs, shown in Figure 6.5(c-1 to c-20). The front view shows that the SWI has significantly reduced after adding the BWs. However, the salt concentration near the coast has increased vastly due to excessive pumping from BWs. This increase is shown as the toe length of SWI has increased. The increase in the salt concentration did not affect the freshwater bore or wells in the Tagabe area. The front view also shows that the SWI contour's length and strength have halved for 10-, 15- and 20-year time-steps compared to the base case scenario.

Moreover, the salt concentrations at bores 1, 3, 7 and 8 were recorded for the 5 time-steps as scenario 1. Figure 6.7b compares the salt concentrations for the four bores after adding the BWs and the base case. The bars in the graph indicate that the salt has significantly decreased for bores 1, 3 and 7. However, not many changes were shown for bore 8. The salt concentration for bore 1 was reduced by 9.55%, 22.96%, 36.58%, 56.11% and 92.29% for 1-, 5-, 10-, 15- and 20-year periods, respectively. Similarly, the salt concentrations for bore 3 of the five time-steps were also reduced by 16.47%, 28.86%, 32.57%, 34.92% and 64. 19%, respectively. The salt concentration of bore 7 at the 20-year time-step was 5.92 kg/m$^3$ for the base case, whereas after adding BWs, the salt concentration was reduced to 0.46 kg/m$^3$, a decrease of 92.19%. The salt concentrations at bore 8 for 1-, 5-, 10-, 15- and 20-year time-steps for this scenario were increased by 0.25%, 0.97%, 0.35%, 2.26% and 391.65%, respectively.

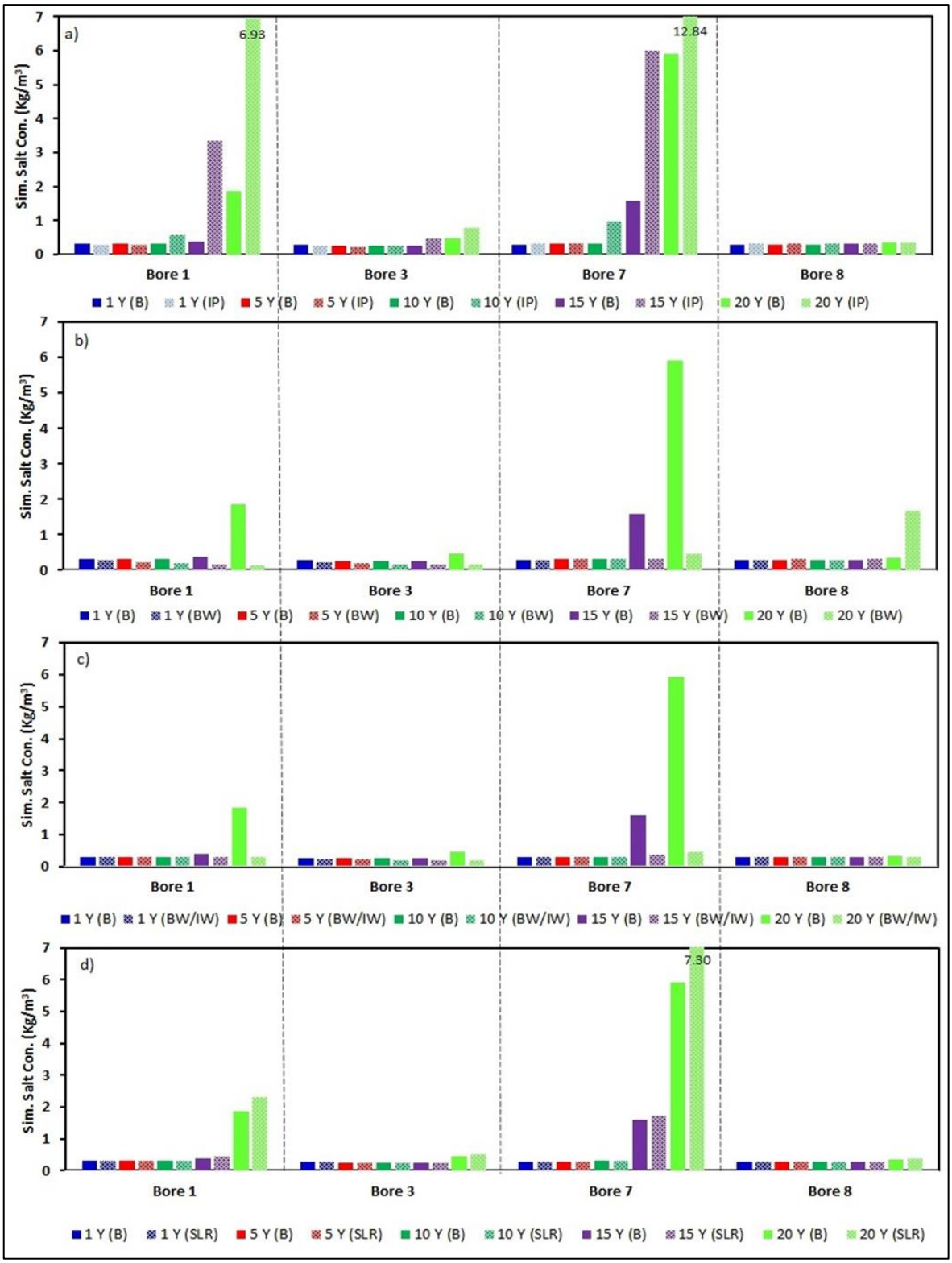



Figure 6.7: a) shows the comparison of simulated salt concentrations for different boreholes for the base case and the increased pumping and the number of pumping wells (scenario 1); b) shows the comparison of simulated salt concentrations for different boreholes for the base case the addition of barrier wells (scenario 2); c) shows the comparison of simulated salt concentrations for different boreholes for the base case the addition of injection well plus barrier wells (scenario 3); d) shows the comparison of simulated salt concentrations for different boreholes for the base case and the sea level rise (scenario 4).

### 6.5.5 Scenario 3: Addition of barrier wells and injection wells

The injection wells (IWs) and BWs were added to the model domain as an SWI management technique for the Tagabe coastal aquifer. In scenario 2, six BWs were added, whereas three BWs were replaced with IWs in this scenario. Therefore, for this scenario, there are three BWs and three IWs. Transient pumping rates, lower than BW pumping, were assigned to the IWs. The model simulation was initiated, and the plan view of the simulated results is given in Figure 6.4(d-1–d-20). The results show significant changes as the SWI is reduced further compared to the base case and scenarios 1 and 2. The length of encroachments from all sides of the model domain, from the coast to the pumping locations, was reduced significantly.

Furthermore, Figure 6.5(d-1–d-20) shows the front view of the simulated salt concentrations after adding BWs and IWs. The length of salt contours has significantly decreased compared to the base case and scenarios 1 and 2. Injecting freshwater also reduces the intensity of salt concentration at the coast. The front view shows the encroachment length is half that of scenario 2, whereas it is a quarter of the base case and scenario 1. Adding IWs has significantly reduced SWI in the Tagabe coastal aquifer.

The salt concentrations for bore 1, 3, 7 and 8 were significantly reduced when compared with the base case, as indicated by the bars of Figure 6.7c. The percentage decrease in salt concentration for bore 1 during 1-, 5-, 10-, 15- and 20-year time-steps are 6.36%, 8.62%, 6.16%, 22.93% and 83.73%, respectively. The percentage decrease for bore 3 for the same respective time-steps as bore 1 are 10.93%, 14.67%, 17.33%, 18.01%, and 54.29%, respectively. Similar decreasing trends were also noted for bore 7. However, the highest decrease in salt concentration was noted at bore 7 for the 20-year time-step, with a decrease of 92.37% compared with the base case. Moreover, bore 8 has shown slight increments of salt concentrations during 1-, 5-, 10- and 15-year time-steps. The percentage increments for these four time-steps were 0.78%, 0.43%, 0.08% and 0.11%, respectively. However, the salt concentration decreased during the 20-year time step by 9.63% when compared with the base case.

### 6.5.6 Scenario 4: Sea level rise

The sea level rise (SLR) is one of the significant natural disasters in Vanuatu. The SLR could also be affecting the Tagabe freshwater aquifer. The SLR was modelled for Tagabe coastal aquifer to validate the previous statement, and the extent of SWI was

noted. The projected SLR for Vanuatu, in general, is shown in Figure 6.8. Based on the projections, the SLR for Vanuatu by 2043 will be approximately raised by 25 cm. Hence, the coastal head boundaries were gradually increased by 1.2 cm each year for 20 years until it reached 25 cm. Using this projected SLR, the model was simulated. The increase in head values for the coastal boundary indicated SLR. The plan view of the simulated results are shown in Figure 6.4(e-1 to e-20). The boundary conditions and other initial conditions used for the simulation of SLR were used from the base case model design.

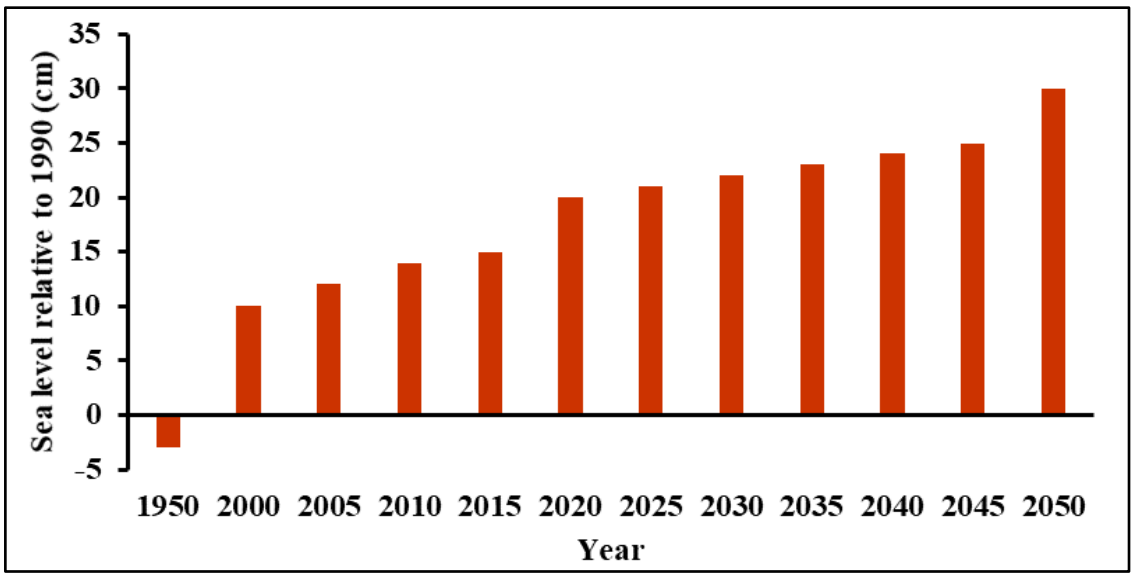



Figure 6.8: Projected sea level rise for Vanuatu, relative to 1990. Source (CRCP, 2021).

Moreover, to see the SLR effects further, the front view for 1-, 5-, 10-, 15- and 20-year time-steps were compiled as shown in Figure 6.5(e-1 to e-20). The front-view results are also similar to the base case results. However, the contour and the salt concentrations for year-20 are higher, as indicated by colour changes. The more orange and yellow colours are noted in the contours, indicating higher salt concentrations. From the front-view, the changes are less significant when compared with the base case. However, to see the effect of SLR on the intensity of SWI, the salt concentration values were plotted using the bar graph to compare the salt concentrations with the base case. The results are shown in Figure 6.7d.

Using the bar graph, it was visible that SLR does have some impact on the water quality in Tagabe coastal aquifer. The percentage increase in salt concentration for bore 1 during 1-, 5-, 10-, 15- and 20-year time-steps are 0.07%, 0.19%, 0.36%, 14.99%, and 24.45%, respectively. Similarly, the percentage increase for the same time-steps for bore 3 is 0.33%, 1.11%, 1.67%, 4.61%, and 16.07%, respectively. Moreover, the percentage

increase in salt concentration for bore 7 is also noted for all time-steps. The highest salinity increases for bore 7 was noted at a 20-year time-step of 23.37% compared to the base case. The salt concentration changes for bore 8 were insignificant, except at the 20-year time-step, which was around 13.28% compared to the base case scenario.

## 6.6 Discussion

The SWI in Tagabe coastal aquifer was modelled using real field data. The simulation results indicated that SWI is currently affecting and will also affect freshwater resources in the future for Tagabe. Using the field data, the model was calibrated and validated. The calibrated model was used to test different scenarios that could help manage SWI in Tagabe coastal aquifer. The scenarios-based sensitivity analysis for this research was the first for Vanuatu and any PICs. Based on the scenarios and sensitivity analysis, robust SWI management regulations can be drawn for Tagabe coastal aquifer.

Using hydraulic barriers like barrier wells (BWs) to abstract the saline water near the coast prevents the extent of SWI from contaminating the freshwater wells. Armanuos et al. (2020) effectively showed that using BWs near the saltwater side reduced the SWI rates or SWI length ratio. Abdoulhalik et al. (2017) also stated that using BWs reduced the SWI rates in coastal aquifers. Similarly, our results also indicated that using BWs near the coast positively affected the SWI in Tagabe coastal aquifer. The scenario that showed exciting results in minimising the extent of SWI in our model domain was using mixed BWs and IWs. Abd-Elaty et al. (2021) investigated the strategies for controlling the SWI due to sea level rise (SLR) and climate change for humid and hyper-arid regions. The authors reported that using recharge wells or IWs, brackish water abstraction, and desalination reduced the SWI rates. The authors suggested using mixed hydraulic barriers to manage SWI. Similar results were noted in our study.

Moreover, Yang et al. (2021) showed how to mitigate the SWI using pumping and injection strategies. The authors reported that IWs and PWs are more effective in managing SWI than using IWs or BWs alone. Our study also revealed that using the combination of hydraulic barriers like BWs and IWs helps to further reduce the extent of SWI in the Tagabe coastal aquifer. The hydraulic barriers implemented in this study showed that SWI could be managed. BWs and IWs alter the hydraulic gradient and prevent the upconing of the saline water. Werner et al. (2013) reported that the hydraulic barriers block the saline water encroachments by increasing the difference between the

groundwater head and seawater head. Similarly, our results indicated that hydraulic barriers effectively block saline water from reaching freshwater wells.

However, physical barriers like subsurface dams and cutoff walls in controlling SWI are also widely used (e.g., Luyun et al., 2011; Abdoulhalik et al., 2022; Kaleris and Ziogas, 2023). These studies have investigated the effect of cutoff walls on SWI in coastal aquifers, and they reported that the use of cutoff walls is effective in managing SWI. However, this study is the first for Tagabe coastal aquifer, therefore only hydraulic barriers were used and modelled for the study area. The use of physical barriers in managing SWI for the Tagabe coastal aquifer will be added to our future scope of work. Moreover, cutoff walls physically prevent the SWI and it does not need any maintenance. However, the initial costs are high (Abdoulhalik et al., 2017). Cutoff walls could be used for Tagabe in the future.

Moreover, the use of BWs can also have some adverse effects on the management of SWI. Pool and Carrera (2010) studied the dynamics of negative hydraulic barriers to prevent SWI and reported that BWs sometimes abstract more freshwater, reducing the freshwater volume in aquifers. Moreover, Kumar (2006) reported that the disposal of abstracted saline water is an issue because it cannot be used anywhere unless the saline water is desalinated. Therefore, this study proposed using the IWs along with BWs. The abstracted saline water can be desalinated and injected using IWs in Tagabe. If this process seems expensive and time-consuming, the abstracted saline water can be disposed of back into the ocean. Disposing saline water back into the ocean will not be costly because most of the population lives near the coast, and the freshwater wells are not far from the coast. Hence, a shorter length of pipes may be required to dispose of the saline water. If the abstracted saline water is disposed of in the ocean, the input for injection wells can be taken from freshwater sources like the Tagabe River or Sono River in Port Vila. Also, due to high rainfalls in Vanuatu, the rainwater could be harvested and injected backing to the aquifer to increase the aquifer volumes.

The hydraulic barriers proposed and modelled for Tagabe coastal aquifer would manage SWI and protect the freshwater wells from over-abstraction of groundwater. However, climate change and sea level rise (SLR) also affects the groundwater in Tagabe. Therefore, the SLR factor was considered and modelled for Tagabe coastal aquifer. The results indicated that the extent of SWI and the strength of salt concentrations in the

freshwater aquifer have increased. Similar results were reported by Casillas-Trasvina et al. (2019) and Romanazzi et al. (2015) for a different study area. Moreover, the SLR by 25 cm was less significant, and fewer variations were noted in our study. The SLR and SWI simulation results were less significant because raising the hydraulic head by 25 cm has significantly less impact on the SWI rates. Loaiciga et al. (2011) and Sharan et al. (2023) also reported that SLR by < 1 m has less effect on the SWI rates in coastal aquifers. However, the length and strength of SWI would be extensive if SLRs by > 1 m in future. The SLR by > 1 m would be considered for the future scope of work for Tagabe coastal aquifer.

Based on the scenario testing and sensitivity analysis, the SWI management strategies for Tagabe coastal aquifer were proposed, as discussed above. Using the results from numerical modelling, the water resource managers, site owners or governing bodies can draw up policies and regulations for using Tagabe groundwater. However, due to uncertainties and the variability of climate conditions in Vanuatu, it is suggested that the policies and regulations be revised every year. Factoring the different boundary conditions, pumping patterns and uncertainties, hydrogeologists can remodel and simulate new sets of SWI management strategies. However, this can be challenging and computationally extensive because numerical modelling is a complex and time-consuming exercise. Hence, using AI-based surrogate and ensemble models would be much easier, more efficient and less computationally extensive to simulate SWI management strategies for coastal aquifers in Vanuatu and in PICs.

## 6.7 Conclusions

The Pacific Island countries (PICs) groundwater resources are threatened by anthropogenic and natural factors. A small PIC, Vanuatu's groundwater system, was studied using real field data from Tagabe coastal aquifer, which supplies freshwater in Port Vila. However, Tagabe is experiencing some salinity concentrations in the freshwater wells. Therefore, the primary aim of this study was to provide saltwater intrusion (SWI) management strategies for Tagabe coastal aquifer.

The SWI management strategies were developed based on numerical modelling results. This is the first study in Vanuatu whereby a numerical model was developed using the SEAWAT code. The developed model was calibrated and validated using the salinity data. The calibrated model was then used to test different scenarios that could effectively

manage SWI. The sensitivity analysis revealed that using hydraulic barriers like barrier wells (BWs) and injection wells (IWs) significantly reduced the extent of SWI in Tagabe coastal aquifers. This study also found that using BWs and IWs in combination was the best technique for managing SWI.

Moreover, the sea level rise (SLR) was modelled to see how it affects the SWI in Tagabe coastal aquifer. It was found that SLR had some effects on SWI rates. The numerical simulation period for the study area was till 2043. Hence the sea level was only raised by the projected level of 2043, which was < 30 cm. Therefore, the effect of SLR was not large. However, simulating the model with higher sea face boundary conditions and for larger stress periods would have a significant effect due to SLR. Moreover, uncertainties need to be catered for while forecasting future scenarios.

The management strategies proposed in this study can be used by the water managers, site owners and governing bodies to draw up policies and regulations to manage the SWI rates in Tagabe coastal aquifer. These strategies will protect the groundwater resources from getting contaminated by SWI in future. Moreover, this study can also benefit some stakeholders or bore drilling companies who want to harvest groundwater from the Tagabe coastal aquifer, as it will give them the benchmark of daily or yearly freshwater production rates without SWI.

The limitation of this study was the availability of quality groundwater data. Also, the hydraulic head values that could have been used to calibrate the flow model were not available. Very limited pumping and salinity data were available. Therefore, the transport model was robustly calibrated. Furthermore, only one bore log was available, which was used to gather hydrogeological parameters and other ground stratigraphy.

The recommendations and future work that are proposed for Tagabe coastal aquifer are (1) setting up proper groundwater heads and water quality data monitoring sites in collaboration with the Government of Vanuatu, (2) developing AI-based modelling techniques, (3) using physical barriers in model to simulate SWI, (4) rising the boundary conditions to factor higher (heads > 1 m) SLR.

The next chapter develops multiple surrogate ensemble models (AI-based) and a simulation-optimisation model for Pareto optimal front solutions in managing saltwater intrusion for a coastal aquifer.

# Chapter 7: A multi-objective simulation-optimisation model for managing saltwater intrusion in a coastal aquifer for a Pacific Island country

A manuscript based on the main contents of this chapter has been submitted for publication and are currently under review, as outlined below:

**Sharan, A**., Roy, D.K, Datta, B., & Lal, A. (Under Review). A multi-objective simulation-optimisation model for managing saltwater intrusion in a coastal aquifer for a Pacific Island country. *Journal of Hydrology.*

## 7.1 Overview

This chapter develops multiple surrogate ensemble models as approximate simulators of the numerical flow and transport simulation model. It also optimises surrogate ensemble models using optimisation algorithms to develop optimal saltwater intrusion management strategies.

## 7.2 Executive Summary

Groundwater resources in Pacific Island countries face threats from climate change, natural disasters, and human activities, with saltwater intrusion (SWI) being a significant issue in coastal aquifers like Vanuatu's Tagabe coastal aquifer. This study developed numerical and machine learning models to manage SWI in the Tagabe aquifer. The SEAWAT was used to create a numerical groundwater model, calibrated and validated with salt concentration data from various monitoring locations (MLs). The model generated input (pumping values) and output (salt concentrations) datasets, which were used to train and test twelve machine learning models or surrogate models. These models were ranked using performance criteria and decision theory, and the top five were used to form ensemble models to predict salt concentrations at four MLs. The Pearson coefficient, Index of Agreement, Kling-Gupta Efficiency and Nash Sutcliffe Efficiency coefficient of four ensemble models at ML1 = 0.745, 0.738, 0.497 and 0.384; ML2 = 0.946, 0.950, 0.753 and 0.848; ML3 = -0.028, 0.166, -0.369 and -0.070; ML4 = 0.415, 0.369, -0.135 and -4.032, respectively. The ensemble models performed better than individual surrogate models, with higher predictive accuracy across different MLs. These models were integrated with the Controlled Elitist Multiple Objective Genetic Algorithm (CEMOGA) to create a simulation-optimisation (S-O) management model, providing Pareto optimal solutions for managing SWI. Verification using the SEAWAT-based

numerical model showed that the ensemble models' predictive accuracy was within 7% of the complex numerical model. This study is novel in its use of limited datasets to train twelve machine learning models and the application of surrogate ensemble and S-O management models in Vanuatu, demonstrating their global applicability for managing SWI in coastal aquifers and aiding policymakers in formulating effective groundwater use policies.

## 7.3 Introduction

Saltwater intrusion (SWI) is a challenging environmental problem in Pacific Island countries (PIC). The majority of the coastal aquifers in PICs are hydraulically linked with the sea merely because the islands are surrounded by the Pacific Ocean. This hydraulic linkage fuels up SWI rates when the sea level rises, variations in tide heights, and over-abstraction of groundwater resources (Sharan et al., 2021). The management of SWI in PICs is critical predominantly because people mostly use groundwater for their daily needs. The SWI problem needs to be addressed not only in PICs but around the globe.

Different techniques are utilised around the globe in managing SWI rates. Sherif et al. (2014) and Song et al. (2018) proposed rules for water resource usage and minimising SWI by reducing pumping and relocation of production bores. However, this approach is costly and temporary and could affect the water supply and demand ratios. The use of physical sub-surface barriers like cut-off walls and dams is proposed by Abdoulhalik et al. (2017). These physical barriers stop SWI and do not need maintenance. However, the cost of installing physical barriers is immense and time-constrained. On the other hand, the use of hydraulic barriers to control SWI has gained particular attention because it has proved that hydraulic barriers control SWI in coastal aquifers (e.g., Dhar and Datta, 2009; Sreekanth and Datta, 2011; Roy and Datta, 2017a; Lal and Datta, 2018).

Dhar and Datta (2009) and Sharan et al. (2023) used hydraulic barriers to manage SWI in coastal aquifers. The authors reported that the use of barrier wells (BWs), injection wells (IWs) and coupled BWs-IWs manages SWI effectively. The authors developed a numerical simulation model and simulated various scenarios, including BW and IW, which managed SWI. However, these hydraulic barriers have some disadvantages, which include the higher BW pumping, availability of freshwater for vertical recharge, and disposal of abstracted brackish or salty water. The method proposed by the authors could be beneficial if the BW pumping could be reduced or minimised and production well

(PW) pumping is maximised. Also, reducing salt concentrations without reducing pumping rates from PWs. These are conflicting and multi-objective problems that can only be tackled by linked simulation-optimisation (S-O) modelling techniques (Dhar and Datta, 2009).

The S-O methodology utilises a simulation model to replicate aquifer processes and an optimisation model to identify the optimal solution. For instance, to increase the groundwater abstraction rates and reduce salt concentration in coastal aquifers, an optimal groundwater abstraction rate has to be employed using a S-O method. The S-O model would give a set of pumping regimes that would maximise pumping from the production bores and minimise pumping from the barrier wells while controlling saltwater intrusion. This approach is essential for determining the most effective abstraction rates from a set of viable solutions found in the Pareto optimal front. The linkage between simulation and optimisation ensures a comprehensive evaluation, allowing the identification of optimal rates amid various feasible alternatives. S-O has been applied by various researchers in managing SWI (e.g., Bhattacharjya et al., 2007; Dhar and Datta, 2009; Roy and Datta, 2017). These studies reported that the S-O model successfully provides Pareto optimal front solutions in managing SWI. Other studies on the application of S-O models in groundwater studies are summarised by Sharan et al. (2021).

The first step in developing a linked S-O model is to develop a 3D numerical simulation model. The numerical simulation model plays a crucial role in comprehending and addressing intricate challenges related to the monitoring and management of saltwater intrusion in coastal aquifers. These models accurately depict the groundwater characteristics of the studied region, providing a comprehensive grasp of the inherent physical processes (Lal and Datta, 2020). To develop a coupled S-O based saltwater intrusion management model, the simulation model needs to be linked to an optimisation algorithm. However, direct linking of a numerical simulation model with an optimisation algorithm is computationally prohibitive. For instance, to couple the 3D numerical model with an optimisation algorithm (linked S-O), the convergence computational time could take upto months for a single solution (Dhar and Datta, 2009).

A method to enhance computational efficiency within a connected S-O approach involves employing reasonably accurate surrogate models. These approximate surrogate models serve as valuable tools for simulating the linked processes of flow and salt

transport in coastal aquifers with a high degree of accuracy (Bhattacharjya et al., 2007). These surrogates can substitute the computationally demanding 3D numerical simulation model, leading to enhanced computational efficiency within a connected S-O framework. The repetitive utilisation of these surrogate models by the optimisation algorithm does not impose a substantial computational burden, as these surrogates are simplified renditions of the intricate simulation models (Roy and Datta, 2017a).

Some of the machine learning-based surrogate approximators which substituted complex 3D numerical simulation models include genetic programming (Shreekant and Datta, 2011), radial basis function (Papadopoulou et al., 2010), evolutionary polynomial regression (Hussain et al., 2015), support vector machine regression (Lal and Datta, 2018), multivariate adaptive regression splines (Roy and Datta, 2017b), Gaussian process regression (Kopsiaftis et al., 2019), Deep Neural Networks (Mo et al., 2020). All the aforementioned prediction artificial intelligence (AI) models are machine learning models. Very few studies have used deep learning models as SWI simulation models. Machine learning models require human interaction, whereas deep learning models learn from the dataset and make their own decisions (Brownlee, 2019). Hence, deep learning models may provide accurate results compared to traditional machine learning models (Ahmed et al., 2023). However, deep learning models require immense input-output data sets to give accurate results.

The majority of the studies have used single machine learning models as surrogate approximators in SWI predictions. This study is the first to utilise a large number of machine learning models as surrogate approximators in predicting the SWI of an island aquifer in Vanuatu. The details of all the machine learning models used in this study are given in Section 7.4.2 of this chapter. This study will also look into the advantages of using ensemble models for SWI predictions. The use of surrogate and ensemble models in predicting SWI in Vanuatu will be applied for the first time. Moreover, this work will also utilise decision theories to select robust surrogate and ensemble models in predicting SWI. To the best of the current knowledge, decision theories have not been used to select the best surrogate and ensemble models for SWI prediction in Pacific Island countries (PICs). Furthermore, the other aspects of the significance of this study include the use of Controlled Elitist Multiple Objective Genetic Algorithm (CEMOGA) in optimising the Pareto optimal front solutions. A detailed discussion of multi-objective optimisation algorithms is given in Section 7.4.3.

The results from this study are of global significance as it builds on the current knowledge of utilising machine learning models in SWI predictions. This study will contribute to the knowledge of which surrogate or ensemble is robust, computer-efficient and accurate in predicting the SWI of a complex and heterogeneous island aquifer. A large number of surrogates and ensembles would also provide a benchmark for the accuracy of SWI predictions in an island coastal aquifer. Another important aspect of this study is that it used a limited number of input-output training patterns to train the surrogate models. This approach saved computational time and provided efficiency in developing the surrogate models. Roy and Datta (2020a) and Roy et al. (2024) used 1,500 input-output patterns to train the surrogate models. However, the author's computational time was high. Hence, using fewer input-output datasets is one of the novelties of this study. The results will also provide justifications of which decision theories are important in selecting surrogate and ensemble models. Moreover, the results will also highlight the importance of using CEMOGA algorithm in drawing up robust multi-objective SWI management strategies in Vanuatu. The results from this study could be used by policymakers and water engineers in modelling, planning, and decision-making to conserve and utilise the water resources of island aquifers.

## 7.4 Methodology

### 7.4.1 Study area

The SWI multi-objective management model was developed in this study. A 3D numerical model of Tagabe coastal aquifer, an island aquifer in Vanuatu, was used to develop a multi-objective management model. The study area is shown in Figure 7.1.

#### *7.4.1.1 Country background*

Vanuatu, situated east of Australia, consists of 83 islands with diverse landscapes ranging from volcanic mountains to coral atolls. With a population of over 300,000, its capital, Port Vila, is renowned for its natural beauty, attracting tourists for activities like snorkelling, diving, and hiking. Tourism contributes significantly to Vanuatu's economy, comprising 35.5% of its GDP in 2019, alongside agriculture, fishing, and forestry (WTTC, 2021). However, Vanuatu faces challenges from natural disasters and climate change impacts, prompting the government to prioritise resilience-building measures (CRCP, 2021; VMGD, 2023; Sharan, 2023).

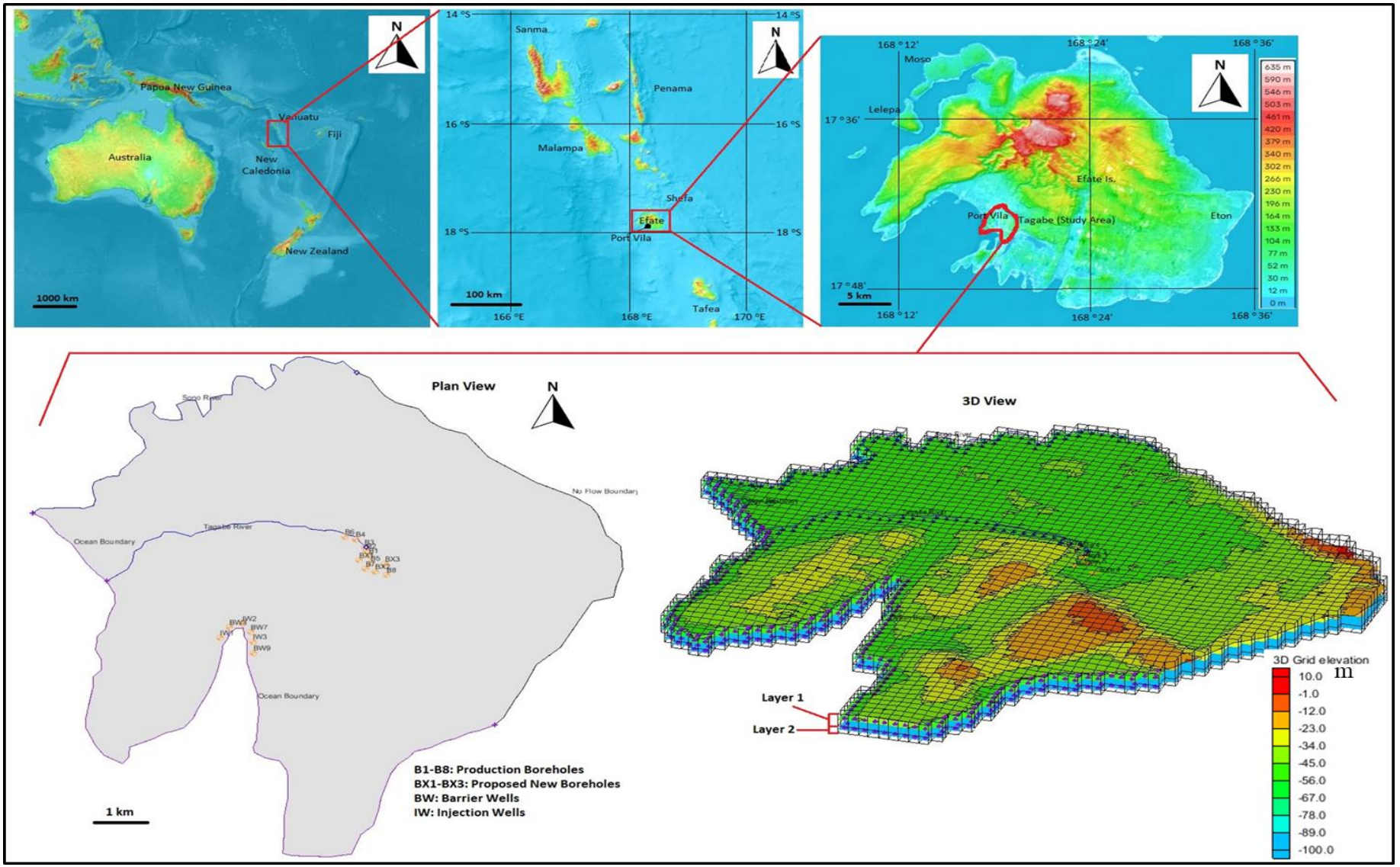



Figure 7.1: Study area. Source (Sharan et al., 2024).

Vanuatu's six provinces, including Shefa, home to the capital, Efate Island, are characterised by diverse geology shaped by volcanic activity, tectonic movements, and erosion. Efate Island boasts volcanic features like the Yasur volcano and limestone formations formed by marine organisms, along with alluvial deposits from nearby rivers (Bath et al., 1986). Geological processes have shaped the island's topography, with tectonic movements creating faults and folds, and erosion impacting coastal areas due to their low elevation. Despite its geological diversity, Vanuatu's vulnerability to natural disasters underscores the importance of integrating climate adaptation and disaster risk reduction strategies into its development planning to ensure resilience for its people and infrastructure (Sharan et al., 2024).

#### *7.4.1.2 Site hydrogeology*

The water supply for Port Vila, sourced from the Tagabe catchment, faces complex hydrogeological challenges influenced by the island's geology, rainfall patterns, and land use. The catchment comprises a fractured volcanic rock aquifer system primarily composed of basalts and andesites, as reported by the Vanuatu Geohazards Observatory (VGO, 2015). Factors affecting groundwater recharge, such as rainfall patterns, land use, and soil characteristics, have been identified by the United Nations Development Programme (UNDP, 2016). With Port Vila experiencing rapid urbanisation, population growth, and increased demands from various sectors, including tourism and infrastructure, the freshwater aquifer in Tagabe is under mounting pressure. Climate change exacerbates these challenges, heightening vulnerability and threatening the ability to sustain current and future water needs for Port Vila and Vanuatu as a whole.

The Tagabe catchment features eight active production boreholes supplying water to Port Vila, revealing a hydrogeological profile with two layers, primarily sand and gravel in the upper layer and limestone below. Considering the uncertainties, the limestone layer is conservatively approximated to extend to 20 meters below ground level. The Tagabe coastal aquifer, characterised by its heterogeneity, shallowness, and unconfined nature, also receives contributions from two active rivers, Sono and Tagabe, further complicating its dynamics. Covering an area of approximately 57 square kilometres, the aquifer supports multiple boreholes nearby, emphasising the importance of sustainable SWI management strategies to ensure the resilience and longevity of Port Vila's water supply (TRCMP, 2018).

#### *7.4.1.3 Numerical simulation model*

The groundwater data provided by the Department of Water Resources, Government of Vanuatu, was limited, comprising bore pumping data from 2017 to 2022 and partial electrical conductivity records from 2019-2021. Critical parameters like hydraulic head values and initial concentrations were absent. Despite these limitations, the 3D numerical simulation model was developed utilising the available data to address saltwater intrusion (SWI) management scenarios in the Tagabe coastal aquifer. The boundary conditions and hydrogeological parameters used to develop a 3D groundwater numerical model are given in Table 7.1.

The numerical 3D groundwater model was developed using flow and transport codes in Groundwater Modelling Systems (GMS) software. SEAWAT was code used in GMS to develop the numerical model. SEAWAT employs a computational framework to simulate three-dimensional groundwater flow in porous materials, accommodating variable density and transient conditions. This is achieved by integrating the functionalities of MODFLOW (develops flow model), which tackles the complexities of variable density flow equations, and MT3DMS (develops transport model), which handles the temporal and spatial aspects of solute transport equations, as outlined by Guo and Langevin (2002).

The conceptual model of the Tagabe coastal aquifer was developed using the MODFLOW-2000 code, encompassing a model domain with dimensions of 7.50 km in the X-direction, 7.61 km in the Y-direction, and 0.1 km in the Z-direction. A 3D finite-difference grid with cell sizes of 100 x 100 m was constructed for the entire domain, consisting of two layers with distinct hydraulic conductivities and porosities. Layer 1, extending from 0 to -80 m, had a hydraulic conductivity of 20 m/d and a porosity of 0.35, while layer 2, from -80 to -100 m, exhibited hydraulic conductivity of 35 m/d and porosity of 0.45. Boundary conditions were applied, with the southern boundary designated as a specified head boundary (CHB), the eastern side as a no-flow boundary, and the northwestern boundary representing the Sono River connected to the ocean boundary and no-flow boundary.

Observed hydraulic head values from boreholes in Tagabe were not available, necessitating the assignment of approximate values based on the provided data. CHB values for western and southeastern nodes were set at 9 m and 8.8 m, respectively,

maintaining a slight hydraulic gradient towards the landward side. Head values for the Sono River and Tagabe River nodes were also assigned accordingly, with consideration for the presence of salinity in the aquifer, indicating a landward-side hydraulic gradient. Boreholes B1-B8 were incorporated into the model domain along with their specific geographic locations, and transient pumping values from 2017 to 2021 were assigned. Finally, all hydrogeological parameters, boundary conditions, wells, pumping values, and head values were integrated into MODFLOW, and a steady-state simulation spanning 20 years was conducted to establish initial conditions.

SEAWAT was initiated for a 5-year period, utilising pumping data from 2017 to 2021, with calibration based on electrical conductivity (EC) data from boreholes B1, B2, B3, B7, and B8 spanning 2019 to 2020 due to missing data in 2021. EC values were converted to parts per million (ppm) or milligrams/litre (mg/L) and then to kg/m$^3$. Despite the absence of observed head values, calibration using secondary data was conducted through trial-and-error methods, adjusting initial salt concentrations, recharge values, hydraulic conductivities, and porosities. Following calibration, the model was simulated for the subsequent 20 years (2022-2043), with the calibrated results serving as the base case for the study. The calibrated model was further employed to get the input (pumping) and output (salt concentrations) at four monitoring locations.

Table 7.1: Model parameters and the values used for the model design. Source (Sharan et al., 2024).

| **Definition** | **Assigned field values** | **Calibrated values** | **S.I. Units** |
|---|---|---|---|
| Layer 1 (Sand and gravel) | Hydraulic Conductivity, K = 20<br>Porosity = 0.35 | Hydraulic Conductivity, K = 25.5<br>Porosity = 0.45 | K = m/d<br>Porosity = dimensionless |
| Layer 2 (Limestone) | Hydraulic Conductivity, K = 35<br>Porosity = 0.45 | Hydraulic Conductivity, K = 40<br>Porosity = 0.55 | |
| Recharge | 0.0004 | 0.000271 | m/d |
| Horizontal Anisotropy | 1 | | dimensionless |
| Freshwater Density | 1000 | | $kg/m^3$ |
| Seawater Density | 1025 | | $kg/m^3$ |
| Saltwater Concentration | 35 | | $kg/m^3$ |
| Specific Storage | 0.000035 | | 1/m |
| River conductance | 1 | | $m^2/dm$ |
| Longitudinal dispersivity | 30 | | m |
| Density/Con. constant, F | 0.7143 | | dimensionless |

#### *7.4.1.4 Input-output patterns*

The calibrated model was used to generate input-output patterns. The decision space was used to generate random pumping values. Decision space consisted of the simulation period (five years), eight production bores and six barrier wells. These decision space values gave seventy variables, where fourteen (total wells) were multiplied by the simulation period. Once the number of variables was fixed, then the number of simulations was set as 200. Hence, the quasi-random sequences for all wells were generated 200 times using the data range between lower bound (0 $m^3$/d) and upper bound (1200 $m^3$/d). Once the decision space was defined and set, the pumping values (input patterns) were randomly generated using the Halton sequence in MATLAB (Halton 1960).

These randomly generated input patterns (spatiotemporal groundwater abstraction from the production bores and barrier wells) were fed to the numerical simulation model to get the salt concentration (output patterns) at four MLs (B1 = ML1, B3 = ML2, B7 = ML3 and B8 = ML4) by running the calibrated 3D numerical simulation model developed for Tagabe coastal aquifer (Sharan et al. 2024). The salt concentrations after running the numerical model were recorded at the end of $5^{th}$ year. The model was simulated 130 times with a different set of spatiotemporal pumping patterns to get the salt concentration at four monitoring locations. These pumping patterns and salt concentrations became the input and output patterns, respectively. Using the input-output patterns from the numerical model, several machine learning-based surrogate models were developed in this study.

A limited number of input-output patterns were generated because the intention was to reduce the computational burden in the coupled S-O approach and to determine whether a smaller number of input-output datasets for a large number of variables (70) could be utilised to effectively and accurately train the surrogate models.

### 7.4.2 Surrogate and ensemble models

The machine learning-based surrogate and ensemble models were developed to mimic the 3D numerical simulation model of the Tagabe coastal aquifer. The various machine learning and deep learning algorithms could be used to develop surrogate and ensemble models. In this study, numerous machine learning-based models were developed as approximate emulators of the numerical simulation model. This study would

be the first to use limited datasets to train numerous machine learning models as surrogate ensembles and decision theories in selecting the best approximators. Past studies have large training datasets and less than five machine learning models as approximate simulators (e.g., Roy and Datta, 2017a; 2017b; Lal and Datta, 2018; 2020). Some of the machine learning and deep learning models used in this study are discussed below.

#### *7.4.2.1 Artificial Neural Network*

The Artificial Neural Network (ANN) has been widely used in various fields of engineering and science (e.g., Rogers et al., 1995; Shreekanth and Datta, 2011; Roy et al., 2024). ANN works similarly to human brains by imitating the process and transferring the information. ANN demonstrates effective performance when tasked with handling complex systems characterised by noisy and ambiguous input data. It can be trained as an approximate simulator of the physical processes (Dhar and Datta, 2009). The ANN model is fully connected through neurons in all its layers. ANN has an input layer, one or more hidden layers and an output layer. These layers interact with each other through weighted connections (Yin et al. 2003). The general ANN structure used in this research is shown in Figure 7.2.

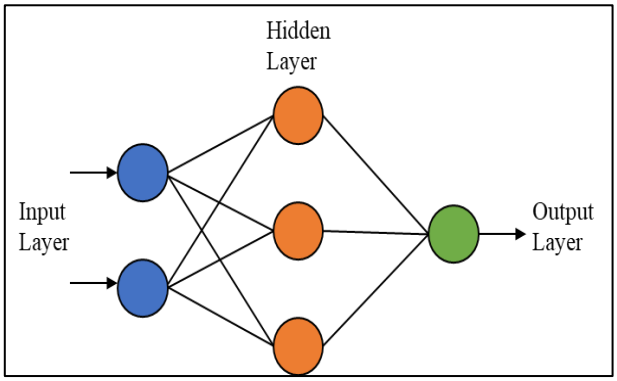



Figure 7.2: Single-layered ANN structure.

The mathematical representation of ANN is given in equation 7.1 (Kumar, 2013).

$$y = f_{sigm}\left\{B_o \sum_{k=1}^{h}\left[w_k \times f_{sigm}\left(B_{hk} + \sum_{i=1}^{m} w_{ik}\, x_i\right)\right]\right\} \tag{7.1}$$

where $B_0$ = bias at the output layer; $w_k$ = connection weight between the *kth* of the hidden layer and single output neuron; $B_{kh}$ = bias at the *kth* neuron of hidden layer; $h$ = number of neurons in the hidden layer; $w_{ik}$ = connection weight between the *ith* input

element and the hidden layer; $x_i$ = input variable $i$; $y$ = output variable; $f_{isgm}$ = transfer function.

#### *7.4.2.2 Support Vector Regression*

Support Vector Regression (SVR) is an influential machine-learning technique which is not sensitive to local optimum and has minimum over-fitting (Tenne and Goh, 2010). Different kernel functions such as polynomial, Gaussian and linear are used in SVR method. SVR consists of a training dataset: $T = [(a_1, b_1), (a_2, b_2),\ldots,(a_n, b_n)]$ so that $a_i$ is a vector of real independent variables and $b_i$ is the matching scaler real dependent variable. The SV regression equation is given in equation 7.2 (Praveen et al., 2016).

$$z(a, w) = (w \cdot \delta[a] + k) \tag{7.2}$$

Where $w$ = weight vector; $k$ is a constant; $\delta[a]$ = feature function; $w \cdot \delta[a]$ = dot product; SVR functions by reducing the equations 7.3 and 7.4.

$$Q(f) = C\frac{1}{N}L_{\propto}(b, z[a, w]) + \frac{1}{2}\|w^2\| \tag{7.3}$$

$$L_{\propto}[b, z(a, w)] = \begin{cases} 0, & if\ |\mathrm{b} - \mathrm{z(a, w)}| \leq \propto \\ |\mathrm{b} - \mathrm{z(a, w)}| - \propto, & otherwise \end{cases} \tag{7.4}$$

Equation 7.3 (first term) describes the empirical error (*ee*) where $C$ = cost function which is a measure of optimisation among the *ee* and the complexity of the model (second term in equation 7.3. The cost function controls the SVR problems. Equation 7.4 illustrates the loss function. The Langrangian multipliers $\gamma_i$ and $\gamma_i^{\circ}$ transform an optimisation problem into two problems. Using the input support vector $a_i$, the SVR equation takes the form given in equation 7.5.

$$z\left(a, \gamma_i - \gamma_i^{\circ}\right) = \sum_{i=1}^{N_{sv}} (\gamma_i - \gamma_i^{\circ})(\delta(a_i) \cdot (\delta(a_j)) + k \tag{7.5}$$

Further, using the support from the kernel function $K$ ($x_i$, $x_j$), the SVR can be expressed as equation 7.6.

$$z\left(a,\ \gamma_i - \gamma_i^{\circ}\right) = \sum_{i=1}^{N_{sv}} \left(\gamma_i - \gamma_i^{\circ}\right) K(a, a_i) + k \tag{7.6}$$

The simple SVR structure is given in Figure 7.3.

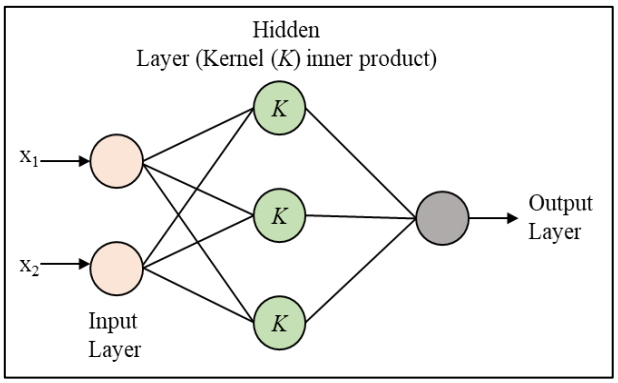



Figure 7.3: Simple S.V.R. model structure.

### *7.4.2.3 Genetic Programming*

The Genetic Programming (GP) model was initially designed by Koza (1992) as an evolutionary algorithm to synthesise programs using the theory of natural selection (Dou et al., 2020). GP is an extension of the genetic algorithm (GA), which employs a generative approach to produce offspring with enhanced fitness by employing fundamental genetic mechanisms such as crossover and mutation. Hierarchical tree formats, comprising predetermined functional and terminal nodes, are used to get the model outcomes. The simple GP model structure (tree) is given in Figure 7.4. Using the figure, the functional expression can be expressed using equation 7.7.

$$y(k) = (-y_{k-1}) + \left(0.2 \times (-u_{k-1})\right) \tag{7.7}$$

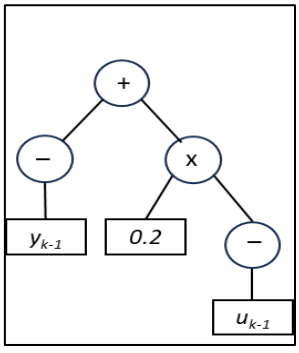



Figure 7.4: Simple Genetic Programming model tree.

#### *7.4.2.4 Multivariate Adaptive Regression Spline*

The Multivariate Adaptive Regression Spline (MARS) model was developed by Friedman (1991) and uses a nonparametric adaptive regression adaptive search strategy in which forward and backward stages modify the search space. MARS is capable of predicting continuous and binary output variables, which makes it an accurate and flexible machine learning model (Salford Predictive Modeler, 2019). MARS categorises and divides the complete input variables into different intervals and creates the regression model by matching single splines to each interval. The process of building a MARS model involves iteratively adding piecewise linear functions called basis functions to improve the fit of the model. These basis functions, including hinge functions and constant functions, are chosen based on their ability to decrease the residual sum of squares, ensuring a better fit to the data.

MARS starts with a simple model, typically a constant term representing the mean response, and then progressively adds basis functions in a forward pass to increase the model's complexity. Subsequently, a backward pass is performed to remove redundant basis functions and simplify the model, thus preventing overfitting. The resulting MARS model provides a balance between flexibility and interpretability, making it valuable for capturing complex relationships in data while remaining comprehensible to users (Friedman, 1991; Salford Predictive Modeler, 2019).

MARS can be further divided into two models: Multivariate Adaptive Regression Spline with Piecewise Cubic Spline (MARS-C) and Multivariate Adaptive Regression Spline with Piecewise Linear (MARS-L). MARS-C uses piecewise cubic splines to model relationships, offering greater flexibility at the cost of increased complexity and potential overfitting. MARS-L, on the other hand, employs piecewise linear functions, which are simpler and may be more interpretable, with potentially lower risk of overfitting, particularly in cases with limited data.

The MARS model can be mathematically represented using equation 7.8.

$$\hat{y} = c_o + \sum_{m=1}^{M} c_m B_m(x) \tag{7.8}$$

Where $\hat{y}$ = dependent variable; $c_o$ = constant; $B_m(x)$ = $m$th basin function; $c_m$ = coefficient of the $m$th basin function.

#### *7.4.2.5 Probabilistic Linear Regression*

Probabilistic linear regression (PLR) enhances traditional linear regression by incorporating uncertainty into both model parameters and predictions (Bishop, 2006). Instead of offering singular point estimates for the response variable based on predictor variables, probabilistic linear regression estimates a probability distribution over potential response variable values, which accounts for inherent noise in the data and uncertainty in model parameters (Gelman et al., 2013). Typically, it assumes a Gaussian distribution for the response variable, with the mean predicted by the linear combination of predictor variables and the variance representing prediction uncertainty (Bishop, 2006).

Bayesian methods, such as Bayesian linear regression, are often employed to infer the posterior distribution of model parameters, leveraging prior knowledge or beliefs about parameters and updating them based on observed data (Gelman et al., 2013). This results in a posterior distribution that comprehensively represents uncertainty in both model parameters and predictions (Bishop, 2006), providing numerous advantages, including robustness to outliers, incorporation of prior knowledge, and the ability to quantify uncertainty, making it a powerful tool in various applications such as decision-making, forecasting, and risk assessment (Gelman et al., 2013).

The mathematical representation of PLR, incorporating uncertainty into both model parameters and predictions is given in equation 7.9 and the simple graphical representation of PLR is shown in Figure 7.5.

$$Y = \beta_0 + \beta_1 x + \varepsilon \tag{7.9}$$

Where $\varepsilon$ = random error; $x$ = independent variable; $y$ = dependent variable; $\beta_0$ = population Y intercept; $\beta_1$ = population slope coefficient.

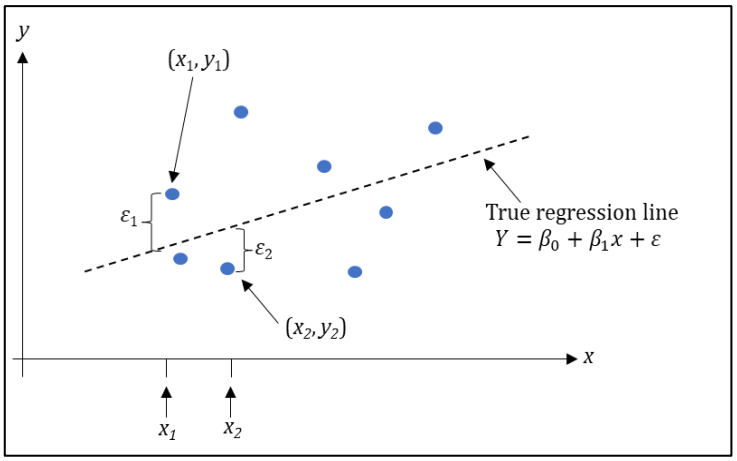



Figure 7.5: Schematic of simple probabilistic linear regression.

### *7.4.2.6 Random Forest Regression*

Random Forest Regression (RFR) is an ensemble learning technique that combines the predictions of multiple decision trees to improve predictive accuracy and robustness. In Random Forest regression, a collection of decision trees is trained on randomly selected subsets of the data and predictor variables. During training, each tree learns to predict the response variable based on a subset of the features and a random subset of the training data. When making predictions, each tree in the forest produces an individual prediction, and the final prediction is obtained by averaging or taking a weighted average of the predictions from all the trees. This ensemble approach helps to mitigate overfitting and provides more stable and accurate predictions compared to individual decision trees. Additionally, Random Forest regression can handle both numerical and categorical data, as well as missing values, making it a versatile and powerful regression technique (Breiman, 2001). The random forest does not have a single regression equation like traditional linear regression. Figure 7.6 shows the RFR using decision trees.

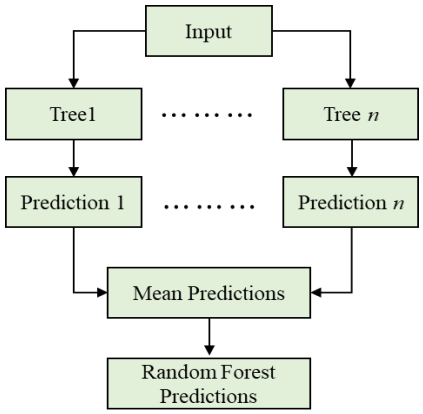



Figure 7.6: Random forest regression structure.

#### *7.4.2.7 Group Method of Data Handling*

The Group Method of Data Handling (GMDH) is a computational algorithm used for modelling complex relationships in data by iteratively selecting and combining simpler mathematical models. GMDH works by progressively refining the model structure through a process of self-organisation and optimisation. Initially, the algorithm generates a pool of potential models, often simple polynomial or linear models. These models are evaluated based on some criterion, such as their predictive accuracy or goodness of fit. Subsequently, GMDH selects the best-performing models and combines them to create more complex models. This process continues iteratively, with the algorithm refining the model structure at each step by selecting and combining models that lead to improved performance. GMDH is known for its ability to automatically generate and optimise models without prior assumptions about the underlying data distribution, making it useful for a wide range of applications in data analysis and modelling (Ivakhnenko, 1968).

#### *7.4.2.8 Long Short-Term Memory*

Long Short-Term Memory (LSTM) is a type of recurrent neural network (RNN) architecture designed to address the vanishing gradient problem in traditional RNNs, enabling them to effectively model and learn long-term dependencies in sequential data. LSTM networks consist of memory cells that maintain a state over time and three gates: input gate, forget gate, and output gate. These gates regulate the flow of information into and out of the memory cells, allowing LSTMs to selectively remember or forget information at each time step. This mechanism enables LSTMs to capture temporal dependencies and patterns in sequential data, making them particularly well-suited for tasks such as time series prediction, natural language processing, and speech recognition. By retaining important information over long sequences and mitigating the effects of the vanishing gradient problem, LSTM networks can learn and represent complex temporal dynamics in data with greater effectiveness (Hochreiter and Schmidhuber, 1997).

Bidirectional Long Short-Term Memory (Bi-LSTM) is an extension of the traditional LSTM (Long Short-Term Memory) recurrent neural network architecture. Bi-LSTM networks enhance the capabilities of LSTM networks by processing input sequences in both forward and backward directions simultaneously.

#### *7.4.2.9 Adaptive Neuro-Fuzzy Inference Systems*

Adaptive Neuro-Fuzzy Inference Systems (ANFIS) combine the adaptability of neural networks with the interpretability of fuzzy logic systems to create hybrid models capable of handling complex nonlinear relationships in data (Jang, 1993). ANFIS models consist of a series of fuzzy if-then rules that are optimised using a hybrid learning algorithm, typically a combination of gradient descent and least squares methods. These rules are organised in a hierarchical structure, with each rule representing a local model capturing a specific region of the input space. The parameters of the fuzzy membership functions and the linear coefficients associated with each rule are adjusted during training to minimise the error between the model's output and the actual data.

The ANFIS learning algorithm proceeds in two phases: a forward pass and a backward pass. During the forward pass, the input data is propagated through the fuzzy inference system to compute the output of each rule. These outputs are then combined to produce the overall model output. In the backward pass, the gradient of the error with respect to the model parameters is computed, and the parameters are updated using gradient descent to minimise the error. ANFIS models offer several advantages, including their ability to capture complex nonlinear relationships, their interpretability due to the fuzzy rule base, and their flexibility in handling both numerical and categorical data. However, they also have limitations, such as the need for careful selection of fuzzy rules and membership functions and the potential for overfitting if not adequately regularised.

#### *7.4.2.10 Asynchronous Successive Halving Algorithm tuned Automatic Model Selection*

The Asynchronous Successive Halving Algorithm tuned Automatic Model Selection (AMS-AHSA) methodology integrates the Asynchronous Successive Halving Algorithm with Automatic Model Selection to automate the process of identifying the optimal machine learning model and its associated hyperparameters for a given dataset. This approach begins by defining a set of candidate models, each with its hyperparameters. Subsequently, the Asynchronous Successive Halving Algorithm is employed, which systematically prunes underperforming models and allocates more resources to promising ones in an asynchronous manner. This process continues through successive rounds until a subset of the best-performing models remains. Finally, based on the performance estimates obtained during the algorithm's execution, the best-

performing model and its hyperparameters are selected. AMS-AHSA efficiently navigates the model space to facilitate automated model selection, which is particularly beneficial in resource-constrained or large-scale hyperparameter optimisation scenarios (Yang et al., 2019).

#### *7.4.2.11 Bayesian Optimisation tuned Automatic Model Selection*

Bayesian Optimisation tuned Automatic Model Selection (AMS-B) is a sophisticated approach that integrates the power of Bayesian Optimisation (BO) with Automatic Model Selection (AMS) to automate the selection of the most suitable machine learning model and its associated hyperparameters for a given dataset. AMS-B harnesses Bayesian Optimization's efficiency in exploring the model space to automate the model selection process and identify high-performing models with minimal manual intervention. This methodology is particularly valuable in scenarios where manual model selection and hyperparameter tuning are time-consuming and resource-intensive (Snoek et al., 2012).

### 7.4.3 Management Model

The ensemble models developed were externally linked to the CEMOGA (Deb and Goel, 2001) optimisation algorithm to obtain optimal groundwater extraction values for developing a management model. The multi-objective saltwater water intrusion management model was developed to find robust SWI management strategies for the Tagabe coastal aquifer. The steps involved in developing the management model are summarised in the flow diagram shown in Figure 7.7.

The management model developed in the current study has a multi-objective type problem of two conflicting objectives. The objectives of the management model include maximising the freshwater abstraction from pumping/production wells (PWs) for beneficial purposes and minimising the pumping from barrier wells (BWs). BW pumping is reduced because it would be an issue to dispose of the saline water if it is abstracted in high volumes. According to Datta and Peralta (1986), the management model solutions would provide Pareto optimal front. The Pareto optimal front would provide the water managers and policymakers with the trade-off between two conflicting solutions. The management model can be mathematically represented in equations 7.10 to 7.15 (Bhattacharjya and Datta, 2005)

$$\text{Maximise: } f_1(Q_{PW}) = \sum_{n=1}^{N}\sum_{t=1}^{T} Q_{PW_n}^t \tag{7.10}$$

$$\text{Minimise: } f_2(Q_{BW}) = \sum_{m=1}^{M}\sum_{t=1}^{T} Q_{BW_m}^t \tag{7.11}$$

Subject to

$$C_i = \varepsilon(Q_{PW}, Q_{BW}) \tag{7.12}$$

$$C_i \leq C_{max} \forall_i \tag{7.13}$$

$$Q_{PW_{min}} \leq Q_{PW_n}^t \leq Q_{PW_{max}} \tag{7.14}$$

$$Q_{BW_{min}} \leq Q_{BW_n}^t \leq Q_{BW_{max}} \tag{7.15}$$

where PW = pumping/production well, BW = barrier well; where $Q_{PW_n}^t$= water extraction from the n$^{th}$ production well during t$^{th}$ time steps; $Q_{BW_m}^t$= water extraction from the n$^{th}$ barrier well during t$^{th}$ time steps; $C_i$ = saltwater concentrations at the i$^{th}$ MLs at the end of the management period; $\varepsilon()$ denotes the density-dependent coupled flow and salt transport surrogate model. The constraint given in equation 7.12 shows the linking of the surrogate ensemble model with the optimisation model; the constraint given in equation 7.13 indicates the maximum allowable salt concentration at various MLs; the constraints given in equations 7.14 and 7.15 outline the upper and lower limits of the water abstraction from pumping and barrier wells, respectively.

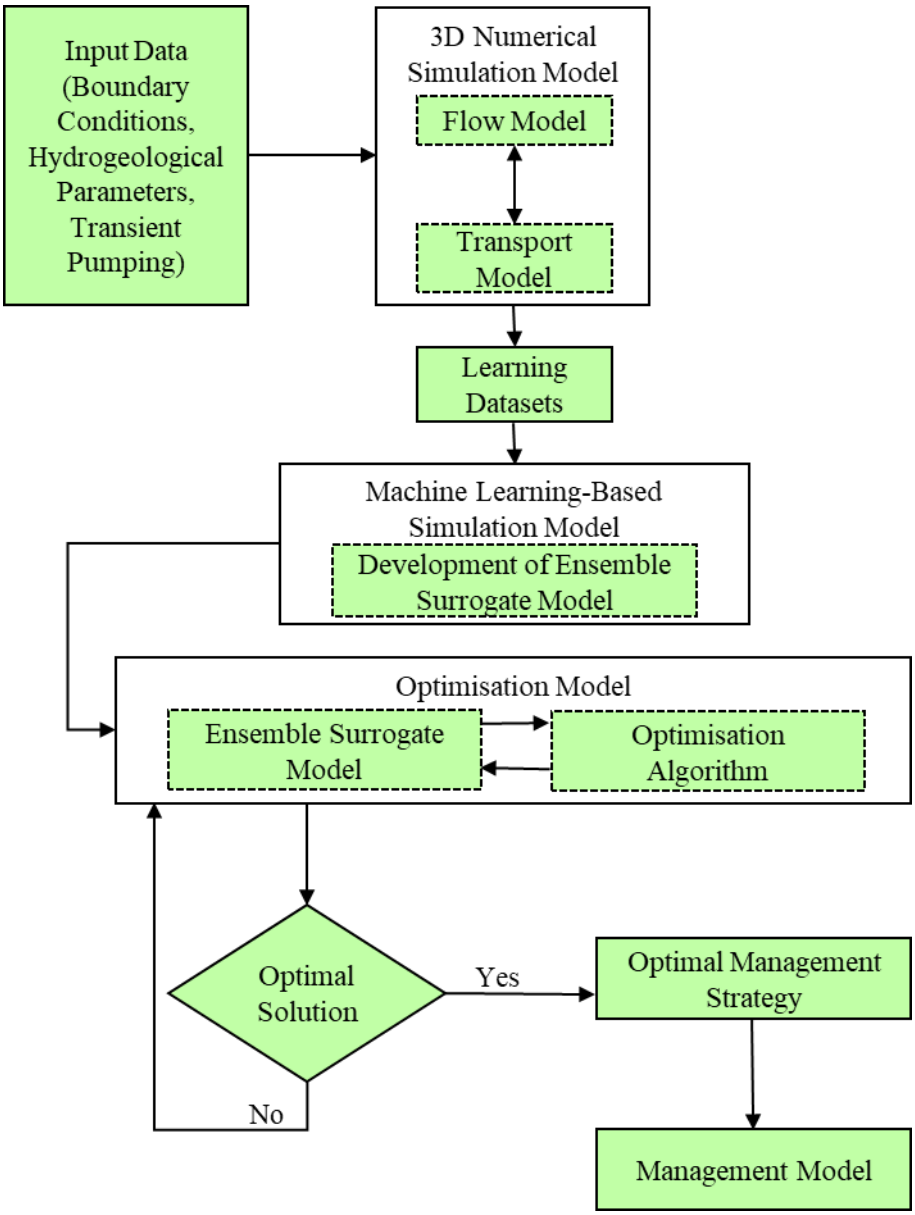



Figure 7.7: Flow diagram of linked simulation-optimisation management model.

### 7.4.4 Model Performance Evaluation Criterion

Various performance evaluation criteria were used to assess the performances of the surrogate models. Correlation coefficient or Pearson's correlation coefficient ($R^2$) (PCC), Index of Agreement (IoA), Kling-Gupta efficiency (KGE), Nash-Sutcliffe efficiency coefficient (NSE), mean absolute error (MAE), root mean square error (RMSE) and mean absolute percentage error (MAPE) were used to evaluate the performance of surrogate and ensemble models.

### 7.4.5 Shannon's entropy-based decision theory

Twelve surrogate models were developed for each ML, along with ensembles of the selected surrogate models for each of the four MLs. Shannon's entropy weight-based decision theory (Shannon, 1948) was applied to select the best-performing model. Entropy weight-based decision theory in model selection employs the concept of entropy to assign weights to different models based on their performance and uncertainty. Shannon's entropy weights (EW) consist of five steps in ranking the models (Li et al., 2011). The steps are as follows:

a). Calculating the entropy value for each index using Shannon's Entropy principles. The entropy value for the j$^{th}$ index was determined using the equations 7.16 – 7.18.

$$Entropy_j = -k \sum_{i=1}^{m} f_{ij} \ln f_{ij} \tag{7.16}$$

$$f_{ij} = S_{ij} \div \sum_{i=1}^{m} S_{ij} \tag{7.17}$$

$$k = 1 \div ln\, m \tag{7.18}$$

b). Determining the entropy weight for each index. The entropy weight for the j$^{th}$ index was calculated using equation 7.19. EW (equation 7.19) signifies the index's importance in decision-making. A higher value of EW suggests that the index contains more information and is more critical in the decision-making process.

$$w(entropy)_j = \frac{1 - entropy_j}{P - \sum_{j=1}^{P} entropy_j} \tag{7.19}$$

c). Determining the rank weight for each model involves adding up the result of multiplying each index's EW by the standardised value of that index. This process is expressed mathematically in equation 7.20.

$$w(entropy)_i = \sum_{j=1}^{P} S_{ij} \times w(entropy)_j \tag{7.20}$$

d). Equation 7.21 gives the step in determining the model ranking.

$$\max\left[w(entropy)_i\right], \ldots, \min\left[w(entropy)_i\right]; \text{for} i = 1,\ 2,\ \ldots, m \tag{7.21}$$

e). Finally, the EWs for individual surrogate prediction models are calculated using equation 7.22.

$$w(entropy)_i = w(entropy)_i \div \sum_{i=1}^{m} w(entropy)_i \qquad (7.22)$$

This approach considers the accuracy of each model and the diversity and reliability of their predictions. By incorporating EW, decision-makers can account for the complexity and uncertainty inherent in real-world datasets, thus making more informed choices when selecting the most suitable model (Wang et al., 2007). This methodology offers a principled way to balance the trade-offs between model accuracy and robustness, ensuring that the selected model effectively captures the underlying patterns in the data while accounting for uncertainty and variability.

## 7.5 Results and Discussion

### 7.5.1 Numerical Simulation Model

The SEAWAT-based numerical simulation model was developed for Tagabe coastal aquifer in Vanuatu. The model indicated that with the current pumping regimes, the SWI rates would increase in Tagabe coastal aquifer. Four scenarios were simulated using the calibrated and validated numerical model to investigate and find the best SWI management strategies. These scenarios included increased population and freshwater pumping rates, the addition of barrier wells and injection wells to prevent saltwater encroachment into freshwater wells, and the effect of rising sea levels on the SWI rates in Tagabe coastal aquifer. The results from the four scenarios are shown in Figure 7.8.

The Tagabe coastal aquifer, which supplies water to the capital city of Vanuatu, has eight operational boreholes. Using current field pumping data, the MODFLOW model interpolated transient pumping data over a 20-year period to predict SWI in the aquifer. The calibrated model ran for 20 years, recording the SWI. Figure 7.8(a-1 to a-20) shows the plan view of the model domain for the base case, with results recorded at five different time steps. The numbers 1, 5, 10, 15, and 20 correspond to 1-year, 5-year, 10-year, 15-year, and 20-year time steps, respectively. The contours represent the SWI in the Tagabe coastal aquifer, with red indicating salt concentrations greater than 30 kg/m³ and light blue indicating approximately 0 kg/m³.

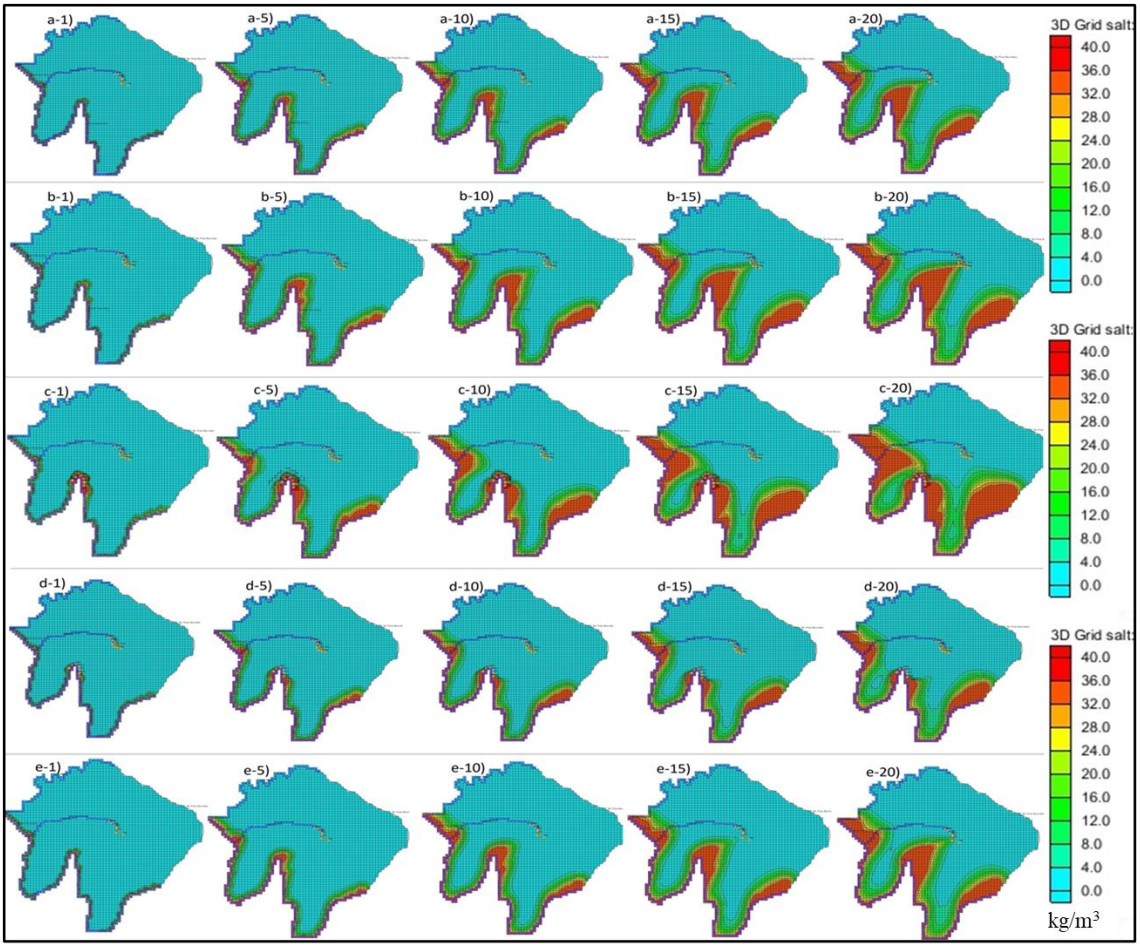



Figure 7.8: (a-1 to a-20) shows the plan view of the simulated results of saltwater intrusion for the base case; (b-1 to b-20) increasing the pumping and number of pumping wells (scenario 1); (c-1 to c-20) addition of barrier wells (scenario 2); (d-1 to d-20) addition of injection well plus barrier wells (scenario 3); (e-1 to e-20) sea level rise (scenario 4). The numbers 1, 5, 10, 15 and 20 represent the time steps 1 year, 5 years, 10 years, 15 years and 20 years, respectively. Source (Sharan et al., 2024).

The addition of barrier wells and injection wells has significantly reduced the SWI rates, as shown in Figure 8(d-1 to d-20). Sea level rise (SLR) (Figure 7.8e-1 to e-20) has some positive effect on the rates of SWI in Tagabe coastal aquifer. In the current simulation, the SLR was only increased by 25 cm upto 20 years (2043). If the sea level rises by over 1m, then the effects would be immense. Sharan et al. (2023; 2024) reported a similar SLR effect in coastal aquifers.

In addition, the results also indicated that the increased freshwater pumping from the production bores in Tagabe coastal aquifer would cause higher rates of SWI. To manage SWI, barrier well and injection well pumping would be required to reverse the hydraulic gradient and prevent the saline water from entering the production bores. Moreover, sea level rise affects SWI rates in Tagabe coastal aquifer. Similar results were reported by Sharan et al. (2024).

The numerical model predicted that increasing the pumping rates with the increased population in future would contaminate the freshwater bores in Tagabe coastal aquifer with increased salinity. Moreover, the model also predicted that using hydraulic barriers would decrease the SWI. However, the use of barrier wells and injection wells is costly. Also, the disposal of abstracted saline water from the barrier wells or the freshwater supply needed to inject into the aquifer to reverse the hydraulic gradients could be an issue. Therefore, optimal SWI management strategies must be provided where the minimum barrier well pumping is required, and maximum allowable salt concentration is allowed in the production bores with the maximum pumping rates. Due to conflicting criteria, this problem can only be tackled with linked simulation-optimisation techniques.

### 7.5.2 Surrogate and Ensemble Model

The input and output patterns gathered from the 3D numerical simulation model were used to develop twelve surrogate and four ensemble models at different (four) MLs. In addition, the twelve surrogate models were ranked using Shannon's entropy and the top five surrogate models (at each of the MLs) were used to develop the weighted average ensembles. The number of input-output patterns was limited based on the computational time taken (20 minutes) by the numerical model. Additionally, the output (salt concentrations) showed minimal variation across all machine learning-based models. Hence, a total of 130 input-output patterns were used to train and test the surrogate models. 80% of the dataset was used to train the surrogates and 20% to test the surrogate models against the actual salt concentrations. MATLAB was used to train the twelve surrogate models and the linear regression graphs were used to compare the actual and predicted values of salt concentrations generated by different algorithms. The actual versus predicted during the training stage is given in Figure 7.9 to Figure 7.12. A limited number of datasets were chosen to achieve computational efficiency from running the numerical model. One of the novelties of the current study was the use of a limited number of input-output patterns. The results indicated that despite using limited training datasets, the surrogates were trained and predicted salt concentrations reasonably well.

Figure 7.9(a-l) shows the actual versus predicted regression analysis of twelve different machine learning models for ML1 during the training period. The majority of the machine learning models predicted better salt concentrations for ML1. The models ANFIS, ANN, MARS_L and GPR outperformed with the $R^2$ greater than 0.96. Bi-LSTM

gave poor prediction results at ML1. Figure 7.10(a-l) shows the actual versus predicted regression analysis of twelve different machine learning models for ML2 during the training period. The models ANFIS, MARS_L, AMS_ASHA and GPR outperformed at ML2 with the $R^2$ greater than 0.98. PLR and SVR also performed well with $R^2$ greater than 0.92. For ML2, ANN, Bi-LSTM and RF did not perform well. Similarly, Figure 7.11 (a-l) shows the actual versus predicted regression analysis of twelve different machine learning models for ML3 during the training period. For ML3, ANFIS, MARS_L, AMS_Bayesian, GPR and RF performed exceptionally well during the training period compared with other machine learning models. Prediction of salt concentration at ML4 [Figure 7.12(a-l)] was exceptionally predicted by MARS_C, MARS_L, AMS_ASHA, and RF. ANN, Bi-LSTM, and SVR did not perform well in predicting accurate results.

After training the twelve models using the 80% dataset, the 20% dataset was used to test the performance of the models. The results of actual versus predicted salt concentrations during the testing periods are given in Figure 7.13 to Figure 7.16. Figure 7.13(a-l) shows the actual versus predicted salt concentrations of twelve surrogate models at ML1. ANFIS, ANN, AMS_Bayesian, AMS_ASHA, GPR, PLR and SVR showed similar patterns of salt concentrations to the actual ones. Similarly, at ML2, MARS_C, MARS_L, AMS_ASHA, GPR, PLR and SVR displayed very close patterns of salt concentrations when compared with the actual values, as shown in Figure 7.14a, c, d, f, i, j and l, respectively.

The ML3 predicted values of salt concentrations by the surrogates are not up to the levels as compared to ML1 and ML2 because the salt concentrations (output patterns) at ML3 were quite similar, which resulted in poor-performing surrogates. However, MARS_C, MARS_L, GPR and RF displayed patterns similar to the actual values, as shown in Figure 7.15c, d, i and k, respectively. The predicted salt concentrations at ML4 during the testing stage are given in Figure 7.16(a-l). The output displayed the variations and patterns following the actual values of salt concentrations. However, only a few surrogates were able to estimate the outputs close to the inputs. These surrogates were MARS_C, MARS_L and RF. Other surrogates did not show many variations in their outputs and followed the patterns of the actual values.

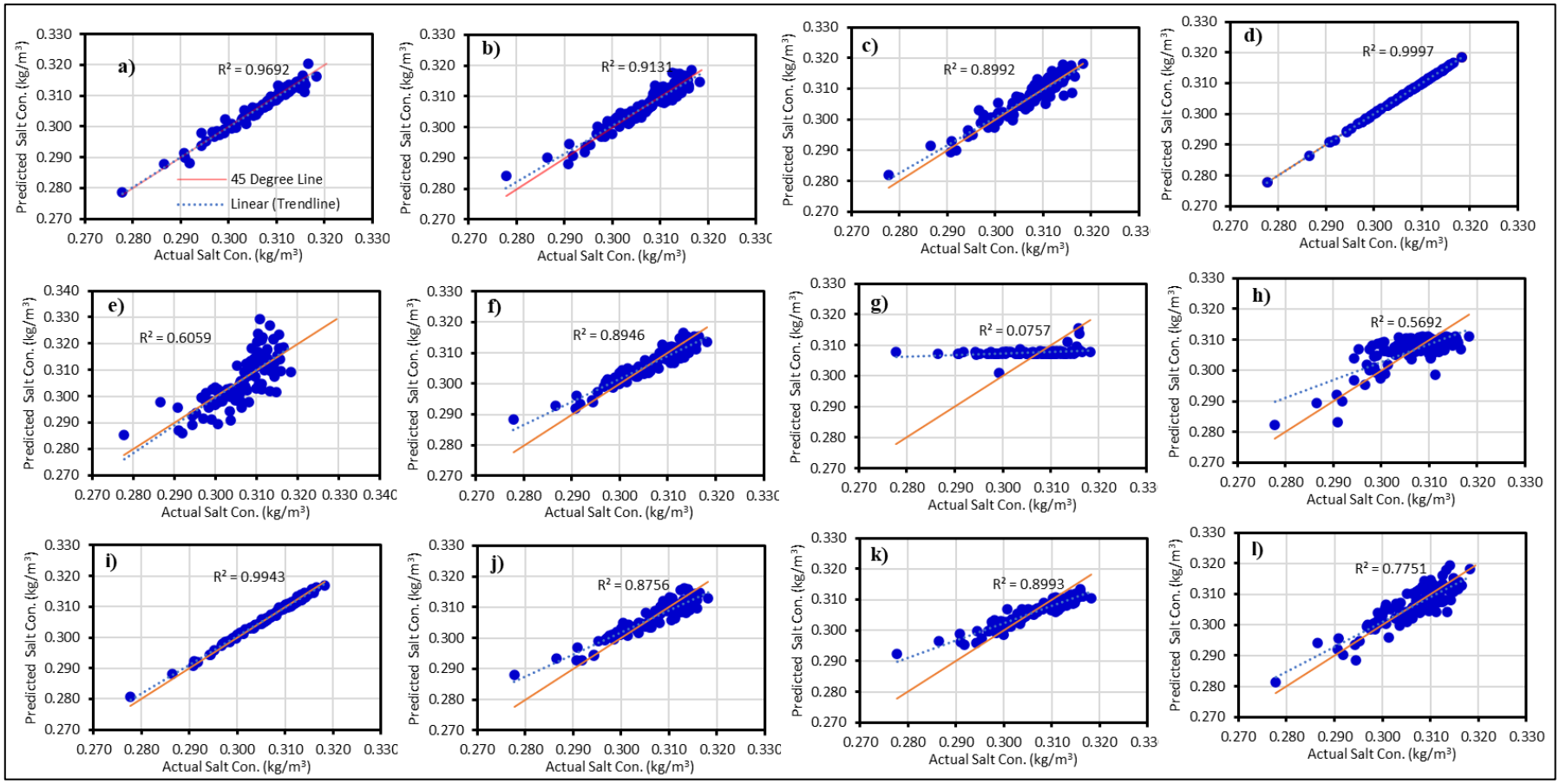



Figure 7.9: Actual versus predicted salt concentrations of monitoring location 1 (ML1) using different machine learning algorithms during training period; **a)** – Adaptive Neuro Fuzzy Inference System (ANFIS), **b)** – Artificial Neural Network (ANN), **c)** – Multivariate Adaptive Regression Spline with Piecewise Cubic Spline (MARS_C), **d)** – Multivariate Adaptive Regression Spline with Piecewise Linear Spline (MARS_L), **e)** – Bayesian Optimization tuned Automatic Model Selection (AMS_Bayesian), **f)** – Asynchronous Successive Halving Algorithm tuned Automatic Model Selection (AMS_ASHA), **g)** – Bi-directional Long Short term Memory Network (Bi-LSTM), **h)** – Group Method of Data Handling (GMDH), **i)** – Gaussian Process Regression (GPR), **j)** – Probabilistic Linear Regression (PLR), **k)** – Random Forest (RF) and **l)** – Support Vector Regression (SVR).

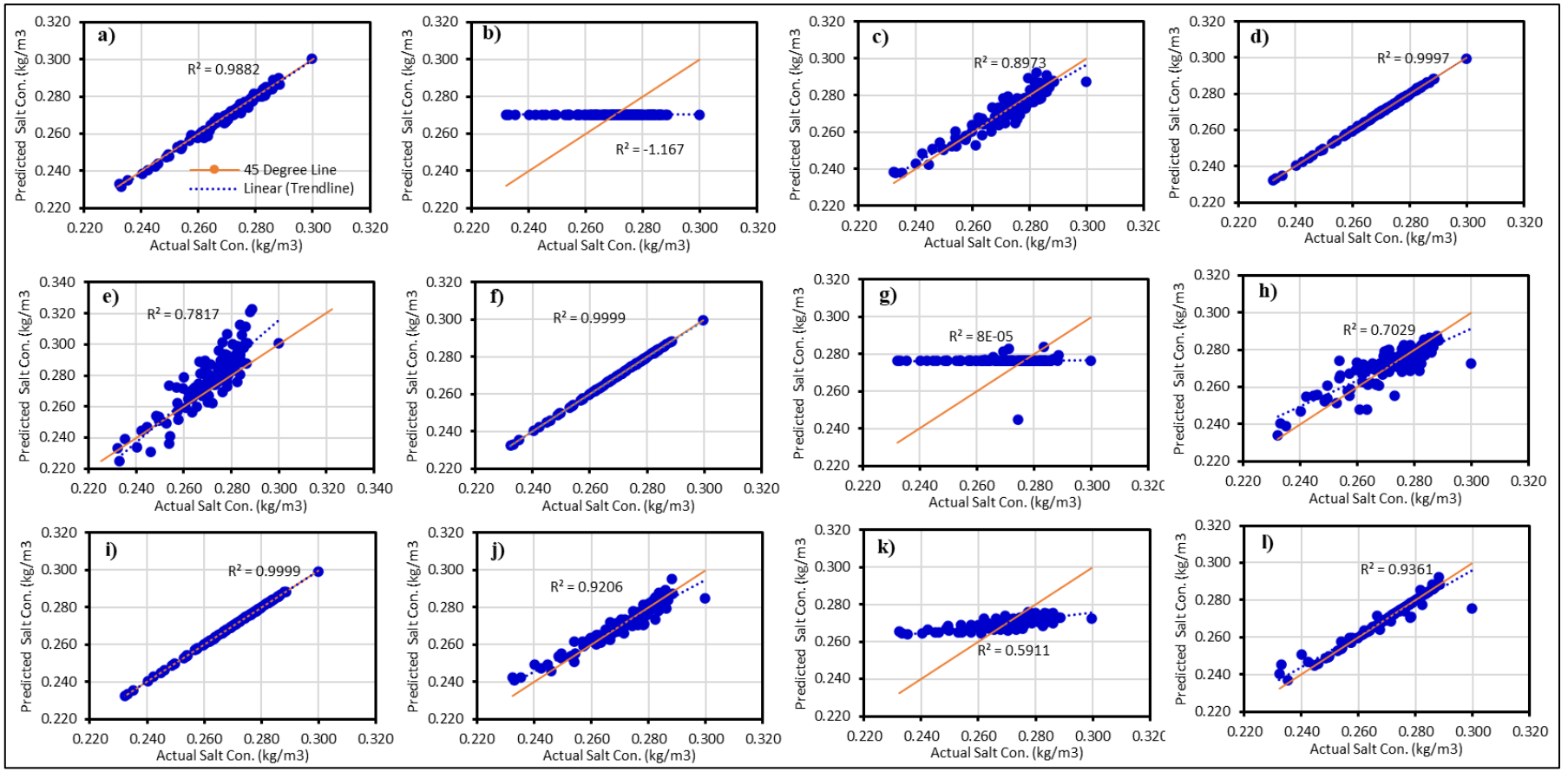



Figure 7.10: Actual versus predicted salt concentrations of monitoring location 2 (ML2) using different machine learning algorithms during training period; **a)** – Adaptive Neuro Fuzzy Inference System (ANFIS), **b)** – Artificial Neural Network (ANN), **c)** – Multivariate Adaptive Regression Spline with Piecewise Cubic Spline (MARS_C), **d)** – Multivariate Adaptive Regression Spline with Piecewise Linear Spline (MARS_L), **e)** – Bayesian Optimization tuned Automatic Model Selection (AMS_Bayesian), **f)** – Asynchronous Successive Halving Algorithm tuned Automatic Model Selection (AMS_ASHA), **g)** – Bi-directional Long Short term Memory Network (Bi-LSTM), **h)** – Group Method of Data Handling (GMDH), **i)** – Gaussian Process Regression (GPR), **j)** – Probabilistic Linear Regression (PLR), **k)** – Random Forest (RF) and **l)** – Support Vector Regression (SVR).

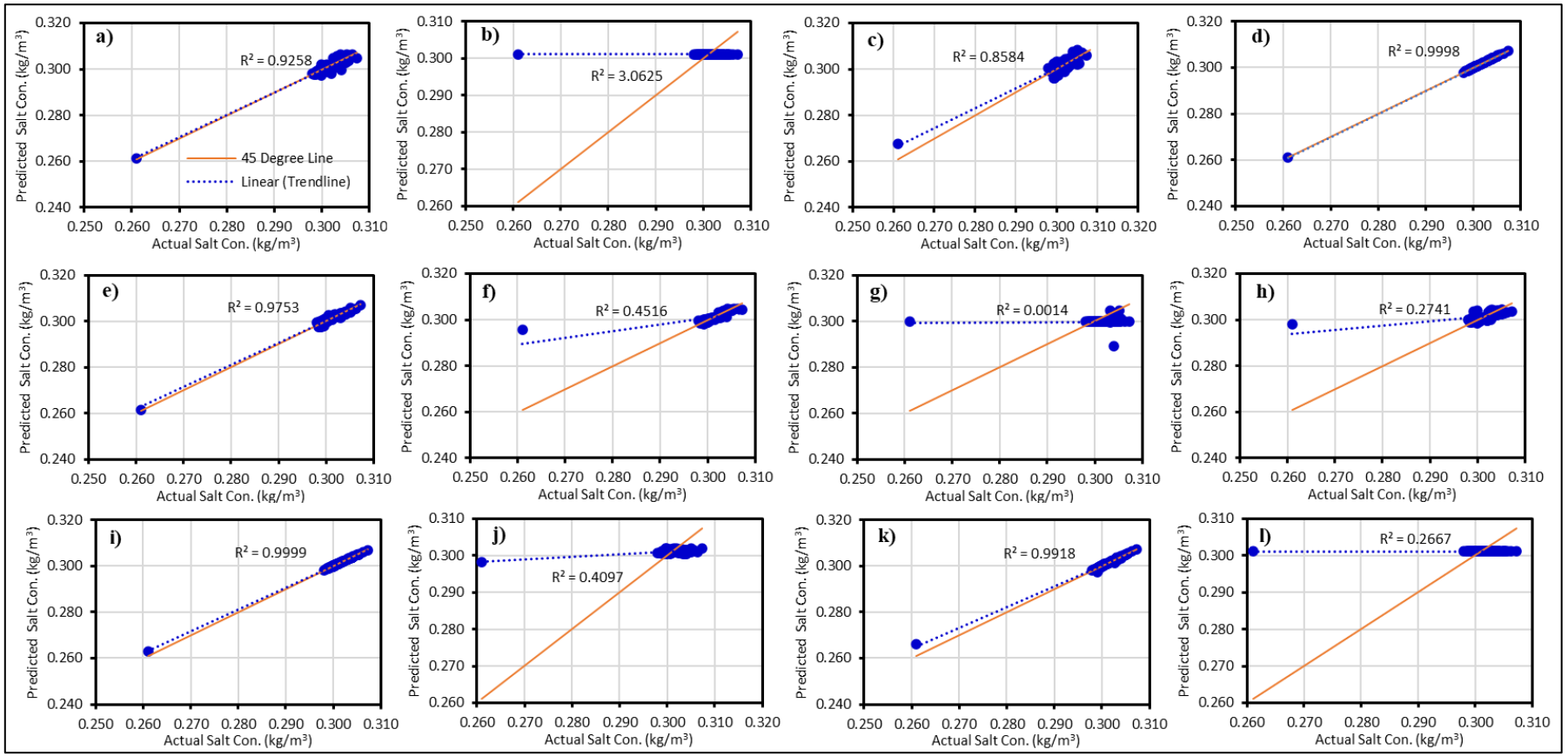



Figure 7.11: Actual Actual versus predicted salt concentrations of monitoring location 3 (ML3) using different machine learning algorithms during training period; **a)** – Adaptive Neuro Fuzzy Inference System (ANFIS), **b)** – Artificial Neural Network (ANN), **c)** – Multivariate Adaptive Regression Spline with Piecewise Cubic Spline (MARS_C), **d)** – Multivariate Adaptive Regression Spline with Piecewise Linear Spline (MARS_L), **e)** – Bayesian Optimization tuned Automatic Model Selection (AMS_Bayesian), **f)** – Asynchronous Successive Halving Algorithm tuned Automatic Model Selection (AMS_ASHA), **g)** – Bi-directional Long Short term Memory Network (Bi-LSTM), **h)** – Group Method of Data Handling (GMDH), **i)** – Gaussian Process Regression (GPR), **j)** – Probabilistic Linear Regression (PLR), **k)** – Random Forest (RF) and **l)** – Support Vector Regression (SVR).

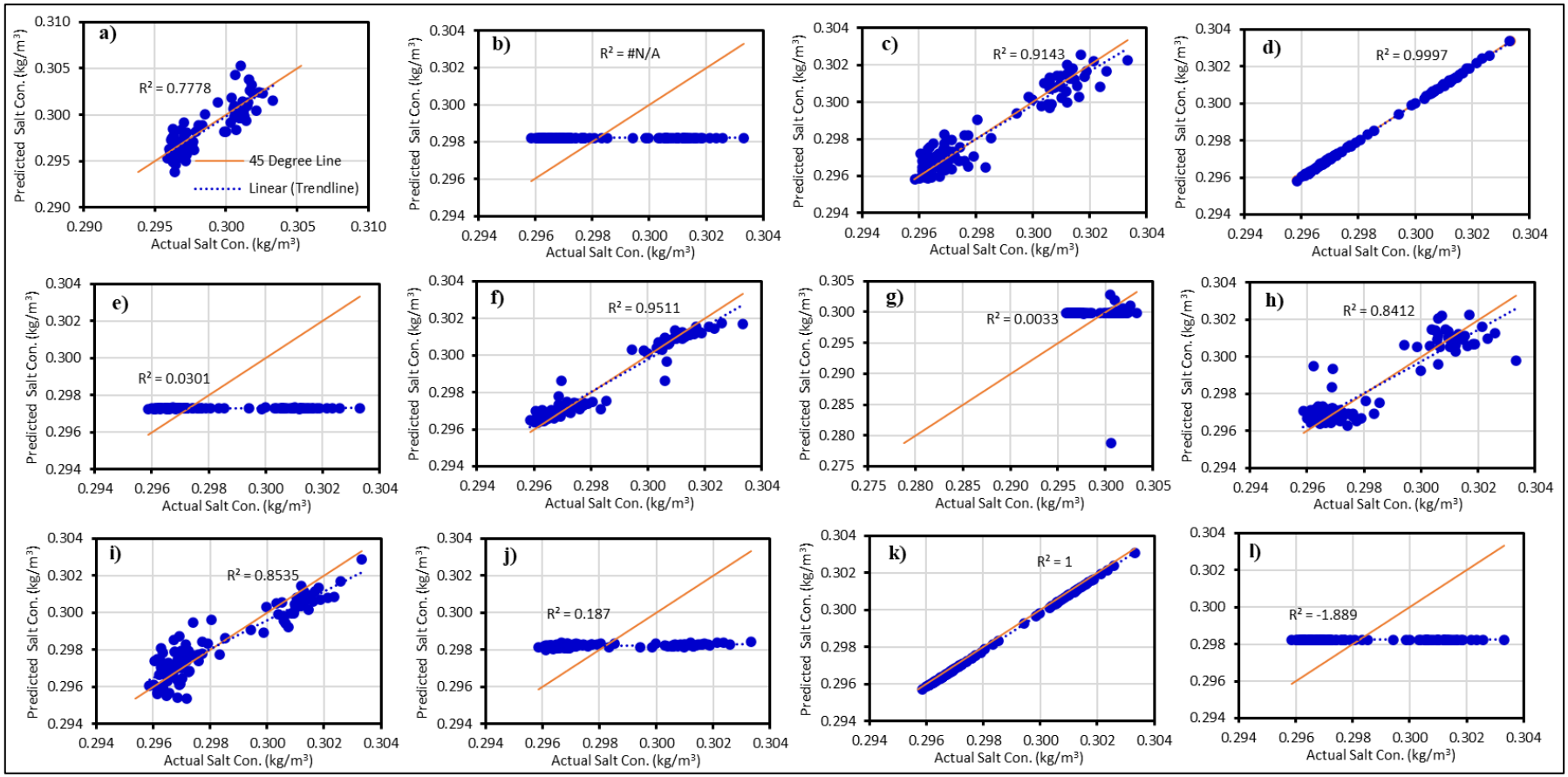



Figure 7.12: Actual versus predicted salt concentrations of monitoring location 4 (ML4) using different machine learning algorithms during training period; **a)** – Adaptive Neuro Fuzzy Inference System (ANFIS), **b)** – Artificial Neural Network (ANN), **c)** – Multivariate Adaptive Regression Spline with Piecewise Cubic Spline (MARS_C), **d)** – Multivariate Adaptive Regression Spline with Piecewise Linear Spline (MARS_L), **e)** – Bayesian Optimization tuned Automatic Model Selection (AMS_Bayesian), **f)** – Asynchronous Successive Halving Algorithm tuned Automatic Model Selection (AMS_ASHA), **g)** – Bi-directional Long Short term Memory Network (Bi-LSTM), **h)** – Group Method of Data Handling (GMDH), **i)** – Gaussian Process Regression (GPR), **j)** – Probabilistic Linear Regression (PLR), **k)** – Random Forest (RF) and **l)** – Support Vector Regression (SVR).

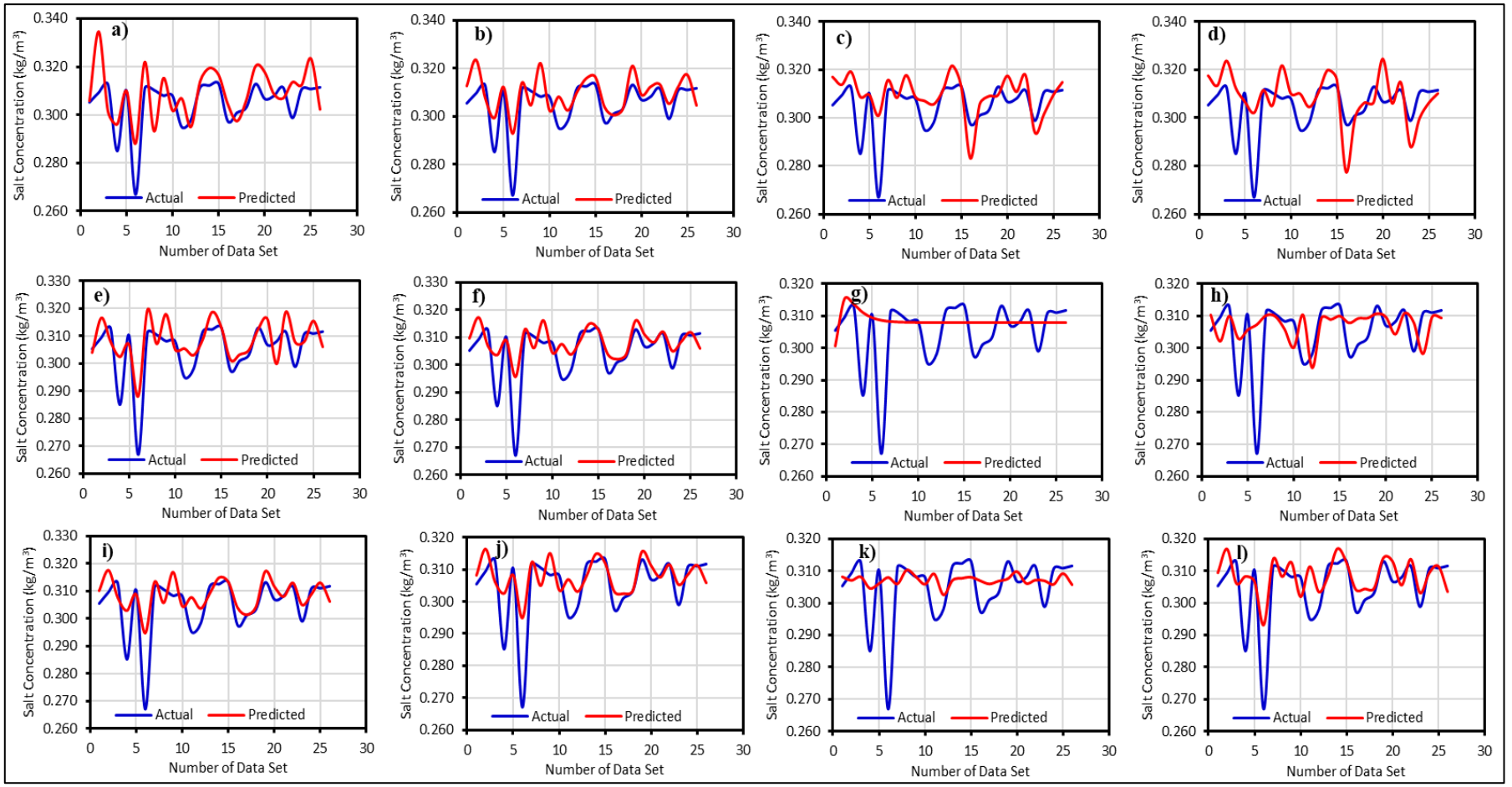



Figure 7.13: Actual versus predicted salt concentrations of monitoring location 1 (ML1) using different machine learning algorithms during testing period; **a)** – Adaptive Neuro Fuzzy Inference System (ANFIS), **b)** – Artificial Neural Network (ANN), **c)** – Multivariate Adaptive Regression Spline with Piecewise Cubic Spline (MARS_C), **d)** – Multivariate Adaptive Regression Spline with Piecewise Linear Spline (MARS_L), **e)** – Bayesian Optimization tuned Automatic Model Selection (AMS_Bayesian), **f)** – Asynchronous Successive Halving Algorithm tuned Automatic Model Selection (AMS_ASHA), **g)** – Bi-directional Long Short term Memory Network (Bi-LSTM), **h)** – Group Method of Data Handling (GMDH), **i)** – Gaussian Process Regression (GPR), **j)** – Probabilistic Linear Regression (PLR) , **k)** – Random Forest (RF) and **l)** – Support Vector Regression (SVR).

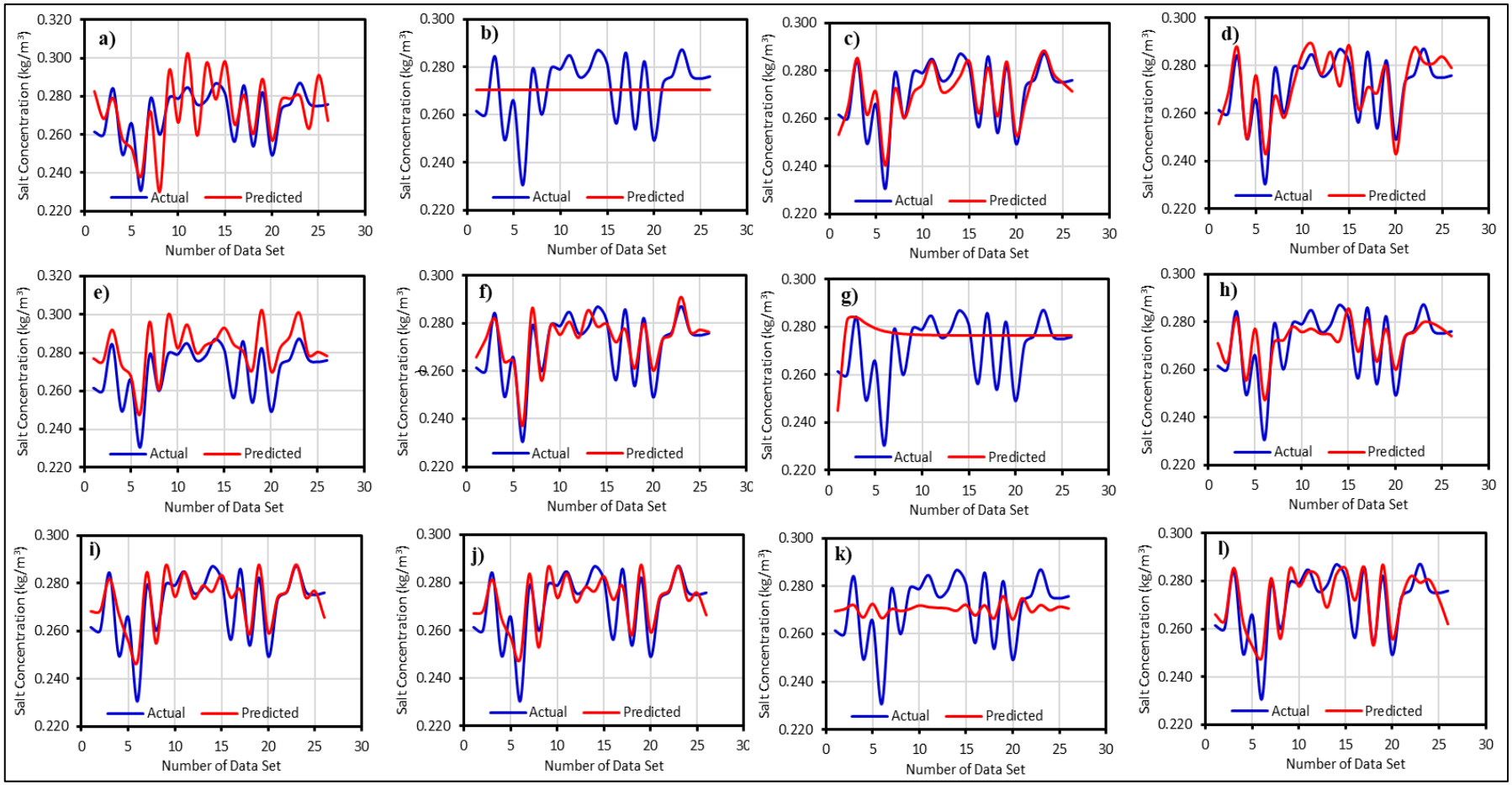



Figure 7.14: Actual versus predicted salt concentrations of monitoring location 2 (ML2) using different machine learning algorithms during testing period; **a)** – Adaptive Neuro Fuzzy Inference System (ANFIS), **b)** – Artificial Neural Network (ANN), **c)** – Multivariate Adaptive Regression Spline with Piecewise Cubic Spline (MARS_C), **d)** – Multivariate Adaptive Regression Spline with Piecewise Linear Spline (MARS_L), **e)** – Bayesian Optimization tuned Automatic Model Selection (AMS_Bayesian), **f)** – Asynchronous Successive Halving Algorithm tuned Automatic Model Selection (AMS_ASHA), **g)** – Bi-directional Long Short term Memory Network (Bi-LSTM), **h)** – Group Method of Data Handling (GMDH), **i)** – Gaussian Process Regression (GPR), **j)** – Probabilistic Linear Regression (PLR), **k)** – Random Forest (RF) and **l)** – Support Vector Regression (SVR).

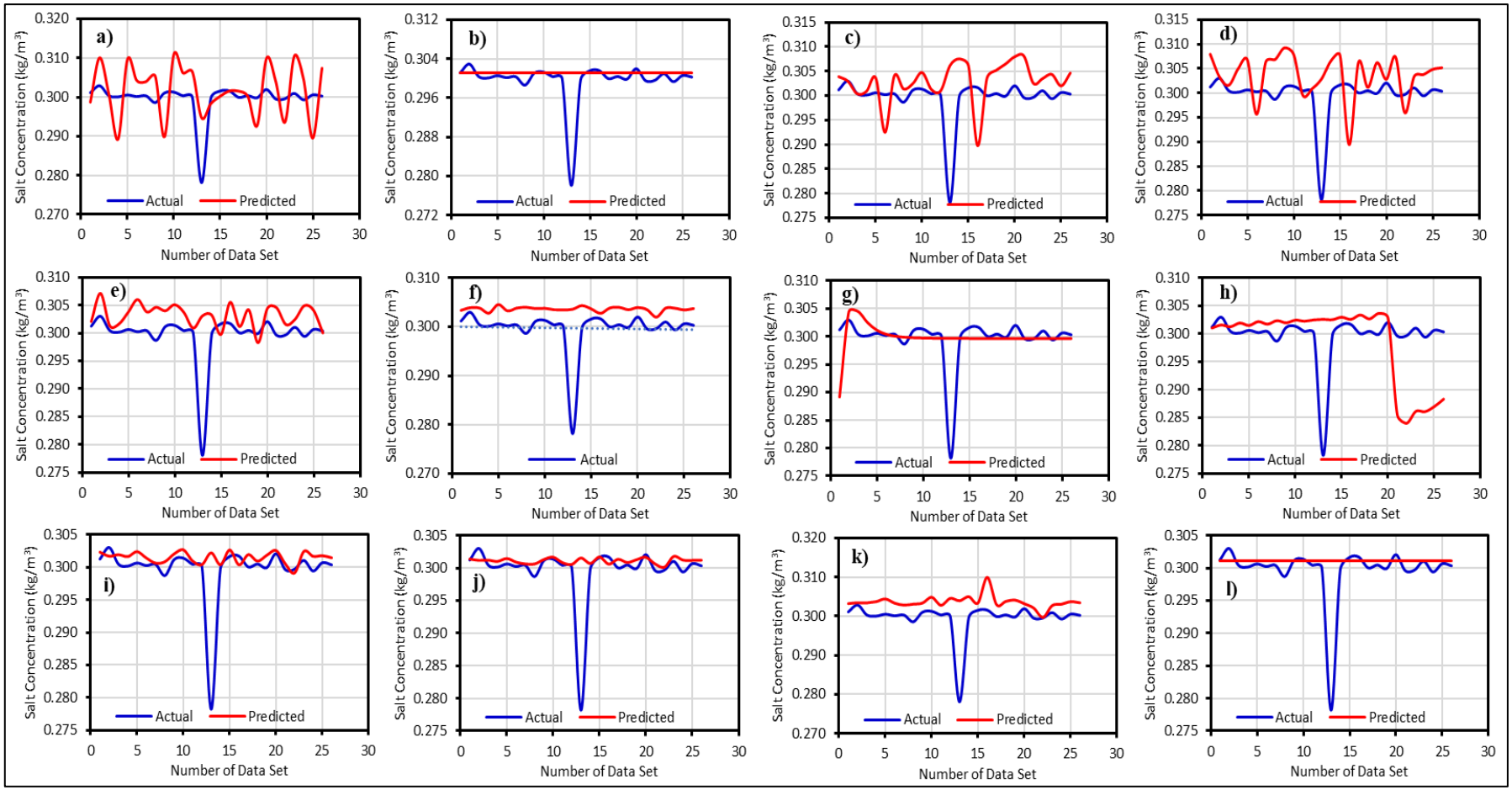



Figure 7.15: Actual versus predicted salt concentrations of monitoring location 3 (ML3) using different machine learning algorithms during testing period; **a)** – Adaptive Neuro Fuzzy Inference System (ANFIS), **b)** – Artificial Neural Network (ANN), **c)** – Multivariate Adaptive Regression Spline with Piecewise Cubic Spline (MARS_C), **d)** – Multivariate Adaptive Regression Spline with Piecewise Linear Spline (MARS_L), **e)** – Bayesian Optimization tuned Automatic Model Selection (AMS_Bayesian), **f)** – Asynchronous Successive Halving Algorithm tuned Automatic Model Selection (AMS_ASHA), **g)** – Bi-directional Long Short term Memory Network (Bi-LSTM), **h)** – Group Method of Data Handling (GMDH), **i)** – Gaussian Process Regression (GPR), **j)** – Probabilistic Linear Regression (PLR), **k)** – Random Forest (RF) and **l)** – Support Vector Regression (SVR).

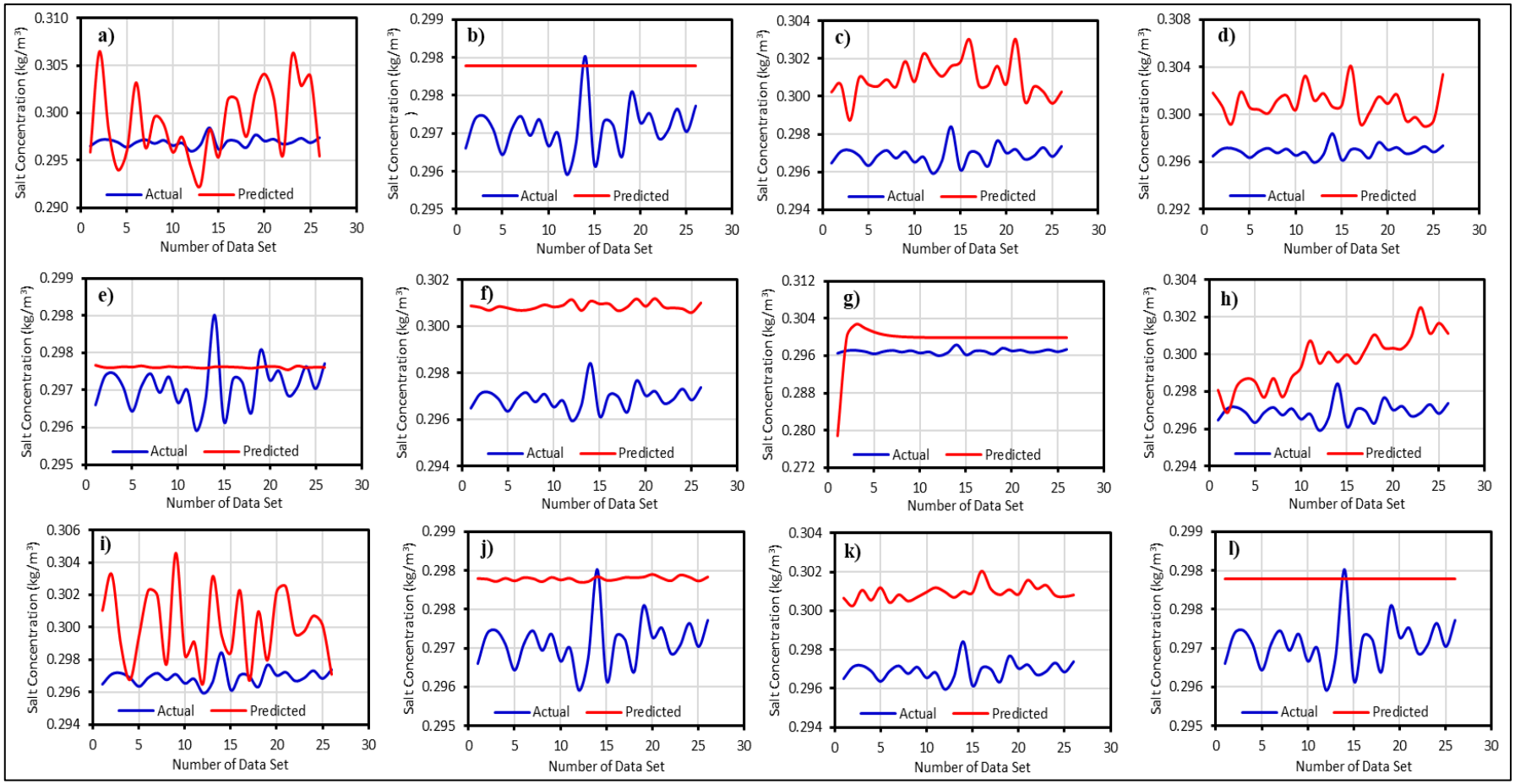



Figure 7.16: Actual versus predicted salt concentrations of monitoring location 4 (ML4) using different machine learning algorithms during testing period; **a)** – Adaptive Neuro Fuzzy Inference System (ANFIS), **b)** – Artificial Neural Network (ANN), **c)** – Multivariate Adaptive Regression Spline with Piecewise Cubic Spline (MARS_C), **d)** – Multivariate Adaptive Regression Spline with Piecewise Linear Spline (MARS_L), **e)** – Bayesian Optimization tuned Automatic Model Selection (AMS_Bayesian), **f)** – Asynchronous Successive Halving Algorithm tuned Automatic Model Selection (AMS_ASHA), **g)** – Bi-directional Long Short term Memory Network (Bi-LSTM), **h)** – Group Method of Data Handling (GMDH), **i)** – Gaussian Process Regression (GPR), **j)** – Probabilistic Linear Regression (PLR), **k)** – Random Forest (RF) and **l)** – Support Vector Regression (SVR).

### 7.5.3 Model Performance and Selection

The different criteria for measuring the performance of the surrogate models for different ML during the model training given in Table 7.2 and Figure 7.17. These performances are for the training stage, where the actual values of the salt concentration were compared with the predicted values by various machine learning models mentioned in Section 7.4.2. The majority of the models performed better in predicting the salt concentration during the testing period. Comparing the MAPE (%), Pearson's coefficient, Index of Agreement, Kling-Gupta efficiency and Nash Sutcliffe efficiency coefficients, it can be seen that ANFIS, ANN, MARS_C, MARS_L, AMS_ASHA, GPR and SVR predicted better salt concentrations. Similarly, ANFIS, MARS_C, MARS_L, AMS_ASHA, GPR, PLR and SVR performed better in predicting the salt concentrations at ML2 during the training stage. ANFIS, MARS_C, MARS_L, AMS_Bayesian, GPR and RF performed better in predicting the salt concentrations at ML3 during the training stage. Finally, MARS_C, MARS_L, AMS_ASHA, GMDH and RF performed better in predicting the salt concentrations at ML4 during the training stage.

Table 7.3 and Figure 7.18 demonstrate the reliable performance of twelve surrogate models at different MLs during the testing period. The actual and predicted salt concentrations were compared using the MAPE (%), Pearson's coefficient, Index of Agreement, Kling-Gupta efficiency, and Nash-Sutcliffe efficiency coefficients. ANN, AMS_Bayesian and PLR consistently predicted better salt concentrations at ML1. ANFIS, MARS_C, MARS_L, AMS_Bayesian, AMS_ASHA, GHD and SVR consistently predicted better salt concentrations at ML2. In addition, the reliable surrogate models in predicting the salt concentrations at ML3 were AMS_Bayesian and ANN. Meanwhile, ANFIS, AMS_ASHA, and SVR performed well. All ensemble models consistently performed better, as shown in Table 7.3.

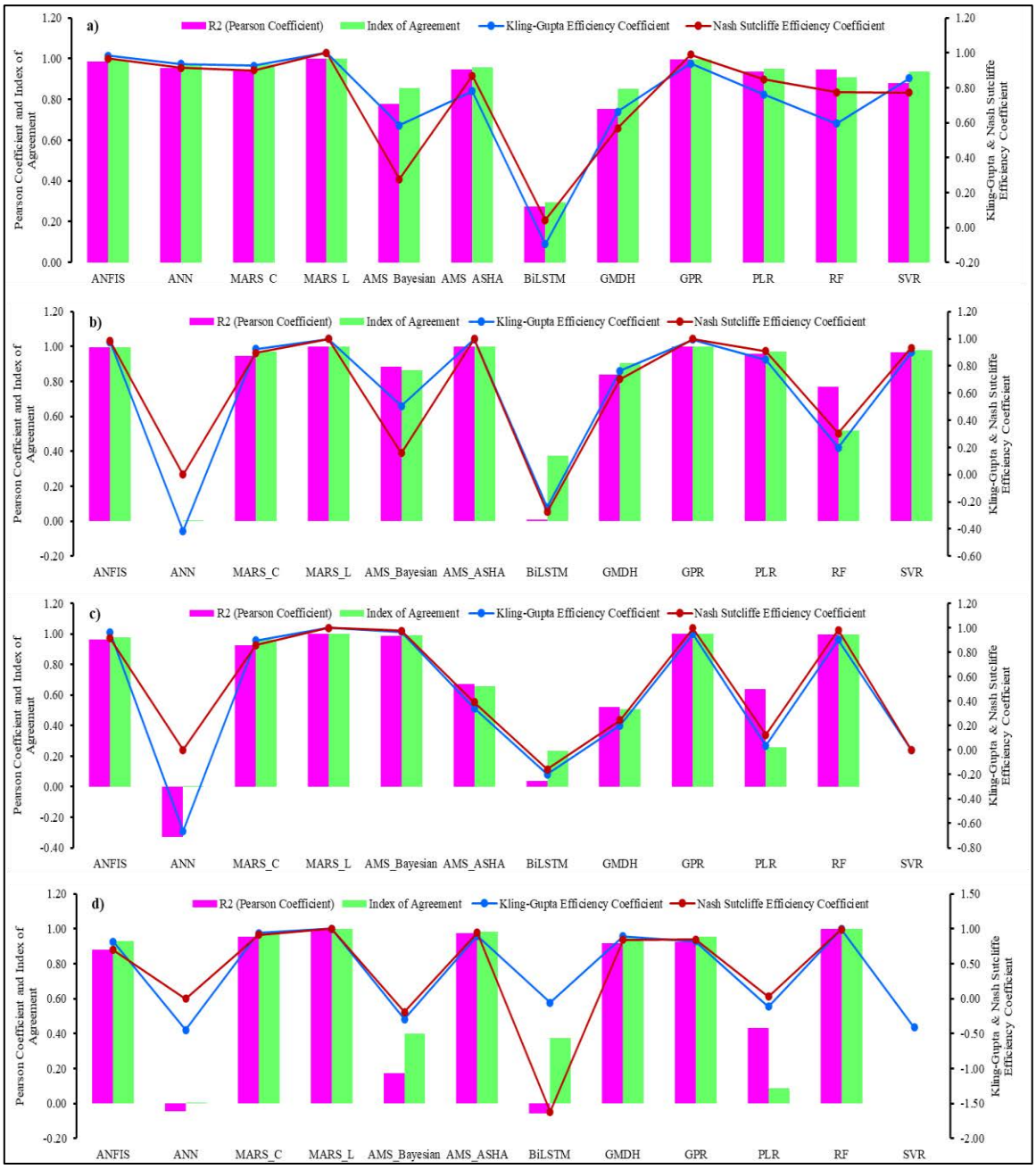



Figure 7.17: Performance of all surrogate models during the training stage using Pearson correlation coefficient, Index of Agreement, Kling-Gupta Efficiency coefficient and Nash-Sutcliffe Efficiency coefficient at **a)** ML2, **b)** ML2, **c)** ML3 and **d)** ML4.

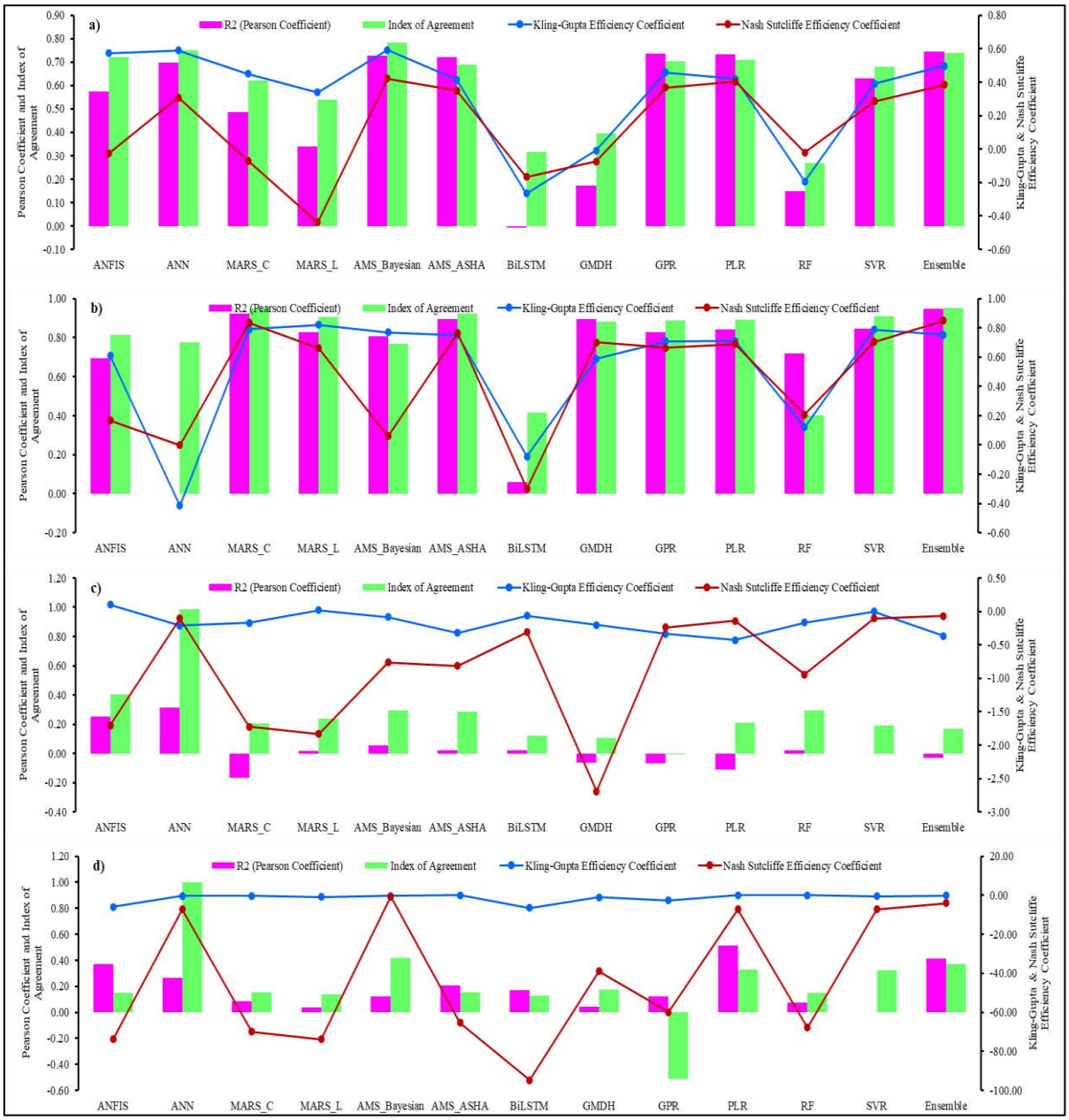



Figure 7.18: Performance of all surrogate models during the training stage using Pearson correlation coefficient, Index of Agreement, Kling-Gupta Efficiency coefficient and Nash-Sutcliffe Efficiency coefficient at **a)** ML2, **b)** ML2, **c)** ML3 and **d)** ML4.

Table 7.2: Performance criteria of twelve surrogate models at four different monitoring locations (MLs) during the model training period.

| | Performance Measure | ANFIS | ANN | MARS_C | MARS_L | AMS_Bayesian | AMS_ASHA | BiLSTM | GMDH | GPR | PLR | RF | SVR |
|---|---|---|---|---|---|---|---|---|---|---|---|---|---|
| **ML1** | Mean Absolute Deviation (MAD) | 0.0009293 | 0.0017723 | 0.0017369 | 0.0000927 | 0.0048193 | 0.0020226 | 0.0052974 | 0.0038625 | 0.0005386 | 0.0021990 | 0.0025491 | 0.0028542 |
| | Mean Square Error (MSE) | 0.0000017 | 0.0000045 | 0.0000052 | 0.0000000 | 0.0000373 | 0.0000067 | 0.0000495 | 0.0000223 | 0.0000005 | 0.0000078 | 0.0000117 | 0.0000118 |
| | RMSE | 0.0012968 | 0.0021187 | 0.0022825 | 0.0001138 | 0.0061111 | 0.0025953 | 0.0070324 | 0.0047200 | 0.0006848 | 0.0027999 | 0.0034223 | 0.0034335 |
| | MAPE (%) | 0.303 | 0.580 | 0.568 | 0.030 | 1.570 | 0.663 | 1.754 | 1.263 | 0.176 | 0.720 | 0.837 | 0.932 |
| **ML2** | Mean Absolute Deviation (MAD) | 0.001235 | 0.010136 | 0.003231 | 0.000171 | 0.009189 | 0.000074 | 0.010648 | 0.005414 | 0.000100 | 0.002983 | 0.008319 | 0.001147 |
| | Mean Square Error (MSE) | 0.000003 | 0.000168 | 0.000017 | 0.000000 | 0.000141 | 0.000000 | 0.000214 | 0.000050 | 0.000000 | 0.000015 | 0.000117 | 0.000011 |
| | RMSE | 0.001600 | 0.012966 | 0.004155 | 0.000212 | 0.011885 | 0.000101 | 0.014639 | 0.007071 | 0.000128 | 0.003913 | 0.010814 | 0.003376 |
| | MAPE (%) | 0.459 | 3.840 | 1.197 | 0.063 | 3.371 | 0.027 | 4.102 | 2.020 | 0.037 | 1.114 | 3.142 | 0.433 |
| **ML3** | Mean Absolute Deviation (MAD) | 0.0009339 | 0.0020962 | 0.0012951 | 0.0000495 | 0.0005557 | 0.0008921 | 0.0023394 | 0.0013296 | 0.0001112 | 0.0020018 | 0.0001535 | 0.0020977 |
| | Mean Square Error (MSE) | 0.0000017 | 0.0000198 | 0.0000028 | 0.0000000 | 0.0000005 | 0.0000121 | 0.0000230 | 0.0000150 | 0.0000001 | 0.0000173 | 0.0000003 | 0.0000198 |
| | RMSE | 0.0012984 | 0.0044534 | 0.0016758 | 0.0000625 | 0.0007043 | 0.0034716 | 0.0047910 | 0.0038725 | 0.0002292 | 0.0041651 | 0.0005843 | 0.0044534 |
| | MAPE (%) | 0.309 | 0.714 | 0.433 | 0.016 | 0.185 | 0.313 | 0.791 | 0.459 | 0.038 | 0.681 | 0.054 | 0.714 |
| **ML4** | Mean Absolute Deviation (MAD) | 0.0008730 | 0.0018996 | 0.0004841 | 0.0000299 | 0.0016707 | 0.0003444 | 0.0026600 | 0.0006084 | 0.0006741 | 0.0018773 | 0.0001878 | 0.0019016 |
| | Mean Square Error (MSE) | 0.0000013 | 0.0000045 | 0.0000004 | 0.0000000 | 0.0000053 | 0.0000002 | 0.0000117 | 0.0000007 | 0.0000007 | 0.0000043 | 0.0000000 | 0.0000045 |
| | RMSE | 0.0011613 | 0.0021146 | 0.0006191 | 0.0000366 | 0.0023100 | 0.0004946 | 0.0034221 | 0.0008436 | 0.0008286 | 0.0020803 | 0.0001883 | 0.0021146 |
| | MAPE (%) | 0.292 | 0.636 | 0.162 | 0.010 | 0.557 | 0.115 | 0.893 | 0.204 | 0.226 | 0.628 | 0.063 | 0.636 |

Table 7.3: Performance criteria of twelve surrogate models and four ensemble models at four different monitoring locations (MLs) during the model testing period.

| | Performance Measure | ANFIS | ANN | MARS_C | MARS_L | AMS_Bayesian | AMS_ASHA | BiLSTM | GMDH | GPR | PLR | RF | SVR | Ensemble |
|---|---|---|---|---|---|---|---|---|---|---|---|---|---|---|
| **ML1** | Mean Absolute Deviation (MAD) | 0.008200 | 0.006349 | 0.007465 | 0.008784 | 0.006097 | 0.005403 | 0.006612 | 0.006838 | 0.005481 | 0.005194 | 0.006468 | 0.005891 | 0.005640 |
| | Mean Square Error (MSE) | 0.000106 | 0.000072 | 0.000111 | 0.000149 | 0.000060 | 0.000068 | 0.000121 | 0.000112 | 0.000066 | 0.000062 | 0.000106 | 0.000074 | 0.000064 |
| | RMSE | 0.010318 | 0.008478 | 0.010540 | 0.012212 | 0.007752 | 0.008220 | 0.011006 | 0.010560 | 0.008094 | 0.007874 | 0.010290 | 0.008610 | 0.007997 |
| | MAPE (%) | 2.718 | 2.072 | 2.528 | 2.965 | 2.045 | 1.839 | 2.270 | 2.333 | 1.861 | 1.767 | 2.210 | 1.998 | 1.909 |
| **ML2** | Mean Absolute Deviation (MAD) | 0.01127 | 0.01195 | 0.00480 | 0.00693 | 0.01124 | 0.00513 | 0.01089 | 0.00620 | 0.00629 | 0.00611 | 0.01070 | 0.00590 | 0.00383 |
| | Mean Square Error (MSE) | 0.00016 | 0.00020 | 0.00003 | 0.00007 | 0.00019 | 0.00005 | 0.00026 | 0.00006 | 0.00007 | 0.00006 | 0.00016 | 0.00006 | 0.00003 |
| | RMSE | 0.01282 | 0.01408 | 0.00570 | 0.00819 | 0.01364 | 0.00682 | 0.01603 | 0.00770 | 0.00815 | 0.00783 | 0.01251 | 0.00767 | 0.00548 |
| | MAPE (%) | 4.169 | 4.465 | 1.808 | 2.569 | 4.232 | 1.945 | 4.245 | 2.345 | 2.396 | 2.330 | 4.036 | 2.237 | 1.469 |
| **ML3** | Mean Absolute Deviation (MAD) | 0.006016 | 0.001744 | 0.004818 | 0.005643 | 0.003692 | 0.003950 | 0.002270 | 0.005475 | 0.002075 | 0.001717 | 0.003989 | 0.001750 | 0.001563 |
| | Mean Square Error (MSE) | 0.000052 | 0.000021 | 0.000053 | 0.000055 | 0.000034 | 0.000035 | 0.000025 | 0.000071 | 0.000024 | 0.000022 | 0.000038 | 0.000021 | 0.000021 |
| | RMSE | 0.007226 | 0.004616 | 0.007253 | 0.007393 | 0.005832 | 0.005922 | 0.005031 | 0.008440 | 0.004896 | 0.004698 | 0.006124 | 0.004620 | 0.004545 |
| | MAPE (%) | 2.019 | 0.585 | 1.632 | 1.904 | 1.254 | 1.341 | 0.777 | 1.849 | 0.716 | 0.596 | 1.354 | 0.606 | 0.544 |
| **ML4** | Mean Absolute Deviation (MAD) | 0.0032556 | 0.0013282 | 0.0040002 | 0.0040240 | 0.0005095 | 0.0039669 | 0.0038250 | 0.0027744 | 0.0031787 | 0.0013349 | 0.0040280 | 0.0013341 | 0.0010268 |
| | Mean Square Error (MSE) | 0.0000180 | 0.0000020 | 0.0000171 | 0.0000180 | 0.0000004 | 0.0000160 | 0.0000231 | 0.0000096 | 0.0000147 | 0.0000020 | 0.0000166 | 0.0000020 | 0.0000012 |
| | RMSE | 0.0042461 | 0.0014021 | 0.0041331 | 0.0042417 | 0.0006236 | 0.0039962 | 0.0048019 | 0.0030969 | 0.0038287 | 0.0014056 | 0.0040709 | 0.0014080 | 0.0011007 |
| | MAPE (%) | 1.096 | 0.445 | 1.348 | 1.356 | 0.172 | 1.336 | 1.289 | 0.935 | 1.071 | 0.450 | 1.357 | 0.450 | 0.346 |

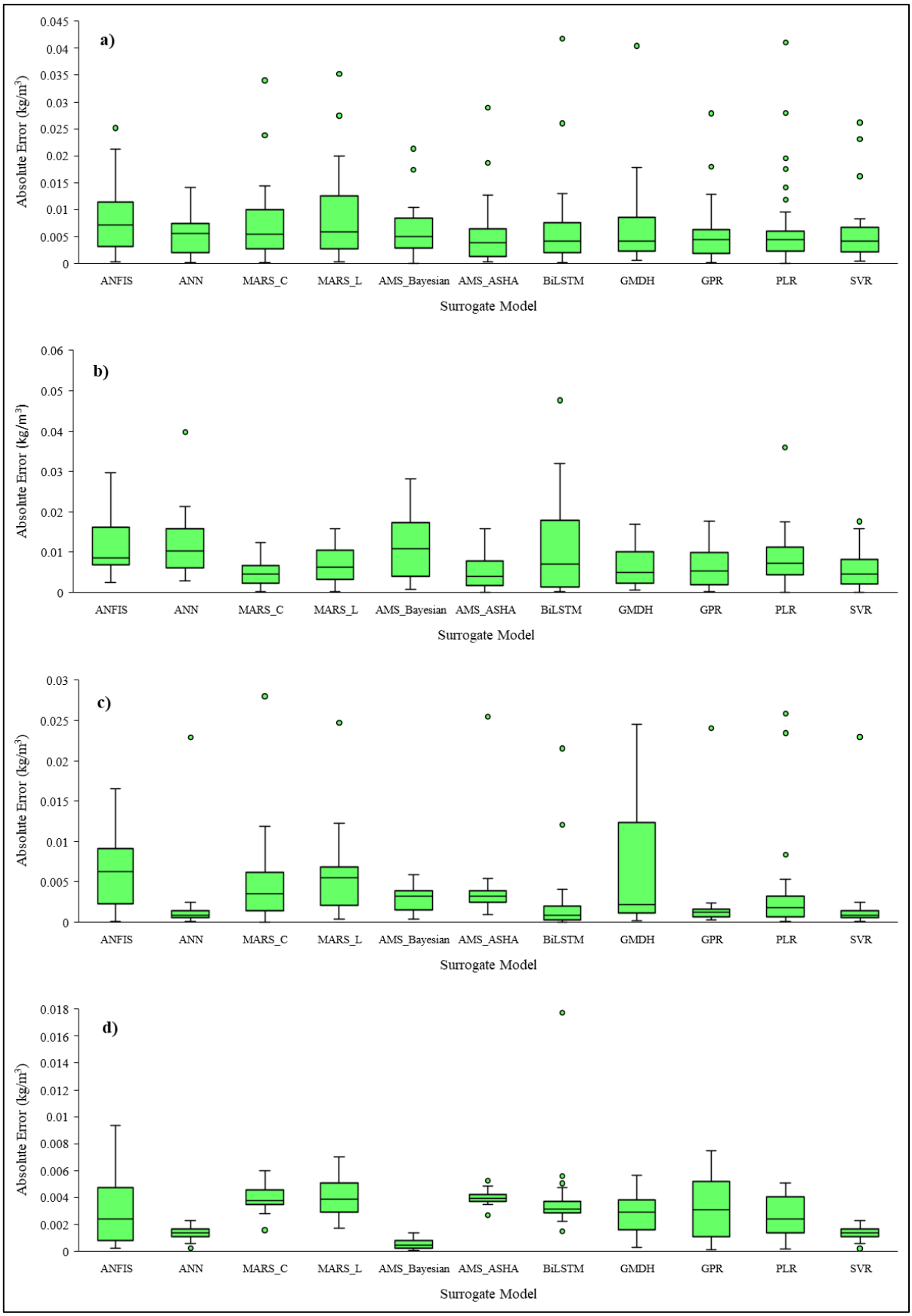



Figure 7.19: Boxplots of absolute errors between actual and predicted salt concentration values at **a)** ML1, **b)** ML2, **c)** ML3, and **d)** ML4 using all twelve surrogate models.

An absolute error boxplot was also used to compare standalone surrogate models, as shown in Figure 7.19. The boxplots revealed that different surrogates perform differently for all four MLs. Also, most surrogate models performed better according to the multiple criteria mentioned in Section 7.4.4. However, different prediction models may excel in various performance metrics. For example, one model might show superior performance in correlation coefficient, while another might perform better in relative error. To reconcile these differences, a comprehensive set of performance metrics should be employed in the decision-making process to address such contradictions objectively. This method categorises performance metrics into benefit indices (where higher values are preferred) and cost indices (where lower values are preferred) (Roy et al. 2021). This study utilised four benefit and four cost indices to evaluate prediction model accuracy. Decision-making involved calculating the weights of each hybridised model using these indices, aided by Shannon's Entropy concepts.

The Shannon's entropy weight (EW) was used to select the best-performing surrogate model based on their weights. The EWs of the performance indices are given in Table 7.4. The higher the entropy weight value of the performance indices, the greater its impact on determining the weight of the individual models. That is to say, higher values of the EW of the performance indices indicate the greater impact of this index in the decision-making process. The EWs of individual prediction models were calculated to rank the best-performing surrogate model in predicting the salt concentrations at four MLs. The ranking of the surrogate model was solely based on their EWs. The surrogate model ranking based on EWs is shown in Table 7.5.

Table 7.4: Entropy weight of performance indices.

| **Performance Indices** | **Entropy Weight** | | | |
|---|---|---|---|---|
| | **ML1** | **ML2** | **ML3** | **ML4** |
| R2 | 0.137 | 0.144 | 0.100 | 0.178 |
| IOA | 0.169 | 0.179 | 0.132 | 0.238 |
| KGE | 0.151 | 0.156 | 0.161 | -0.084 |
| MAD | 0.181 | 0.173 | 0.192 | 0.218 |
| RMSE | 0.181 | 0.174 | 0.221 | 0.231 |
| MAPE (%) | 0.181 | 0.173 | 0.193 | 0.218 |
| Sum | 1.0 | 1.0 | 1.0 | 1.0 |

Table 7.5: Entropy weight of the individual prediction models.

| Standalone models | ML1 | | ML2 | | ML3 | | ML4 | |
|---|---|---|---|---|---|---|---|---|
| | EW | Rank | EW | Rank | EW | Rank | EW | Rank |
| ANFIS | 0.745 | 7 | 0.605 | 9 | 0.425 | 9 | 0.191 | 7 |
| ANN | 0.918 | 1 | 0.436 | 11 | 0.915 | 1 | 0.598 | 2 |
| MARS_C | 0.697 | 8 | 0.994 | 1 | 0.423 | 10 | 0.151 | 10 |
| MARS_L | 0.572 | 9 | 0.820 | 5 | 0.300 | 12 | 0.125 | 11 |
| AMS_Bayesian | 0.912 | 2 | 0.639 | 8 | 0.444 | 7 | 0.806 | 1 |
| AMS_ASHA | 0.877 | 5 | 0.926 | 2 | 0.505 | 6 | 0.201 | 6 |
| Bi-LSTM | 0.533 | 11 | 0.315 | 12 | 0.542 | 5 | 0.093 | 12 |
| GMDH | 0.508 | 12 | 0.815 | 7 | 0.351 | 11 | 0.172 | 8 |
| GPR | 0.891 | 4 | 0.817 | 6 | 0.673 | 4 | 0.238 | 5 |
| PLR | 0.904 | 3 | 0.833 | 4 | 0.822 | 3 | 0.525 | 3 |
| RF | 0.549 | 10 | 0.446 | 10 | 0.442 | 8 | 0.152 | 9 |
| SVR | 0.816 | 6 | 0.865 | 3 | 0.840 | 2 | 0.341 | 4 |

EW = Entropy Weight, ANFIS = Adaptive Neuro Fuzzy Inference System, ANN = Artificial Neural Network, MARS_C = Multivariate Adaptive Regression Spline with Piecewise Cubic Spline, MARS_L = Multivariate Adaptive Regression Spline with Piecewise Linear Spline, AMS_Bayesian = Bayesian Optimization tuned Automatic Model Selection, AMS_ASHA = Asynchronous Successive Halving Algorithm tuned Automatic Model Selection, Bi-LSTM = Bi-directional Long Short term Memory Network, GMDH = Group Method of Data Handling, GPR = Gaussian Process Regression, PLR = Probabilistic Linear Regression, SVR = Support Vector Regression.

EWs easily allowed the ranking of best-predicting models. The ranking of surrogate models was used to develop an ensemble model that would predict better results than the standalone surrogate models. The top-ranked five surrogate models were used to form the ensembles at each of the MLs. Although combining a larger number of surrogates to form an ensemble provides better assurance in predicting salt concentrations, it may also incur a computational burden, particularly in the development of a coupled S-O-based saltwater intrusion management model. As such, the number of surrogate models in the ensemble formation was limited to the top five, as determined by Shannon's entropy. Hence, five surrogates were chosen to form an ensemble model for predicting the salt concentrations at ML1. Based on the EW ranking given in Table 7.5, the ensemble model for ML1 was formulated using ANN, AMS_Bayesian, PLR, GPR and AMS_ASHA.

Similarly, the ensemble at ML2 included MARS_C, AMS_ASHA, SVR, PLR and MARS_L. The ensemble model consisted of ANN, SVR, PLR, GPR and BiLSTM surrogate approximators for ML3. Lastly, the surrogates used to develop an ensemble model at ML4 were AMS_Bayesian, ANN, PLR and SVR. For ML4, only four surrogates were used in forming the ensemble model because using the fifth surrogate (GPR) based on ranking gave poor results. The performance of four ensemble models is given in Table

7.3. The results indicated that all the ensemble models performed better than the standalone surrogate models. The residual of the surrogate ensemble model is also shown in Figure 7.20. The residuals indicate fewer variations between the actual and predicted salt concentrations at different MLs.

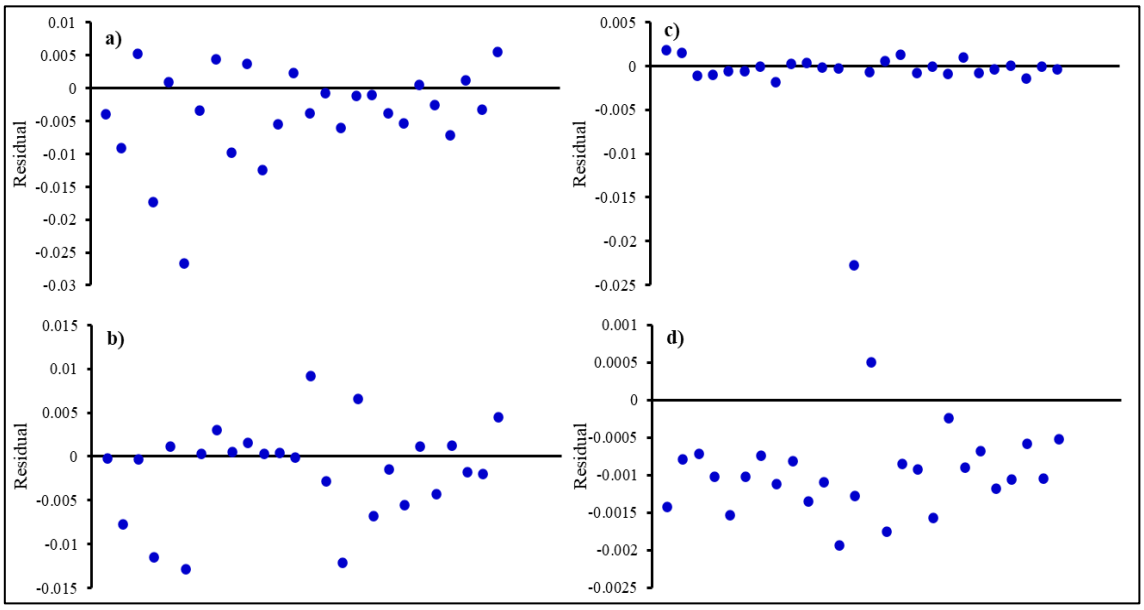



Figure 7.20: Residual of actual versus predicted salt concentrations of ensemble models. **a)** residual of an ensemble model at ML1, **b)** residual of an ensemble model at ML2, **c)** residual of an ensemble model at ML3 and **d)** residual of an ensemble model at ML4.

### 7.5.4 Management Model

The four ensemble models developed at the MLs were separately linked with the CEMOGA, and a multi-objective saltwater intrusion management model was formulated for the Tagabe coastal aquifer. The two conflicting objectives of the management model were maximising the production well pumping and minimising the barrier well pumping. The constraint of the optimisation formulation was to maintain a specific maximum permissible salt concentration at different MLs. Several combinations of different parameters were simulated using different optimum parameter values in optimisation formulation.

The population size is an important factor that determines how many individuals are present in each generation of a genetic algorithm. Having a large population size enables the algorithm to explore the solution space more extensively, improving the likelihood of finding a global solution. Conversely, a smaller population size limits the search space and impacts the distribution of solutions along the Pareto optimal front. This

study selected a population size of 2,000 to balance population diversity and computational efficiency based on various trials and the interplay with other parameters.

The optimisation algorithm was executed for 16,000 generations to achieve the global optimal solution. This required a total of 32,000,000 evaluations, calculated as 2,000 individuals per generation multiplied by 16,000 generations. The algorithm employed a tournament selection method with a tournament size of two. The crossover and mutation rates were set at 0.92 and 0.1, respectively. The migration parameter used a forward direction with a fraction of 0.2 and an interval of 20. A Pareto front population fraction of 0.7 was used, resulting in 1,400 (2,000 × 0.7) non-dominated optimal solutions from the 2,000 individuals. The function and constraint tolerances were set at $1 \times 10^{-4}$. The optimisation routine took 11354 seconds to converge to optimal solutions.

The Pareto-optimal front obtained by CEMOGA-ensemble models are shown in Figure 7.21.

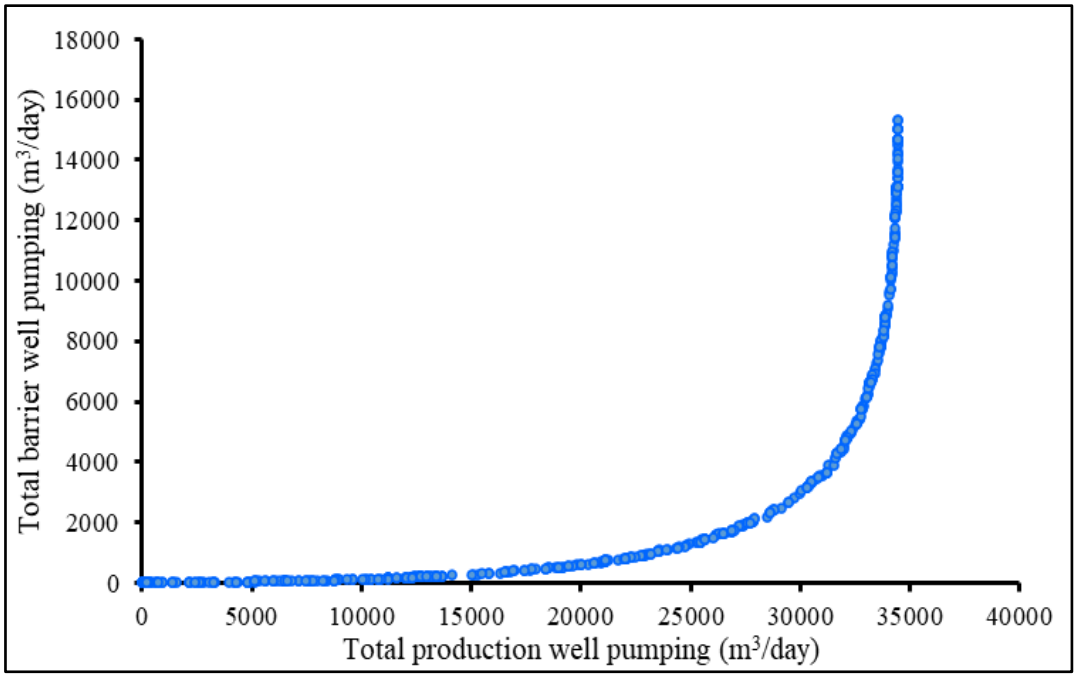



Figure 7.21: Pareto optimal front of the linked simulation-optimisation management model.

The 1,400 Pareto optimal front solutions related to groundwater abstractions from the combined eight production bores and six barrier wells are shown in Figure 7.21. This Pareto optimal front provides numerous solutions for maximising pumping from the production wells and minimising the pumping from the barrier wells while maintaining the allowable salt concentrations at different monitoring locations within the specified limits in equations 10 to 15. The Pareto optimal front demonstrates the balance between

two competing objectives. Its extensive nature indicates that the trade-offs between these objectives are thoroughly represented. Figure 7.21 illustrates that 15,000 $m^3$/d could be extracted from the production bores from Tagabe coastal aquifer with a relatively small amount of barrier well abstraction (253 $m^3$/d). However, if higher production bore pumping is performed, then higher barrier well pumping would be required to keep the hydraulic gradient towards the seaward side.

A similar method was used by Roy and Datta (2017a; 2017b), Lal and Datta (2018). The authors compared a few surrogate models (less than five) and formed ensembles out of them. In this study, a total of 12 surrogate models were developed and compared. Then, the top-performing 5 surrogate models, determined by Shannon's Entropy based decision theory, were used to form the weighted-average ensemble model. Moreover, other studies (e.g., Bhattacharjya and Datta 2005; Hussain et al. 2015) used a linked S-O technique. However, these authors used single surrogate models that were linked with the optimisation algorithms. Linking multiple surrogates and developing an ensemble reduces the uncertainty in the prediction of salt concentrations (outputs). The ensembles developed in this study performed exceptionally well compared with standalone surrogates.

### 7.5.5 Validation of Pareto Optimal Solutions

The effectiveness of the surrogate-based saltwater intrusion management model was assessed by checking how well it met the specified constraints. The results showed that the saltwater concentrations from the optimisation model, which used surrogate models, consistently stayed below the set maximum allowable levels at all monitoring sites. This indicates that the constraints were fully satisfied without any breaches during the optimisation process. Additionally, the saltwater concentrations closely matched the specified limits, suggesting that the optimisation model effectively converged near the upper limits of the constraints.

The Pareto optimal solutions obtained using the ensemble-CEMOGA optimisation models at respective MLs were verified and validated. Five randomly selected optimal solutions (pumping values) were fed into the SEAWAT-based numerical groundwater model, and the outputs (salt concentrations) of the numerical model were compared with the salt concentrations prespecified by the linked S-O model. The validation results are given in Table 7.6. The results (Table 7.6) indicated that the relative error (RE) between

the simulated and predicted salt concentrations at four MLs ranged between 0.47% and 6.66%. The salinity concentrations of both models had a minimal difference (RE < 7%), which indicated that the optimal solutions converged to the upper limit of the constraints. Also, it can be reported that all the constraints are satisfied with no constraint violations. The findings in this study are similar to the results reported by Roy and Datta (2017b). The authors suggested that relative errors of less than 10% are considered appropriate and effective for developing an optimal management strategy using an integrated S–O approach. Hence, it could be stated that the machine learning-based ensemble model developed could be replaced with the complex nonlinear coupled density-dependent SEAWAT-based model for developing optimal groundwater management solutions for Tagabe coastal aquifer. Moreover, this methodology could be utilised for other aquifers.

The limitation of this study was the number of data sets used to train and test the surrogate models. The current study used 130 sets of input-output data from the numerical model to train and test the surrogate models. Hence, some of the deep learning models did not perform that well when compared with the machine learning models. Also, larger datasets will be used to train and test the deep learning models in future.

Table 7.6: Validation of Pareto optimal front solutions with the numerical simulation model.

| Solution Number | ML1 | | | ML2 | | | ML3 | | | ML4 | | |
|---|---|---|---|---|---|---|---|---|---|---|---|---|
| | NSM ($kg/m^3$) | SEM ($kg/m^3$) | RE (%) | NSM ($kg/m^3$) | SEM ($kg/m^3$) | RE (%) | NSM ($kg/m^3$) | SEM ($kg/m^3$) | RE (%) | NSM ($kg/m^3$) | SEM ($kg/m^3$) | RE (%) |
| 1 | 0.320 | 0.301 | 6.547 | 0.282 | 0.300 | 5.930 | 0.299 | 0.300 | 0.481 | 0.314 | 0.300 | 4.814 |
| 2 | 0.312 | 0.300 | 3.783 | 0.283 | 0.300 | 5.721 | 0.299 | 0.300 | 0.473 | 0.285 | 0.300 | 5.157 |
| 3 | 0.313 | 0.304 | 2.916 | 0.290 | 0.300 | 3.237 | 0.299 | 0.301 | 0.658 | 0.311 | 0.300 | 3.525 |
| 4 | 0.321 | 0.301 | 6.658 | 0.282 | 0.300 | 5.886 | 0.299 | 0.300 | 0.485 | 0.314 | 0.300 | 4.734 |
| 5 | 0.320 | 0.301 | 6.407 | 0.283 | 0.300 | 5.509 | 0.299 | 0.300 | 0.443 | 0.294 | 0.300 | 2.065 |

NSM – Numerical simulation model; SEM = surrogate ensemble model; RE = absolute relative error between the simulated and the predicted salt concentrations; ML = Monitoring location; C = Concentration

## 7.6 Conclusions

Saltwater intrusion is a concern in Vanuatu for Tagabe coastal aquifer based on current groundwater pumping regimes. To manage the saltwater intrusion, optimal management strategies need to be developed. The current study developed a methodology using a linked simulation-optimisation (S-O) technique that provided optimal management strategies of managing saltwater intrusion in Tagabe coastal aquifer. S-O methodology was developed using a surrogate ensemble modelling approach where twelve surrogate models were trained with the input-output patterns from the SEAWAT-based numerical simulation model. Using Shannon's entropy weight (decision theory), the top five surrogates were ranked and selected to form an ensemble model for each monitoring location. All the ensemble models performed exceptionally well compared with standalone surrogates. Later, the ensemble models were externally linked in MATLAB with the Controlled Elitist Multiple Objective Genetic Algorithm (CEMOGA) to optimise the saltwater intrusion management solutions.

The constraints fixed for the S-O model were maximising the pumping from the production wells, minimising the pumping from the barrier well, and maintaining the maximum allowable salt concentrations at each monitoring location. Conflicting constraints were easily solved with the S-O methodology developed in this study. The S-O model gave Pareto optimal front solutions, maximising the pumping from production wells and minimising the pumping from barrier wells. To verify the Pareto optimal solutions, five random pumping values (Pareto solutions) were fed into the numerical simulation model, and the same was fed into the surrogate ensemble model. The results indicated that the salt concentrations (outputs) from both models had a minimal relative error of less than 7%, satisfying the constraints.

In addition, the results from this study indicated that the use of machine learning in groundwater modelling is a robust tool for predicting the saltwater intrusion in Tagabe coastal aquifer. The use of surrogate ensemble models reduced the computational burden and exertions faced during the optimisation stage. The results also indicated that training different machine learning surrogates with limited datasets was also successful. The S-O management model also proved to be robust in generating optimal solutions for managing the saltwater intrusion in Tagabe coastal aquifer. The methodology proposed in this study is of global significance and can be used by policymakers and water monitoring

authorities to draw up policies and regulations for groundwater use in Vanuatu. The methodology presented in this study could also be used in other coastal aquifers to manage saltwater intrusion and conserve groundwater.

The future scope of work has also been planned for Tagabe coastal aquifer, where other constraints would be considered in the S-O methodology to manage SWI. For instance, minimising the recharge, maximising the evapotranspiration and salt concentrations at monitoring locations, using other optimising algorithms and using larger input-output data sets in training and testing surrogate and ensemble models.

The next chapter uses the multi-objective simulation-optimisation framework to develop a digital twin model for Tagabe coastal aquifer.

# Chapter 8: Conceptual development and implementation of a digital twin model for managing saltwater intrusion of an island coastal aquifer

A manuscript based on the main contents of this chapter has been submitted for publication and is currently under review, as outlined below:

**Sharan, A**., Roy, D.K, Datta, B., & Lal, A. (Under Review). Conceptual development and implementation of a digital twin model for managing saltwater intrusion of an island coastal aquifer. *Water Resources Research.*

## 8.1 Overview

This chapter develops a digital twin model that can feed the real-time data into the virtual model from the field.

## 8.2 Executive Summary

Saltwater intrusion (SWI) poses a significant environmental challenge for coastal aquifers in Pacific Island nations, including Port Vila, Vanuatu. This study utilised a 3D numerical simulation model to evaluate SWI in the Tagabe coastal aquifer under current pumping regimes. To address SWI, optimal pumping patterns were identified through machine learning-based surrogate ensemble models and a simulation-optimisation (S-O) management model. A digital twin (DT) framework of the Tagabe coastal aquifer was developed, incorporating a 3D numerical model, surrogate ensemble models, and the S-O approach. The DT framework, linked with illustrative field data, was used to generate and analyse five illustrative scenarios based on varying salt concentrations (0.45, 0.55, 0.75, 0.90 and 1.15 kg/m$^3$; Scenarios 1 to 5, respectively). Results indicated that scenario 3, with a salt concentration of 0.75 kg/m$^3$, yielded the highest pumping rates from production wells (17,317 m$^3$/d) and the lowest from barrier wells (202 m$^3$/d). Conversely, using the Pareto frontier (knee of Pareto solutions), scenario 5 solutions showed maximum pumping values of 31,676 m$^3$/d from production wells and 5,000 m$^3$/d from barrier wells. The S-O model results were validated with less than 10% relative error compared to the numerical model outputs. To the best of the current knowledge, the application of DT in managing SWI has not been applied before. The results from the study indicated that DT can be successfully employed in a coastal aquifer for managing the SWI. The methodology developed and implemented in this study is of global significance and could be used to manage water resources wisely. The study demonstrated

that with the help of S-O approach, the DT is vital in predicting future scenarios, changes in pumping patterns and other uncertainties.

## 8.3 Introduction

Saltwater intrusion (SWI) is a major challenge in Pacific Island countries (PICs), and managing SWI is a far more complex and costly process (Sharan et al., 2021). Globally, including PICs, various techniques and methodologies are designed to tackle SWI. However, the severity of the problem keeps on increasing with the changing climate, natural disasters and human activities. Different strategies for managing SWI in coastal aquifers are needed. However, accessing the field data is becoming costly and time-consuming. Hence, developing the SWI management strategies can get delayed, which would cause the freshwater aquifers to be contaminated with saline water. Therefore, getting the field data about the changes in the hydrogeological parameters and boundary conditions on time is needed. Currently, smart sensors and data loggers feed the data to personal computers (PCs), but they are not yet used in groundwater modelling.

The use of smart sensors in remote monitoring and the feedback information is crucial in managing SWI and water resources. Based on the literature search and the best of the current knowledge, management of SWI using smart techniques has not yet been applied yet. The current study employs a novel approach to develop and implement a digital twin (DT) model for a coastal aquifer. Based on the literature and the current knowledge, the DT model has not been applied globally or in PICs' SWI management processes. The DT model is emerging as a transformative technology in various industries, offering unparalleled opportunities for optimisation and innovation (Liu et al., 2021). Essentially, a DT is a virtual representation of a physical asset, system, or process that is continuously updated with real-time data (Tao et al., 2022). This dynamic model enables predictive analysis, performance monitoring, and decision support, enhancing operational efficiency and reducing risks. The concept has evolved from its early applications in aerospace to diverse fields such as manufacturing, healthcare, urban planning, and beyond (Attaran and Celik, 2023).

DTs and virtual representations of physical systems have seen growing applications in groundwater management. Ortega (2023) developed a DT model for monitoring the groundwater table in Enschede, Netherlands. The author used smart sensors, which fed the information to the 3D geospatial model through the Internet of Things (IoT). These

sensors monitored the groundwater table from rainfall variations and based on the head heights, the water pumps were activated or deactivated in physical space. The results demonstrated that the DT effectively visualises historical data, current conditions, and anticipated changes in the groundwater table, aiding in identifying areas needing pumping. By integrating forecasts, the system can predict potential groundwater table depths, visualise possible scenarios, and support decision-making processes regarding pumping or retaining groundwater levels through automated messages or physical actions.

Henrik et al. (2023) developed and implemented the hydrological information and prediction (HIP) system in Denmark. The authors used a combination of real-time data integration, advanced hydrological models, and machine learning techniques to create a DT that can dynamically update and predict hydrological conditions. The study area covered various aspects of Denmark's water systems, including groundwater levels, soil moisture, and streamflow. The HIP portal, developed by the Danish Agency for Data Supply and Infrastructure, provided a platform for these models and data to be accessed and utilised by various stakeholders, including municipal planners, water supply workers, and environmental consultants. The authors reported that their study highlighted the effectiveness of the HIP DT in improving climate change adaptation, water management, disaster risk reduction, real-time monitoring and forecasting, helping to identify potential risks and manage water resources more efficiently. The authors recommend further development of the DT approach, emphasising the importance of real-time data updates and collaborative efforts across different sectors to maximise the benefits of this technology for climate resilience and sustainable water management.

Huang et al. (2022) developed a DT of the Earth systems in predicting and analysing floods. The authors used various artificial intelligence (AI), geological and 3D software to formulate a DT model. Their study focused on surface water hydrology, specifically targeting flood detection and prediction in Earth's rivers and lakes. The DT framework allows users to explore current Earth system states, predict future conditions, and run hypothetical scenarios to understand potential system evolutions. The authors reported that DT can accurately predict flood events, analyse their impacts, and provide actionable insights for flood management. The authors recommended expanding the DT framework to incorporate more environmental variables and geographic areas and enhancing

collaboration between agencies for broader data integration and improved predictive capabilities.

Tsakiridis et al. (2023) developed a DT to assess and monitor soil ecosystems. The authors developed DT by integrating various data sources, including IoT, sensors, remote sensing data, field measurements, digital cartography, surveys, and other Earth observation data. The integration created a cohesive digital representation of the physical, chemical, and biological characteristics of soil. The authors used multiple environments to test and validate the DT model. The authors reported that DT could provide detailed insights into soil health, including nutrient cycles, microbial communities, and physical soil structure. The DT framework developed has the potential to do scenario analysis, visualising environmental impacts such as climate change and land use alterations and aiding in decision-making processes for various stakeholders.

Lari et al. (2022) designed a DT to monitor natural source zone depletion (NSZD) of light non-aqueous phase liquids (LNAPLs) at petroleum-impacted sites in Bemidji Minnesota (USA). The authors used a TMVOCBio (finite volume numerical simulator) multi-phase multi-component multi-microbe transport phenomena at a Darcy scale to mimic the significant NSZD process, hence a DT. The approach integrated partitioning, biodegradation, and fluid dynamics to predict long-term trends and validate the model against field data. The authors reported that the DT accurately simulated complex subsurface processes, providing a detailed and reliable representation of NSZD. The authors also reported that the DT's ability to predict future depletion trends and support site management decisions underscored its potential utility in their study. The authors recommended further developing and applying DT for complex subsurface systems to enhance decision-making and management strategies for contaminated sites, emphasising the benefits of detailed computational approaches for environmental monitoring and restoration.

The application of DT in groundwater is growing, yet minimal. However, DT has been applied in other disciplines extensively (e.g., Ayani et al., 2018; Uhlemann et al., 2017; Cia et al., 2017; Bottani et al., 2017; Lindstrom et al., 2017; Silva et al., 2023). These studies have shown the exploration and application of the DT paradigm across various domains of manufacturing and production systems. These studies collectively emphasise the integration of real-time data acquisition, sensor data fusion, and cyber-

physical systems to create virtual representations, or DTs, of physical entities. This integration enhanced operational efficiency, predictive maintenance, and system optimisation.

The application of DT in SWI management in coastal aquifers has not been applied yet. Hence, this work aims to develop a DT that would be applied to a coastal aquifer of a small Pacific Island country. This study will use a 3D numerical simulation model, various machine learning algorithms, surrogate ensemble models and optimisation algorithms to design a DT. The detailed steps in the DT model development are given in Section 8.4.5. The DT developed in this study will be used to predict various scenarios for managing the SWI. The advantage of using DT in coastal aquifers is that it can provide real-time feedback from the field, and based on the information, optimal SWI management strategies can be developed. The methodology and findings from this study could aid researchers, policymakers and water engineers in modelling, planning, and making informed decisions to conserve and utilise the groundwater.

## 8.4 Methodology

### 8.4.1 Study area

The study area for this research is a small Pacific Island country, Vanuatu. Vanuatu, an island nation east of Australia, is comprised of 83 islands with a mix of volcanic mountains and coral atolls. With a population exceeding 300,000, Port Vila's capital is famous for its natural beauty and attracts tourists. Tourism is crucial to Vanuatu's economy, contributing 35.5% to its GDP in 2019, alongside agriculture, fishing, and forestry (WTTC, 2021). Despite these economic drivers, Vanuatu faces significant challenges from natural disasters and climate change, leading the government to focus on resilience-building measures (CRCP, 2021; VMGD, 2023; Sharan, 2023). The six provinces of Vanuatu, including Shefa, where the capital, Efate Island, is located, feature diverse geology influenced by volcanic activity, tectonic movements, and erosion. Efate Island is notable for its volcanic features, such as the Yasur volcano, limestone formations created by marine organisms, and alluvial deposits from nearby rivers (Bath et al., 1986). The island's topography has been shaped by tectonic movements causing faults and folds and by erosion affecting the low-elevation coastal areas. This geological diversity, coupled with Vanuatu's susceptibility to natural disasters, highlights the need for integrating climate adaptation and disaster risk reduction into a development plan.

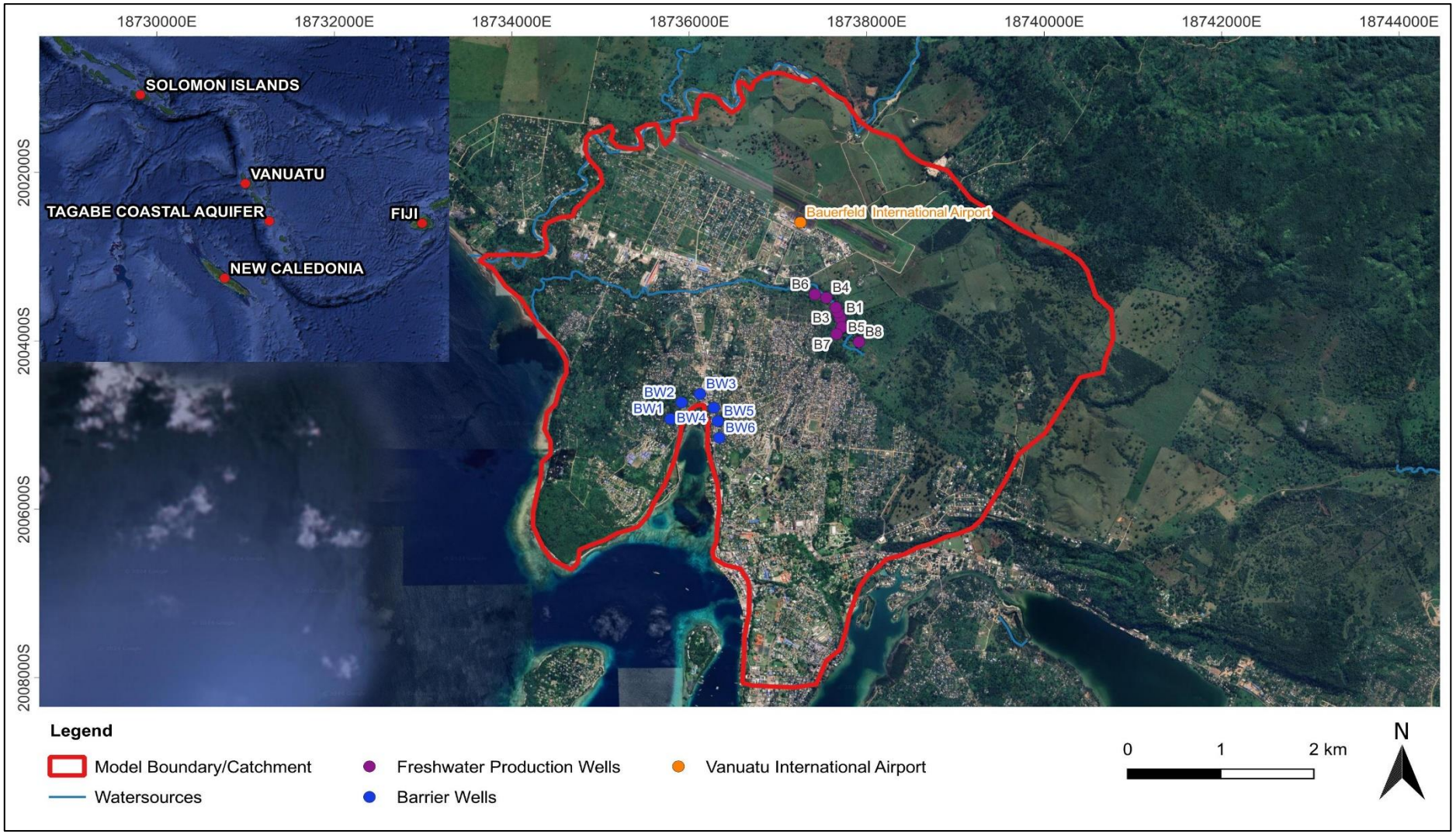



Figure 8.1: Location of the study area.

The methodology developed in this study was applied to the Tagabe coastal aquifer in Vanuatu. The location of the study area is shown in Figure 8.1. Eight freshwater wells (B1-B8) pump the freshwater from Tagabe coastal aquifer, which supplies water in Port Vila. The model boundary or the catchment was selected based on the geology and water feeding into Tagabe coastal aquifer. To minimise the SWI, six barrier wells (BW1-W6) were added near the sea boundary.

### 8.4.2 3D Numerical Simulation Model

Modelling the groundwater processes of a coastal aquifer is a complex and lengthy process because of its heterogeneity. Actuate field data from Tagabe coastal aquifer, including the hydrogeological parameters and boundary conditions, were used to develop a 3D groundwater model. The groundwater data provided by the Department of Water Resources, Vanuatu, was limited, consisting of bore pumping data from 2017 to 2022 and electrical conductivity values from 2019 to 2021. Limited data on critical parameters, such as hydraulic head values and initial concentrations, were provided. Despite these limitations, a 3D numerical simulation model was developed using the available data to manage SWI scenarios in the Tagabe coastal aquifer. The model was calibrated and validated using the salt concentration data (Sharan et al., 2024a). Table 8.1 details the boundary conditions and hydrogeological parameters used to develop the 3D model.

Table 8.1: Model parameters and the values used for the model design. Source (Sharan et al., 2024a).

| Definition | Assigned field values | Calibrated values | SI Units |
|---|---|---|---|
| Layer 1 (Sand and gravel) | Hydraulic Conductivity, K = 20<br>Porosity = 0.35 | Hydraulic Conductivity, K = 25.5<br>Porosity = 0.45 | K = m/d<br>Porosity = |
| Layer 2 (Limestone) | Hydraulic Conductivity, K = 35<br>Porosity = 0.45 | Hydraulic Conductivity, K = 40<br>Porosity = 0.55 | dimensionless |
| Recharge | 0.0004 | 0.000271 | m/d |
| Horizontal Anisotropy | 1 | | dimensionless |
| Freshwater Density | 1000 | | $kg/m^3$ |
| Seawater Density | 1025 | | $kg/m^3$ |
| Saltwater Concentration | 35 | | $kg/m^3$ |
| Specific Storage | 0.000035 | | 1/m |
| River conductance | 1 | | $m^2/dm$ |
| Longitudinal dispersivity | 30 | | m |
| Density/Con. constant, F | 0.7143 | | dimensionless |

The 3D groundwater model was developed using flow and transport codes in Groundwater Modelling Systems software, explicitly using the SEAWAT code. SEAWAT simulates three-dimensional groundwater flow in porous materials, accommodating variable density and transient conditions by integrating MODFLOW

(solves flow model) and MT3DMS (solves solute transport model) using the equations provided by Guo and Langevin (2002).

The conceptual model of the Tagabe coastal aquifer was created with the MODFLOW, covering a model domain of 7.50 km by 7.61 km by 0.1 km. A 3D finite-difference grid with 100 x 100 m cells was used, consisting of two layers with different hydraulic conductivities and porosities. Layer 1 (0 to -80 m) had a hydraulic conductivity of 20 m/d and a porosity of 0.35, while layer 2 (-80 to -100 m) had a hydraulic conductivity of 35 m/d and a porosity of 0.45. Boundary conditions included a specified head boundary (CHB) on the southern side, a no-flow boundary on the eastern side, and the Sono River on the northwestern boundary connected to the ocean boundary.

Due to the lack of observed hydraulic head values from boreholes in Tagabe, approximate values were assigned based on available data. CHB values for the western and southeastern nodes were set at 9 m and 8.8 m, respectively, maintaining a slight hydraulic gradient towards the sea. Head values for the Sono River and Tagabe River nodes were assigned accordingly, considering the presence of salinity in the aquifer. Boreholes B1-B8 (Figure 8.1) were included in the model domain, with transient pumping values from 2017 to 2021. All hydrogeological parameters, boundary conditions, wells, pumping values, and head values were integrated into MODFLOW, and a 20-year steady-state simulation was conducted to establish initial conditions.

SEAWAT was initiated for a 5-year period, utilising pumping data from 2017 to 2021. The model was calibrated using electrical conductivity (EC) data from boreholes B1, B2, B3, B7, and B8 from 2019 to 2020 (2021 data missing). Despite the lack of observed head values, calibration was performed using secondary data through trial-and-error methods, adjusting initial salt concentrations, recharge values, hydraulic conductivities, and porosities (Sharan et al., 2024a). After calibration, the model was simulated for the next 20 years (2022-2043), with the calibrated results serving as the base case for the study. The calibrated model was also used to obtain output (salt concentrations) values at four monitoring locations (MLs) using randomly generated input (pumping) values. The four MLs were selected from the current production wells. Hence ML1 = B1, ML2 = B3, ML3 = B7 and ML4 = B8 (Figure 8.1).

The 3D numerical model was run 130 times using different spatiotemporal pumping patterns to determine the salt concentration at four monitoring sites. These pumping

patterns served as the inputs, while the resulting salt concentrations were the outputs. Using these input-output patterns, this study developed an ensemble of several machine learning-based surrogate models. The limited number of input-output patterns aimed to reduce computational demands in the coupled S-O approach and to evaluate whether a small dataset, despite having 70 variables, could effectively and accurately train the surrogate ensemble models.

### 8.4.3 Surrogate Ensemble Model

Machine learning-based surrogate and ensemble models were developed to replicate the 3D numerical simulation model of the Tagabe coastal aquifer. Various machine learning and deep learning algorithms can be employed to build these surrogate and ensemble models. This study developed an ensemble of several surrogate models as approximations of the numerical simulation model. Notably, this study establishes the use of limited datasets to train multiple machine learning models as surrogate ensembles and the application of decision theories to choose the best surrogate ensemble model.

The machine learning and deep learning algorithims used to develp surrogate ensemble models were Artificial Neural Network (ANN), Support Vector Regression (SVR), Genetic Programming (GP), MARS_C = Multivariate Adaptive Regression Spline with Piecewise Cubic Spline, MARS_L = Multivariate Adaptive Regression Spline with Piecewise Linear Spline, Probabilistic linear regression (PLR), Random Forest Regression (RFR), Group Method of Data Handling (GMDH), Long Short-Term Memory (LSTM), Adaptive Neuro-Fuzzy Inference Systems (ANFIS), Asynchronous Successive Halving Algorithm tuned Automatic Model Selection (AMS-AHSA) and Bayesian Optimisation tuned Automatic Model Selection (AMS-Bayesian).

The input-output patterns generated from the 3D numerical simulation model were used to train the machine learning and deep learning models mentioned above.

#### *8.4.3.1 Model Performance*

Several performance evaluation criteria were employed to assess the surrogate models. These included the correlation coefficient or Pearson's correlation coefficient ($R^2$) (PCC), Index of Agreement (IoA), Kling-Gupta efficiency (KGE), Nash-Sutcliffe efficiency coefficient (NSE), mean absolute error (MAE), root mean square error

(RMSE), and mean absolute percentage error (MAPE). These metrics were used to evaluate both surrogate and ensemble models.

Moreover, Shannon's entropy-based decision theory was used to select the best-performing model (Shannon, 1948). Using the steps outlined in Li et al. (2011), the model ranking was done. After ranking the best surrogate models, the first five ranked surrogates were used to form an ensemble model for each monitoring location.

### 8.4.4 Management Model

Using the ensemble models developed in Section 8.4.3, a management model or simulation-optimisation (S-O) model was developed. The ensemble models were externally linked with the Controlled Elitist Multiple Objective Genetic Algorithm (CEMOGA) (Deb and Goel, 2001) to find the optimal groundwater management pumping values. The flow diagram of developing a management model using 3D numerical simulation and surrogate ensemble models is given in Figure 8.2.

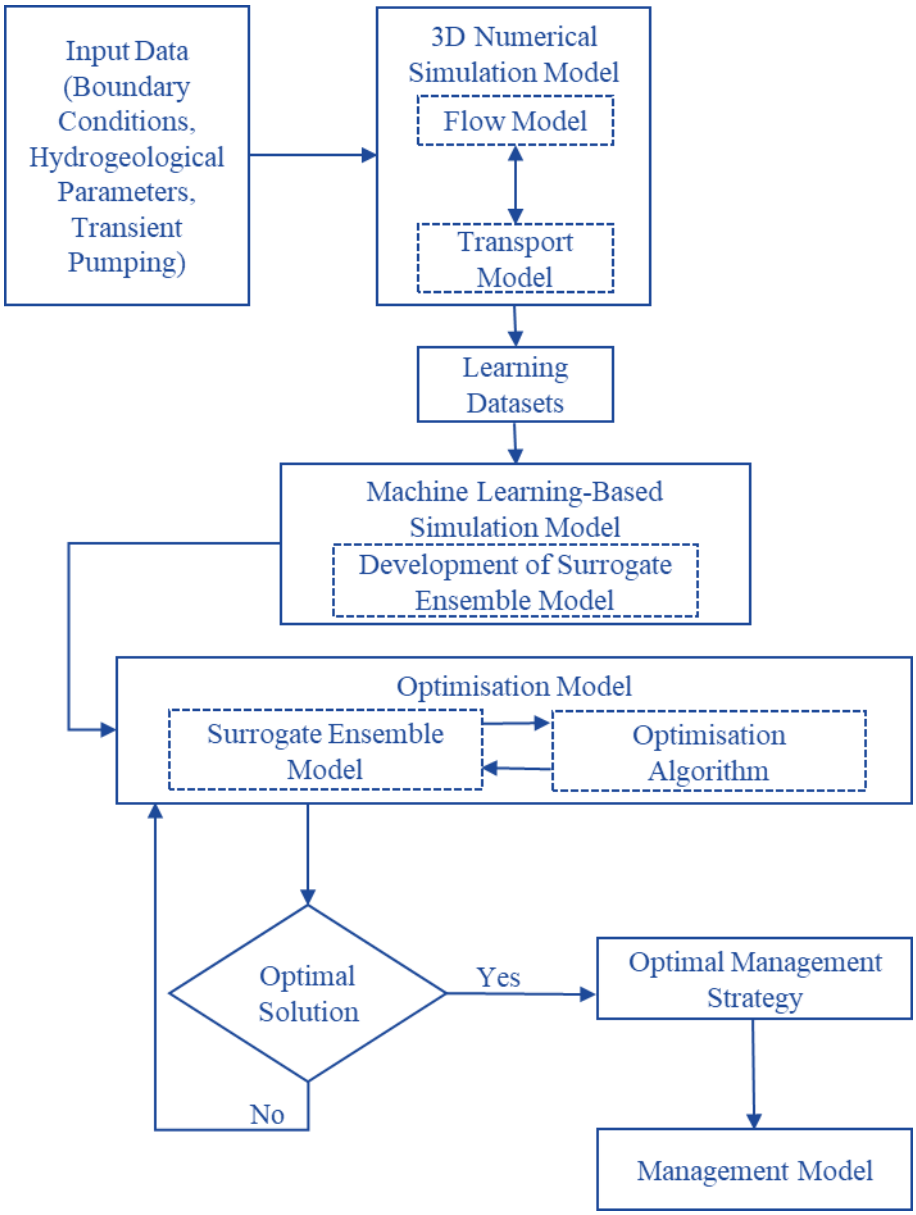



Figure 8.2: Flow diagram of linked simulation-optimisation management model.

The management model developed in this study addresses a multi-objective problem with two conflicting objectives. The objectives are to maximise freshwater extraction from PWs for beneficial use and to minimise pumping from BWs. Reducing BW pumping is important because disposing of large volumes of saline water can be problematic. According to Datta and Peralta (1986), the solutions from the management model will yield a Pareto optimal front, offering water managers and policymakers a clear trade-off between the two conflicting objectives. The mathematical representation of this management model is provided in equations (8.1) to (8.6) (Bhattacharjya and Datta, 2005).

$$\text{Maximise: } f_1(Q_{PW}) = \sum_{n=1}^{N}\sum_{t=1}^{T} Q_{PW_n}^t \tag{8.1}$$

$$\text{Minimise: } f_2(Q_{BW}) = \sum_{m=1}^{M}\sum_{t=1}^{T} Q_{BW_m}^t \tag{8.2}$$

Subject to

$$C_i = \varepsilon(Q_{PW}, Q_{BW}) \tag{8.3}$$

$$C_i \leq C_{max} \forall_i \tag{8.4}$$

$$Q_{PW_{min}} \leq Q_{PW_n}^t \leq Q_{PW_{max}} \tag{8.5}$$

$$Q_{BW_{min}} \leq Q_{BW_n}^t \leq Q_{BW_{max}} \tag{8.6}$$

where PW = production well, BW = barrier well; where $Q_{PW_n}^t$= water extraction from the n$^{th}$ production well during t$^{th}$ time steps; $Q_{BW_m}^t$= water extraction from the n$^{th}$ barrier well during t$^{th}$ time steps; $C_i$ = saltwater concentrations at the i$^{th}$ MLs at the end of the management period; $\varepsilon()$ denotes the density-dependent coupled flow and salt transport surrogate model. The constraint given in equation 8.3 shows the linking of the surrogate ensemble model with the optimisation model; the constraint given in equation 8.4 indicates the maximum allowable salt concentration at various MLs; the constraints given in equations 8.5 and 8.6 outline the upper and lower limits of the water abstraction from pumping and barrier wells, respectively.

### 8.4.5 Digital Twin

In this study, the virtual representation of a coastal aquifer was used using the digital twin (DT) framework. The DT framework and model design is shown in Figure 8.3. The development of the DT for a coastal aquifer is a complex and challenging task. Initially, the 3D numerical simulation model was developed using the field data as described in Section 8.4.2. Secondly, using the learning datasets, 12 surrogate and 4 ensemble models were developed (Section 8.4.3). Thirdly, a management model (S-O model) was developed using the ensemble model, MOGA optimisation algorithm and sets of constraints (Equations 8.1 to 8.6) (Section 8.4.4). These three models represent the virtual

space component of the DT framework. The physical space of the DT framework represents the actual coastal aquifer (Tagabe coastal aquifer).

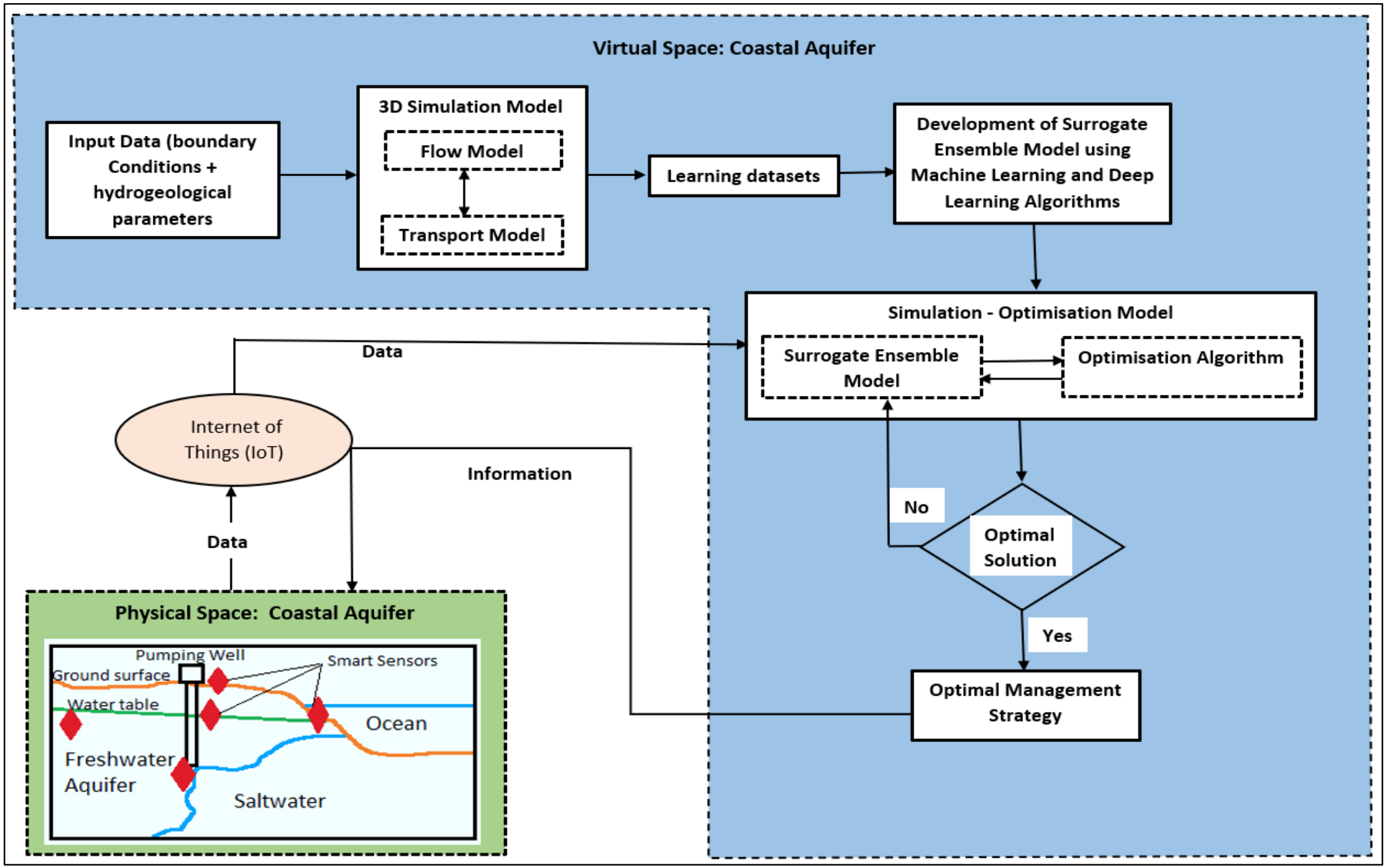



Figure 8.3: Digital twin framework of a coastal aquifer.

The DT is where the physical and virtual spaces are connected. Hence, the smart sensors supply the field data through the Internet of Things (IoTs) to the computers where the virtual model is located. Using the field data supplied by the IoTs, new sets of constraints (Equations 8.1 to 8.6) are set, and the optimal management strategy is developed for managing the saltwater intrusion. Due to time, budget and government approval constraints, the smart sensors were not placed in Tagabe coastal aquifer. Instead, it was assumed that the smart sensors were placed in the field to measure the standing water levels in bores, rainfall (recharge) rates, and the salt concentration of the water, as illustrated in Figure 8.3. These sensors fed the data daily to the computer hardware, and based on these data, a new set of optimal groundwater pumping rates was decided at the end of every month. The governing body implemented the optimal pumping rates to the groundwater users in Port Vila.

The physical space (actual aquifer) has smart sensors, constantly monitoring the water levels, salinity and rainfall rates in Tagabe coastal aquifer. These field data are transmitted using IoT to the surrogate ensemble model, which then re-runs and gives different sets of Pareto optimal fronts (optimal pumping values). The optimal management strategy is then fed back to the physical space. For instance, the smart sensors recorded the drop in groundwater level. Hence, the constraints have to be changed and the maximum pumping limit has to be reduced in equations 8.1 and 8.2 due to the drop in the groundwater level. Using modified constraints, the optimisation algorithm will provide the optimal pumping values, which will then be passed to the users of groundwater. These optimal pumping values would be safe and would prevent saltwater intrusion in coastal aquifers. For this study, the DT works in the steps discussed above.

Using the physical space data provided by IoTs and the constraints outlined in equations 8.1 to 8.6, five scenarios were simulated using the DT for Tagabe coastal aquifer. The sensors have triggered and sent five sets of data/scenarios. The sensors that were illustratively placed in the field measured the salt concentrations of the groundwater in four different MLs and sent the data to the computer, which has the virtual system in place. Based on the new maximum allowable concentrations, Pareto optimal pumping values were simulated. The five scenarios/trigger limits given by the field sensors include;

*Scenario 1:* The maximum allowable salt concentration has decreased from 0.5 to 0.45 kg/m$^3$. The concentration, 0.5 kg/m3, was estimated from the numerical model.

Based on this new constraint, the total allowable salt concentration is 0.45 kg/m$^3$. However, the maximum (1200 m$^3$/d) and minimum pumping (0 m$^3$/d) remain the same. The twelve surrogates and four ensemble models developed in Section 8.4.2 were used to optimise the pumping rate for this scenario. However, the Pareto optimal fronts were generated using the 0.45 kg/m$^3$ allowable salt concentration at all MLs.

*Scenario 2:* The maximum allowable salt concentration has increased from 0.45 to 0.55 kg/m$^3$. Based on this new constraint, the total allowable salt concentration is 0.55 kg/m$^3$. However, the maximum (1200 m$^3$/d) and minimum pumping (0 m$^3$/d) remain the same. The surrogate models used in scenario 1 were used to optimise the pumping rate for this scenario. However, the Pareto optimal fronts were generated using the 0.55 kg/m$^3$ allowable salt concentration at all MLs.

*Scenario 3:* The maximum allowable salt concentration has increased from 0.55 to 0.75 kg/m$^3$. Based on this new constraint, the total allowable salt concentration is 0.75 kg/m$^3$. However, the maximum (1200 m$^3$/d) and minimum pumping (0 m$^3$/d) remain the same. The surrogate models used in scenario 1 were used to optimise the pumping rate for this scenario. However, the Pareto optimal fronts were generated using the 0.75 kg/m$^3$ allowable salt concentration at all MLs.

*Scenario 4:* The maximum allowable salt concentration has increased from 0.75 to 0.9 kg/m$^3$. Based on this new constraint, the total allowable salt concentration is 0.9 kg/m$^3$. However, the maximum (1200 m$^3$/d) and minimum pumping (0 m$^3$/d) remain the same. The surrogate models used in scenario 1 were used to optimise the pumping rate for this scenario. However, the Pareto optimal fronts were generated using the 0.9 kg/m$^3$ allowable salt concentration at all MLs.

*Scenario 5:* The maximum allowable salt concentration has increased from 0.9 to 1.1 kg/m$^3$. Based on this new constraint, the total allowable salt concentration is 1.1 kg/m$^3$. However, the maximum (1200 m$^3$/d) and minimum pumping (0 m$^3$/d) remain the same. The surrogate models used in scenario 1 were used to optimise the pumping rate for this scenario. However, the Pareto optimal fronts were generated using the 1.1 kg/m$^3$ allowable salt concentration at all MLs.

These scenarios were simulated using four surrogate ensembles and the S-O model for different constraints. The Pareto optimal front values were generated, and with the help of the local government, water managers, and local municipal office, these optimal

pumping rates could be sent to the groundwater users of Tagabe coastal aquifer. The optimal pumping rates would be sent to the users using the smart information boards placed near the nested bore networks by IoTs. These smart information boards would show the optimal pumping rates based on different scenarios. The use of machine learning, smart sensors, DT and smart information boards will significantly reduce remote travel, cost, time and improve the sustainability of groundwater resources in Tagabe coastal aquifers and other aquifers as well.

## 8.5 Results and Discussion

### 8.5.1 3D Numerical Simulation Model

The numerical simulation model was developed, calibrated, and validated using the salt concentration data. Using the calibrated data and the current pumping regimes, the numerical model was simulated for 20 years, starting from 2022 to 2043. The extent of SWI for three time steps (5, 10 and 20 years) is shown in Figure 8.4. The length of SWI is clearly shown in the figure. With the current pumping regime, the wells would be contaminated, and the freshwater Tagabe aquifer would have saline water with concentrations reaching up to 20 kg/m$^3$ (20,000 mg/L). Moreover, Figure 8.5 shows the cross-sections of the SWI extents/lengths. These cross-sections clearly show when the saline water would reach the production wells (B1-B8). Hence, the water would not be suitable for drinking and irrigation.

Therefore, managing SWI is essential as Tagabe coastal aquifer supplies fresh water to the capital city (Port Vila). The use of barrier wells, injection/recharge wells, and managing pumping rates were effective for managing SWI in Tagabe coastal aquifer (Sharan et al., 2024a). However, knowing the optimum pumping rates from barrier wells (BWs) and production wells (PWs) is challenging and cannot be fully achieved by the numerical simulation model. Also, optimising the numerical simulation model would take an immense amount of computational time (Bhattacharjya and Datta, 2005). Hence, this study developed a methodology to maximise the pumping from the PW and minimise the pumping from the BW, maintaining the maximum allowable salt concentration. The machine learning surrogate ensembles and S-O models were developed to tackle the multi-objective simulation-optimisation problem. However, the main aim of this study is to develop a digital twin (DT) of Tagabe coastal aquifer. Hence, machine learning surrogate ensembles and S-O models need to be developed initially to develop the DT.

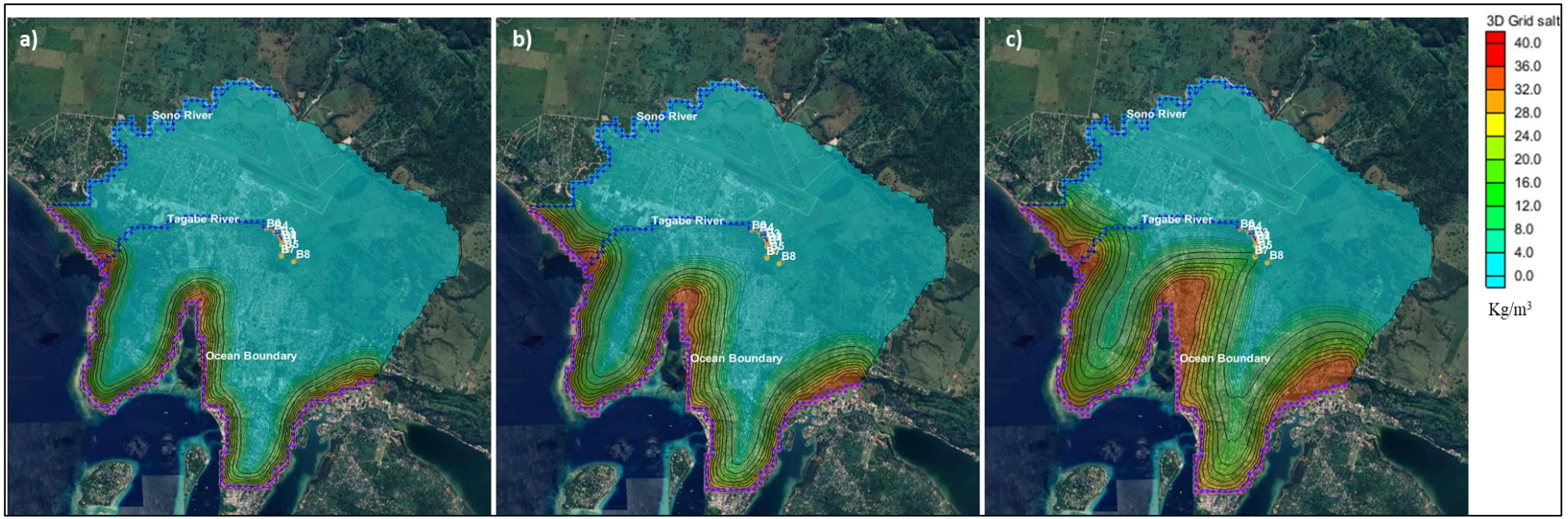



Figure 8.4: Numerical model simulated saltwater intrusion rates in Tagabe coastal aquifer with production bores (B1-B8): **a)** length of saltwater intrusion after 5 years of current pumping regimes in Tagabe; **b)** length of saltwater intrusion after 10 years of current pumping regimes in Tagabe; **c)** length of saltwater intrusion after 20 years of current pumping regimes in Tagabe.

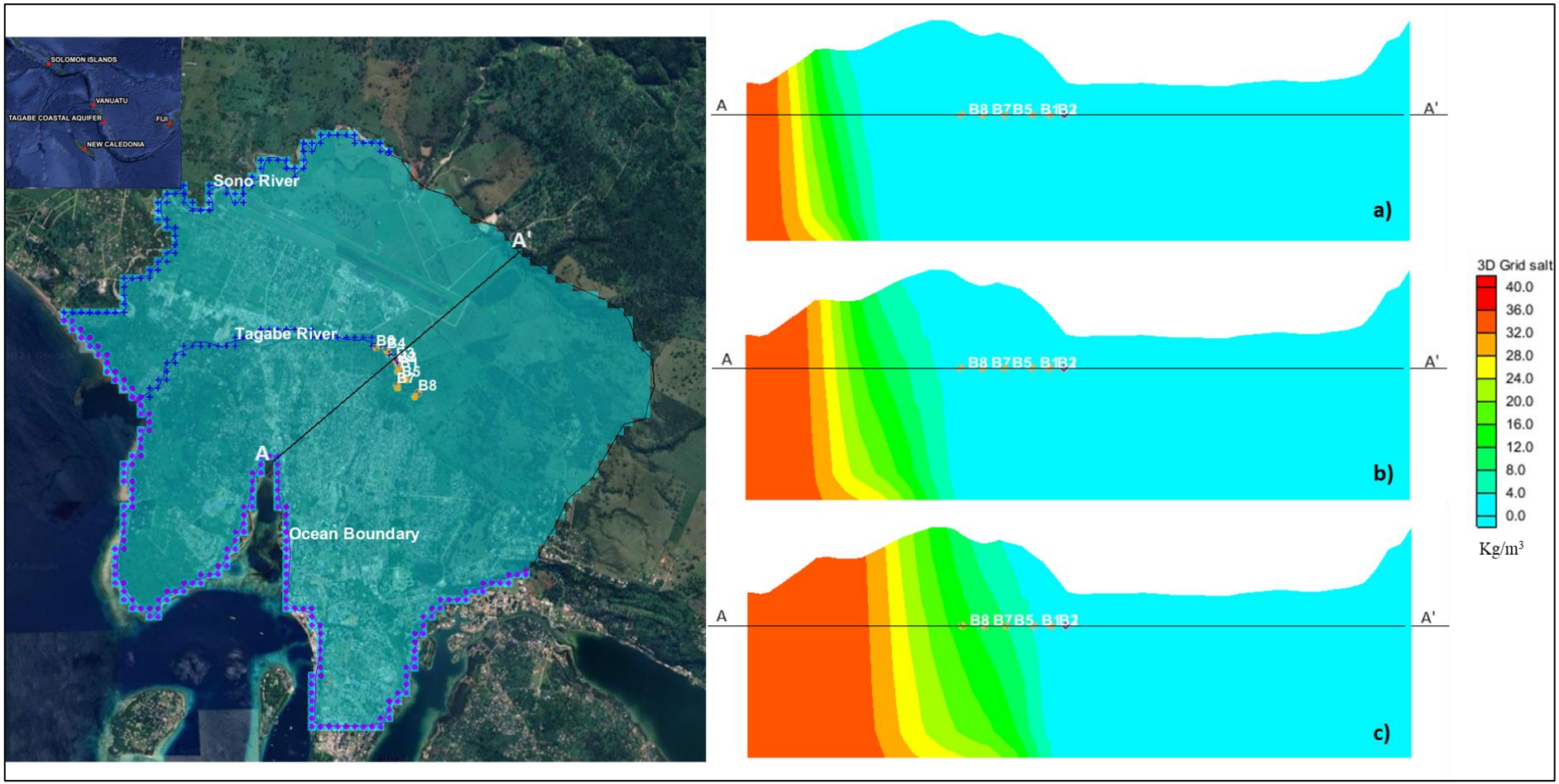



Figure 8.5: Side view cross-sections of salt concentration of layer 1 with production bores (B1-B8): **a)** length of saltwater intrusion after 5 years of current pumping rates in Tagabe; **b)** length of saltwater intrusion after 10 years of current pumping rates in Tagabe; **c)** length of saltwater intrusion after 20 years of current pumping rates in Tagabe.

### 8.5.2 Machine learning surrogate ensemble model

Twelve surrogate models were trained using the machine learning algorithms mentioned in Section 8.4.3. Figure 8.6 to Figure 8.9 illustrate the actual versus predicted results during the training phase. A limited dataset was chosen to enhance computational efficiency when running the numerical model. One of the innovative aspects of this study is the use of a limited number of input-output patterns. The results demonstrated that even with limited training data, the surrogates were able to predict salt concentrations with reasonable accuracy for all MLs, as shown in Figure 8.6 to Figure 8.9. The majority of the surrogate models performed exceptionally well during the model training stage, with few giving poor prediction results. The following surrogates did not perform well in the training stage: BiLSTM for ML1; ANN, BiLSTM and RF for ML2; ANN, BiLSTM, PLR and SVR for ML3; ANN, AMS_Bayesian, BiLSTM, PLR and SVR for ML4. These surrogates did not do well in predicting the salt concentrations at various MLs. However, to further investigate and find the accuracy of model prediction, different performance measures were employed, as outlined in Section 8.4.3.1.

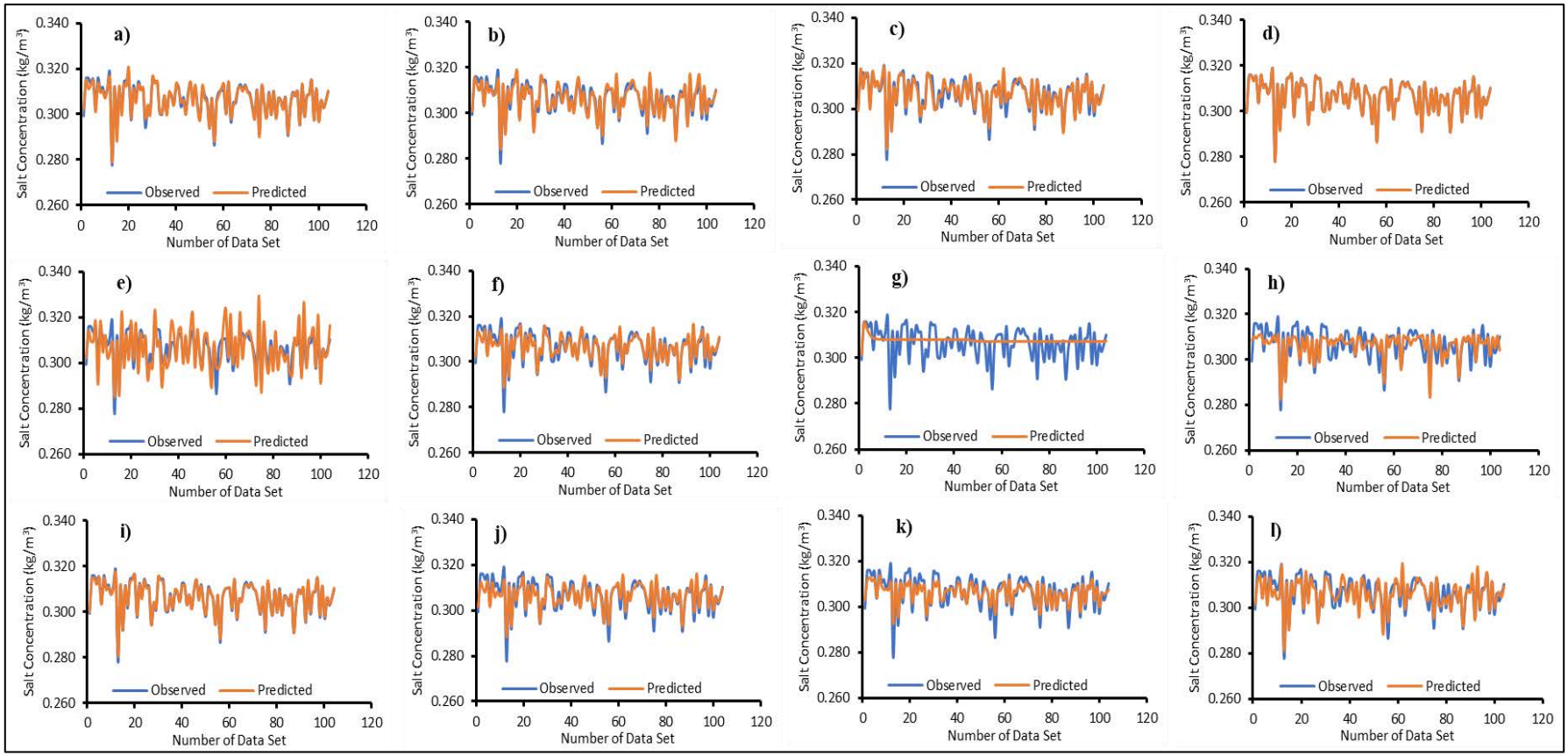



Figure 8.6: Actual versus predicted salt concentrations of monitoring location 1 (ML1) using different machine learning algorithms during training period; **a)** – Adaptive Neuro Fuzzy Inference System (ANFIS), **b)** – Artificial Neural Network (ANN), **c)** – Multivariate Adaptive Regression Spline with Piecewise Cubic Spline (MARS_C), **d)** – Multivariate Adaptive Regression Spline with Piecewise Linear Spline (MARS_L), **e)** – Bayesian Optimization tuned Automatic Model Selection (AMS_Bayesian), **f)** – Asynchronous Successive Halving Algorithm tuned Automatic Model Selection (AMS_ASHA), **g)** – Bi-directional Long Short term Memory Network (Bi-LSTM), **h)** – Group Method of Data Handling (GMDH), **i)** – Gaussian Process Regression (GPR), **j)** – Probabilistic Linear Regression (PLR), **k)** – Random Forest (RF) and **l)** – Support Vector Regression (SVR).

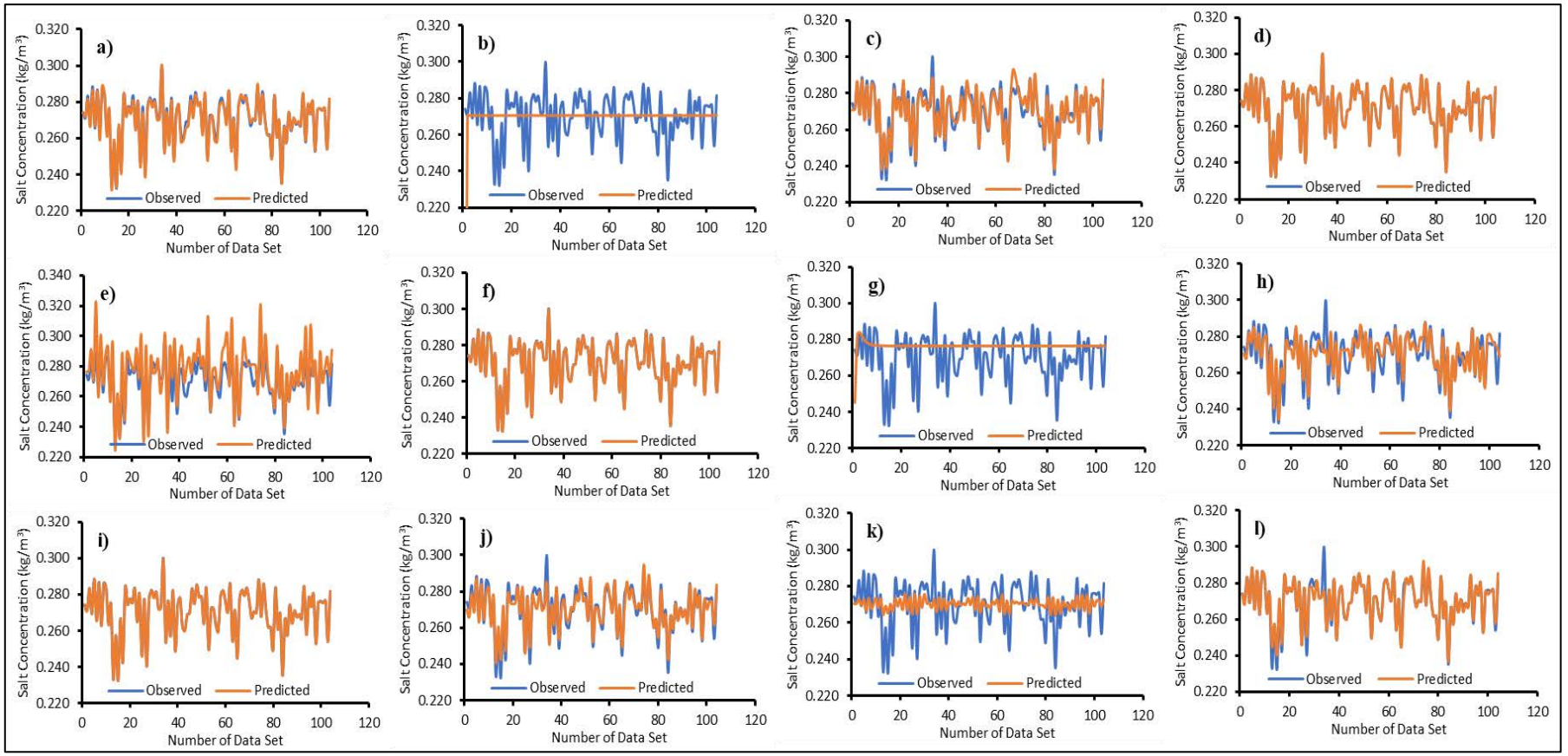



Figure 8.7: Actual versus predicted salt concentrations of monitoring location 2 (ML2) using different machine learning algorithms during training period; **a)** – Adaptive Neuro Fuzzy Inference System (ANFIS), **b)** – Artificial Neural Network (ANN), **c)** – Multivariate Adaptive Regression Spline with Piecewise Cubic Spline (MARS_C), **d)** – Multivariate Adaptive Regression Spline with Piecewise Linear Spline (MARS_L), **e)** – Bayesian Optimization tuned Automatic Model Selection (AMS_Bayesian), **f)** – Asynchronous Successive Halving Algorithm tuned Automatic Model Selection (AMS_ASHA), **g)** – Bi-directional Long Short term Memory Network (Bi-LSTM), **h)** – Group Method of Data Handling (GMDH), **i)** – Gaussian Process Regression (GPR), **j)** – Probabilistic Linear Regression (PLR), **k)** – Random Forest (RF) and **l)** – Support Vector Regression (SVR).

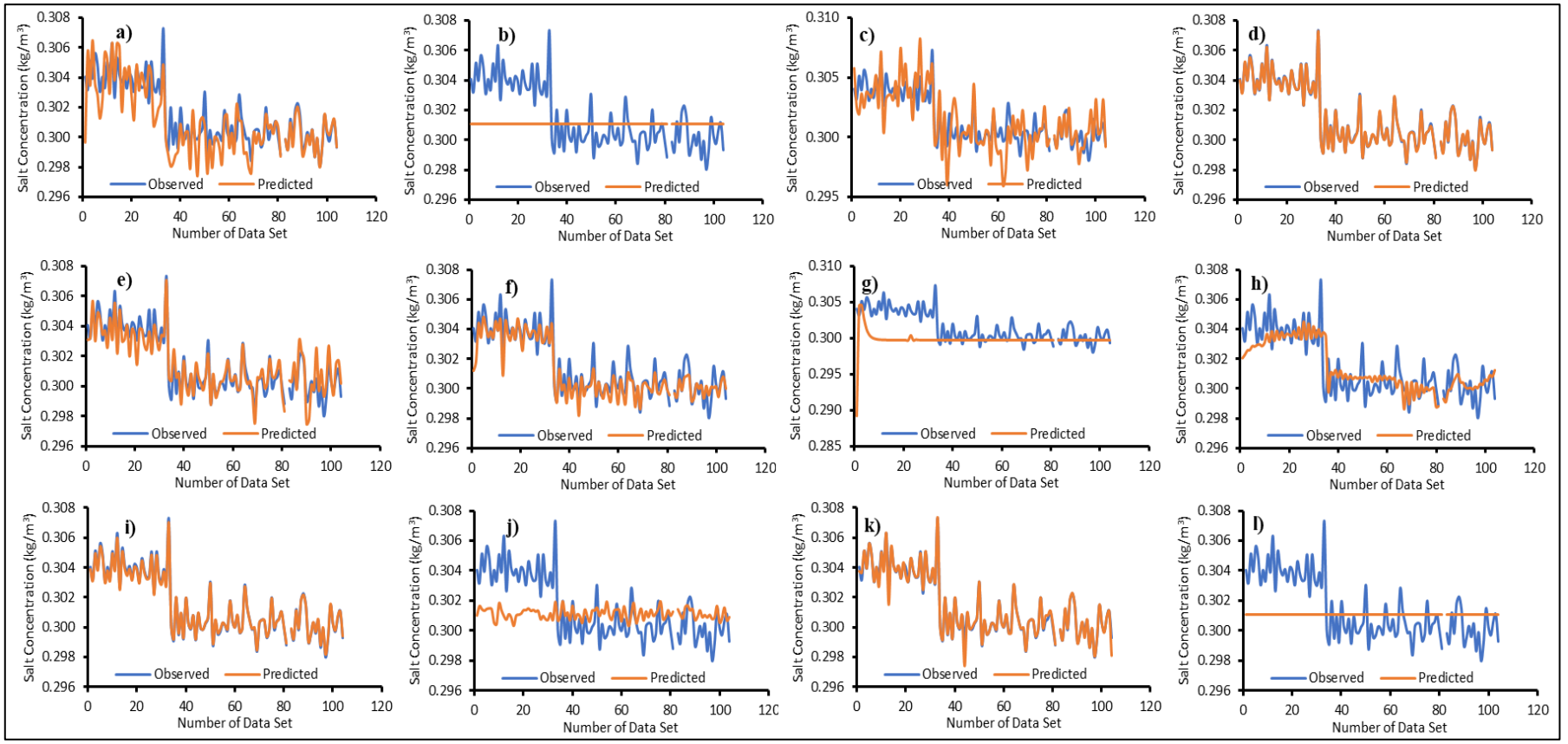



Figure 8.8: Actual versus predicted salt concentrations of monitoring location 3 (ML3) using different machine learning algorithms during training period; **a)** – Adaptive Neuro Fuzzy Inference System (ANFIS), **b)** – Artificial Neural Network (ANN), **c)** – Multivariate Adaptive Regression Spline with Piecewise Cubic Spline (MARS_C), **d)** – Multivariate Adaptive Regression Spline with Piecewise Linear Spline (MARS_L), **e)** – Bayesian Optimization tuned Automatic Model Selection (AMS_Bayesian), **f)** – Asynchronous Successive Halving Algorithm tuned Automatic Model Selection (AMS_ASHA), **g)** – Bi-directional Long Short term Memory Network (Bi-LSTM), **h)** – Group Method of Data Handling (GMDH), **i)** – Gaussian Process Regression (GPR), **j)** – Probabilistic Linear Regression (PLR), **k)** – Random Forest (RF) and **l)** – Support Vector Regression (SVR).

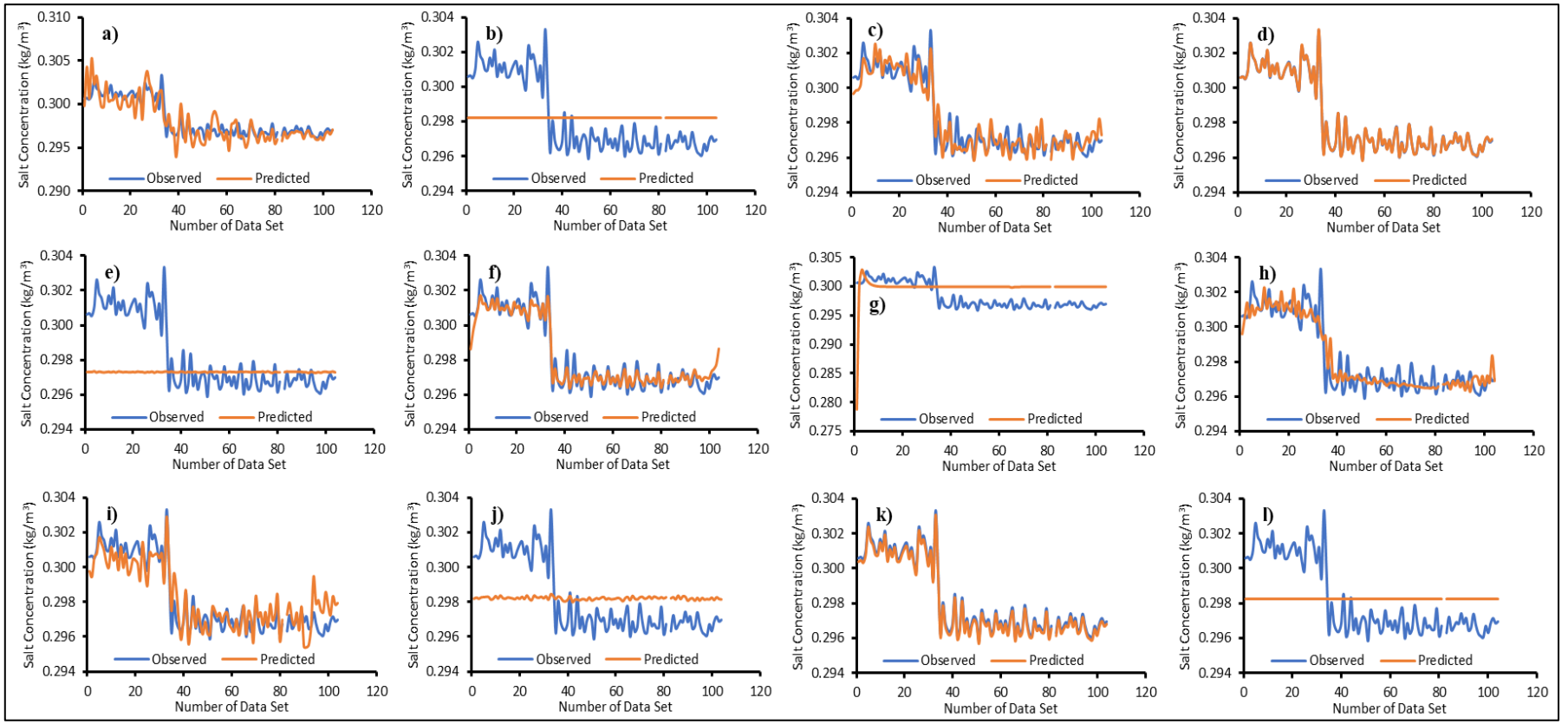



Figure 8.9: Actual versus predicted salt concentrations of monitoring location 4 (ML4) using different machine learning algorithms during training period; **a)** – Adaptive Neuro Fuzzy Inference System (ANFIS), **b)** – Artificial Neural Network (ANN), **c)** – Multivariate Adaptive Regression Spline with Piecewise Cubic Spline (MARS_C), **d)** – Multivariate Adaptive Regression Spline with Piecewise Linear Spline (MARS_L), **e)** – Bayesian Optimization tuned Automatic Model Selection (AMS_Bayesian), **f)** – Asynchronous Successive Halving Algorithm tuned Automatic Model Selection (AMS_ASHA), **g)** – Bi-directional Long Short term Memory Network (Bi-LSTM), **h)** – Group Method of Data Handling (GMDH), **i)** – Gaussian Process Regression (GPR), **j)** – Probabilistic Linear Regression (PLR), **k)** – Random Forest (RF) and **l)** – Support Vector Regression (SVR).

#### *8.5.2.1 Model Performance*

The criteria used to assess the performance of the surrogate models for various monitoring locations during the training stage are detailed Table 8.2 and Figure 8.10d-f. These performance metrics focus on the training phase, where the predicted salt concentration values from the different ML models described in Section 8.4.2 were compared with the actual measurements. Similar techniques were used and results were reported by Roy et al. (2020) and Roy et al. (2024). Most models showed improved accuracy in predicting salt concentrations during the training phase. When examining the Mean Absolute Percentage Error (MAPE), Pearson's coefficient, Index of Agreement, Kling-Gupta efficiency, and Nash Sutcliffe efficiency, it is evident that ANFIS, ANN, MARS_C, MARS_L, AMS_ASHA, GMDH, RF, GPR, and SVR excelled in predicting salt concentrations at ML1 during the training stage. Similarly, ANFIS, MARS_C, MARS_L, AMS_ASHA, GPR, PLR, and SVR were more effective at predicting salt concentrations at ML2. At ML3, ANFIS, MARS_C, MARS_L, AMS_Bayesian, GPR, and RF outperformed others in the training stage predictions. Lastly, at ML4, MARS_C, MARS_L, AMS_ASHA, GMDH, and RF demonstrated superior performance during training in predicting salt concentrations.

Table 8.3 and Figure 8.10a-c highlights the performance of twelve surrogate models across various MLs during the testing phase. The actual and predicted salt concentrations were compared using metrics such as MAPE (%), Pearson's correlation coefficient, Index of Agreement, Kling-Gupthighlightsa efficiency, and Nash-Sutcliffe efficiency. At ML1, the models ANN, AMS_Bayesian, and PLR demonstrated superior predictive accuracy. For ML2, the models ANFIS, MARS_C, MARS_L, AMS_Bayesian, AMS_ASHA, GHD, and SVR consistently produced more accurate predictions. At ML3, AMS_Bayesian and ANN were the most reliable, with a strong performance from ANFIS, AMS_ASHA, and SVR.

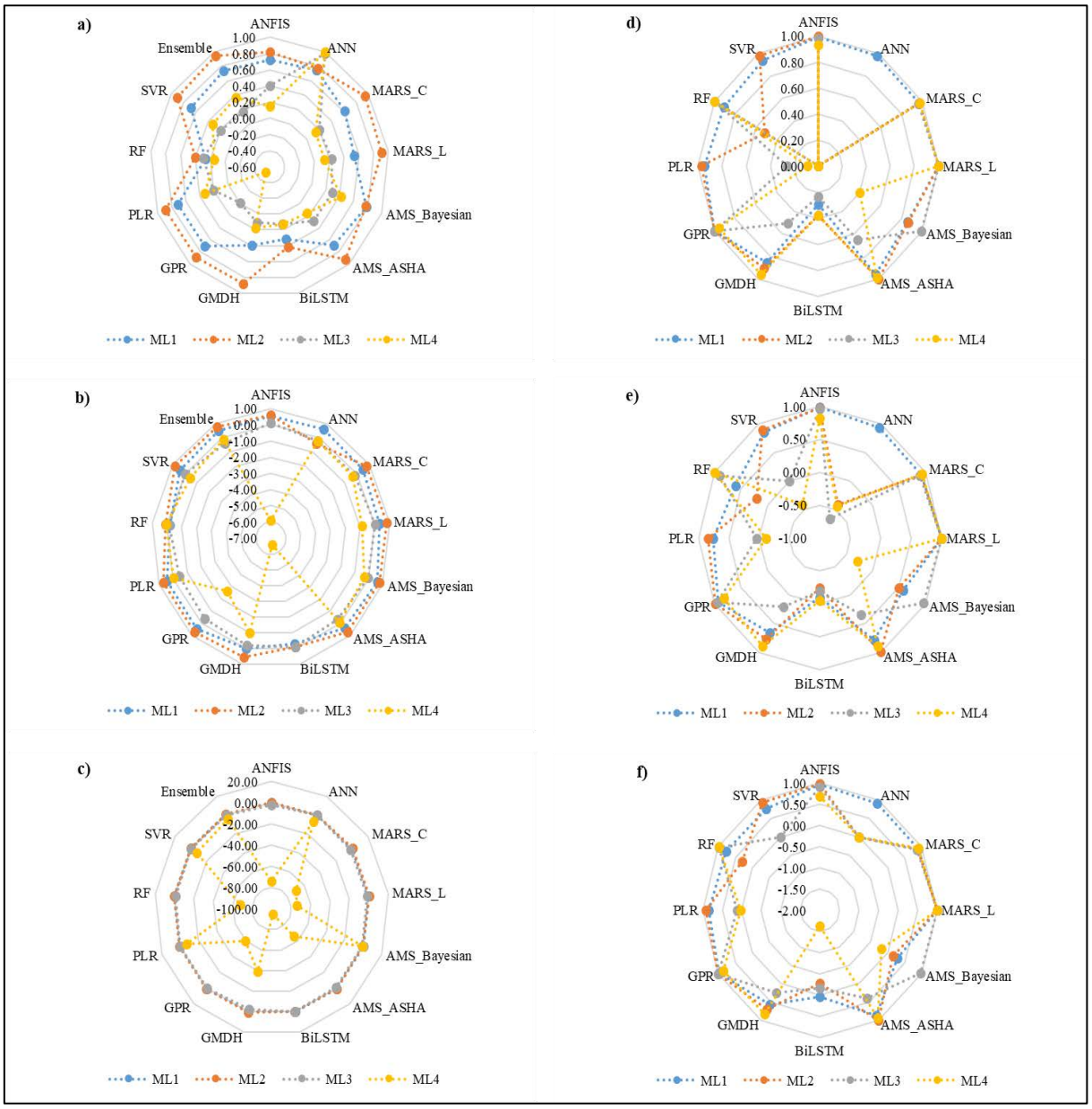



Figure 8.10: Spider plots of three major performance measures of twelve surrogate models for different monitoring locations: **a)** Index of Agreement values for twelve surrogate models during the testing period; **b)** Kling-Gupta Efficiency Coefficient values for twelve surrogate models during the testing period; **c)** Nash Sutcliffe Efficiency Coefficient values for twelve surrogate models during the testing period; **d)** Index of Agreement values for twelve surrogate models during the training period; **e)** Kling-Gupta Efficiency Coefficient values for twelve surrogate models during the training period; **f)** Nash Sutcliffe Efficiency Coefficient values for twelve surrogate models during the training period.

Table 8.2: Performance criteria of twelve surrogate models at four different monitoring locations (MLs) during the model training period. Source (Sharan et al., 2024b).

| | Performance Measure | ANFIS | ANN | MARS_C | MARS_L | AMS_Bayesian | AMS_ASHA | BiLSTM | GMDH | GPR | PLR | RF | SVR |
|---|---|---|---|---|---|---|---|---|---|---|---|---|---|
| **ML1** | Mean Absolute Deviation (MAD) | 0.0009293 | 0.0017723 | 0.0017369 | 0.0000927 | 0.0048193 | 0.0020226 | 0.0052974 | 0.0038625 | 0.0005386 | 0.0021990 | 0.0025491 | 0.0028542 |
| | Mean Square Error (MSE) | 0.0000017 | 0.0000045 | 0.0000052 | 0.0000000 | 0.0000373 | 0.0000067 | 0.0000495 | 0.0000223 | 0.0000005 | 0.0000078 | 0.0000117 | 0.0000118 |
| | RMSE | 0.0012968 | 0.0021187 | 0.0022825 | 0.0001138 | 0.0061111 | 0.0025953 | 0.0070324 | 0.0047200 | 0.0006848 | 0.0027999 | 0.0034223 | 0.0034335 |
| | MAPE (%) | 0.303 | 0.580 | 0.568 | 0.030 | 1.570 | 0.663 | 1.754 | 1.263 | 0.176 | 0.720 | 0.837 | 0.932 |
| **ML2** | Mean Absolute Deviation (MAD) | 0.001235 | 0.010136 | 0.003231 | 0.000171 | 0.009189 | 0.000074 | 0.010648 | 0.005414 | 0.000100 | 0.002983 | 0.008319 | 0.001147 |
| | Mean Square Error (MSE) | 0.000003 | 0.000168 | 0.000017 | 0.000000 | 0.000141 | 0.000000 | 0.000214 | 0.000050 | 0.000000 | 0.000015 | 0.000117 | 0.000011 |
| | RMSE | 0.001600 | 0.012966 | 0.004155 | 0.000212 | 0.011885 | 0.000101 | 0.014639 | 0.007071 | 0.000128 | 0.003913 | 0.010814 | 0.003376 |
| | MAPE (%) | 0.459 | 3.840 | 1.197 | 0.063 | 3.371 | 0.027 | 4.102 | 2.020 | 0.037 | 1.114 | 3.142 | 0.433 |
| **ML3** | Mean Absolute Deviation (MAD) | 0.0009339 | 0.0020962 | 0.0012951 | 0.0000495 | 0.0005557 | 0.0008921 | 0.0023394 | 0.0013296 | 0.0001112 | 0.0020018 | 0.0001535 | 0.0020977 |
| | Mean Square Error (MSE) | 0.0000017 | 0.0000198 | 0.0000028 | 0.0000000 | 0.0000005 | 0.0000121 | 0.0000230 | 0.0000150 | 0.0000001 | 0.0000173 | 0.0000003 | 0.0000198 |
| | RMSE | 0.0012984 | 0.0044534 | 0.0016758 | 0.0000625 | 0.0007043 | 0.0034716 | 0.0047910 | 0.0038725 | 0.0002292 | 0.0041651 | 0.0005843 | 0.0044534 |
| | MAPE (%) | 0.309 | 0.714 | 0.433 | 0.016 | 0.185 | 0.313 | 0.791 | 0.459 | 0.038 | 0.681 | 0.054 | 0.714 |
| **ML4** | Mean Absolute Deviation (MAD) | 0.0008730 | 0.0018996 | 0.0004841 | 0.0000299 | 0.0016707 | 0.0003444 | 0.0026600 | 0.0006084 | 0.0006741 | 0.0018773 | 0.0001878 | 0.0019016 |
| | Mean Square Error (MSE) | 0.0000013 | 0.0000045 | 0.0000004 | 0.0000000 | 0.0000053 | 0.0000002 | 0.0000117 | 0.0000007 | 0.0000007 | 0.0000043 | 0.0000000 | 0.0000045 |
| | RMSE | 0.0011613 | 0.0021146 | 0.0006191 | 0.0000366 | 0.0023100 | 0.0004946 | 0.0034221 | 0.0008436 | 0.0008286 | 0.0020803 | 0.0001883 | 0.0021146 |
| | MAPE (%) | 0.292 | 0.636 | 0.162 | 0.010 | 0.557 | 0.115 | 0.893 | 0.204 | 0.226 | 0.628 | 0.063 | 0.636 |

Table 8.3: Performance criteria of twelve surrogate models and four ensemble models at four different monitoring locations (MLs) during the model testing period. Source (Sharan et al., 2024b).

| | Performance Measure | ANFIS | ANN | MARS_C | MARS_L | AMS_Bayesian | AMS_ASHA | BiLSTM | GMDH | GPR | PLR | RF | SVR | Ensemble |
|---|---|---|---|---|---|---|---|---|---|---|---|---|---|---|
| **ML1** | Mean Absolute Deviation (MAD) | 0.008200 | 0.006349 | 0.007465 | 0.008784 | 0.006097 | 0.005403 | 0.006612 | 0.006838 | 0.005481 | 0.005194 | 0.006468 | 0.005891 | 0.005640 |
| | Mean Square Error (MSE) | 0.000106 | 0.000072 | 0.000111 | 0.000149 | 0.000060 | 0.000068 | 0.000121 | 0.000112 | 0.000066 | 0.000062 | 0.000106 | 0.000074 | 0.000064 |
| | RMSE | 0.010318 | 0.008478 | 0.010540 | 0.012212 | 0.007752 | 0.008220 | 0.011006 | 0.010560 | 0.008094 | 0.007874 | 0.010290 | 0.008610 | 0.007997 |
| | MAPE (%) | 2.718 | 2.072 | 2.528 | 2.965 | 2.045 | 1.839 | 2.270 | 2.333 | 1.861 | 1.767 | 2.210 | 1.998 | 1.909 |
| **ML2** | Mean Absolute Deviation (MAD) | 0.01127 | 0.01195 | 0.00480 | 0.00693 | 0.01124 | 0.00513 | 0.01089 | 0.00620 | 0.00629 | 0.00611 | 0.01070 | 0.00590 | 0.00383 |
| | Mean Square Error (MSE) | 0.00016 | 0.00020 | 0.00003 | 0.00007 | 0.00019 | 0.00005 | 0.00026 | 0.00006 | 0.00007 | 0.00006 | 0.00016 | 0.00006 | 0.00003 |
| | RMSE | 0.01282 | 0.01408 | 0.00570 | 0.00819 | 0.01364 | 0.00682 | 0.01603 | 0.00770 | 0.00815 | 0.00783 | 0.01251 | 0.00767 | 0.00548 |
| | MAPE (%) | 4.169 | 4.465 | 1.808 | 2.569 | 4.232 | 1.945 | 4.245 | 2.345 | 2.396 | 2.330 | 4.036 | 2.237 | 1.469 |
| **ML3** | Mean Absolute Deviation (MAD) | 0.006016 | 0.001744 | 0.004818 | 0.005643 | 0.003692 | 0.003950 | 0.002270 | 0.005475 | 0.002075 | 0.001717 | 0.003989 | 0.001750 | 0.001563 |
| | Mean Square Error (MSE) | 0.000052 | 0.000021 | 0.000053 | 0.000055 | 0.000034 | 0.000035 | 0.000025 | 0.000071 | 0.000024 | 0.000022 | 0.000038 | 0.000021 | 0.000021 |
| | RMSE | 0.007226 | 0.004616 | 0.007253 | 0.007393 | 0.005832 | 0.005922 | 0.005031 | 0.008440 | 0.004896 | 0.004698 | 0.006124 | 0.004620 | 0.004545 |
| | MAPE (%) | 2.019 | 0.585 | 1.632 | 1.904 | 1.254 | 1.341 | 0.777 | 1.849 | 0.716 | 0.596 | 1.354 | 0.606 | 0.544 |
| **ML4** | Mean Absolute Deviation (MAD) | 0.0032556 | 0.0013282 | 0.0040002 | 0.0040240 | 0.0005095 | 0.0039669 | 0.0038250 | 0.0027744 | 0.0031787 | 0.0013349 | 0.0040280 | 0.0013341 | 0.0010268 |
| | Mean Square Error (MSE) | 0.0000180 | 0.0000020 | 0.0000171 | 0.0000180 | 0.0000004 | 0.0000160 | 0.0000231 | 0.0000096 | 0.0000147 | 0.0000020 | 0.0000166 | 0.0000020 | 0.0000012 |
| | RMSE | 0.0042461 | 0.0014021 | 0.0041331 | 0.0042417 | 0.0006236 | 0.0039962 | 0.0048019 | 0.0030969 | 0.0038287 | 0.0014056 | 0.0040709 | 0.0014080 | 0.0011007 |
| | MAPE (%) | 1.096 | 0.445 | 1.348 | 1.356 | 0.172 | 1.336 | 1.289 | 0.935 | 1.071 | 0.450 | 1.357 | 0.450 | 0.346 |

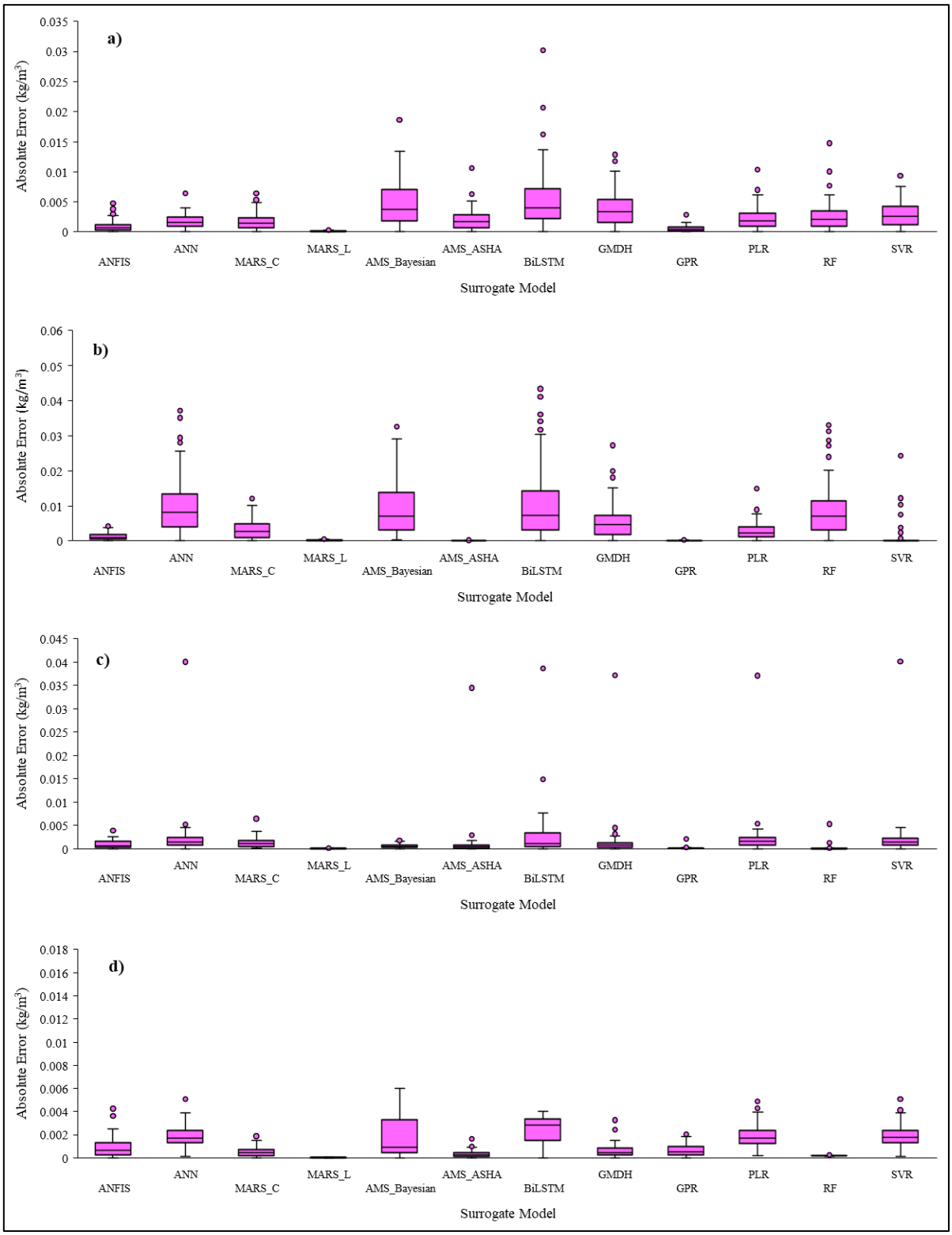



Figure 8.11: Boxplots of absolute errors between actual and predicted salt concentration during the training stage at **a)** ML1, **b)** ML2, **c)** ML3, and **d)** ML4 using all twelve surrogate models. Pink dots indicate outliers.

The boxplots of absolute error between the observed and computed values for all MLs during the surrogate model training are given in Figure 8.11. The absolute error close to zero indicates a better-performing model.

Different MLs had different surrogate models that outperformed amongst each other. Hence, to further narrow it down and choose the best performing models, Shannon's Entropy weights (EW) were used to rank the model (Sharan et al., 2024b). EW method was applied to identify the best-performing surrogate model based on their assigned weights (Sharan et al., 2024b). A higher EW for a performance metric signifies a stronger influence on determining the weight of individual models. In other words, larger EW values indicate that the corresponding performance metric plays a more significant role in the decision-making process. The EWs for each prediction model were calculated to rank their effectiveness in predicting salt concentrations across four MLs. The ranking of the models was determined entirely by their EWs, as presented in Table 8.4.

Table 8.4: Entropy weight of the individual prediction models. Source (Sharan et al., 2024b).

| Standalone models | ML1 | | ML2 | | ML3 | | ML4 | |
|---|---|---|---|---|---|---|---|---|
| | EW | Rank | EW | Rank | EW | Rank | EW | Rank |
| ANFIS | 0.745 | 7 | 0.605 | 9 | 0.425 | 9 | 0.191 | 7 |
| ANN | 0.918 | 1 | 0.436 | 11 | 0.915 | 1 | 0.598 | 2 |
| MARS_C | 0.697 | 8 | 0.994 | 1 | 0.423 | 10 | 0.151 | 10 |
| MARS_L | 0.572 | 9 | 0.820 | 5 | 0.300 | 12 | 0.125 | 11 |
| AMS_Bayesian | 0.912 | 2 | 0.639 | 8 | 0.444 | 7 | 0.806 | 1 |
| AMS_ASHA | 0.877 | 5 | 0.926 | 2 | 0.505 | 6 | 0.201 | 6 |
| Bi-LSTM | 0.533 | 11 | 0.315 | 12 | 0.542 | 5 | 0.093 | 12 |
| GMDH | 0.508 | 12 | 0.815 | 7 | 0.351 | 11 | 0.172 | 8 |
| GPR | 0.891 | 4 | 0.817 | 6 | 0.673 | 4 | 0.238 | 5 |
| PLR | 0.904 | 3 | 0.833 | 4 | 0.822 | 3 | 0.525 | 3 |
| RF | 0.549 | 10 | 0.446 | 10 | 0.442 | 8 | 0.152 | 9 |
| SVR | 0.816 | 6 | 0.865 | 3 | 0.840 | 2 | 0.341 | 4 |

EW = Entropy Weight, ANFIS = Adaptive Neuro Fuzzy Inference System, ANN = Artificial Neural Network, MARS_C = Multivariate Adaptive Regression Spline with Piecewise Cubic Spline, MARS_L = Multivariate Adaptive Regression Spline with Piecewise Linear Spline, AMS_Bayesian = Bayesian Optimization tuned Automatic Model Selection, AMS_ASHA = Asynchronous Successive Halving Algorithm tuned Automatic Model Selection, Bi-LSTM = Bi-directional Long Short term Memory Network, GMDH = Group Method of Data Handling, GPR = Gaussian Process Regression, PLR = Probabilistic Linear Regression, SVR = Support Vector Regression.

The top 5 ranked surrogate models (Table 8.4) were used to form surrogate ensemble models for each ML. The prediction results of surrogate ensemble models are

shown in Figure 8.12. The performance of each ensemble is also shown in Table 8.3. The ensemble outperforms standalone surrogates. The surrogate ensemble for ML4 (Figure 8.12d) did not predict the variations as shown by other surrogate ensembles for MLs 1-3. However, the results of all surrogate ensemble models performed better than the standalone surrogate models.

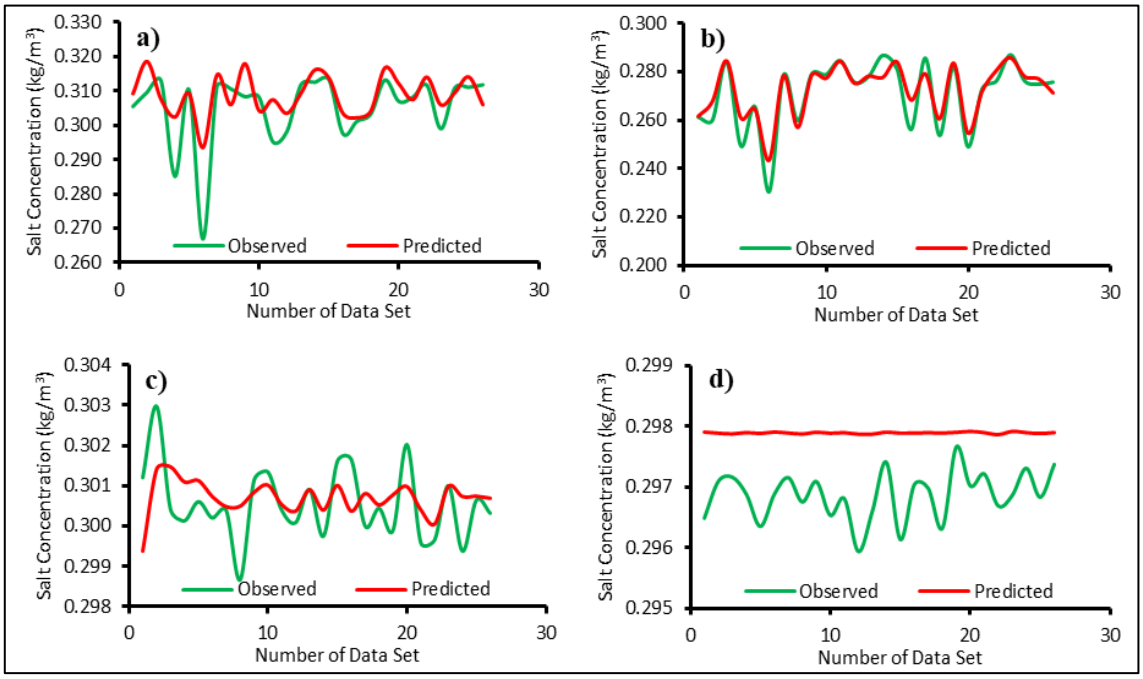



Figure 8.12: Observed versus predicted salt concentrations using surrogate ensemble models at **a)** ML1, **b)** ML2, **c)** ML3 and **d)** ML4.

### 8.5.3 Digital Twin

The four surrogate ensembles for each ML were linked with MOGA to develop a multi-objective saltwater intrusion management model (simulation-optimisation model; S-O) for the Tagabe coastal aquifer. The management model aimed to balance two conflicting objectives: maximising production well pumping while minimising barrier well pumping. The optimisation process was constrained by the requirement to maintain salt concentrations below a specified maximum (0.5 kg/m$^3$) at various MLs. Multiple simulations were conducted using different combinations of parameters, with the optimal values applied to the optimisation framework. The results from the S-O model were used to make informed decisions in managing the freshwater pumping rates at Tagabe coastal aquifer. The 3D numerical simulation model results, surrogate ensemble model results, and S-O model results were used as a DT for Tagabe coastal aquifer. The DT working

framework is given in Figure 8.3. The scenarios tested under DT are given in Section 8.4.5. The different illustrative field sensors triggered and fed the data to the S-O model were simulated.

Initially, a S-O model was developed based on a maximum allowable salt concentration of 0.5 kg/$m^3$ (Sharan et al., 2024b). In this chapter for scenario 1, the sensors triggered and sent the data indicating that the maximum salt concentration was decreased from 0.5 kg/$m^3$ to 0.45 kg/$m^3$. Hence, optimal pumping rates need to be simulated based on the new concentration data received by the DT. The population size of 2000 executed 16000 generations to achieve the Pareto optimal solutions. The crossover and mutation rates were set at 0.92 and 0.1, respectively. The migration parameter was set to move in a forward direction with a fraction of 0.2 and an interval of 20. A population fraction of 0.7 was applied to the Pareto front, yielding 1400 non-dominated optimal solutions out of 2000 individuals (2000 × 0.7). Both the function and constraint tolerances were established at $1 \times 10^{-4}$. The optimisation process required 7286 seconds to reach convergence and simulate the optimal solutions. The Pareto optimal generated for scenario 1 is given in Figure 8.13a. The maximum pumping from all bores in Tagabe aquifer with a maximum salt concentration of 0.45 kg/$m^3$ is predicted as 11500 $m^3$/d with 219 $m^3$/d extraction from the barrier well. Increasing the pumping from production wells will also increase the pumping from barrier wells, as shown in Figure 8.13a.

Similarly, the Pareto optimal fronts for scenarios 2-5 were generated using the same method and optimisation algorithm as used for scenario 1. However, the maximum allowable salt concentrations varied as triggered by the illustrative sensors from the field. The Pareto optimal fronts for scenarios 2-4 are shown in Figure 8.13b-e, respectively. The optimisation time taken to generate the Pareto optimal fronts for scenarios 2-5 was 11353 s, 16532 s, 16577 s and 18655 s, respectively. Increasing the allowable salt concentration took more time than the lower concentration constraint. The maximum production well pumping for scenarios 2-5 are 15107 $m^3$/d, 17317 $m^3$/d, 10044 $m^3$/d and 15155 $m^3$/d, respectively. Similarly, based on these maximum production well pumping, the barrier well pumping for scenarios 2-5 are 280 $m^3$/d, 202 $m^3$/d, 293 $m^3$/d and 269 $m^3$/d, respectively.

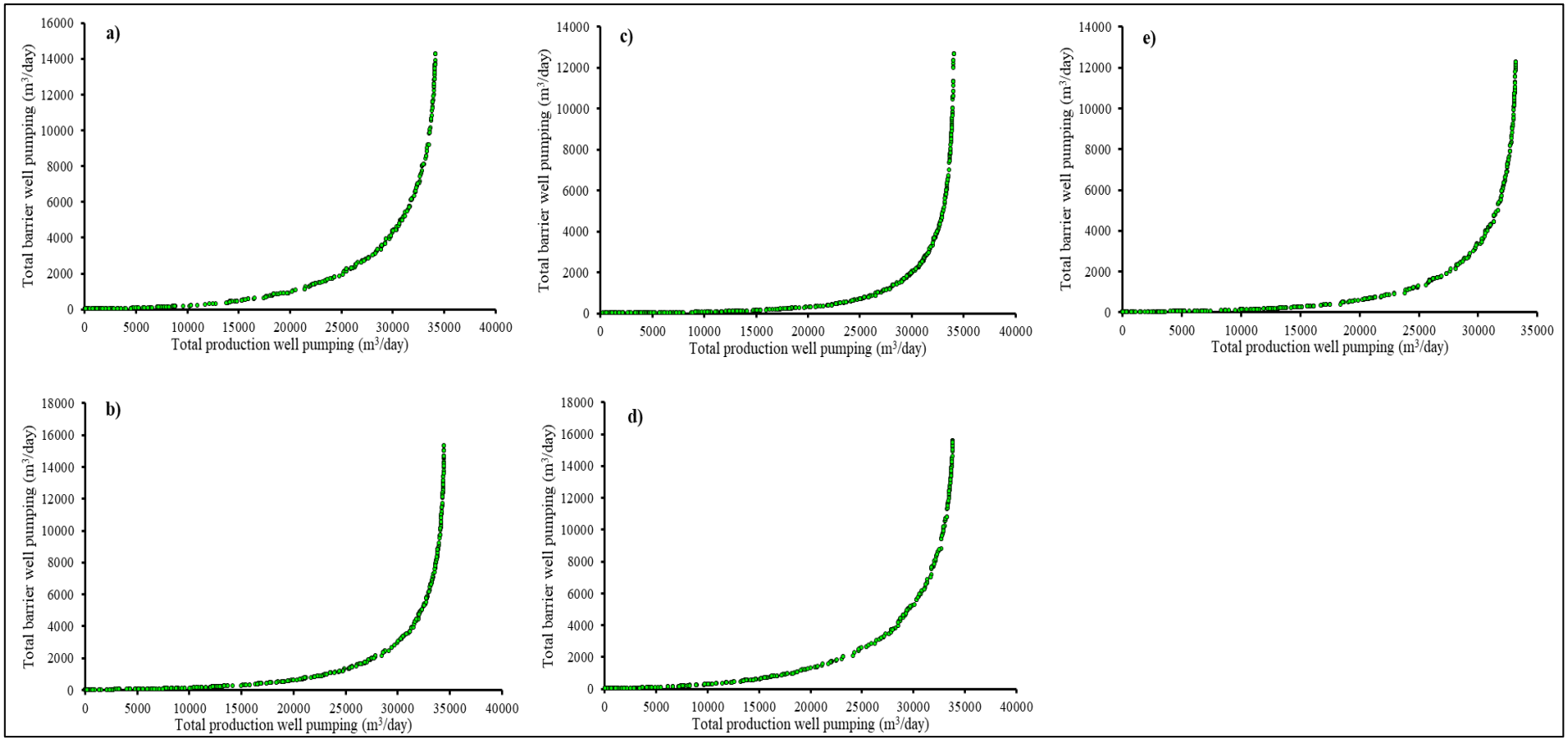



Figure 8.13: Pareto optimal fronts of the linked simulation-optimisation management models based on different scenarios for digital twin models. **a)** Scenario 1 with a maximum allowable salt concentration of 0.45 kg/m3, **b)** Scenario 2 with a maximum allowable salt concentration of 0.55 kg/m3, **c)** Scenario 3 with a maximum allowable salt concentration of 0.75 kg/m3, **d)** Scenario 4 with a maximum allowable salt concentration of 0.90 kg/m3, **e)** Scenario 5 with a maximum allowable salt concentration of 1.15 kg/m3.

Roy and Datta (2017a; 2017b) and Lal and Datta (2018) used a similar approach to simulate the Pareto optimal fronts. However, they compared a small number of surrogate models (fewer than five) and created ensembles from them. In contrast, this study developed and compared a total of 12 surrogate models. The five top-performing models identified through Shannon's Entropy-based decision theory were then used to create a weighted-average ensemble model. Previous studies, such as those by Bhattacharjya and Datta (2005) and Hussain et al. (2015), applied a linked S-O technique but relied on single surrogate models combined with optimisation algorithms. By incorporating multiple surrogates into an ensemble, this study reduced the uncertainty in predicting salt concentrations. The ensembles developed here outperformed standalone surrogate models significantly. Moreover, this is the first time the multiple surrogate ensemble and S-O model have been used to develop a DT model for a coastal aquifer.

Pareto-optimal pumping values can be shared with groundwater users of Tagabe coastal aquifer through collaboration with the local government, water managers, and municipal offices. These optimal rates would be communicated via smart information boards powered by IoT installed near the nested bore networks. The boards would display recommended pumping rates for various scenarios. By integrating machine learning, smart sensors, DT, and smart information boards, this approach minimises the need for remote travel, reduces costs and time, and enhances the sustainable management of groundwater resources in the Tagabe aquifer and beyond.

### 8.5.4 Validation of Pareto optimal fronts

The performance of the surrogate-based saltwater intrusion management model was evaluated by examining its ability to meet the predefined constraints. The results demonstrated that the saltwater concentrations predicted by the optimisation model, which utilised surrogate models, consistently remained below the maximum permissible levels at all monitoring locations. This indicates that the model successfully adhered to the constraints without any violations throughout the optimisation process. Furthermore, the saltwater concentrations were found to be close to the specified limits, suggesting that the optimisation model effectively converged near the upper bounds of the constraints.

Table 8.5: Validation of Pareto optimal front solutions with the numerical simulation model for all five scenarios of the digital twin approach.

| Scenario | Solution Number | ML1 | | | ML2 | | | ML3 | | | ML4 | | |
|---|---|---|---|---|---|---|---|---|---|---|---|---|---|
| | | NSM ($kg/m^3$) | SEM ($kg/m^3$) | RE (%) | NSM ($kg/m^3$) | SEM ($kg/m^3$) | RE (%) | NSM ($kg/m^3$) | SEM ($kg/m^3$) | RE (%) | NSM ($kg/m^3$) | SEM ($kg/m^3$) | RE (%) |
| 1 | 1 | 0.297 | 0.320 | 7.858 | 0.296 | 0.283 | 4.340 | 0.296 | 0.295 | 0.479 | 0.296 | 0.325 | 9.710 |
| | 2 | 0.300 | 0.320 | 6.549 | 0.297 | 0.287 | 3.424 | 0.297 | 0.299 | 0.808 | 0.296 | 0.325 | 9.677 |
| | 3 | 0.301 | 0.320 | 6.364 | 0.297 | 0.288 | 3.110 | 0.297 | 0.300 | 0.970 | 0.296 | 0.325 | 9.642 |
| | 4 | 0.301 | 0.320 | 6.289 | 0.297 | 0.288 | 2.968 | 0.297 | 0.300 | 0.921 | 0.297 | 0.325 | 9.637 |
| | 5 | 0.301 | 0.320 | 6.250 | 0.297 | 0.288 | 2.876 | 0.297 | 0.300 | 0.944 | 0.297 | 0.325 | 9.627 |
| 2 | 1 | 0.297 | 0.326 | 9.630 | 0.296 | 0.283 | 4.244 | 0.296 | 0.300 | 1.078 | 0.296 | 0.315 | 6.322 |
| | 2 | 0.297 | 0.326 | 9.630 | 0.296 | 0.290 | 2.181 | 0.296 | 0.300 | 1.185 | 0.296 | 0.310 | 4.635 |
| | 3 | 0.299 | 0.326 | 9.042 | 0.297 | 0.287 | 3.231 | 0.297 | 0.300 | 1.020 | 0.296 | 0.320 | 7.999 |
| | 4 | 0.300 | 0.326 | 8.661 | 0.297 | 0.289 | 2.652 | 0.297 | 0.300 | 0.986 | 0.296 | 0.320 | 7.981 |
| | 5 | 0.299 | 0.326 | 8.893 | 0.297 | 0.288 | 3.015 | 0.297 | 0.300 | 1.023 | 0.296 | 0.320 | 8.010 |
| 3 | 1 | 0.301 | 0.330 | 9.737 | 0.297 | 0.287 | 3.415 | 0.297 | 0.300 | 1.051 | 0.296 | 0.326 | 9.958 |
| | 2 | 0.301 | 0.330 | 9.715 | 0.297 | 0.282 | 5.026 | 0.297 | 0.300 | 1.038 | 0.296 | 0.326 | 9.842 |
| | 3 | 0.300 | 0.330 | 9.820 | 0.297 | 0.289 | 2.839 | 0.297 | 0.300 | 1.076 | 0.296 | 0.325 | 9.736 |
| | 4 | 0.297 | 0.325 | 9.393 | 0.296 | 0.289 | 2.222 | 0.296 | 0.300 | 1.313 | 0.296 | 0.325 | 9.702 |
| | 5 | 0.300 | 0.325 | 8.467 | 0.297 | 0.289 | 2.497 | 0.297 | 0.300 | 1.147 | 0.296 | 0.325 | 9.691 |
| 4 | 1 | 0.301 | 0.326 | 8.463 | 0.297 | 0.284 | 4.442 | 0.297 | 0.300 | 1.010 | 0.296 | 0.325 | 9.750 |
| | 2 | 0.299 | 0.325 | 8.756 | 0.297 | 0.281 | 5.207 | 0.297 | 0.300 | 0.996 | 0.296 | 0.325 | 9.779 |
| | 3 | 0.300 | 0.326 | 8.748 | 0.297 | 0.288 | 3.002 | 0.297 | 0.300 | 1.037 | 0.296 | 0.325 | 9.768 |
| | 4 | 0.297 | 0.324 | 9.223 | 0.296 | 0.287 | 3.215 | 0.296 | 0.300 | 1.208 | 0.296 | 0.325 | 9.797 |
| | 5 | 0.297 | 0.327 | 9.954 | 0.296 | 0.290 | 2.177 | 0.296 | 0.300 | 1.183 | 0.296 | 0.325 | 9.791 |
| 5 | 1 | 0.300 | 0.321 | 7.114 | 0.297 | 0.285 | 3.820 | 0.297 | 0.300 | 1.086 | 0.296 | 0.325 | 9.697 |
| | 2 | 0.297 | 0.322 | 8.331 | 0.296 | 0.282 | 4.754 | 0.296 | 0.300 | 1.177 | 0.296 | 0.325 | 9.700 |
| | 3 | 0.300 | 0.324 | 8.081 | 0.297 | 0.288 | 2.942 | 0.296 | 0.300 | 1.169 | 0.296 | 0.325 | 9.697 |
| | 4 | 0.297 | 0.326 | 9.897 | 0.297 | 0.284 | 4.470 | 0.296 | 0.300 | 1.150 | 0.296 | 0.325 | 9.678 |
| | 5 | 0.297 | 0.325 | 9.282 | 0.296 | 0.286 | 3.314 | 0.297 | 0.300 | 1.012 | 0.296 | 0.325 | 9.708 |

NSM – Numerical simulation model; SEM = surrogate ensemble model; RE = absolute relative error between the simulated and the predicted salt concentrations; ML = Monitoring location; C = Concentration

The Pareto fronts generated by the surrogate ensemble-CEMOGA optimisation models at each ML were verified and validated. To achieve this validation, five randomly selected production and barrier well pumping solutions were added as inputs into the 3D numerical model. The resulting salt concentrations from the numerical model were then compared with the salt concentrations predicted by the S-O model. The outcomes of this validation process are presented in Table 8.5. The relative error (RE) between the observed and computed ranges between 0.5 to 9.99%. The RE is less than 10%, indicating that optimal solutions converged for the upper limit of the constraints.

The results of this study align with those reported by Roy and Datta (2017b), who indicated that relative errors below 10% are suitable for devising an optimal management strategy using an integrated S-O approach. Therefore, it can be concluded that the machine learning-based surrogate ensemble model developed in this study could serve as an effective substitute for the complex nonlinear, density-dependent SEAWAT model in optimising groundwater management for the Tagabe coastal aquifer. Furthermore, this methodology could potentially be applied to other aquifers as well.

The current chapter used the methodology developed by Sharan et al. (2024b). Hence, some of the results overlap. The limitation of this study was the small dataset used to train the surrogate models with 130 input-output patterns. Hence, deep learning models did not perform well during the training and testing stages. Moreover, the illustrative sensors were used during the development of the digital twin for Tagabe coastal aquifer instead of real sensors. Getting government approvals from Vanuatu, the cost of buying the sensors, smart water quality meters, solar panels and other types of equipment needed to feed data from the field to the virtual space (virtual Tagabe aquifer) was not available. Hence, the digital twin was developed using illustrative data. In the future, with funding, the illustrative sensors and scenarios will be replaced with actual sensors and field data.

## 8.6 Summary and Conclusions

Saltwater intrusion (SWI) is a major environmental concern for coastal aquifers in Pacific Island countries, including Port Vila and Vanuatu. Based on current pumping regimes, sea level rise and anthropogenic activities, Tagabe coastal aquifer would have SWI as demonstrated by the 3D numerical model simulation model in this study. To manage SWI in Tagabe coastal aquifer, optimal pumping patterns were generated using machine learning-based surrogate ensemble models and simulation-optimisation

management model (S-O). The S-O model was later used to create the digital twin (DT) of Tagabe coastal aquifer.

The current study developed a digital twin (DT) framework for Tagabe coastal aquifer. The DT was developed using a 3D numerical simulation model, surrogate and ensemble models and S-O. The DT framework was designed and linked using the illustrative field data. Due to funding constraints and government approvals, the real field sensors were not placed in Tagabe coastal aquifer. Hence, illustrative sensors were used to generate five different scenarios. These illustrative sensors triggered and sent the data from the physical space (Tagabe aquifer) to the virtual space with changes in the salt concentration values at different MLs. Based on these illustrative data, the maximum allowable salt concentrations for scenarios 1 to 5 were 0.45, 0.55, 0.75, 0.90, and 1.15 kg/m3, respectively. Using these allowable salt concentrations and maximum and minimum pumping values, the simulation model (surrogate ensemble) was optimised using Controlled Elitist Multiple Objective Genetic Algorithm.

The S-O gave Pareto optimal fronts or solutions that could be used to maximise the pumping from the production wells and minimise the pumping from the barrier wells. Five sets of Pareto optimal fronts were generated for each constraint (different salt concentrations). Scenario 3 (concentration of 0.75 kg/m3) gave higher pumping (17,317 m3/d) from the production wells and lowest pumping (202 m3/d) from the barrier wells, compared with other scenarios. However, the selected compromise solutions or the Pareto frontier (knee of the curve) of generated optimal solutions kept on increasing as the maximum allowable salt concentrations increased. Hence, scenario 5 had the higher Pareto frontier or solutions of 31,676 and 5,000 m3/d pumping from production wells and barrier wells, respectively. The results from the S-O model were validated using randomly selected solutions from each scenario. The relative error was less than 10% when outputs from the numerical model were compared with the outputs from the S-O model.

To the best of the current knowledge, the application of DT in managing SWI has not been applied before. The results from the study indicated that DT works for a coastal aquifer in managing the SWI. The methodology developed and implemented in this study is of global significance and could be used to manage water resources wisely. The study demonstrated that the DT is vital in predicting future scenarios, changes in pumping patterns and other uncertainties. DT helped attain outcomes based on feedback

information from continuous monitoring with sensors with a smaller time interval (a month in this study). Overall, the study demonstrated that DT helps modify management strategies more efficiently and effectively based on field data transmitted back.

Using the DT of an aquifer offers a powerful tool for enhancing water resource management and sustainability. By creating a virtual replica of the aquifer, this technology allows for real-time monitoring, simulation, and analysis of the aquifer's behaviour under various conditions. This helps in understanding complex hydrological processes, predicting the impacts of human activities and climate change, and optimising water extraction and conservation strategies, as demonstrated by the results in this study. The DT can integrate data from sensors, historical records, and predictive models to provide actionable insights, leading to more informed decision-making and improved management of vital water resources.

The use of field smart sensors, smart water quality meters, smart information boards and other components of DT would be considered for future scope of work in Tagabe coastal aquifer, including other Pacific Island countries.

The next chapter summarises the overall thesis findings and provides recommendations, limitations and future scope of work.

# Chapter 9: Conclusions and Recommendations

## 9.1 Conclusions

Saltwater intrusion (SWI) is a significant threat to coastal aquifers for small Pacific Island countries (PICs). The major causes of SWI in PICs coatal aquifers are anthropogenic and natural factors. Hence, the main goal of this thesis was to develop more efficient, reliable, and robust mathematical, machine learning, simulation-optimisation, and digital twin models for managing SWI of Pacific Island coastal aquifers for the long-term sustainability of groundwater resources. This thesis also examined the anthropogenic factors and natural disasters affecting groundwater resources PICs.

To understand and validate how anthropogenic and natural factors affect groundwater resources in PICs, the climate change effects and freshwater over-abstraction on groundwater resources in Tonga have been analysed using climate and groundwater data. The findings reveal that increased groundwater pumping in Tongatapu has led to higher salinity levels over 42 years. In comparison, long-term rainfall and net recharge have declined over 61 years due to reduced rainfall and rising atmospheric heat from $CO_2$ emissions. Rising sea levels have also increased the SWI rates, contaminating coastal aquifers. $CO_2$ emissions have surged, threatening groundwater quality. To manage groundwater and make informed decisions, there is a need for 3D and AI-based (machine learning) models to understand SWI and provide critical insights for reducing abstraction rates, lowering carbon footprints, and addressing climate change, benefiting both Tonga and the global scientific community.

The SWI and climate change problem has been identified through a thorough literature review and quantitative data analysis for PICs. To develop a methodology that can effectively manage the SWI, a 3D numerical simulation model was developed for an illustrative study area in the context of the PICs aquifer system. Initially, an actual aquifer and pumping locations were treated as illustrative study areas because the hydraulic head and some pumping data were unavailable to calibrate and validate the model. However, some hydrogeological parameters and boundary conditions were from the field data. The multi-species solute and heat transport module, SEAWAT, was used to model the study area. Seven different scenarios and sensitivity analyses were modelled and tested using SEAWAT. The scenarios that provided the best SWI management strategies were using injection wells (IWs) to pump freshwater near the toe of the saltwater wedge, increasing

the recharge of the system, using barrier wells (BWs) and decreasing or increasing the hydraulic conductivities. The location of placing the BWs is essential, and it can be achieved by placing the wells within the model domain using the trial-and-error method and simulating the lowest salt concentrations at various monitoring locations and pumping wells. Furthermore, the sea level rise (SLR) by 0.3 to 1 m was also simulated to see the effect of the SWI rates, and the results indicated that the SLR by 0.3 to 1 m did not substantially impact SWI rates. However, SLR above 1 m would be an issue for coastal aquifers.

In addition, further modelling and heterogeneity of the aquifer need to be tested and used so that the actual geology of the aquifer is modelled. Hence, the hydraulic conductivities were randomised to test the heterogeneity and use field-like soil characteristics. The use of randomised hydraulic conductivities (RHCs) in the SEAWAT-based numerical simulation model was developed for three different hydraulic conductivity (K) ranges. Random integers and Halton sequence techniques were used to generate more than 10000 random values of K for the range K-1=15 m/d to 25 m/d, K-2 = 5 m/d to 40 m/d and K-3 = 2 m/d to 100 m/d. All three ranges of K were generated in MATLAB. The K values were imported in MODFLOW, and the SEAWAT was simulated. The study area, Suva, Fiji, was chosen to run the 3D model using RHCs. However, the study area was treated as an illustrative study area due to the unavailability of the groundwater data. However, some hydrogeological parameters, boundary conditions, elevations and raster data were taken from Suva. The results indicated that using the RHCs reduces the computational burden on numerical simulation models. Also, the realisation of the hydraulic conductivities was included in the model simulations, which made the study area heterogeneous and realistic. Also, the SEAWAT code was successfully applied, showing that the numerical model converges using heterogeneous and anisotropic randomised hydraulic conductivities.

After successfully developing and simulating the 3D numerical model using the SEAWAT code for the illustrative study area, a similar methodology was applied, and a 3D model was developed for a real study area. The study focused on managing SWI in the Tagabe coastal aquifer, which mainly supplies groundwater in Port Vila, Vanuatu. A SEAWAT-based numerical model was developed, calibrated, and validated using field data, making it the first of its kind in Vanuatu. The model tested various scenarios and revealed that combining BWs and IWs is the most effective strategy to mitigate SWI.

Additionally, SLR impacts were modelled for a projection up to 2043, showing minimal effects under the current estimates but highlighting the need for long-term modelling to account for higher SLR and uncertainties. However, excessive pumping from BWs poses an issue when disposing of abstracted saline water. Similarly, excessive pumping from production wells (PWs) could increase SWI rates. Hence, the BW and PW pumping needs to be optimised.

To manage the SWI effectively, the optimal SWI management strategies were developed using a linked simulation-optimisation (S-O) technique that provided optimal management strategies for managing SWI in the Tagabe coastal aquifer. S-O methodology was developed using a surrogate ensemble modelling approach where twelve surrogate models were trained with the input-output patterns from the SEAWAT-based numerical simulation model. Using Shannon's entropy weight (decision theory), the top five surrogates were ranked and selected to form an ensemble model for each monitoring location. All the ensemble models performed exceptionally well compared with standalone surrogates. Later, the ensemble models were externally linked in MATLAB with the Controlled Elitist Multiple Objective Genetic Algorithm (CEMOGA) to optimise the saltwater intrusion management solutions.

The constraints fixed for the S-O model were maximising the pumping from the PWs, minimising the pumping from the BWs, and maintaining the maximum allowable salt concentrations at each monitoring location. Conflicting constraints were easily solved with the S-O methodology developed in this study. The S-O model gave Pareto optimal front solutions, maximising the pumping from PWs and minimising the pumping from BWs. Five random pumping values (Pareto solutions) were fed into the numerical simulation model, and the same was fed into the surrogate ensemble model to verify the Pareto optimal solutions. The results indicated that both models' salt concentrations (outputs) had a minimal relative error of less than 7%, satisfying the constraints.

In addition, the multi-objective S-O model results indicated that using machine learning in groundwater modelling is a robust tool for predicting the SWI in Tagabe coastal aquifer. Using surrogate ensemble models reduced the computational burden and exertions during optimisation. The results also indicated that training different machine learning surrogates with limited datasets was also successful. The S-O management model also proved to be robust in generating optimal solutions for managing the saltwater

intrusion in Tagabe coastal aquifer. However, using feedback from the field, testing different uncertainties and passing optimal SWI management strategies in the field was lacking in the S-O model alone. Hence, a replica of Tagabe coastal aquifer was developed that could easily solve these issues.

A digital twin (DT) model (virtual replica) of the Tagabe coastal aquifer was developed, incorporating a 3D numerical model, surrogate ensemble models, and the S-O approach. Due to funding constraints, illustrative field sensors were used to generate scenarios that simulated salt concentration changes and triggered data transmission from the physical to the virtual space. The DT optimised pumping strategies using a CEMOGA, generating Pareto optimal solutions for different maximum allowable salt concentrations (0.45, 0.55, 0.75, 0.90 and 1.15 kg/m$^3$; Scenarios 1 to 5, respectively). Scenario 3 (0.75 kg/m$^3$) provided an optimal balance with 17,317 m$^3$/day from production wells and 202 m$^3$/day from barrier wells. Higher salt concentration scenarios increased pumping rates but required more from barrier wells. The DT framework was validated with a relative error of less than 10%, demonstrating its reliability and accuracy for managing SWI.

This innovative application of DT for SWI management showcases its global potential for sustainable water resource management. By creating a virtual replica of the aquifer, the DT enables real-time monitoring, simulation, and optimisation of water extraction strategies. It proved vital for predicting future scenarios, adjusting management plans, and efficiently addressing uncertainties. The DT can improve decision-making and resource conservation by integrating smart sensors and feedback loops. This thesis's various studies (chapters) proved that numerical models, surrogate ensemble models, S-O models, and digital twin models successfully manage the SWI in coastal aquifers. The SWI management strategies can guide policymakers, water managers, and stakeholders in protecting groundwater resources and optimising sustainable freshwater extraction in PICs. A similar methodology could be applied in other parts of the world where groundwater is used.

## 9.2 Limitations and future scope of work

The present study used illustrative study area, simulated-synthetic data, real study area and field data to develop numerical and machine learning-based models. One of the major limitations was the availability of the groundwater data. Due to the unavailability of quality and complete data, the study areas were treated as an illustrative study area.

Moreover, the limited data on groundwater standing water levels, pumping, and hydrogeological parameters further stressed the calibration and validation of 3D numerical simulation models. Secondary data, such as salt concentration in calibration and validation, was used to improve model calibrations further. Furthermore, a limited borelog was available that was used to gather hydrogeological parameters and other ground stratigraphy. A larger dataset with quality data is needed for developing, calibrating and validating complex and heterogeneous groundwater models.

Another limitation of this study was the small dataset (130 input-output patterns) used to train the surrogate models. Hence, deep learning models did not perform well during the training and testing stages. It is recommended that larger input-output patterns be used to train surrogate ensemble models and compare their results. Moreover, automating the numerical model in fetching the input data from a folder, simulating the model, and adding the corresponding outputs in the same folder is also recommended to save an immense amount of time when generating input-output patterns.

Moreover, the illustrative sensors were used during the development of the digital twin for Tagabe coastal aquifer instead of real sensors. Getting government approvals from Vanuatu, the cost of buying the sensors, smart water quality meters, solar panels and other types of equipment needed to feed data from the field to the virtual space (virtual Tagabe aquifer) was not available. Hence, the digital twin was developed using illustrative data.

In future, with funding, the illustrative sensors and scenarios will be replaced with actual sensors and field data. Future work aims to implement smart water quality meters, information boards, and sensors in the Tagabe aquifer and other Pacific Island nations, enhancing the scope and effectiveness of DT in managing coastal aquifers. In future, other constraints could be considered in the S-O methodology to manage SWI. For instance, minimising the recharge, maximising the evapotranspiration and salt concentrations at monitoring locations, using other optimising algorithms and using larger input-output data sets in training and testing surrogate and ensemble models.

# Reference


Abarca, E., Vázquez-Suñé, E., Carrera, J., Capino, B., Gámez, D., & Batlle, F. (2006). Optimal design of measures to correct seawater intrusion. *Water Resources Research, 42*(9). doi:10.1029/2005wr004524

Abd-Elaty, I., & Polemio, M. (2023). Saltwater intrusion management at different coastal aquifers bed slopes considering sea level rise and reduction in fresh groundwater storage. *Stochastic Environmental Research and Risk Assessment*, 1-16. https://doi.org/10.1007/s00477-023-02381-9

Abd-Elaty, I., Straface, S., & Kuriqi, A. (2021). Sustainable saltwater intrusion management in coastal aquifers under climatic changes for humid and hyper-arid regions. *Ecological Engineering, 171*, Article 106382. https://doi.org/10.1016/j.ecoleng.2021.106382

Abd-Elhamid, H. F., & Javadi, A. A. (2011). A cost-effective method to control seawater intrusion in coastal aquifers. *Water Resources Management, 25*(11), 2755–2780.

Abdoulhalik, A., Abdelgawad, A. M., Ahmed, A. A., Moutari, S., & Hamill, G. (2022). Assessing the protective effect of cutoff walls on groundwater pumping against saltwater upconing in coastal aquifers. *Journal of Environmental Management, 323*, Article 116200. https://doi.org/10.1016/j.jenvman.2022.116200

Abdoulhalik, A., Ahmed, A., & Hamill, G. A. (2017). A new physical barrier system for seawater intrusion control. *Journal of Hydrology, 549*, 416–427. https://doi.org/10.1016/j.jhydrol.2017.04.005

ACASA. (2011). *Saltwater intrusion and climate change: A primer for local and provincial decision-makers.* Atlantic Climate Adaptation Solutions Association (ACASA). Prince Edward Island Department of Environment, Labour and Justice. Retrieved from http://www.gov.pe.ca/photos/original/cle_WA1.pdf

Acworth, R. I., & Dasey, G. R. (2003). Mapping of the hyporheic zone around a tidal creek using a combination of borehole logging, borehole electrical tomography, and cross-creek electrical imaging, New South Wales, Australia. *Hydrogeology Journal, 11*, 368–377. https://doi.org/10.1007/s10040-003-0258-4

Aharmouch, A., & Larabi, A. (2001). Numerical modelling of saltwater interface upconing in coastal aquifers. In *Proceedings of the 1st International Conference and Workshop on Saltwater Intrusion and Coastal Aquifers: Monitoring, Modelling, and Management*, Essaouira, Morocco, April 23–25.

Ahmed, S. F., Alam, M. S. B., Hassan, M., Rozbu, M. R., Ishtiak, T., Rafa, M., Mofijur, M., Ali, A. M. B. S., & Gandomi, A. H. (2023). Deep learning modelling techniques: Current progress, applications, advantages, and challenges. *Artificial Intelligence Review, 56*, 13521–13617. https://doi.org/10.1007/s10462-023-10466-8

Alberti, L., La Licata, I., & Cantone, M. (2017). Saltwater intrusion and freshwater storage in sand sediments along the coastline: Hydrogeological investigations and groundwater modeling of Nauru Island. *Water, 9*(10), Article 788. https://doi.org/10.3390/w9100788

Al-Hashimi, O., Hashim, K., Loffill, E., Marolt Čebašek, T., Nakouti, I., Faisal, A., & Al-Ansari, N. (2021). A comprehensive review for groundwater contamination and remediation: Occurrence, migration and adsorption modelling. *Molecules (Basel, Switzerland)*, *26*(19), 5913. https://doi.org/10.3390/molecules26195913

Allen, D. M., Mastuo, G., Suchy, M., & Abbey, D. G. (2001). A multidisciplinary approach to studying the nature and occurrence of saline groundwater in the Gulf

Islands, British Columbia, Canada. In *Proceedings of the 1st International Conference and Workshop on Saltwater Intrusion and Coastal Aquifers: Monitoring, Modelling, and Management*, Canada.

Alley, W. M., Healy, R. W., LaBaugh, J. W., & Reilly, T. E. (1999). Flow and storage in groundwater systems. *Science*, *296*(5575), 1985–1990. https://doi.org/10.1126/science.1067123

Alley, W. M., Reilly, T. E., & Franke, O. L. (1999). Sustainability of groundwater resources. *US Department of the Interior, US Geological Survey*, Denver, Colorado.

Amosa, D. U. (2012). Social policies in Samoa. In *Wayzgoose (Ed.)*, Commonwealth Secretariat and United Nations Research Institute for Social Development Report (64 pages). Published by the Commonwealth Secretariat.

Andersen, P. F., Mercer, J. W., & White, H. O. (1988). Numerical modeling of saltwater intrusion at Hallandale, Florida. *Groundwater*, *26*(5), 619–630. https://doi.org/10.1111/j.1745-6584.1988.tb00796.x

Antoniou, A., Loco, A., Kumar, A., & Sinclair, P. (2018). Strengthening water security of vulnerable island states: Groundwater investigation Aitutaki, Cook Islands. *SPC* (50 pages).

Anumalla, S., Ramamurthy, B., Gosselin, D. C., & Burbach, M. (2005). Groundwater monitoring using smart sensors. In *IEEE International Conference on Electro Information Technology*. https://doi.org/10.1109/eit.2005.1626962

Armanuos, A. M., Al-Ansari, N., & Yaseen, Z. M. (2020). Underground barrier wall evaluation for controlling saltwater intrusion in sloping unconfined coastal aquifers. *Water*, *12*(9), 2403. https://doi.org/10.3390/w12092403

Ataie-Ashtiani, B., & Ketabchi, H. (2011). Elitist continuous ant colony optimization algorithm for optimal management of coastal aquifers. *Water Resources Management*, *25*(1), 165–190.

Ataie-Ashtiani, B., Ketabchi, H., & Rajabi, M. M. (2013). Optimal management of a freshwater lens in a small island using surrogate models and evolutionary algorithms. *Journal of Hydrologic Engineering*, *19*(2), 339–354.

Attaran, M., & Celik, B. G. (2023). Digital twin: Benefits, use cases, challenges, and opportunities. *Decision Analytics Journal*, *6*, Article 100165. https://doi.org/10.1016/j.dajour.2023.100165

Auken, E., Pellerin, L., Christensen, N. B., & Sørensen, K. I. (2006). A survey of current trends in near-surface electrical and electromagnetic methods. *Geophysics*, *71*(5), G249–G260.

Aung, T., Singh, A., & Prasad, U. (2009). A study of sea-level changes in the Kiribati area for the last 16 years. *Weather*, *64*(8), 203–206. https://doi.org/10.1002/wea.396

Ayani, M., Ganeback, M., & Ng, A. H. C. (2018). Digital twin: Applying emulation for machine reconditioning. In *Proceedings of the 51st CIRP Conference on Manufacturing Systems, Procedia*, *72*. https://doi.org/10.1016/j.procir.2018.03.139

Ayolabi, E. A., Folorunso, A. F., Odukoya, A. M., & Adeniran, A. E. (2013). Mapping saline water intrusion into the coastal aquifer with geophysical and geochemical techniques: The University of Lagos campus case (Nigeria). *SpringerPlus*, *2*, Article 433. https://doi.org/10.1186/2193-1801-2-433

Babu, R., Park, N., Yoon, S., & Kula, T. (2018). Sharp interface approach for regional and well scale modeling of small island freshwater lens: Tongatapu Island. *Water*, *10*(11), 1636. https://doi.org/10.3390/w10111636

Bakker, M., Essink, O. G. H. P., & Langevin, C. D. (2004). The rotating movement of three immiscible fluids—a benchmark problem. *Journal of Hydrology*, *287*(1–4), 270–278. https://doi.org/10.1016/j.jhydrol.2003.10.007

Baldwin, H. L., & McGuinness, C. L. (1963). *A primer on groundwater*. United States Department of the Interior and Geological Survey, Washington, D.C. Retrieved from https://pubs.usgs.gov/gip/7000056/report.pdf

Barbieri, M., Barberio, M. D., Banzato, F., Billi, A., Boschetti, T., Franchini, S., Gori, F., & Petitta, M. (2021). Climate change and its effect on groundwater quality. *Environmental Geochemistry and Health*. https://doi.org/10.1007/s10653-021-01140-5

Barnett, B., Townley, L. R., Post, V., Evans, R. E., Hunt, R. J., Peeters, L., Richardson, S., Werner, A. D., Knapton, A., & Boronkay, A. (2012). *Australian groundwater modelling guidelines*. Waterlines Report, National Water Commission, Canberra. Retrieved from https://www.groundwater.com.au/media/W1siZiIsIjIwMTIvMTAvMTcvMjFfNDFfMzZfOTYwX0F1c3RyYWxpYW5fZ3JvdW5kd2F0ZXJfbW9kZWxsaW5nX2d1aWRlbGluZXMucGRm

Barrett, B., Heinson, G., Hatch, M., & Telfer, A. (2002). Geophysical methods in saline groundwater studies: Locating perched water tables and fresh-water lenses. *Exploration Geophysics*, *33*(2), 115–121.

Bates, B. C., Kundzewicz, Z. W., Wu, S., & Palutikof, J. P. (2008). *Climate change and water* (Technical Paper of the Intergovernmental Panel on Climate Change).

Bath, A. H., Burgess, W. G., & Carney, J. N. (1986). The chemistry and hydrology of thermal springs on Efate, Vanuatu, SW Pacific. *Geothermics*, *15*(3), 277–294.

Bear, J., & Verruijt, A. (2012). *Modeling groundwater flow and pollution*. Springer Science & Business Media.

Bear, J., Cheng, A. H.-D., Sorek, S., Ouazar, D., & Herrera, I. (1999). *Seawater intrusion in coastal aquifers: Concepts, methods and practices*. Springer Science & Business Media, Kluwer, Dordrecht.

Bendixson, V. M., Jenson, J. W., & Habana, N. C. (2014). The Northern Guam Lens Aquifer Database. University of Guam.

Berthe, L., Seng, D. C., & Asora, L. (2014). Multiple stresses, veiled threat: Saltwater intrusion in Samoa. Paper presented at the *Samoa Conference III: Opportunities and challenges for a sustainable cultural and natural environment*, 25-29 August, National University of Samoa, Apia, Samoa.

Bhattacharjya, R. K., & Datta, B. (2005). Optimal management of coastal aquifers using linked simulation optimization approach. *Water Resources Management, 19*, 293-320. https://doi.org/10.1007/s11269-005-3180-9

Bhattacharjya, R. K., Datta, B., & Satish, M. G. (2007). Artificial neural networks approximation of density dependent saltwater intrusion process in coastal aquifers. *Journal of Hydrologic Engineering, 12*(3). https://doi.org/10.1061/(ASCE)1084-0699(2007)12:3(273)

Bishop, C. M. (2006). *Pattern Recognition and Machine Learning*. Springer.

Bloomfield, J. P., Lewis, M. A., Newell, A. J., Loveless, S. E., & Stuart, M. E. (2020). Characterising variations in the salinity of deep groundwater systems: A case study from Great Britain (GB). *Journal of Hydrology: Regional Studies, 28*, 1-16. https://doi.org/10.1016/j.ejrh.2020.100684

Bobba, A. G. (2002). Numerical modelling of saltwater intrusion due to human activities and sea-level change in the Godavari Delta, India. *Hydrological Sciences Journal, 47*, S67–S80. https://doi.org/10.1080/02626660209493023

Bosserelle, A., Jakovovic, D., Post, V., Rodriguez, S. G., Werner, A., & Sinclair, P. (2015). Assessment of sea-level rise and inundation effects on Bonriki Freshwater Lens, Tarawa Kiribati - Groundwater Modelling report. *Bonriki Inundation Vulnerability Assessment*, ISBN: 978-982-00-0935-6, 1-167.

Bottani, E., Cammardella, A., Murino, T., & Vespoli, S. (2017). From the Cyber-Physical System to the Digital Twin: The process development for behaviour modelling of a Cyber Guided Vehicle in M2M logic.

Boufadel, M. C., Xia, Y., & Li, H. (2011). Modeling solute transport and transient seepage in a laboratory beach under tidal influence. *Environmental Modelling & Software, 26*, 899–912.

Bouwer, H. (2002). Artificial recharge of groundwater: Hydrogeology and engineering. *Hydrogeology Journal, 10*(1), 121-142.

Bower, J. W., Motez, L. H., & Durden, D. W. (1999). Analytical solution for the critical conditions of saltwater upconing in a leaky artesian aquifer. *Journal of Hydrology, 221*, 43–5Breiman, L. (2001). *Random forests*. *Machine Learning, 45*(1), 5-32. https://doi.org/10.1023/A:1010933404324

Brownlee, J. (2019). What is deep learning? *Machine Learning Mastery*. Accessed online on 03/06/2024. Accessed from https://machinelearningmastery.com/what-is-deep-learning/

Burns, W. C. (2002). Pacific island developing country water resources and climate change. *The World's Water, 2003*, 113-132.

Butler, D. J. (2004). National assessment of the priority environmental concerns of Niue. *IWP-Pacific Technical Report (International Waters Project)* no. 2. SPREP's Publications Unit, ISBN: 982-04-0263-8, ISSN: 1818-5614, 68 pages.

C2ES. (2022). Extreme Precipitation and Climate Change. *Centre for Climate and Energy Solutions (C2ES)*. Accessed from https://www.c2es.org/content/extreme-precipitation-and-climate-change/. Date accessed 29.02.2022.

Cai, Y., Starly, B., Cohen, P., & Lee, Y.-S. (2017). Sensor data and information fusion to construct digital-twins virtual machine tools for cyber-physical manufacturing. In *Proceedings of the 45th SME North American Manufacturing Research Conference (NAMRC 45)*, LA, USA, *Procedia Manufacturing, 10*.

Calvache, M., & Pulido-Bosch, A. (1997). Effects of geology and human activity on the dynamics of salt-water intrusion in three coastal aquifers in southern Spain. *Environmental Geology, 30*(3-4), 215-223.

Carpenter, C., Ganilau, L., Chandra, A., Nakamura, T., Duda, A., Bower, R., & Overmars, M. (2007). Integrated Water Resources Management in Pacific Island Countries: A Synopsis. *Dreamwise Limited*, Fiji, 52 pages.

Carroll, S., Hao, Y., & Aines, R. (2009). Geochemical detection of carbon dioxide in dilute aquifers. *Geochem Trans, 10*(4). https://doi.org/10.1186/1467-4866-10-4

Carruthers, P. (2009). *Cook Islands Coastal Vulnerability Assessments. A Small Pacific Island Nation's Experience*. *Pacific Island Climate Change Assistance Program, Environment Service*, 1-8.

Carson, Y., & Maria, A. (1997). Simulation optimization: methods and applications. *WSC 97: Proceedings of the 29th Conference on Winter Simulation*, December 1997, Pages 118–126. https://doi.org/10.1145/268437.268460

Casillas-Trasvina, A., Zhou, Y., Stigter, T.Y., Mussaa, F.E.F., & Juizo, D. (2019). Application of numerical models to assess multi-source saltwater intrusion under natural and pumping conditions in the Great Maputo aquifer, Mozambique. *Hydrogeology Journal, 27*, 2973–2992. https://doi.org/10.1007/s10040-019-02053-5

Chakraborty, S., & Pal, U. (2021). Towards growth and sustainable research in phase change materials. *Journal of Phase Change Materials, 2*(1). https://doi.org/10.6084/jpcm.v1i1.9

Chakraborty, S., Aggarwal, V., Mukherjee, D., & Andras, K. (2012). Biomass to biofuel: a review on production technology. *Asia-Pacific Journal of Chemical Engineering, 7*(Suppl. 3), S254–S262. https://doi.org/10.1002/apj.1642

Chakraborty, S., Li, J., & Bhattacharya, P. (2021). The solution to the global energy crisis with new materials, and sustainability. *Journal of Phase Change Materials, 1*(2).

Chang, S.W., & Clement, T.P. (2012). Experimental and numerical investigation of saltwater intrusion dynamics in flux-controlled groundwater systems. *Water Resource Journal, 48*, 1–10.

Cheng, A. H.-D., Halhal, D., Naji, A., & Ouazar, D. (2000). Pumping optimization in saltwater-intruded coastal aquifers. *Water Resources Research, 36*(8), 2155–2165. https://doi.org/10.1029/2000wr900149

Cherubini, C., & Pastore, N. (2011). Critical stress scenarios for a coastal aquifer in southeastern Italy. *Nat Hazard Earth System, 11*(13), 81–93.

Choquet, C., Diédhiou, M.M., & Rosier, C. (2016). Derivation of a Sharp-Diffuse Interfaces Model for Seawater Intrusion in a Free Aquifer. Numerical Simulations. *SIAM Journal on Applied Mathematics, 76*(1), 138-158.

Christelis, V., & Mantoglou, A. (2016). Pumping optimization of coastal aquifers assisted by adaptive metamodelling methods and radial basis functions. *Water Resources Management, 30*(15), 5845–5859.

Christiansen, J. E. (1944). Effect of entrapped air upon the permeability of soils. *Soil Sciences, 58*(5), 355–365.

CIA. (2021). The World Factbook – Australia – Oceania. Accessed on 31.05.2021, Retrieved from https://www.cia.gov/the-world-factbook/australia-oceania/

Clifford, M.J., Ali, S.H., & Matsubae, K. (2018). Mining, land restoration and sustainable development in isolated islands: An industrial ecology perspective on extractive transitions on Nauru. *Ambio*. https://doi.org/10.1007/s13280-018-1075-2

Cobaner, M., Yurtal, R., Dogan, A., & Motz, L.H. (2012). Three dimensional simulation of seawater intrusion in coastal aquifers: A case study in the Goksu Deltaic Plain. *Journal of Hydrology, 464-465*, 262-280. https://doi.org/10.1016/j.jhydrol.2012.07.022

Collins, G. (2015). Blue Gold: Commoditize Groundwater and Use Correlative Management to Balance City, Farm, and Frac Use in Texas. *Natural Resource Journal, 55*(2), 441-478. https://digitalrepository.unm.edu/nrj/vol55/iss2/9

Cooper, H. H. (1959). A hypothesis concerning the dynamic balance of fresh water and salt water in a coastal aquifer. *Journal of Geophysical Research, 64*(4), 461–467. https://doi.org/10.1029/jz064i004p00461

Costall, A. R., Harris, B. D., Teo, B., Schaa, R., Wagner, F. M., & Pigois, J. P. (2020). Groundwater throughflow and seawater intrusion in high quality coastal aquifers. *Scientific Reports, 10*(1). https://doi.org/10.1038/s41598-020-66516-6

CP. (2023). City Population (CP). Port Vila, population. Online report accessed on 23.03.2023. Retrieved from https://www.citypopulation.de/en/vanuatu/admin/shefa/02__port_vila/

CRCP. (2021). Report on Climate Risk Country Profile (CRCP): Vanuatu (2021): The World Bank Group. Retrieved from https://climateknowledgeportal.worldbank.org/sites/default/files/country-profiles/15825-WB_Vanuatu%20Country%20Profile-WEB.pdf

Datta, B., & Peralta, R. C. (1986). Interactive computer graphics-based multi-objective decision-making for regional groundwater management. *Agricultural Water Management, 11*(2), 91–116.

Dausman, A., & Langevin, C. D. (2005). Movement of the saltwater interface in the surficial aquifer system in response to hydrologic stresses and water-management practices, Broward County, Florida. (U.S. Department of the Interior, U.S. Geological Survey, 2005).

Dawe, P. (2001). Review of the Rotuma Water Supply and Distribution System, Fiji Islands. SOPAC Secretariat.

Deb, K., & Goel, T. (2001). Controlled elitist non-dominated sorting genetic algorithms for better convergence. In E. Zitzler, L. Thiele, K. Deb, C. A. Coello Coello, & D. Corne (Eds.), *Evolutionary Multi-Criterion Optimization* (Vol. 1993, pp. 75–89). Springer, Berlin, Heidelberg. https://doi.org/10.1007/3-540-44719-9_5

Depledge, D. (1994). The urban water resources of Port Vila. Hydrogeological report, Government of Vanuatu.

Devlin, M., Smith, A., Graves, C. A., Petus, C., Tracey, D., Maniel, M., Hooper, E., Kotra, K., Samie, E., Loubser, D., & Lyons, B. P. (2020). Baseline assessment of coastal water quality in Vanuatu, South Pacific: Insights gained from in-situ sampling. *Marine Pollution Bulletin, 160*, 111651. https://doi.org/10.1016/j.marpolbul.2020.111651

Dhar, A., & Datta, B. (2009). Saltwater intrusion management of coastal aquifers. I: Linked simulation-optimization. *Journal of Hydrologic Engineering, 14*(12), 1263–1272. https://doi.org/10.1061/(ASCE)HE.1943-5584.0000097

Dibaj, M., Javadi, A. A., Akram, M., Ke, K. Y., Farmani, R., Tan, Y. C., & Chen, A. S. (2019). Modelling seawater intrusion in the Pingtung coastal aquifer in Taiwan, under the influence of sea-level rise and changing abstraction regime. *Hydrogeology Journal, 28*, 2085–2103. https://doi.org/10.1007/s10040-020-02172-4

Dogan, A., & Fares, A. (2008). Effects of land-use changes and groundwater pumping on saltwater intrusion in coastal watersheds (Chapter 8). In *Coastal Watershed Management* (pp. 219–249). WIT Press, ISSN 1755-8336. https://doi.org/10.2495/978-1-84564-091-0/08

Dore, M. H. I. (2005). Climate change and changes in global precipitation patterns: What do we know? *Environmental International, 31*(8), 1167–1181. https://doi.org/10.1016/j.envint.2005.03.004

Dou, T., Lopes, Y. K., Rockett, P., Hatchway, E. A., & Saber, E. (2020). Model predictive control of non-domestic heating using genetic programming dynamic models. *Applied Soft Computing Journal, 97*(Part B). https://doi.org/10.1016/j.asoc.2020.106695

Dror, I., Berkowitz, B., & Gorelick, S. M. (2004). Effects of air injection on flow through porous media: Observations and analyses of laboratory-scale processes. *Water Resources Research, 40*, WO9203, 1-18. https://doi.org/10.1029/2003WR002960

Duncan, R. (2016). Sources of growth spurts in Pacific Island economies. *Asia and the Pacific Policy Studies, 3*(2), 351–365. https://doi.org/10.1002/app5.125

Edet, A. E., & Okereke, C. S. (2001). A regional study of saltwater intrusion in southeastern Nigeria based on the analysis of geoelectrical and hydrochemical data. *Environmental Geology, 40*(10), 1278–1289. https://doi.org/10.1007/s002540100313

Ekwurzel, B., Moran, J. E., Hudson, G. B., Bissani, M., Blake, R., Krimissa, M., Mosleh, N., Marah, H., Safsaf, N., Hsissou, Y., & Bouchaou, M. (2001). An isotopic

investigation of salinity and water sources in the Souss-Massa Basin, Morocco. In *Proceedings of the 1st international conference on saltwater intrusion and coastal aquifers, monitoring, modelling, and management*, Essaouira, Morocco, April 23–25.

Epting, J., Michel, A., Affolter, A., & Huggenberger, P. (2021). Climate change effects on groundwater recharge and temperatures in Swiss alluvial aquifers. *Journal of Hydrology X, 11*, 1-18. https://doi.org/10.1016/j.hydroa.2020.100071

Falkland, T. (2002). From vision to action – towards sustainable water management in the Pacific, Theme 1 Overview Report Water Resources Management, Pacific Regional Consultation on Water in Small Island Countries, Sigatoka, Fiji, 29 July 2002–3 August 2002.

Famiglietti, J. S. (2014). The global groundwater crisis. *Nature Climate Change, 4*, 945–948.

Ferguson, G., & Gleeson, T. (2012). Vulnerability of coastal aquifers to groundwater use and climate change. *Nature Climate Change, 2*, 342–345. https://doi.org/10.1038/Nclimate1413

Fitterman, D. V., & Deszcz-Pan, M. (2001). Saltwater intrusion in Everglades National Park, Florida, measured by airborne electromagnetic surveys. In *Proceedings of the 1st international conference and workshop on saltwater intrusion and coastal aquifers, monitoring, modelling, and management*, Essaouira, Morocco, April 23–25.

Fletcher, C. H., & Richmond, B. M. (2010). Climate change in the Federated States of Micronesia: Food and water security, climate risk management, and adaptive strategies. University of Hawaii, Sea Grant College Program.

Forrester, A., Sobester, A., & Keane, A. (2008). *Engineering design via surrogate modelling: a practical guide*. John Wiley & Sons, USA.

Foster, S., & Chilton, P. (2003). Groundwater: the processes and global significance of aquifer degradation. *Philosophical Transactions of the Royal Society B, Biological Sciences, 358*(1440), 1957–1972.

Foster, T., & Willetts, J. (2018). Multiple water source use in rural Vanuatu: Are households choosing the safest option for drinking? *International Journal of Environmental Health Research*, 1–11. https://doi.org/10.1080/09603123.2018.1491953

Foster, T., Willetts, J., & Kotra, K. K. (2019). Faecal contamination of groundwater in rural Vanuatu: Prevalence and predictors. *Journal of Water and Health, 17*(5), 737–748. https://doi.org/10.2166/wh.2019.016

Francesco, P., Coppola, G., & Curcio, S. (2021). Modeling aspects in simulation of phase change materials used for thermal regulation of buildings. *Journal of Phase Change Materials, 1*(2). https://doi.org/10.6084/jpcm.v1i2.16

Frankel, T. C. (2015). New NASA data show how the world is running out of water. *Economic Policy, The Washington Post*, June 16. Retrieved from https://www.washingtonpost.com/news/wonk/wp/2015/06/16/new-nasa-studies-show-how-the-world-is-running-out-of-water/?variant=c44b726edf25a662

Freeze, R. A., & Cherry, J. A. (1979). *Groundwater*. Prentice-Hall, Inc., Englewood Cliffs, New Jersey 07632. ISBN-13: 978-0133653120.

Friedman, J. H. (1991). Multivariate adaptive regression splines. *Annals of Statistics, 19*(1), 1–67. https://doi.org/10.1214/aos/1176347963

Frolov, A. P., & Yushmanov, I. O. (1998). Interaction between fresh groundwater and salt water at the Baltic Sea Coast. *Vodn. Resur.*, 25(1), 5–8 [*Water Resour.* (Engl. Transl.), 25(1), 1–3].

Fujita, M., Suzuki, J., Sato, D., Kuwahara, Y., Yokoki, H., & Kayanne, H. (2013). Anthropogenic impacts on water quality of the lagoonal coast of Fongafale Islet, Funafuti Atoll, Tuvalu. *Sustainability Science, 8*(3), 381–390. https://doi.org/10.1007/s11625-013-0204-x

Füssel, H.-M. (2012). Vulnerability of coastal populations. In *Climate Change, Justice and Sustainability* (pp. 45–57). Springer.

Gay, D. (2016). Productive capacity and trade in the Solomon Islands. *CDP Background Paper No. 31*. Department of Economic and Social Affairs, New York. Retrieved from http://www.un.org/en/development/desa/papers/

Gelman, A., Carlin, J. B., Stern, H. S., Dunson, D. B., Vehtari, A., & Rubin, D. B. (2013). *Bayesian Data Analysis* (3rd ed.). CRC Press.

Gharsallah, A., Tahri, N., Duplay, J., & Amar, R. B. (2022). Performances of NF and RO applied in a combined system and separately for the treatment and recycling of biologically pretreated real textile wastewater. *Journal of Phase Change Materials, 2*(1), 24–47.

Ghassemi, F., Jakeman, A., Jacobson, G., & Howard, K. (1996). Simulation of seawater intrusion with 2D and 3D models: Nauru Island case study. *Hydrogeology Journal, 4*(3), 4–22.

Giambastiani, B. M. S., Antonellini, M., Oude Essink, G. H. P., & Stuurman, R. J. (2007). Saltwater intrusion in the unconfined coastal aquifer of Ravenna (Italy): A numerical model. *Journal of Hydrology, 340*, 91–104.

Giordana, G. A., & Montginoul, M. (2006). Policy instruments to fight against seawater intrusion in coastal aquifers: An overview. *Vie et Milieu / Life & Environment, 56*(4), 287–294. hal-00453815f.

Goldscheider, N., Chen, Z., Auler, A. S., et al. (2020). Global distribution of carbonate rocks and karst water resources. *Hydrogeology Journal, 28*, 1661–1677. https://doi.org/10.1007/s10040-020-02139-5

Goode, D., Senior, L., Subah, A., & Jaber, A. (2013). Groundwater-level trends and forecasts, and salinity trends, in the Azraq, Dead Sea, Hammad, Jordan side valleys, Yarmouk, and Zarqa groundwater basins, Jordan. United States Geological Survey, Reston, VA.

Gorelick, S. M., & Zheng, C. (2015). Global change and the groundwater management challenge. *Water Resources Research, 51*, 3031–3051. https://doi.org/10.1003/2014WR016825

Gounder, N. (2020). Fiji economic survey: Low growth the new normal? *Asia & the Pacific Policy Studies, 7*(2), 145–157. https://doi.org/10.1002/app5.307

Green, T. R. (2016). Linking Climate Change and Groundwater. In A. J. Jakeman, O. Barreteau, R. J. Hunt, J. D. Rinaudo, & A. Ross (Eds.), *Integrated Groundwater Management* (pp. 107–125). Springer, Cham. https://doi.org/10.1007/978-3-319-23576-9_5

Green, T. R., Taniguchi, M., Kooi, H., Gurdak, J. J., Allen, D. M., Hiscock, K. M., Treidel, H., & Aureli, A. (2011). Beneath the surface of global change: Impacts of climate change on groundwater. *Journal of Hydrology, 405*(3-4), 532–560. https://doi.org/10.1016/j.jhydrol.2011.05.002

Gregorauskas, M. M., Mokrik, R. V., & Iokshas, K. K. (1986). Hydrochemical aspects of studying fresh groundwater discharge into the Baltic Sea. *Vodn. Resur.*, 4, 13–22.

Gregorauskas, M. M., Mokrik, R. V., & Meeris, S. A. (1987). On the issue of modeling seawater intrusion into aquifers. *Vodn. Resur.*, 4, 21–30.

Grinat, M., Südekum, W., Epping, D., Grelle, T., & Meyer, R. (2010). An automated electrical resistivity tomography system to monitor the freshwater/saltwater zone on a North Sea island. In *Near Surface 2010–16th EAGE European Meeting of Environmental and Engineering Geophysics*. EAGE Publications. https://doi.org/10.3997/2214-4609.20144785

Guo, Q., Huang, J., Zhou, Z., & Wang, J. (2019). Experiment and numerical simulation of seawater intrusion under the influences of tidal fluctuation and groundwater exploitation in coastal multilayered aquifers. *Geofluids*. https://doi.org/10.1155/2019/2316271

Guo, W., & Langevin, C. D. (2002). *User's Guide to SEAWAT: A computer program for simulation of three-dimensional variable density groundwater flow*. Techniques of water-resources investigations of the US Geological Survey, Book 6, Chapter A7.

GWPR (2016). Groundwater Protection Regulations (GWPR), British Columbia. Retrieved from https://www2.gov.bc.ca/gov/content/environment/air-land-water/water

Hagagg, K. H. (2019). Numerical modeling of seawater intrusion in karstic aquifer, Northwestern Coast of Egypt. *Modeling Earth Systems and Environment, 5*, 431–441. https://doi.org/10.1007/s40808-018-0549-3

Halton, J. H. (1960). On the efficiency of certain quasi-random sequences of points in evaluating multi-dimensional integrals. *Numer. Math., 2*(1), 84–90. https://doi.org/10.1007/bf01386213

Hamed, Y., Hadji, R., Redhaounia, B., Zighmi, K., Baali, F., & Gayar, E. A. (2018). Climate impact on surface and groundwater in North Africa: A global synthesis of findings and recommendations. *Euro-Mediterranean Journal for Environmental Integration, 3*(25). https://doi.org/10.1007/s41207-018-0067-8

Hamidi, M. J. E. L., Larabi, A., & Faouzi, M. (2021). Numerical modeling of saltwater intrusion in the Rmel-Oulad Ogbane Coastal Aquifer (Larache, Morocco) in the climate change and sea-level rise context (2040). *Water, 13*(16), 2167. https://doi.org/10.3390/w13162167

Hanjra, M. A., & Qureshi, M. E. (2010). Global water crisis and future food security in an era of climate change. *Food Policy, 35*(5), 365–377.

Hao, A., Zhang, Y., Zhang, E., Li, Z., Yu, J., Wang, H., & Wang, Y. (2018). Review: Groundwater resources and related environmental issues in China. *Hydrogeology Journal*, 1–13. https://doi.org/10.1007/s10040-018-1787-1

Harkness, L. (2001). Recent economic developments in the Kingdom of Tonga. *Pacific Economic Bulletin, 16*(1), 19–43.

Hay, J. E., & Kaluwin, C. (1993). Climate change and sea level rise in the South Pacific region: Proceedings of the second SPREP meeting. South Pacific Regional Environment Programme, Apia, Western Samoa, 238 pp.

Hay, J. E., Kaluwin, C., & Koop, N. (1995). Implications of climate change and sea level rise for small island nations of the South Pacific: A regional synthesis. *Weather and Climate, 15*(2), 5–20. https://www.jstor.org/stable/44280015

Henriksen, H. J., Schneider, R., Koch, J., Ondracek, M., Troldborg, L., Seidenfaden, I. K., et al. (2023). A new digital twin for climate change adaptation, water management, and disaster risk reduction (HIP Digital Twin). *Water, 15*(1), 25. https://doi.org/10.3390/w15010025

Henry, H. R. (1959). Salt intrusion into freshwater aquifers. *Journal of Geophysical Research, 64*(11), 1911–1919. https://doi.org/10.1029/jz064i011p01911

Hess, C. (2017). Improving water quality in Tonga. *The Borgen Project, blog*. Accessed from https://borgenproject.org/water-quality-in-tonga/. Accessed date: 25 March 2022.

Hillel, D. (2000). *Salinity management for sustainable irrigation integrating science, environment, and economics*. Environmentally and socially sustainable development: Rural development department, the World Bank, Washington.

Hochreiter, S., & Schmidhuber, J. (1997). Long short-term memory. *Neural Computation, 9*(8), 1735–1780.

Holding, S., Allen, D. M., Foster, S., Hsieh, A., Larocque, I., Klassen, J., & Van Pelt, S. C. (2016). Groundwater vulnerability on small islands. *Nature Climate Change, 6*, 1100–1103. https://doi.org/10.1038/nclimate3128

Howard, K. F. (2015). Sustainable cities and the groundwater governance challenge. *Environmental Earth Sciences, 73*, 2543–2554. https://doi.org/10.1007/s12665-014-3370-y

Howes, S., Fox, R., Laveil, M., Nguyen, B. H., & Sum, D. J. (2019). 2019 Papua New Guinea economic survey. *Asia & the Pacific Policy Studies, 6*(3), 271–289. https://doi.org/10.1002/app5.287

Huang, T., David, C., Oadia, C., Roberts, J. T., Kumar, S. V., Stackhouse, P., et al. (2022). An Earth System Digital Twin for Flood Prediction and Analysis. *IGARSS 2022 IEEE International Geoscience and Remote Sensing Symposium*, Kuala Lumpur, Malaysia, 4735–4738. https://doi.org/10.1109/IGARSS46834.2022.9884830

Hunt, B. (1979). An analysis of the groundwater resources of Tongatapu Island, Kingdom of Tonga. *Journal of Hydrology, 40*, 185–196. https://doi.org/10.1016/0022-1694(79)90097-0

Hussain, M. S., Abd-Elhamid, H. F., Javadi, A. A., & Sherif, M. M. (2019). Management of seawater intrusion in coastal aquifers: A review. *Water, 11*(12). https://doi.org/10.3390/w11122467

Hussain, M. S., Javadi, A. A., Ahangar-Asr, A., & Farmani, R. (2015). A surrogate model for simulation–optimisation of aquifer systems subjected to seawater intrusion. *Journal of Hydrology, 523*. https://doi.org/10.1016/j.jhydrol.2015.01.079

IGRAC. (2016). Groundwater monitoring in small island developing states in the Pacific. In *Proceedings of the Workshop Summary on Advancing Groundwater Monitoring in Pacific SIDS*, Suva, Fiji, 29 August–2 September 2016; International Groundwater Resources Assessment Centre (IGRAC). Delft, Netherlands.

IMF. (2019). 2018 Article IV Consultation – Press Release; Staff Report, and Statement by the Executive Director for the Republic of Palau. *International Monetary Fund (IMF) Country Report No. 19/43*. Retrieved from: http://www.imf.org/

Iodkazis, V. I., & Mokrik, R. V. (1981). Hydrogeology of the submarine part of the Pribaltic Artesian Basin, in *Osadkoobrazovanie v Baltiiskom more* (Sediment Formation in the Baltic Sea), Moscow: Nedra, 35–44.

Ivakhnenko, A. G. (1968). The group method of data handling—arrival of the method of stochastic approximation. *Soviet Automatic Control, 13*(3), 43–55.

Jang, J. S. R. (1993). ANFIS: Adaptive-network-based fuzzy inference system. *IEEE Transactions on Systems, Man, and Cybernetics, 23*(3), 665–685.

Jasechko, S., Perrone, D., Seybold, H., Fan, Y., & Kirchner, J. W. (2020). Groundwater level observations in 250,000 coastal US wells reveal scope of potential seawater

intrusion. *Nature Communications, 11*(3229). https://doi.org/10.1038/s41467-020-17038-2

Javadi, A., Hussain, M., Sherif, M., & Farmani, R. (2015). Multi-objective optimization of different management scenarios to control seawater intrusion in coastal aquifers. *Water Resources Management, 29*(6), 1843–1857.

Kacimov, A., & Sherif, M. (2006). Sharp interface, one-dimensional seawater intrusion into a confined aquifer with controlled pumping: Analytical solution. *Water Resources Research, 42*(6).

Kaleris, V. K., & Ziogas, A. I. (2023). The effect of cutoff walls on saltwater intrusion and groundwater extraction in coastal aquifers. *Journal of Hydrology, 476*, 370-383. https://doi.org/10.1016/j.jhydrol.2012.11.007

Karterakis, S. M., Karatzas, G. P., Nikolos, I. K., & Papadopoulou, M. P. (2007). Application of linear programming and differential evolutionary optimization methodologies for the solution of coastal subsurface water management problems subject to environmental criteria. *Journal of Hydrology, 342*, 270–282.

Kelly, D. J. (2006). Development of seawater intrusion protection regulations. *Proceedings of the 1st SWIM-SWICA Joint Saltwater Intrusion Conference*, Cagliari-Chia Laguna, Italy - September 24-29, 135-146.

Khatri, N., & Tyagi, S. (2015). Influences of natural and anthropogenic factors on surface and groundwater quality in rural and urban areas. *Frontiers in Life Science, 8*(1), 23-39. https://doi.org/10.1080/21553769.2014.933716

Khublaryan, M. G., Frolov, A. P., & Yushmanov, I. O. (2008). Seawater intrusion into coastal aquifers. *Water Resources, 35*(3), 274–286. https://doi.org/10.1134/s0097807808030032

Kirkegaard, C., Sonnenborg, T. O., Auken, E., & Jorgensen, F. (2011). Salinity distribution in heterogeneous coastal aquifers mapped by airborne electromagnetics. *Vadose Zone Journal, 10*(1), 125–35. https://doi.org/10.2136/vzj2010.0038

Koch, M., & Starke, B. (2001). Experimental and numerical investigation of macrodispersion of density-dependent flow and transport in stochastically heterogeneous media. In: *Proceedings of the 1st International Conference and Workshop on Saltwater Intrusion and Coastal Aquifers, Monitoring, Modelling, and Management*, Essaouira, Morocco, April 23–25.

Kohout, F. A. (1960). Cyclic flow of salt water in the Biscayne aquifer of southeastern Florida. *Journal of Geophysical Research, 65*(7), 2133–2141. https://doi.org/10.1029/jz065i007p02133

Kopsiaftis, G., Protopapadakis, E., Voulodimos, A., Doulamis, N., & Mantoglou, A. (2019). Gaussian process regression tuned by Bayesian optimisation for seawater intrusion prediction. *Computational Intelligence and Neuroscience*. https://doi.org/10.1155/2019/2859429

Kotra, K. K., Bathula, S., & Sami, E. (2022). Delineation of groundwater salinity zones in Shefa and Malampa Provinces, Vanuatu. *Nature Environment and Pollution Technology, 21*(2), 803-812. https://doi.org/10.46488/NEPT.2022.v21i02.045

Kourakos, G., & Mantoglou, A. (2009). Pumping optimization of coastal aquifers based on evolutionary algorithms and surrogate modular neural network models. *Advances in Water Resources, 32*, 507–521.

Kourakos, G., & Mantoglou, A. (2013). Development of a multi-objective optimization algorithm using surrogate models for coastal aquifer management. *Journal of Hydrology, 479*, 13-23.

Koza, J. R. (1992). *Genetic Programming: On the Programming of Computers by Means of Natural Selection*; MIT Press: Cambridge, MA, USA, 1992; Volume 1.

Kumar, C. P. (2016). Modelling of seawater intrusion using SUTRA. Roorkee: National Institute of Hydrology. https://doi.org/10.13140/RG.2.1.2857.0005

Kumar, D. S. (2013). Artificial neural networks in geotechnical engineering: Modeling and application issues. *Metaheuristics in Water, Geotechnical and Transport Engineering*. Elsevier, London, 231-270.

Kumar, M., Thakur, A. K., Mazumder, P., et al. (2020). Frontier review on the propensity and repercussion of SARS-CoV-2 migration to aquatic environment. *Journal of Hazardous Materials Letters, 1*, 100001. https://doi.org/10.1016/j.hazl.2020.100001

Kwame, K. R., & Bawa, M. (2022). Variability of carbonate chemistry of seawater of the central Atlantic coastline of Ghana. *Journal of Phase Change Materials, 2*(1), 12–23.

Lal, A., & Datta, B. (2017). Modelling saltwater intrusion processes and development of a multi-objective strategy for management of coastal aquifers utilizing planned artificial freshwater recharge. *Model. Earth Syst. Environ.*, 4, 111–126.

Lal, A., & Datta, B. (2018a). Development and implementation of support vector machine regression surrogate models for predicting groundwater pumping-induced saltwater intrusion into coastal aquifers. *Water Resources Management, 32*(7), 2405-2419. https://doi.org/10.1007/s11269-018-1936-2

Lal, A., & Datta, B. (2018b). Multiple objective management strategies for coastal aquifers utilising new surrogate models. *International Journal of GEOMATE, 15*(48), 79-85. https://doi.org/10.21660/2018.48.7169

Lal, A., & Datta, B. (2019a). Application of monitoring network design and feedback information for adaptive management of coastal groundwater resources. *Int. J. Environ. Res. Public Health, 16*(22). https://doi.org/10.3390/ijerph16224365

Lal, A., & Datta, B. (2019b). Multi-objective groundwater management strategy under uncertainties for sustainable control of saltwater intrusion: Solution for an island country in the South Pacific. *J. Environ. Manage.*, 234, 115–130.

Lal, A., & Datta, B. (2019c). Optimal groundwater-use strategy for saltwater intrusion management in a Pacific Island country. *Journal of Water Resources Planning and Management, 145*(9), 04019032. https://doi.org/10.1061/(asce)wr.1943-5452.0001090

Landscape-SA. (2015). Measuring salinity. Online fact sheet from the Department of Environment, Water and Natural Resources, South Australia (SA). Retrieved from https://www.landscape.sa.gov.au/mr/publications/measuring-salinity#:~:text=Simply%20times%20(x)%20EC%20(,get%20an%20approximate%20ppm%20equivalent

Langevin, C. D., Thorne Jr, D. T., Dausman, A. M., Sukop, M. C., & Guo, W. (2008). SEAWAT Version 4: A Computer Program for Simulation of Multi-Species Solute and Heat Transport [Report] (6-A22). (Techniques and Methods, Issue. S. Geological). http://pubs.er.usgs.gov/publication/tm6A22

Lari, K. S., Davis, G. B., & Rayner, J. L. (2022). Towards a digital twin for characterising natural source zone depletion: A feasibility study based on the Bemidji site. *Water Research, 208*. https://doi.org/10.1016/j.watres.2021.117853

Lee, D., Park, J., Lee, H. A., & Woo, N. C. (2023). A numerical approach to evaluating groundwater vulnerability to seawater intrusion on Jeju volcanic island, South Korea. *Sustainability, 15*(4), 3081. https://doi.org/10.3390/su15043081

Leopold, L. B. (1974). *Water: A Primer*. W. H. Freeman & Co., San Francisco.

Lese, V., Kiem, A. S., Mariner, A., et al. (2021). Historical and future drought impacts in the Pacific islands and atolls. *Climatic Change, 166*(19). https://doi.org/10.1007/s10584-021-03112-1

Li, H., & Boufadel, M. C. (2011). A tracer study in an Alaskan gravel beach and its implications on the persistence of the Exxon Valdez oil. *Marine Pollution Bulletin, 62*(6), 1261–1269. https://doi.org/10.1016/j.marpolbul.2011.03.011

Li, P., Karunanidhi, D., Subramani, T., & Srinivasamoorthy, K. (2021). Sources and consequences of groundwater contamination. *Archives of Environmental Contamination and Toxicology, 80*, 1–10. https://doi.org/10.1007/s00244-020-00805-z

Li, X., Wang, K., Liu, L., Xin, J., Yang, H., & Gao, C. (2011). Application of the entropy weight and TOPSIS method in safety evaluation of coal mines. *Procedia Engineering, 26*, 2085–2091. https://doi.org/10.1016/j.proeng.2011.11.2410

Lin, J., Snodsmith, J. B., Zheng, C., & Wu, J. (2009). A modeling study of seawater intrusion in Alabama Gulf Coast, USA. *Environmental Geology, 57*, 119–130. https://doi.org/10.1007/s00254-008-1288-y

Lindsey, R. (2020). Climate change: Atmospheric carbon dioxide. Online article by National Oceanic and Atmospheric Administration (NOAA). Accessed on 25 March 2020. Retrieved from https://www.climate.gov/news-features/understanding-climate/climate-change-atmospheric-carbon-dioxide

Lindstrom, J., Larsson, H., Jonsson, M., & Lejon, E. (2017). Towards intelligent and sustainable production. Combining and integrating online predictive maintenance and continuous quality control. *Procedia CIRP, 63*, 443–448.

Liu, M., Fang, S., Dong, H., & Xu, C. (2021). Review of digital twin about concepts, technologies, and industrial applications. *Journal of Manufacturing Systems, 58*, Part B, 346-361. https://doi.org/10.1016/j.jmsy.2020.06.017

Livingston, M. L., & Garrido, A. (2004). Entering the policy debate: An economic evaluation of groundwater policy in flux. *Water Resource Research, 40*(12). https://doi.org/10.1029/2003WR002737

Loaiciga, H. A., Pingel, T. J., & Garcia, E. S. (2011). Sea water intrusion by sea-level rise: Scenarios for the 21st century. *Groundwater, 50*(1), 37–47. https://doi.org/10.1111/j.1745-6584.2011.00800.x

Maity, P. K., Das, S., & Das, R. (2018). Remedial measures for saline water ingression in coastal aquifers of South West Bengal in India. *MOJ Ecology & Environmental Sciences, 3*(1), 00061. https://doi.org/10.15406/mojes.2018.03.00061

Malekpour, A., Sadeghiyan, N., & Mohammadi, M. (2018). Effect of uncertainty of hydraulic conductivity and number of samples in Monte-Carlo method on time-dependent variation of soil consolidation. *Iranian Journal of Soil and Water Research, 49*(4), 749–739. https://doi.org/10.22059/IJSWR.2017.235350.667701

Mantoglou, A. (2003). Pumping management of coastal aquifers using analytical models of saltwater intrusion. *Water Resources Research, 39*(12). https://doi.org/10.1029/2002WR001891

Mantoglou, A., Papantoniou, M., & Giannoulopoulos, P. (2004). Management of coastal aquifers based on nonlinear optimization and evolutionary algorithms. *Journal of Hydrology, 97*, 209–228.

Manu, V. T. (2000). Effects of cropping on soil C and nutrient availability, and the amelioration practices that enhance optimum and sustainable crop yields in Tonga. PhD thesis, University of New England, New South Wales, Australia.

Margat, J., & Gun, J. V. D. (2013). *Groundwater around the World - A Geographic Synopsis* (372 pages). Taylor & Francis Group.

Mcleod, E., Bruton-Adams, M., Forster, J., Franco, C., Gaines, G., Gorong, B., James, R., Posing-Kulwaum, G., Tara, M., & Terk, E. (2019). Lessons from the Pacific Islands – Adapting to climate change by supporting social and ecological resilience. *Frontiers in Marine Science, 6*(289). https://doi.org/10.3389/fmars.2019.00289

MEIDECC. (2021). 2020–2021 Tropical Cyclone Season Updated Outlook for Tonga. Ministry Of Meteorology, Energy, Information, Disaster Management, Environment, Climate Change and Communications (MEIDECC) Nuku'alofa, Tonga. https://reliefweb.int/sites/reliefweb.int/files/resources/TC-Outlook-for-Tonga-March-2021.pdf

Mellor, C. S. (2003). An economic survey of Tuvalu. *Pacific Economic Bulletin, 18*(2), 20–28.

Melloul, A. J., & Goldenberg, L. C. (1997). Monitoring of seawater intrusion in coastal aquifers: Basics and local concerns. *Journal of Environmental Management, 51*(1), 73–86. https://doi.org/10.1006/jema.1997.0136

Menberg, K., Blum, P., Kurylyk, B. L., & Bayer, P. (2014). Observed groundwater temperature response to recent climate change. *Hydrology and Earth System Sciences, 18*(11), 4453–4466. https://doi.org/10.5194/hess-18-4453-2014

Meyer, R., Engesgaard, P., & Sonnenborg, T. O. (2019). Origin and dynamics of saltwater intrusion in a regional aquifer: Combining 3D saltwater modelling with geophysical and geochemical data. *Water Resources Research*. https://doi.org/10.1029/2018WR023624

Michael, H. A., Post, V. E. A., Wilson, A. M., & Werner, A. D. (2017). Science, society, and the coastal groundwater squeeze. *Water Resources Research, 53*(4), 2610–2617. https://doi.org/10.1002/2017WR020851

Milan, A., Oakes, R., & Campbell, J. (2016). *Tuvalu: Climate change and migration – Relationships between household vulnerability, human mobility and climate change* Report No.18. Bonn: United Nations University Institute for Environment and Human Security (UNU-EHS).

Miles, W., Grecni, Z., Matsutaro, E. X., Colin, P., Keener, V., & Golbuu, Y. (2020). Climate change in Palau: Indicators and considerations for key sectors: Report for the Pacific Islands Regional Climate Assessment (PIRCA). Honolulu, HI: East-West Center. https://www.eastwestcenter.org/PIRCA-Palau

Mimura, N. (1999). Vulnerability of island countries in the South Pacific to sea level rise and climate change. *Climate Research, 12*(137–143), 137–143.

Mimura, N. (2013). Sea-level rise caused by climate change and its implications for society. *Proceedings of the Japan Academy. Series B, Physical and Biological Sciences, 89*(7), 281–301. https://doi.org/10.2183/pjab.89.281

Mishra, V., Asoka, A., Vatta, K., & Lall, U. (2018). Groundwater depletion and associated CO2 emissions in India. *Earth's Future*. https://doi.org/10.1029/2018EF000939

Mo, S., Zabaras, N., Shi, X., & Wu, J. (2020). Integration of adversarial autoencoders with residual dense convolutional networks for estimation of non-Gaussian hydraulic conductivities. *Water Resources Research, 56*(2), e2019WR026082.

Mohsen, M. S., Singh, V. P., & Amer, A. M. (1990). A note on saltwater intrusion in coastal aquifers. *Water Resources Management, 4*(2), 123–134.

Mokhtar, M. E., Chibout, M., Mansouri, B. E., Chao, J., Kili, M., & Kanti, S. M. E. (2018). Modeling of the groundwater flow and saltwater intrusion in the coastal

aquifer of Fum Al Wad, Province of Laayoun, Morocco. *International Journal of Geosciences, 9*, 71–92. https://doi.org/10.4236/ijg.2018.91005

Morris, B. L., Lawrence, A. R., Chilton, P., Adams, B., Calow, R. C., & Klinck, B. A. (2003). Groundwater and its susceptibility to degradation: A global assessment of the problem and options for management. United Nations Environment Programme, 126pp. (Early warning and assessment report series, 03-3).

Motallebian, M., Ahmadi, H., Raoof, A., & Cartwright, N. (2019). An alternative approach to control saltwater intrusion in coastal aquifers using a freshwater surface recharge canal. *Journal of Contaminant Hydrology, 222*, 56–64. https://doi.org/10.1016/j.jconhyd.2019.02.007

Mourits, L. J. (1996). An assessment of saltwater intrusion in Babai pits and some water supply projects on Makin, Butaritari, and Abaiang, Republic of Kiribati. *SOPAC Technical Report 229*, funded by the United Nations Development Programme, 39 pages. http://www.pacificwater.org/userfiles/file/TR0229.pdf

Mulhern, O. (2020). Sea level rise projection map – Tonga. *Earth.org*. Accessed on 24/01/2021, from https://earth.org/data_visualization/sea-level-rise-by-2100-tonga/

Neumann, B., Vafeidis, A. T., Zimmermann, J., & Nicholls, R. J. (2015). Future coastal population growth and exposure to sea-level rise and coastal flooding, a global assessment. *PLOS One, 10*(3), e0118571. https://doi.org/10.1371/journal.pone.0118571

Nguyen, B. (2016). Coupling geophysical and isotopic approaches to better simulate saltwater intrusion into coastal aquifers: A case study in the Crau aquifer. *Université d'Avignon*.

Nishikawa, T., Siade, A. J., Reichard, E. G., Ponti, D. J., Canales, A. G., & Johnson, T. A. (2009). Stratigraphic controls on seawater intrusion and implications for groundwater management, Dominguez Gap area of Los Angeles, California, USA. *Hydrogeology Journal, 17*, 1699–1725.

NOAA. (2021). What is the largest ocean basin on Earth? *National Ocean Services, National Oceanic and Atmospheric Administration, U.S. Department of Commerce*. Retrieved from: https://oceanservice.noaa.gov

NOC (2022). Permanent Service for Mean Sea Level, Nuku'alofa B. National Oceanography Centre (NOC), Accessed online on 20 March 2022, accessed from https://psmsl.org/data/obtaining/stations/1842.php

NRW. (2015). *Nauru water and sanitation master plan*, Government of the Republic of Nauru, Non-revenue Water (NRW) Specialists Pty Ltd and NRW Macallan (Fiji) Ltd, 1-273.

Ortega, L. R. M. (2023). A digital twin model for groundwater table monitoring. *Masters Thesis*. Retrieved from https://essay.utwente.nl/97168/1/Morales_MA_ITC.pdf. University of Twente.

Oviedo-Vargas, D., Genereux, D. P., Dierick, D., & Oberbauer, S. F. (2015). The effect of regional groundwater on carbon dioxide and methane emissions from a lowland rainforest stream in Costa Rica. *Journal of Geophysical Research: Biogeosciences, 120*, 2579–2595. doi:10.1002/2015JG003009

Owuor, S. O., Butterbach-Bahl, K., Guzha, A. C., et al. (2016). Groundwater recharge rates and surface runoff response to land use and land cover changes in semi-arid environments. *Ecological Processes, 5*(16). https://doi.org/10.1186/s13717-016-0060-6

Palmer, C. D., Blowes, D. W., Frind, E. O., & Molson, J. W. (1992). Thermal-energy storage in an unconfined aquifer. 1. Field injection experiment. *Water Resource Research, 28*(10), 2845–2856.

Papadopoulou, M. P., Karatzas, G. P., Koukadaki, M. A., & Trichakis, Y. (2005). Modelling the saltwater intrusion phenomenon in coastal aquifers—a case study in the industrial zone of Herakleio in Crete. *Global NEST Journal, 7*, 197–203.

Papadopoulou, M. P., Nikolos, I. K., & Karatzas, G. P. (2010). Computational benefits using artificial intelligent methodologies for the solution of an environmental design problem: Saltwater intrusion. *Water Science & Technology, 62*(7), 1479–1490. https://doi.org/10.2166/wst.2010.442

Parveen, N., Zaidi, S., & Danish, M. (2016). Support vector regression model for predicting the sorption capacity of lead (II). *Perspectives in Science, 8*, 629–631.

Pastor, J., & Post, W. (1988). Response of northern forests to CO2-induced climate change. *Nature, 334*, 55–58. https://doi.org/10.1038/334055a0

Person, M., Taylor, J. Z., & Dingman, S. L. (1998). Sharp interface models of saltwater intrusion and wellhead delineation on Nantucket Island, Massachusetts. *Ground Water, 36*(5), 731–742.

Pfeiffer, T. (2023). Yasur Volcano. *Volcano Discovery*. Online Article retrieved on 21 March 2023, link: https://www.volcanodiscovery.com/yasur.html

Pool, M., & Carrera, J. (2010). Dynamics of negative hydraulic barriers to prevent seawater intrusion. *Hydrogeology Journal, 18*, 95–105. https://doi.org/10.1007/s10040-009-0516-1

Post, V., & Abarca, E. (2009). Preface: Saltwater and freshwater interactions in coastal aquifers. *Hydrogeology Journal, 18*, 1–4. https://doi.org/10.1007/s10040-009-0561-9

Presley, T. K. (2005). Effects of the 1998 drought on the freshwater lens in the Laura area, Majuro Atoll, Republic of the Marshall Islands. *Geological Survey (US)*.

Quigley, N., Beavis, S. G., & White, I. (2016). Rainwater harvesting augmentation of domestic water supply in Honiara, Solomon Islands. *Australian Journal of Water Resources, 20*(1), 65–77. doi:10.1080/13241583.2016.1173314

Rao, S., Bhallamudi, S. M., Thandaveswara, B., & Mishra, G. (2004). Conjunctive use of surface and groundwater for coastal and deltaic systems. *Journal of Water Resources Planning and Management, 130*(3), 255–267.

Rastogi, A., Choi, G. W., & Ukarande, S. K. (2004). Diffused interface model to prevent ingress of seawater in multi-layer coastal aquifers. *Journal of Spatial Hydrology, 4*, 1–31.

Rebecca, L. (2022). Climate Change: Global Sea Level. *NOAA, Climate.gov*. Adapted online on 01 November 2022. Retrieved from https://www.climate.gov/news-features/understanding-climate/climate-change-global-sea-level#:~:text=Global%20average%20sea%20level%20has,3.8%20inches)%20above%201993%20levels.

Reilly, T., & Goodman, A. (1987). Analysis of saltwater upconing beneath a pumping well. *Journal of Hydrology, 89*(3), 169–204.

Rogers, L. L., Dowla, F. U., & Johnson, V. M. (1995). Optimal field-scale groundwater remediation using neural networks and the genetic algorithm. *Environmental Science & Technology, 29*(5), 1145–1155. https://doi.org/10.1021/es00005a003

Romanazzi, A., Gentile, F., & Polemio, M. (2015). Modelling and management of a Mediterranean karstic coastal aquifer under the effects of seawater intrusion and climate change. *Environmental Earth Sciences, 74*, 115–128. https://doi.org/10.1007/s12665-015-4423-6

Ronczka, M., Günther, T., Grinat, M., & Wiederhold, H. (2020). Monitoring freshwater-saltwater interfaces with SAMOS - installation effects on data and inversion. *Near Surface Geophysics*. doi:10.1002/nsg.12115

Roy, D. K., & Datta, B. (2017a). Genetic algorithm tuned fuzzy inference system to evolve optimal groundwater extraction strategies to control saltwater intrusion in multi-layered coastal aquifers under parameter uncertainty. *Modeling Earth Systems and Environment*, 1–19.

Roy, D. K., & Datta, B. (2017b). Multivariate adaptive regression spline ensembles for management of multilayered coastal aquifers. *Journal of Hydrologic Engineering, 22*(9). https://doi.org/10.1061/(ASCE)HE.1943-5584.0001550

Roy, D. K., & Datta, B. (2018). A surrogate-based multi-objective management model to control saltwater intrusion in multi-layered coastal aquifer systems. *Civil Engineering and Environmental Systems, 34*, 238–263. https://doi.org/10.1080/10286608.2018.1431777

Roy, D. K., & Datta, B. (2020a). Modelling and management of saltwater intrusion in a coastal aquifer system: A regional-scale study. *Groundwater for Sustainable Development, 11*, 1–12. https://doi.org/10.1016/j.gsd.2020.100479

Roy, D. K., & Datta, B. (2020b). Saltwater intrusion prediction in coastal aquifers utilizing a weighted-average heterogeneous ensemble of prediction models based on Dempster-Shafer theory of evidence. *Hydrological Sciences Journal*. https://doi.org/10.1080/02626667.2020.1749764

Roy, D. K., Barzegar, R., Quilty, J., & Adamowski, J. (2020). Using ensembles of adaptive neuro-fuzzy inference system and optimisation algorithms to predict reference evapotranspiration in subtropical climatic zones. *Journal of Hydrology, 591*. https://doi.org/10.1016/j.jhydrol.2020.125509

Roy, D. K., Lal, A., Sarker, K. K., Saha, K. K., & Datta, B. (2021). Optimisation algorithms as training approaches for prediction of reference evapotranspiration using adaptive neuro fuzzy inference system. *Agricultural Water Management, 255*. https://doi.org/10.1016/j.agwat.2021.107003

Roy, D. K., Paul, C. R., Munmun, T. H., & Datta, B. (2024). An automatic model selection-based machine learning approach to predict seawater intrusion into coastal aquifers. *Environmental Earth Science, 83*, 287. https://doi.org/10.1007/s12665-024-11589-z

Roy, T., Schütze, N., Grundmann, J., Brettschneider, M., & Jain, A. (2016). Optimal groundwater management using state-space surrogate models: A case study for an arid coastal region. *Journal of Hydroinformatics*, jh2016086.

Ru, Y., Jinno, K., Hosokawa, T., & Nakagawa, K. (2001). Study on effect of subsurface dam in coastal seawater intrusion. In *Proceedings of the 1st International Conference on Saltwater Intrusion and Coastal Aquifers, Monitoring, Modelling, and Management*, Essaouira, Morocco, April 23–25.

Rusydi, A. F. (2018). Correlation between conductivity and total dissolved solid in various types of water: A review. *IOP Conference Series: Earth and Environmental Science, 118*(1), IOP Publishing. doi:10.1088/1755-1315/118/1/012019

SachinAmreiss, G. N., Karthikeyan, B., & Premkumar, K. (2020). Groundwater monitoring system using Internet of Things. *IOP Conference Series: Materials Science and Engineering, 937*, 012017. https://doi.org/10.1088/1757-899X/937/1/012017

Salford Predictive Modeler (2019). Introducing MARS: Multivariate adaptive regression spline. Minitab, 1–35.

https://www.minitab.com/content/dam/www/en/uploadedfiles/content/products/spm/IntroMARS.pdf

Sbai, M. A., Larabi, A., & De-Smedt, F. (1998). Modelling saltwater intrusion by a 3-D sharp interface finite element model. *Transactions on Ecology and the Environment, 17*, ISSN 1743–3541, 201–208.

Scanlon, B. R., Faunt, C. C., Longuevergne, L., Reedy, R. C., Alley, W. M., McGuire, V. L., & McMahon, P. B. (2012). Groundwater depletion and sustainability of irrigation in the US High Plains and Central Valley. *Proceedings of the National Academy of Sciences, 109*(24), 9320–9325. https://doi.org/10.1073/pnas.1200311109

Scheidleder, A., Grath, J., Winkler, G., Stärk, U., Koreimann, C., Gmeiner, C., Nixo, S., Casillas, J., Gravesen, P., Leonard, J., & Elvira, M. (1999). Groundwater quality and quantity in Europe. *European Environment Agency Report*, Copenhagen.

Schmidt, E., Mueller, V., & Rosenbach, G. (2020). Rural households in Papua New Guinea afford better diets with income from small businesses. *Food Policy, 97*, 1–15. https://doi.org/10.1016/j.foodpol.2020.101964

Senthilkumar, S., Vinodh, K., Johnson Babu, G., Gowtham, B., & Arulprakasam, V. (2019). Integrated seawater intrusion study of coastal region of Thiruvallur district, Tamil Nadu, South India. *Applied Water Science, 9*(5). https://doi.org/10.1007/s13201-019-1005-x

Shammas, M. I. (2008). The effectiveness of artificial recharge in combating seawater intrusion in Salalah coastal aquifer, Oman. *Environmental Geology, 55*(1), 191–204.

Shannon, C. E. (1948). A mathematical theory of communication. *The Bell System Technical Journal, 27*, 379–423. https://doi.org/10.1002/j.1538-7305.1948.tb01338.x

Sharan, A. (2022). Analyzing the effects of geomagnetic storms on the F2-region ionosphere in South Pacific region. *Geomagnetism and Aeronomy, 62*, 802–814. https://doi.org/10.1134/S0016793222060147

Sharan, A. (2023). Analysing the effects of tropical cyclone on critical frequency of the F2-region ionosphere in South Pacific region. *Geomagnetism and Aeronomy, 62*(Suppl 1), S128–S141. https://doi.org/10.1134/S0016793222600175

Sharan, A., & Kumar, S. (2021). Long-term trends of the F2-region at mid-latitudes in the Southern Hemisphere. *Journal of Atmospheric and Solar-Terrestrial Physics, 220*, 1–11. https://doi.org/10.1016/j.jastp.2021.105683

Sharan, A., Datta, B., & Lal, A. (2023). Integrating numerical modelling and scenario-based sensitivity analysis for saltwater intrusion management: Case study of a complex heterogeneous island aquifer system. *Environmental Monitoring and Assessment, 195*(5), 553. https://doi.org/10.1007/s10661-023-11159-z

Sharan, A., Datta, B., & Lal, A. (2024a). Management of saltwater intrusion using 3D numerical modelling: A first for the Pacific Island country of Vanuatu. *Environmental Monitoring and Assessment, 196*(120). https://doi.org/10.1007/s10661-023-12245-y

Sharan, A., Lal, A., & Datta, B. (2021). A review of groundwater sustainability crisis in the Pacific Island countries: Challenges and solutions. *Journal of Hydrology, 603*, 1–15. https://doi.org/10.1016/j.jhydrol.2021.127165

Sharan, A., Lal, A., & Datta, B. (2023). Evaluating the impacts of climate change and water over-abstraction on groundwater resources in the Pacific island country of Tonga. *Groundwater for Sustainable Development, 20*, 1–7. https://doi.org/10.1016/j.gsd.2022.100890

Sharan, A., Roy, D. K., Datta, B., & Lal, A. (2024b) (Under review). A multi-objective simulation-optimisation model for managing saltwater intrusion in a coastal aquifer for a Pacific Island country: Case study of Vanuatu.

Sherif, M., & Al-Rashed, M. (2001). Vertical and horizontal simulation of seawater intrusion in the Nile Delta Aquifer. In: Proceedings of the 1st International Conference on Saltwater Intrusion and Coastal Aquifers, Monitoring, Modelling, and Management, Essaouira, Morocco, April 23–25.

Sherif, M., & Hamza, K. (2001). Mitigation of seawater intrusion by pumping brackish water. *Transport in Porous Media, 43*, 29–44. https://doi.org/10.1023/A:1010601208708

Sherif, M., & Singh, V. (2002). Effect of groundwater pumping on seawater intrusion in coastal aquifers. *Agricultural Sciences, 7*(2), 61-67.

Sherif, M., Kacimov, A., Ebraheem, A., & AlMulla, M. (2010). Three-dimensional mapping of seawater intrusion using geophysical methods. *World Environmental and Water Resources Congress 2010*. doi:10.1061/41114(371)124

Sherif, M., Mahmoudi, A. E., Garamoon, H., Kacimov, A., Akram, S., Ebraheem, A., & Shetty, A. (2005). Geoelectrical and hydrogeochemical studies for delineating seawater intrusion in the outlet of Wadi Ham, UAE. *Environmental Geology, 49*(4), 536–551. doi:10.1007/s00254-005-0081-4

Sherif, M., Sefelnasr, A., Ebraheem, A. A., & Javadi, A. (2014). Quantitative and qualitative assessment of seawater intrusion in Wadi Ham under different pumping scenarios. *Journal of Hydrologic Engineering, 19*(5), 855-866. doi:10.1061/(ASCE)HE.1943-5584.0000907

Shiklomanov, I. (1993). Chapter 2: World freshwater resources. In *Water in Crisis, A Guide to the World's Freshwater Resources*, edited by Peter H. Gleick, Oxford University Press, New York.

Shorten, G. G. (1990). Structural geology of Suva Peninsula and Harbour and its implications for the Neogene tectonics of Fiji. *New Zealand Journal of Geology and Geophysics, 33*, 495-506. https://doi.org/10.1080/00288306.1990.10425704

Sialaoa, A. (2003). The Samoa economy. *Pacific Economic Bulletin, 18*(2), 1-19.

Silva, L., Rodríguez-Sedano, F., Baptista, P., & Coelho, J. P. (2023). The digital twin paradigm applied to soil quality assessment: A systematic literature review. *Sensors, 23*, 1-30. https://doi.org/10.3390/s23021007

Singh, A. (2014). Post Tropical Cyclone Ian rapid water resources assessment, SPC Technical Report 202, Lifuka, Ha'apai, Kingdom of Tonga, 1-88.

Singh, R. B., Hales, S., Wet, N. D., Raj, R., Hearnden, M., & Weinstein, P. (2001). The influence of climate variation and change on diarrheal disease in the Pacific Islands. *Environmental Health Perspectives, 109*(2), 155.

Siohane, A., Chapman, C. (2009). Niue Drinking Water Safety Plan. Division of Water Supply, Niue, 1-57.

Snoek, J., Larochelle, H., & Adams, R. P. (2012). Practical Bayesian optimization of machine learning algorithms. In *Advances in Neural Information Processing Systems*, pp. 2951-2959.

Soldal, O., Mauring, E., Halvorsen, E., & Rye, N. (1994). Seawater intrusion and fresh groundwater hydraulics in fjord delta aquifers inferred from ground penetrating radar and resistivity profiles- Sunndalsøra and Esebotn, western Norway. *Journal of Applied Geophysics, 32*(4), 305-319.

Song, J., Yang, Y., Wu, J., Wu, J., Sun, X., & Lin, J. (2018). Adaptive surrogate model based multi-objective optimisation for coastal aquifer management. *Journal of Hydrology, 561*, 98-111. https://doi.org/10.1016/j.jhydrol.2018.03.063

SOPAC (2007a). Sustainable Integrated Water Resources and Wastewater Management in Pacific Island Countries, National Integrated Water Resource Management Diagnostic Report, Palau, 1-64.

SOPAC (2007b). Sustainable Integrated Water Resources and Wastewater Management in Pacific Island Countries, National Integrated Water Resource Management Diagnostic Report, Solomon Islands, 1-86.

SOPAC (2007c). Sustainable Integrated Water Resources and Wastewater Management in Pacific Island Countries, National Integrated Water Resource Management Diagnostic Report, Vanuatu, 1-71.

SPC. (2015). Vanuatu Climate Change and Disaster Risk Reduction Policy 2016-2030. Report by Secretariat of the Pacific Community (SPC). Retrieved from https://www.preventionweb.net/files/46449_vanuatuccdrrpolicy2015.pdf

Sreekanth, J., & Datta, B. (2010). Multi-objective management of saltwater intrusion in coastal aquifers using genetic programming and modular neural network based surrogate models. *Journal of Hydrology, 393*, 245–256.

Sreekanth, J., & Datta, B. (2011). Coupled simulation-optimisation model for coastal aquifer management using genetic programming-based ensemble surrogate models and multiple-realisation optimisation. *Water Resources Research, 47*(4). https://doi.org/10.1029/2010WR009683

Stein, S., Shalev, E., Sivan, O., & Yechieli, Y. (2023). Challenges and approaches for management of seawater intrusion in coastal aquifers. *Hydrogeology Journal, 31*, 19–22. https://doi.org/10.1007/s10040-022-02575-5

Stewart, R. B., Nemeth, K., & Cronin, S. J. (2010). Is Efate (Vanuatu, SW Pacific) a result of subaerial or submarine eruption? An alternative model for the 1 Ma Efate Pumice Formation. *Central European Journal of Geosciences, 2*(3), 306-320. DOI: 10.2478/v10085-010-0020-9

Strack, O. D. L., Stoeckl, L., Damm, K., Houben, G., Ausk, B. K., & de Lange, W. J. (2016). Reduction of saltwater intrusion by modifying hydraulic conductivity. *Water Resources Research, 52*, 6978-6988. https://doi.org/10.1002/2016WR019037

Tal, A., Weinstein, Y., Baïsset, M., Golan, A., & Yechieli, Y. (2019). High resolution monitoring of seawater intrusion in a multi-aquifer system—Implementation of a new downhole geophysical tool. *Water, 11*(9), 1877. doi:10.3390/w11091877

Tao, F., Xiao, B., Qi, Q., Cheng, J., & Ji, P. (2022). Digital twin modeling. *Journal of Manufacturing Systems, 64*, 372-389. https://doi.org/10.1016/j.jmsy.2022.06.015

Tenne, Y., & Goh, C. K. (2010). Computational intelligence in expensive optimisation problems. Springer-Verlag, Berlin Heidelberg, 707 pages. DOI 10.1007/978-3-642-10701-6

Todd, D. K. (1974). Salt-water intrusion and its control. *Water Technology/Resources, Journal of American Water Works Association, 66*(3), 180–187. https://www.jstor.org/stable/41266996

TRCMP. (2018). Tagabe River Catchment Management Plan (TRCMP) 2017-2030. Report by Tagabe River Management Committee. Retrieved from https://www.pacific-r2r.org/sites/default/files/2020-03/Tagabe%20River%20Management%20Plan%20%282017-2030%29.pdf

Treanor, S., & Watson, K. (2015). Tonga facing up to rising sea levels. *BBC Business Report News*, reported on 1 December 2015. Accessed on 25 March 2022, from https://www.bbc.com/news/business-34738408

Tsakiridis, N. L., Samarinas, N., Kalopesa, E., & Zalidis, G. C. (2023). Cognitive soil digital twin for monitoring the soil ecosystem: A conceptual framework. *Soil Systems, 7*(4), 88. https://doi.org/10.3390/soilsystems7040088

Uhlemann, T. H.-J., Schock, C., Lehmann, C., Freiberger, S., & Steinhilper, R. (2018). The Digital Twin: Demonstrating the potential of real-time data acquisition in production systems. In *Proceedings of the 51st CIRP Conference on Manufacturing Systems*, Procedia Manufacturing 9.

UNDP (2016). State of the Environment Report for Port Vila, Vanuatu. Report from United Nations Development Programme (UNDP). Retrieved from https://www.vu.undp.org/content/vanuatu/en/home/library/environment_energy/State_of_Environment_Report_2016.html

UNESCO (2021). Groundwater. Retrieved from https://en.unesco.org/themes/water-security/hydrology/groundwater

UNESCO. (2021). World Heritage List: Vanuatu. Retrieved from https://whc.unesco.org/en/statesparties/vu

Van, M. N., Jaeggi, D., Herfort, M., Low, S., Lods, G., Pezard, P., & Gouze, P. (2004). Development of a test site for the investigation of saltwater intrusion process in a karstified limestone aquifer (Campos Mallorca, Spain). In: *Proceeding of the 18th Salt Water Intrusion Meeting, Cartagena*.

Vandenbohede, A., & Lebbe, L. (2011). Heat transport in a coastal groundwater flow system near De Panne, Belgium. *Hydrogeology Journal, 19*, 1225–1238. https://doi.org/10.1007/s10040-011-0756-8

Velde, v. d. M., Green, S., Vanclooster, M., & Clothier, B. (2007). Sustainable development in small island developing states: Agricultural intensification, economic development, and freshwater resources management on the coral atoll of Tongatapu. *Ecological Economics, 61*(2), 456-468.

Vengadesan, M., & Lakshmanan, E. (2019). Management of coastal groundwater resources. In *Coastal Management* (pp. 383-397). Academic Press.

Verdone, M., & Seidl, A. (2012). Fishing and Tourism in the Vanuatu Economy. *IUCN Environmental Economics Occasional Paper 3*, Gland, Switzerland. 20pp.

VGO (2015). Port Vila urban geohazard assessment. Report from Vanuatu Geohazards Observatory (VGO). Retrieved from http://www.vmgd.gov.vu/vmgd/images/stories/Publications/Reports/Port%20Vila%20Urban%20Geohazard%20Assessment%20Report.pdf

Vidal, J. (2002). Blue gold: Earth's liquid asset. *The Guardian*. Retrieved from https://www.theguardian.com/environment/2002/aug/22/worldsummit2002.earth2

VMGD. (2023). Vanuatu Meteorology & Geohazards Department (VMGD). Retrieved from https://www.vmgd.gov.vu/vmgd/index.php/forecast-division/tropical-cyclone

Voss, C. I., & Souza, W. R. (1987). Variable density flow and solute transport simulation of regional aquifers containing a narrow freshwater-saltwater transition zone. *Water Resources Research, 23*(10), 1851-1866.

WAF (2019). Water Authority of Fiji – 2016 Annual Report, Parliamentary Paper No.113 of 2019, 1-60.

Wang, M., Han, M., Hui, H., & Li, Y. (2019). Study on seawater intrusion in Laizhou bay coastal zone based on groundwater model. *International Journal of Low-Carbon Technologies, 14*(2), 222–226. https://doi.org/10.1093/ijlct/ctz021

Wang, Y. M., Chin, K. S., & Poon, G. K. (2007). Entropy Weighting Based Decision Making in Multicriteria Fuzzy Systems. *International Journal of Approximate Reasoning, 44*(2), 124-140.

Waterloo, M. J., & Ijzermans, S. (2017). Groundwater availability in relation to water demands in Tongatapu. Technical Report - DRR-Team scoping mission Kingdom of Tonga.

Watson, T. A., Werner, A. D., & Simmons, C. T. (2010). Transience of seawater intrusion in response to sea level rise. *Water Resources Research, 46*, W12533. http://dx.doi.org/10.1029/2010WR00956

WBG (2022). Tonga, World Bank Group (WBG). Accessed online on 20 March 2022, accessed from https://data.worldbank.org/country/tonga?view=chart

Webb, J. (2020). Kiribati economic survey: Oceans of opportunity. *Asia & the Pacific Policy Studies, 7*(1), 5–26. doi:10.1002/app5.297

Webb, M. D., & Howard, K. W. F. (2010). Modeling the Transient Response of Saline Intrusion to Rising Sea-Levels. *Ground Water, 49*(4), 560–569. doi:10.1111/j.1745-6584.2010.00758

Weber, E. (2007). Water in the Pacific Islands: Case studies from Fiji and Kiribati, in *WATER: A Source of Conflict or Cooperation?* V. I. Grover, Editor, Science Publisher: USA. 38 pages.

Weinrich, L., Hubler, J. F., & Spatari, S. (2012). Urban water supply: Modeling watersheds and treatment facilities (Chapter 16). *Understanding and Improving the Urban Environment*, Woodhead Publishing Series in Energy, 370-389. https://doi.org/10.1533/9780857096463.3.370

Werner, A. D., Bakker, M., Post, V. E., Vandenbohede, A., Lu, C., Ataie-Ashtiani, B., Simmons, C. T., & Barry, D. A. (2013). Seawater intrusion processes, investigation, and management: Recent advances and future challenges. *Advances in Water Resources, 51*, 3-26. http://dx.doi.org/10.1016/j.advwatres.2012.03.004

Werner, A., Simmons, C. T. (2009). Impact of sea-level rise on seawater intrusion in coastal aquifers. *Groundwater, 47*(2), 197–204. doi:10.1111/j.1745-6584.2008.00535.x

White, I., & Falkland, A. (2010). Practical responses to climate change: Developing national water policy and implementation plans for Pacific small island countries. Proc., Water and Climate: Policy Implementation Challenges; *Proceedings of the 2nd Practical Responses to Climate Change Conference*, Engineers Australia, 439.

White, I., Falkland, A., Etuati, B., Metai, E., Metutera, T. (2001). Recharge of Fresh Groundwater Lenses: Field Study, Tarawa Atoll, Kiribati. In J. S. Gladwell (Ed.) *Proc. Second International Colloquium on Hydrology and Water Resources Management in the Humid Tropics, Panama, 22-25 March 1999*, UNESCO-IHP, CATHALAC, Panama City (in press).

White, I., Falkland, A., Fatai, T. (2009). Vulnerability of Groundwater in Tongatapu, Kingdom of Tonga Groundwater Evaluation and Monitoring Assessment. Report for SOPAC/EU EDF, SOPAC/EU Reducing the Vulnerability of Pacific APC States; Australian National University: Canberra, Australia, 373 pages. Link: https://tonga-data.sprep.org/system/files/Tongatapu%20Groundwater%20Vulnerability%20%26%20Monitoring%20Report%2C%2022Sep09.pdf

White, I., Falkland, A., Fatai, T. (2011). Vulnerability of Groundwater Resources in Tongatapu. *Proceedings of 34th IAHR World Congress* - Balance and Uncertainty, 26 – 1 July 2011, Brisbane, Australia.

White, I., Falkland, T. (2010). Management of freshwater lenses on small Pacific islands. *Hydrogeology Journal, 18*, 227–246. https://doi.org/10.1007/s10040-009-0525-0

White, I., Falkland, T., Kula, T. (2020). Meeting SDG6 in the Kingdom of Tonga: The Mismatch between National and Local Sustainable Development Planning for Water Supply. *Hydrology, 7*(81), 1-25. https://doi.org/10.3390/hydrology7040081

White, I., Falkland, T., Metutera, T., Metai, E., Overmars, M., Perez, P., Dray, A. (2007). Climatic and Human Influences on Groundwater in Low Atolls. *Vadose Zone Journal*, Special Section: Groundwater Resources Assessment under the Pressures of Humanity and Climate.

Wiyot (2015). Wiyot Tribe Water Quality Monitoring Program, Samoa Channel. 1-5.

Wolanski, E., King, B., & Galloway, D. (1997). Salinity Intrusion in the Fly River Estuary, Papua New Guinea. *Journal of Coastal Research, 13*(4). http://www.jstor.org/stable/4298709

Wood, W. W., Hyndman, D. W. (2017). Groundwater depletion: A significant unreported source of atmospheric carbon dioxide. *Earth's Future*. Doi. 10.1002/2017EF000586

World Population Review. (2021). World population history/world population projections. Accessed on 25.5.21. Retrieved from: https://worldpopulationreview.com/

World Population Review. (2022). World population history/world population projections. Accessed on 02.07.22. Retrieved from: https://worldpopulationreview.com/

World-Bank. (2018). Urban Water Supply and Sanitation Sector Project (P165872). Project Information Document/Integrated Safeguards Data Sheet (PID/ISDS), Report No: PIDISDSC24841; Solomon Islands Water Authority, the World Bank: Washington, DC, USA. http://www.worldbank.org/projects

World-data. (2022). Volcanos in Tonga. Online article by World Data info., Accessed on 25 March 2020, accessed from https://www.worlddata.info/oceania/tonga/volcanos.php

Worldometer (2021). Water use by country. Accessed from Worldometer website on 28.06.2021 https://www.worldometers.info/water/

WPR. (2023). World Population Review (WPR). Vanuatu Population 2023 (Live). Online report accessed on 23.03.2023. Retrieved from https://worldpopulationreview.com/countries/vanuatu-population

WTTC (2021). Vanuatu: Travel & Tourism Economic Impact 2021. Retrieved from https://wttc.org/Research/Economic-Impact/Country-Analysis-Reports

Wu, X., Kumar, V., Quinlan, J.R., Ghosh, J., Yang, Q., Motoda, H., McLachlan, G.J., Ng, A., Liu, B., & Philip, S.Y. (2008). Top 10 algorithms in data mining. *Knowledge and Information Systems, 14*(1), 1-37.

Xylem. (2013). Water monitoring solutions. YSI Integrated Systems & Services, E58-07 0113, USA.

Yang, T., Feng, B., Chien, J., Krishnan, S., & Agrawal, G. (2019). AdaFLO: Adaptive Fuzzy Linear Optimization for Online Hyperparameter Tuning. In *Proceedings of the 2019 SIAM International Conference on Data Mining (SDM)*, pp. 221-229.

Yang, Y., Song, J., Simmons, C. T., Ataie-Ashtiani, B., Wu, J., Wang, J., & Wu, J. (2021). A conjunctive management framework for the optimal design of pumping and injection strategies to mitigate seawater intrusion. *Journal of Environmental Management, 282*, 111964, 1-18. https://doi.org/10.1016/j.jenvman.2021.111964

Zektser, S., Loáiciga, H. A., & Wolf, J. (2005). Environmental impacts of groundwater overdraft: selected case studies in the southwestern United States. *Environmental Geology, 47*(3), 396-404.

Zhang, D. (2002). *Stochastic methods for flow in porous media*. Academics Press, San Diego, California, USA.

Zhang, Y., & Pinder, G. F. (2000). Latin Hypercube Sampling of Random Hydraulic-Conductivity Fields for Monte-Carlo Analysis of Groundwater Flow and Mass Transport. *American Society of Civil Engineers Joint Conference on Water Resource Engineering and Water Resources Planning and Management 2000* - Minneapolis, Minnesota, United States (July 30-August 2, 2000), Building Partnerships, 1–4. doi:10.1061/40517(2000)389

Zheng, C., & Wang, P. P. (1999). MT3DMS, A modular three-dimensional multi-species transport model for simulation of advection, dispersion, and chemical reactions of contaminants in groundwater systems; documentation and user's guide, contract report SERDP-99-1. Vicksburg, MS: US Army Engineer Research and Development Center, p 169.

Zhou, Q., Bear, J., & Bensabat, J. (2005). Saltwater upconing and decay beneath a well pumping above an interface zone. *Transport in Porous Media, 61*(3), 337-363.

Zhou, X., Ma, Y., Tu, Y., & Feng, Y. (2013). Ensemble of surrogates for dual response surface modeling in robust parameter design. *Quality and Reliability Engineering International, 29*(2), 173-197.

Zhou, Z. -H. (2012). *Ensemble methods: foundations and algorithms*, CRC Press.

# Appendix A



Figure A1: The 56 locations of freshwater wells in Tongatapu.

Table A2: Groundwater well locations in Tongatapu. Source (White et al., 2009)

| Location | No. of Wells | Longitude | Latitude |
|---|---|---|---|
| Niutoua | 45 | -175.048 | -21.150 |
| Afa | 57 | -175.058 | -21.138 |
| Kolonga | 49 | -175.074 | -21.141 |
| Manuka | 62 | -175.093 | -21.133 |
| Navutoka | 56 | -175.104 | -21.137 |
| Talafo'ou | 61 | -175.113 | -21.139 |
| Makaunga | 59 | -175.117 | -21.148 |
| Nukuleka | 254 | -175.115 | -21.143 |
| Hoi | 47 | -175.110 | -21.163 |
| Lapaha | 37 | -175.110 | -21.184 |
| Tatakamatonga | 18 | -175.118 | -21.188 |
| Alakifonua | 53 | -175.135 | -21.204 |
| Holonga | 190 | -175.142 | -21.197 |
| Malapo | 55 | -175.154 | -21.204 |
| Pelehake | | -175.135 | -21.221 |
| Airport township | 9 | -175.134 | -21.238 |
| Fua'amotu | 268 | -175.137 | -21.251 |
| Fua'amotu | 182 | -175.140 | -21.256 |

| Location | No. of Wells | Longitude | Latitude |
|---|---|---|---|
| Nakolo | 40 | -175.125 | -21.265 |
| Hamula | 256 | -175.114 | -21.252 |
| Haasini | 42 | -175.110 | -21.249 |
| Lavengatonga | 236 | -175.111 | -21.232 |
| Fatumu | 14 | -175.110 | -21.213 |
| Haveluliku | 50 | -175.106 | -21.200 |
| Vaini | 5 | -175.166 | -21.201 |
| Vaini | 29 | -175.181 | -21.190 |
| Longoteme | 76 | -175.171 | -21.176 |
| Nukuhetulu | 81 | -175.194 | -21.166 |
| Folaha | 78 | -175.185 | -21.174 |
| LDS Nualei | 252 | -175.195 | -21.188 |
| Veitongo | 201 | -175.210 | -21.190 |
| Haateiho | 83 | -175.231 | -21.182 |
| Pea | 88 | -175.242 | -21.170 |
| Utulau | 250 | -175.271 | -21.188 |
| Ha'alalo | 162 | -175.280 | -21.183 |
| Ha'akame | 163 | -175.285 | -21.180 |
| Houma | 166 | -175.300 | -21.166 |
| Vaotu'u | 66 | -175.313 | -21.157 |
| Ha'utu | 157 | -175.330 | -21.140 |
| Kala'au | 156 | -175.338 | -21.138 |
| Ha'avakatolo | 155 | -175.342 | -21.107 |
| Fo'ui | 152 | -175.333 | -21.126 |
| Masilamea | 68 | -175.326 | -21.127 |
| Matahau | 147 | -175.318 | -21.144 |
| Te'ekiu | 65 | -175.320 | -21.131 |
| Nukunuku | 144 | -175.302 | -21.136 |
| Fatai | 133 | -175.278 | -21.139 |
| Lakepa | 134 | -175.278 | -21.143 |
| Matangiake | 139 | -175.273 | -21.164 |
| Kahoua | 170 | -175.269 | -21.161 |
| Lomaiviti | 192 | -175.258 | -21.169 |
| Tokomololo | 86 | -175.250 | -21.174 |
| Hofoa | 89 | -175.230 | -21.134 |
| Vaini | 3 | -175.174 | -21.200 |
| Puke | 217 | -175.242 | -21.133 |
| Sia'atoutai | 93 | -175.258 | -21.138 |